Defining the interactions between components of RND efflux complexes in *Salmonella* Typhimurium

by

Ilyas Alav

A thesis submitted to the University of Birmingham for the degree of

DOCTOR OF PHILOSOPHY

Institute of Microbiology and Infection

College of Medical and Dental Sciences

University of Birmingham

February 2022

UNIVERSITY OF
BIRMINGHAM

University of Birmingham Research Archive

e-theses repository

This unpublished thesis/dissertation is copyright of the author and/or third parties. The intellectual property rights of the author or third parties in respect of this work are as defined by The Copyright Designs and Patents Act 1988 or as modified by any successor legislation.

Any use made of information contained in this thesis/dissertation must be in accordance with that legislation and must be properly acknowledged. Further distribution or reproduction in any format is prohibited without the permission of the copyright holder.

Abstract

Resistance-nodulation-division (RND) efflux pumps contribute to the multidrug resistance of Gram-negative bacteria by exporting clinically relevant antibiotics and preventing them from accumulating at sufficient concentrations. RND pumps, including the principal multidrug efflux pump AcrAB-TolC in *Salmonella enterica*, are tripartite systems with an inner membrane RND-transporter, a periplasmic adaptor protein (PAP) and an outer membrane factor (OMF). The role of the PAPs in the assembly of tripartite efflux complexes and the specific residues involved in the interaction between the PAP and RND-transporter is poorly understood. Previous work in this laboratory predicted four 3D sites involved in the interaction between the PAP AcrA and the AcrB-transporter that corresponded to nine discrete binding sequences referred to as binding boxes within the β-barrel domain and membrane-proximal domain (MPD) of AcrA. These binding boxes are highly conserved within the phylogenetically and structurally related PAPs AcrA and AcrE, which have been shown to be interchangeable.

In this study, the functional role of the residues within these predicted binding boxes was validated by site-directed mutagenesis. Mutations mapping to binding boxes 1, 4, 5, 6 and 9 of AcrA had a significant impact on antimicrobial susceptibility, efflux function, and virulence, indicating their importance in AcrB-binding. Furthermore, a mutation mapping to the MPD of AcrA was found to impact the access of substrates to the entry channels of AcrB, suggesting a potential role for the PAP MPD in modulating substrate channel access. Using the newly defined RND-binding boxes, the PAPs AcrA and AcrE were shown to bind to the AcrB-transporter in the same way by using equivalent residues. Furthermore, the AcrD-transporter was also found to function with AcrA and AcrE to form an efflux competent pump by using the same residues identified based upon AcrA-AcrB interaction.

Overall, this study demonstrates that AcrA and AcrE use the same residues to interact with their RND-transporter partners to form functional tripartite efflux pumps. Targeting the PAP AcrA has been shown to be a good strategy to inhibit the activity of the AcrAB-TolC pump. However, since AcrA and AcrE are interoperable, any potential PAP-inhibitor would need to inhibit the function of both proteins. The sequence and function of the RND-binding boxes defined in this study are conserved between AcrA and AcrE and so could be attractive drug target sites for the development of efflux inhibitors capable of inhibiting both PAPs.

Acknowledgements

First and foremost, I owe my supervisor, Dr. Jessica Blair, endless gratitude for her constant support and guidance throughout my PhD. You were always there to lend an ear whether it be my scientific or personal struggles. I would like to thank all the past and present members of the Blair Lab Group, especially Hannah, Lizzy, Enea, Pauline, and Emily for being so fun and supportive throughout the past three years. Special thanks go to Dr. Helen McNeil for putting up with my whining when my experiments failed and for answering my never-ending stream of questions. I would also like to thank my collaborators Dr. Ricardo Corona Torres for his help with the site-directed mutagenesis work and Prof. Vassiliy Bavro for his help with the structural aspects of my project.

I would like to thank the BBSRC for funding this project and the MIBTP for providing me with the opportunity to undertake a PhD.

I would like to thank all my friends and family for believing in me. Finally, I am grateful to my partner Szymon for putting up with me for the past three years and for being so supportive throughout my PhD.

Declaration of authorship I

This is to confirm that Ilyas Alav was the first author and a major contributor to the following publication: **Alav, I.**, Kobylka, J., Kuth, M. S., Pos, K. M., Picard, M., Blair, J. M. A. & Bavro, V. N. 2021. Structure, Assembly, and Function of Tripartite Efflux and Type 1 Secretion Systems in Gram-Negative Bacteria. *Chemical Reviews,* 121**,** 5479-5596.

Text from this publication has been included in Chapters 1 of the following thesis entitled "Defining the interactions between components of RND efflux complexes in *Salmonella* Typhimurium" submitted to the University of Birmingham in 2022.

Signed:

Ilyas Alav



Dr Jessica Blair (corresponding author)



Declaration of authorship II

This is to confirm that Ilyas Alav was a major contributor to the following publication: McNeil, H. E., **Alav, I.**, Torres, R. C., Rossiter, A. E., Laycock, E., Legood, S., Kaur, I., Davies, M., Wand, M., Webber, M. A., Bavro, V. N. & Blair, J. M. A. 2019. Identification of binding residues between periplasmic adapter protein (PAP) and RND efflux pumps explains PAP-pump promiscuity and roles in antimicrobial resistance. *PLoS Pathog,* 15**,** e1008101.

Data from this publication has been included in Chapter 3 of the following thesis entitled "Defining the interactions between components of RND efflux complexes in *Salmonella* Typhimurium" submitted to the University of Birmingham in 2022.

Signed:

Ilyas Alav



Dr Jessica Blair (corresponding author)



Declaration of authorship III

This is to confirm that Ilyas Alav was the first author and a major contributor to the following publication: Alav, I., Bavro, V. N. & Blair, J. M. A. 2022. A role for the periplasmic adaptor protein AcrA in vetting substrate access to the RND efflux transporter AcrB. *Sci Rep*, 12, 4752. Data from this preprint has been included in Chapter 4 of the following thesis entitled "Defining the interactions between components of RND efflux complexes in *Salmonella* Typhimurium" submitted to the University of Birmingham in 2022.

Signed:

Ilyas Alav



Dr Jessica Blair (corresponding author)



Declaration of authorship IV

This is to confirm that Ilyas Alav was the first author and a major contributor to the following publication: **Alav, I.**, Bavro, V. N. & Blair, J. M. A. 2021. Interchangeability of periplasmic adaptor proteins AcrA and AcrE in forming functional efflux pumps with AcrD in *Salmonella enterica* serovar Typhimurium. *J Antimicrob Chemother*, 76, 2558-2564.

Data from this publication has been included in Chapter 6 of the following thesis entitled "Defining the interactions between components of RND efflux complexes in *Salmonella* Typhimurium" submitted to the University of Birmingham in 2022.

Signed:

Ilyas Alav



Dr Jessica Blair (corresponding author)



Publications resulting from this study

Research articles

Alav, I., Bavro, V. N. & Blair, J. M. A. 2022. A role for the periplasmic adaptor protein AcrA in vetting substrate access to the RND efflux transporter AcrB. *Sci Rep*, 12, 4752.

Alav, I., Bavro, V. N. & Blair, J. M. A. 2021. Interchangeability of periplasmic adaptor proteins AcrA and AcrE in forming functional efflux pumps with AcrD in *Salmonella enterica* serovar Typhimurium. *J Antimicrob Chemother,* 76**,** 2558-2564.

McNeil, H. E., **Alav, I.**, Torres, R. C., Rossiter, A. E., Laycock, E., Legood, S., Kaur, I., Davies, M., Wand, M., Webber, M. A., Bavro, V. N. & Blair, J. M. A. 2019. Identification of binding residues between periplasmic adapter protein (PAP) and RND efflux pumps explains PAP-pump promiscuity and roles in antimicrobial resistance. *PLoS Pathog,* 15**,** e1008101.

Review articles

Alav, I., Kobylka, J., Kuth, M. S., Pos, K. M., Picard, M., Blair, J. M. A. & Bavro, V. N. 2021. Structure, Assembly, and Function of Tripartite Efflux and Type 1 Secretion Systems in Gram-Negative Bacteria. *Chemical Reviews,* 121**,** 5479-5596.

Colclough, A. L.*, **Alav, I.***, Whittle, E. E.*, Pugh, H. L.*, Darby, E. M.*, Legood, S. W.*, McNeil, H. E. & Blair, J. M. 2020. RND efflux pumps in Gram-negative bacteria; regulation, structure, and role in antibiotic resistance. *Future Microbiol,* 15**,** 143-157.

*Contributed equally

Clarification of results produced in collaboration

Chapter 3:

The initial set of plasmids carrying the AcrA mutations used in Section 3.4 was constructed by Dr Ricardo Corona Torres.

The rationale for producing the new AcrA mutations listed in Table 3.2 were discussed in collaboration with Prof. Vassiliy Bavro.

Table of contents

CHAPTER 1. Introduction 1
1.1 *Salmonella* 2
1.2 Overview and impact of *Salmonella* infections 2
1.3 *Salmonella* cell envelope 5
1.3.1 Inner membrane 6
1.3.2 Periplasm 6
1.3.3 Outer membrane 7
1.4 Treatment and prevention of *Salmonella* infections 8
1.5 Antibiotic resistance 11
1.5.1 Mechanisms of antibiotic resistance 14
1.5.2 Efflux-mediated antibiotic resistance 18
1.6 The RND superfamily of efflux pumps 19
1.7 Physiological roles of RND efflux pumps 24
1.7.1 Biofilm formation 24
1.7.2 Virulence 26
1.7.3 Quorum sensing 28
1.8 Regulation of RND efflux pumps 29
1.9 The AcrAB-TolC multidrug efflux pump 34
1.9.1 AcrB 39
1.9.2 AcrA 47
1.9.3 TolC 52
1.9.4 AcrZ 56
1.9.5 Interactions between components of the AcrAB-TolC pump 57
1.10 PAP-RND transporter promiscuity 62
1.11 Efflux inhibitors 64
1.11.1 Targeting the inner membrane transporter 66
1.11.2 Targeting the outer membrane factor 71
1.11.3 Targeting the periplasm adaptor protein 71
1.12 Hypotheses 74
1.13 Aims and objectives 74

CHAPTER 2. Materials and Methods 76
2.1 Bacterial strains and growth conditions 77
2.2 Molecular microbiology techniques 84
2.2.1 Preparation of bacterial lysates 84
2.2.2 Routine PCR amplification primers and conditions 84
2.2.3 Plasmid purification 89
2.2.4 Preparation of electrocompetent cells 89
2.2.5 Electroporation 89
2.2.6 DNA sequencing of plasmids and PCR products 90
2.2.7 Determination of antimicrobial susceptibility 90
2.2.8 Growth kinetic assays 91
2.3 Disruption of genes in *Salmonella* Typhimurium 92
2.3.1 Generation of the PCR product for gene inactivation 92
2.3.2 Transformation of *Salmonella* Typhimurium containing pSIM18 with the PCR construct 93
2.3.3 Verification of gene disruption in candidate colonies 93
2.3.4 Removal of the *aph* gene using the pCP20 plasmid 94
2.3.5 Disruption of multiple genes in *Salmonella* Typhimurium 94
2.4 Ethidium bromide efflux assay 94
2.5 Doxorubicin efflux assay 95
2.6 Site directed mutagenesis (SDM) 96
2.6.1 Validation of SDM 97
2.7 Overexpression of *acrD* and *acrA* or *acrE* in the same *Salmonella* Typhimurium cell 97
2.7.1 Generating an *acrD* cloning amplicon 98
2.7.2 Generating *acrA* and *acrE* cloning amplicons 98
2.7.3 Restriction digest reactions 99
2.7.4 Ligation reactions 102
2.7.5 Transformation of ligation products 102
2.7.6 Verification of cloning 102
2.7.7 Generating the pACYC177Kan^{R} control plasmid 103
2.8 Cloning of *acrAB* into pET-20b (+) 103
2.9 Western blotting 106

2.9.1 Preparation of membrane fractions....106
2.9.2 Western blotting....106
2.10 *Galleria mellonella* infection model of *in vivo* virulence....107
CHAPTER 3. Defining the interactions between periplasmic adaptor protein AcrA and the RND-transporter AcrB in *Salmonella* Typhimurium....109
3.1 Background....110
3.2 Aims....113
3.3 Hypotheses....113
3.4 Defining the binding box model of PAP-RND interactions....113
3.5 Refining the binding box model of PAP-RND interactions....119
3.5.1 Impact of disruptive mutations mapping to binding boxes 6, 7 and 9....123
3.5.2 Impact of mutations mapping to binding boxes 1, 4 and 5....124
3.6 Effect of AcrA point mutations on the *in vivo* virulence of *Salmonella* Typhimurium SL1344....128
3.7 Western blotting of AcrA mutant proteins....132
3.8 Discussion....135
3.9 Key findings....143
3.10 Future work....143
CHAPTER 4. A potential role for periplasmic adaptor protein AcrA in vetting substrate channel access to the RND transporter AcrB....145
4.1 Background....146
4.2 Aims....147
4.3 Hypotheses....147
4.4 Effect of the K366D AcrA mutation on the antimicrobial susceptibility of the AcrAB-TolC pump....147
4.5 Probing the impact of the K366D AcrA mutation on AcrB substrate channels....151
4.6 The impact of the K366D AcrA mutation on channel 3 of the AcrB-transporter....160
4.7 Western blotting of AcrB proteins....166
4.8 The impact of the K366D AcrA mutation on channel 1 of the AcrB-transporter....168
4.9 Discussion....173
4.10 Key finding....175
4.11 Future work....175

CHAPTER 5. Functional validation of the conserved binding box boxes in the related periplasmic adaptor protein AcrE of *Salmonella* Typhimurium 177
5.1 Background 178
5.2 Aims 179
5.3 Hypothesis 179
5.4 Investigating the functional role of the binding box model in AcrE 179
5.5 Western blotting of AcrE mutant proteins 184
5.6 Discussion 186
5.7 Key findings 189
5.8 Future work 189
CHAPTER 6. Investigating the interchangeability of periplasmic adaptor proteins AcrA and AcrE in forming functional efflux pumps with AcrD in *Salmonella* Typhimurium 191
6.1 Background 192
6.2 Aims 192
6.3 Hypotheses 193
6.4 Construction of the *acrAB*, *acrD* and *acrEF*-deletion *Salmonella* Typhimurium mutant strain 193
6.4.1 Verification of gene deletion 194
6.5 Verification of cloning 196
6.6 Verifying the expression of cloned genes 200
6.7 Substrate specificity of the AcrD-transporter in *Salmonella* Typhimurium SL1344 204
6.8 Investigating the functionality of AcrE with AcrD 204
6.9 The role of RND-binding residues of AcrA and AcrE in forming functional tripartite efflux system with AcrD 209
6.10 Discussion 210
6.11 Key findings 215
6.12 Further work 215
CHAPTER 7. Overall Discussion and Conclusions 217
7.1 Increased understanding of PAP-RND binding and the role of PAPs in substrate efflux 218
7.2 Targeting RND-binding residues to inhibit the function of PAPs 222

References.....226
Appendix I. List of drugs used for antimicrobial susceptibility testing. 250
Appendix II. List of primers used for site-directed mutagenesis reactions. 251
Appendix III. Antimicrobial susceptibility of the *Salmonella* Typhimurium SL1344 Δ4PAP strain carrying different versions of AcrA on the pTrcHis2 plasmid. 253
Appendix IV. Structural formulae of AcrB-substrates.....254
Appendix V. Mean generation times of the *Salmonella* Typhimurium SL1344 Δ4PAP strain carrying plasmid different versions of AcrA in the presence of AcrB-substrates. 255
Appendix VI. Mean generation times of the *Salmonella* Typhimurium SL1344 Δ4PAP strain carrying the plasmid with the K366D AcrA mutation in the presence of different linezolid concentrations.....256
Appendix VII. Mean generation times of the *Salmonella* Typhimurium Δ4PAP Δ*acrB* strain carrying the plasmid with the K366D AcrA and channel 4 (F380A) AcrB mutations in the presence of different fusidic acid concentrations. 257

List of figures

Figure 1.1. Schematic diagram of the main mechanisms of antibiotic resistance in bacteria. . 15
Figure 1.2. A schematic diagram of a tripartite RND efflux pump. 22
Figure 1.3. Schematic diagram of the different mechanisms of RND efflux pump expression. 32
Figure 1.4. The structure of the AcrAB(Z)-TolC complex. 38
Figure 1.5. Structure of AcrB and top view of its transmembrane and pore domains. 40
Figure 1.6. The asymmetric structure of AcrB showing its substrate entry channels and binding sites. 43
Figure 1.7. Schematic representation of the functional rotation mechanism of AcrB. 46
Figure 1.8. The structure of a single AcrA protomer labelled with its main domains. 49
Figure 1.9. The structure of TolC labelled with its main domains. 54
Figure 1.10. The interactions between AcrA and TolC. 59
Figure 1.11. The interactions between AcrA and AcrB. 61
Figure 1.12. Schematic diagram of the five characterised tripartite RND efflux systems in *S. enterica*. 63
Figure 1.13. Schematic diagram of the different mechanisms of action of efflux inhibitors. .. 65
Figure 1.14. The structural formulae of representative efflux inhibitors that have been discussed in this section. 70
Figure 2.1. pHSG398 vector map. 100
Figure 2.2. pACYC177 vector map. 101
Figure 2.3. pET-20b (+) vector map. 105
Figure 3.1. The predicted 3D binding sites of AcrA correspond to linear stretches of highly conserved residues. 112
Figure 3.2. Efflux of ethidium bromide by the *Salmonella* Typhimurium SL1344 Δ4PAP strain carrying plasmid with different versions of AcrA. 117
Figure 3.3. The structure of AcrA labelled with the residues selected for mutagenesis to refine the binding box model. 122
Figure 3.4. Refinement of the RND-binding box model to identify the most critical AcrA residues. 126
Figure 3.5. Effect of *Galleria mellonella* infection by different *Salmonella* Typhimurium SL1344 strains. 131

Figure 3.6. Western blotting of mutant AcrA. 134
Figure 3.7. Interaction between the AcrA β-barrel domain with AcrB. 136
Figure 3.8. Structure of AcrA labelled with the important RND-binding boxes. 137
Figure 3.9. Interaction between the AcrA membrane-proximal domain with AcrB. 140
Figure 4.1. The structure of the trimeric AcrB transporter and the hexameric AcrA assembly (TolC not shown for clarity). 152
Figure 4.2. Efflux of doxorubicin by the *Salmonella* Typhimurium SL1344 Δ4PAP strain carrying plasmid with different versions of AcrA. 155
Figure 4.3. Growth kinetics of the *Salmonella* Typhimurium SL1344 Δ4PAP strain carrying plasmid with different versions of AcrA in the presence of AcrB-substrates. 159
Figure 4.4. PCR check of the *acrAB* cloning insert. 161
Figure 4.5. Accumulation of ethidium bromide in the *Salmonella* Typhimurium SL1344 Δ4PAP Δ*acrB* strain carrying the plasmid with the K366D AcrA and channel 3 AcrB (A33W T37W N298W AcrB) mutations. 163
Figure 4.6. Western blotting of the channel 3 AcrB mutant protein. 167
Figure 4.7. Growth kinetics of the *Salmonella* Typhimurium SL1344 Δ4PAP strain carrying plasmid with the K366D AcrA mutation in the presence of different concentrations of linezolid (LZD), a channel 1-substrate of AcrB. 169
Figure 4.8. Growth kinetics of the *Salmonella* Typhimurium SL1344 Δ4PAP Δ*acrB* strain carrying the plasmid with the K366D AcrA and channel 4 (F380A) AcrB mutations in the presence of fusidic acid (FA), a channel 1- and channel 4-substrate 172
Figure 5.1. Accumulation of ethidium bromide in the *Salmonella* Typhimurium SL1344 Δ4PAP Δ*acrF* strain carrying plasmid with different versions of AcrE. 182
Figure 5.2. Western blotting of mutant AcrE. 185
Figure 5.3. The predicted structure of AcrE. 188
Figure 6.1. Agarose gel electrophoresis of PCR amplified products using check primers for *acrAB*, *acrD* and *acrEF* from *Salmonella* Typhimurium SL1344 Δ*acrAB* Δ*acrD* Δ*acrEF* (Δ3RND). 195
Figure 6.2. PCR check of the *acrA*, *acrE* and *acrD* cloning inserts. 197
Figure 6.3. Map of pHSG398 containing an insert corresponding to a region 100 bp upstream to the stop codon of *acrD*. 198

Figure 6.4. Maps of pACYC177 with an insert corresponding to a region 141 bp upstream to 22 bp downstream of *acrA* or 22 bp upstream to stop codon of *acrE*. 199
Figure 6.5. Efflux of ethidium bromide by the *Salmonella* Typhimurium SL1344 Δ4PAP strain complemented with pACYC177 *acrA* or pACYC177 *acrE*. 202
Figure 6.6. Pairwise sequence alignment of AcrD of *Escherichia coli* K-12 and AcrD of *Salmonella* Typhimurium SL1344. 214

List of tables

Table 1.1. Substrate profiles of the five characterised RND efflux pumps in *Salmonella enterica*. 23
Table 2.1. List of strains used in this study. 78
Table 2.2. List of plasmids used in this study. 83
Table 2.3. List of primers used for generating gene knockouts, checking sizes of genes and for cloning of inserts. 86
Table 3.1. Antimicrobial susceptibility of the *Salmonella* Typhimurium SL1344 Δ4PAP strain carrying plasmid with different versions of AcrA. 118
Table 3.2. List of AcrA mutations produced for the refinement of the binding box model of PAP-RND interactions and the rationale for producing the mutations. 120
Table 3.3. Antimicrobial susceptibility of the *Salmonella* Typhimurium SL1344 Δ4PAP strain carrying plasmid with different versions of AcrA to refine the binding box model. 127
Table 4.1. Antimicrobial susceptibility of the *Salmonella* Typhimurium SL1344 Δ4PAP strain carrying plasmid with the F292V, Q311F or K366D AcrA mutations to drugs with different physicochemical characteristics. 150
Table 4.2. List of AcrB-substrates with their predicted channel preference (s). 158
Table 4.3. The antimicrobial susceptibility of the *Salmonella* Typhimurium SL1344 Δ4PAP Δ*acrB* strain carrying the plasmid with the K366D AcrA and channel 3 (A33W T37W N298W) AcrB mutations. 165
Table 5.1. Antimicrobial susceptibility of the *Salmonella* Typhimurium SL1344 Δ4PAP Δ*acrF* strain carrying plasmid with different versions of AcrE. 183
Table 6.1. The susceptibility of the *Salmonella* Typhimurium SL1344 Δ*acrB* strain complemented with pSHG398 *acrD* to AcrD-substrates. 201
Table 6.2. The susceptibility of the *Salmonella* Typhimurium SL1344 Δ4PAP strain complemented with pACYC177 *acrA* or pACYC177 *acrE* to AcrB-substrates. 203
Table 6.3. The antimicrobial susceptibility of *Salmonella* Typhimurium SL1344 Δ*acrB* complemented with pHSG398 *acrD*. 206
Table 6.4. The antimicrobial susceptibility of the *Salmonella* Typhimurium SL1344 Δ*acrAB* Δ*acrD* Δ*acrEF* (Δ3RND) strain complemented with pHSG398 *acrD* and pACYC177 *acrA* or pACYC177 *acrE*. 207

List of abbreviations

Abbreviation	Definition
ABC	ATP-binding cassette
ACR	Acriflavine
AHL	Acyl homoserine lactone
AI	Autoinducer
Amp^R	Ampicillin resistant
AMR	Antimicrobial resistance
ANOVA	One-way analysis of variance
APPE	Aryl-polyene pigment extrusion
ATCC	American Type Culture Collection
ATP	Adenosine triphosphate
AZT	Aztreonam
BER	Berberine
BL	β-lactam
bp	Base pair
BZK	Benzalkonium chloride
CAR	Carbenicillin
CCCP	Carbonyl cyanide *m*-chlorophenyl hydrazone
CFU	Colony forming unit
CH1	Channel 1
CH2	Channel 2
CH3	Channel 3
CH4	Channel 4
CHL	Chloramphenicol
CHO	Cholate
Chl^R	Chloramphenicol resistant
CIP	Ciprofloxacin
CLI	Clindamycin
CLX	Cloxacillin
CV	Crystal violet
DBP	Distal binding pocket

DHFR	Dihydrofolate reductase
DHPS	Dihydropteroate acid synthase
DMSO	Dimethyl sulfoxide
DNA	Deoxyribonucleic acid
DOC	Deoxycholate
DOX	Doxorubicin
DSP	Dithiobis (succinimidyl propionate)
EtBr	Ethidium bromide
EDTA	Ethylenediaminetetraacetic acid
EI	Efflux inhibitor
EM	Electron microscopy
EPS	Extracellular polymeric substance
ERY	Erythromycin
FA	Fusidic acid
FQ	Fluoroquinolone
FRT	Flp recombinase target
g	Gravity
GEN	Gentamicin
HAE-1	Hydrophobe/amphiphile efflux 1
HC	Hexaamminecobalt
HGT	Horizontal gene transfer
HME	Heavy metal efflux
HMMD	High-molecular-mass drug
HYG	Hygromycin B
Hyg^R	Hygromycin resistant
IM	Inner membrane
KAN	Kanamycin
Kan^R	Kanamycin resistant
kb	kilobase
kDa	Kilodalton
L	Litre
LB	Luria Bertani

LMMD	Low-molecular-mass drug
LPS	Lipopolysaccharide
LZD	Linezolid
M	Molar
mA	Milliamp
MATE	Multidrug and toxin extrusion
MB	Methylene blue
MDR	Multidrug resistance
MFS	Major facilitator superfamily
MIC	Minimum inhibitory concentration
MIN	Minocycline
mL	Millilitre
mM	Millimolar
MPD	Membrane-proximal domain
NAF	Nafcillin
NDM	New-Delhi metallo-β-lactamase
NFE	Nodulation factor exporter
NICE	National Institute for Health and Care Excellence
nm	Nanometre
no.	Number
NOV	Novobiocin
NTS	Non-typhoidal *Salmonella*
OD	Optical density
OD_{600}	Optical density at 600 nm
OM	Outer membrane
OMF	Outer membrane factor
OMP	Outer membrane protein
OXA	Oxacillin
PAC	Planar aromatic cation
PACE	Proteobacterial antimicrobial compound efflux
PAP	Periplasmic adaptor protein
PAβN	Phenylalanine-arginine β-naphthylamide

PBP	Proximal binding pocket
PBS	Phosphate buffered saline
PDB	Protein Data Bank
PCR	Polymerase chain reaction
PMF	Proton motive force
PPB	Potassium phosphate buffer
PPMO	Peptide-conjugated phosphorodiamidate morpholino oligomer
PVDF	Polyvinylidene fluoride
QS	Quorum sensing
R6G	Rhodamine 6G
RIF	Rifampicin
RNA	Ribonucleic acid
RND	Resistance-nodulation-division
SDM	Site directed mutagenesis
SDS-PAGE	Sodium dodecyl sulphate-polyacrylamide gel electrophoresis
SDW	Sterile distilled water
SMR	Small multidrug resistance
STC	Spectinomycin
STP	Streptomycin
SUL	Sulbenicillin
TCS	Two-component systems
TET	Tetracycline
TFTR	TetR-family transcriptional regulator
TIC	Ticarcillin
TMD	Transmembrane domain
TMP-SMX	Trimethoprim-sulfamethoxazole
TOB	Tobramycin
TPP	Tetraphenylphosphonium
TRI	Triclosan
TRX	Triton X-10
T1SS	Type-1 secretion system
U	Unit

UV	Ultraviolet
V	Volt
WT	Wild type
w/v	weight per volume
µg	Microgram
µL	Microlitre
µM	Micromolar

CHAPTER 1. Introduction

1.1 *Salmonella*

Salmonella is a genus of rod-shaped bacteria belonging to the Enterobacteriaceae family of Gram-negative bacteria that comprise two species, *Salmonella enterica* and *Salmonella bongori*. The species *S. enterica* is highly diverse and is subdivided into six subspecies: *S. enterica* subsp. *enterica* (I), *S. enterica* subsp. *salamae* (II), *S. enterica* subsp. *arizonae* (IIIa), *S. enterica* subsp. *diarizonae* (IIIb), *S. enterica* subsp. *houtenae* (IV) and *S. enterica* subsp. *indica (*VI). However, *S. enterica* subsp. *arizonae* has been recently recommended to be reclassified as a separate species. Furthermore, five novel subspecies have been recently defined: *S. enterica* subsp. *londinensis* (VII), *S. enterica* subsp. *brasiliensis* (VIII), *S. enterica* subsp. *hibernicus* (IX), *S. enterica* subsp. *essexiensis* (X), and *S. enterica* subsp. *reptilium* (XI) (Pearce *et al.*, 2021). Among the subspecies, *S. enterica* subsp. *enterica* predominantly infects warm-blooded animals, such as mammals. On the other hand, *S. bongori* and the other *S. enterica* subspecies inhabit the environment and are generally restricted to cold-blooded animals, and thus seldom seen in humans (Giammanco *et al.*, 2002). *Salmonella* can further be differentiated into more than 2500 serovars according to the Kaufmann-White classification system, which classifies salmonellae based on antigenic presentation. The serovars can possess different host specificities and clinically present themselves as very distinct illnesses (Eng *et al.*, 2015, Ferrari *et al.*, 2019).

1.2 Overview and impact of *Salmonella* infections

From the perspective of human disease, *Salmonella* serovars fall into two groups: non-typhoidal and typhoidal. The two groups of serovars cause very different diseases. Non-typhoidal *Salmonella* (NTS) serovars, such as *Salmonella enterica* serovar Enteriditis and *Salmonella enterica* serovar Typhimurium, are commonly associated with gastroenteritis and bacteraemia

(Gal-Mor *et al.*, 2014). The primary reservoir of NTS serovars are the intestinal tracts of food producing animals and wildlife species (Hilbert *et al.*, 2012). Certain NTS serovars such as *S.* Enteriditis and *S.* Typhimurium have a broad host range and can infect many different animals (Monack, 2012). On the other hand, some NTS serovars are more commonly associated with a particular host. For example, *Salmonella enterica* serovar Gallinarum is associated with fowl typhoid in chickens, and *Salmonella enterica* serovar Dublin and *Salmonella enterica* serovar Choleraesuis are associated with bacteraemia in cattle and pigs, respectively (Tanner and Kingsley, 2018). Transmission of NTS serovars from animals to humans occurs via the faecal-oral route through consumption of contaminated food products and water, or direct contact (Berger *et al.*, 2010, Monack, 2012). Wildlife can acquire NTS through direct contact with food producing animals or through the consumption of contaminated feed or water (Hilbert *et al.*, 2012). NTS can persist in the environment for extended periods of time and has been found to survive in soil for at least a year and up to several months in water and on plants (Monack, 2012).

NTS is prevalent worldwide and causes gastroenteritis in over 95.1 million people, resulting in more than 50,770 deaths (Stanaway *et al.*, 2019a). Main symptoms include abdominal cramps, diarrhoea, headache, muscle pain, nausea, and vomiting. NTS infections typically have an incubation period of 6 to 12 hours, last no more than a week and usually require no medical treatment. However, young children, elderly people and immunosuppressed individuals infected with NTS are at a higher risk of developing severe symptoms that require hospitalisation. The most severe complication of gastroenteritis is bacteraemia, which is defined as the presence of viable bacteria in the bloodstream that affects approximately 5% of patients infected with NTS. In vulnerable patients, bacteraemia can result in a bloodstream infection

and progress to septic shock, a life-threatening condition with a mortality rate of up to 80% (Hohmann, 2001, Jawad *et al.*, 2012, Eng *et al.*, 2015). Globally, the most common NTS serovars responsible for gastroenteritis are Enteriditis and Typhimurium (Stanaway *et al.*, 2019a). In 2019, these two serovars accounted for 48.6% of all NTS infections in England (UK Health Security Agency, 2021). In sub-Saharan Africa, NTS serovars, such as Enteriditis and Typhimurium, frequently cause bacteraemia. In 2017, it was estimated that 78.8% of the 535,000 global cases of invasive NTS infections occurred in sub-Saharan Africa. Furthermore, 85% of the estimated 77,500 global deaths due to invasive NTS also occurred in this region (Stanaway *et al.*, 2019a).

The typhoidal serovars, such as *Salmonella enterica* serovar Typhi and *Salmonella enterica* serovar Paratyphi cause typhoid and paratyphoid fevers, respectively (Hiyoshi *et al.*, 2018). Clinically, symptoms of typhoid and paratyphoid fever are very similar, hence they are often both referred to as enteric fever (Eng *et al.*, 2015). Compared to NTS, the typhoidal *Salmonella* serovars have no significant animal reservoir and are primarily spread from person-to-person via the faecal-oral route. Asymptomatic human carriers of *S.* Typhi can also serve as a reservoir of infections as the bacteria are periodically shed and transmitted to new hosts (Monack, 2012). The most famous example is Mary Mallon (nicknamed 'Typhoid Mary'), who was the first person to be identified as an asymptomatic carrier of *S.* Typhi in the United States and was believed to have infected 122 people resulting in the death of 5 people (Marineli *et al.*, 2013). The characteristic symptom of enteric fever is the gradual onset of persistent fever (which can reach 38-40°C), as well as symptoms associated with the digestive tract. Enteric fever is strongly endemic in low-to-middle-income countries that lack access to clean water and adequate sanitation, which promotes the spread of *Salmonella* through the faecal-oral route

(Gal-Mor *et al.*, 2014). Globally, *S.* Typhi and *S.* Paratyphi cause enteric fever in over 14.3 million people annually, resulting in greater than 135,900 deaths (Stanaway *et al.*, 2019b).

In addition to the significant social burden, *Salmonella* infections also have a profound economic impact. The United States Department of Agriculture estimates that the annual cost of NTS infections amounts to a total of $3.3 billion, which includes productivity loss and medical costs (Hoffmann *et al.*, 2012). Furthermore, *Salmonella* can also contaminate food products, resulting in product recalls and significant economic loss. In the United States, presence of *Salmonella* in fresh fruit and vegetables, such as cucumbers, lettuce, mushrooms, mangos, onions, peaches, and tomatoes, has resulted in 1,611 food-related outbreaks between 2010–2020 (Centers for Disease Control and Prevention). *Salmonella* can colonise fruit and vegetables through adhesion, which is mediated by different proteins amongst the NTS serovars. This means that the *Salmonella* are not washed away easily during processing and packing, resulting in contaminated produce. This can be especially problematic for foods which are often consumed raw, such as fruits and salads (Berger *et al.*, 2010). In the UK, the latest data from the Foods Standards Agency reported that in 2018, foodborne diseases caused by NTS resulted in a loss of £210 million (Daniel *et al.*, 2020). Therefore, despite improved food safety measures, *Salmonella* still causes frequent outbreaks and food product recalls every year, resulting in major social and economic burdens.

1.3 *Salmonella* cell envelope

The cell envelope of *Salmonella* is comprised of three essential layers: the outer membrane (OM), the periplasm, and the inner membrane (IM). Fundamentally, the cell envelope is

responsible for protecting cells from environmental insults, maintaining cell shape and preventing osmotic lysis (Costerton *et al.*, 1974).

1.3.1 Inner membrane

The cytoplasm is separated from the cell envelope by the IM, which consists of a phospholipid bilayer embedded with IM proteins and lipoproteins. Unlike eukaryotic cells, bacteria lack intracellular organelles; thus, IM proteins in bacteria carry out membrane-associated functions of eukaryotic organelles, such as ATP and lipid biosynthesis, protein secretion and small molecule transport (Silhavy *et al.*, 2010).

1.3.2 Periplasm

Above the IM is the periplasm, which constitutes 20 to 40% of the total *Salmonella* cell volume (Stock *et al.*, 1977). It compartmentalizes some of the degradative enzymes, such as phosphatases and nucleases, to prevent potential damage to intracellular components (Miller and Salama, 2018) Hence, it has been proposed that the periplasm may have been the precursor to the lysosomes found in the eukaryotic cells (De Duve and Wattiaux, 1966). It also contains chaperone proteins that function to assist protein folding, and periplasmic binding proteins, which are involved in sugar and amino acid transport (Silhavy *et al.*, 2010, Miller and Salama, 2018). The periplasm houses a thin layer of peptidoglycan, a polymer of linear glycan chains made up of repeating units of N-acetyl glucosamine-N-acetyl muramic acid, which are cross-linked by short peptides. Owing to its rigidity, peptidoglycan determines bacterial cell shape and protects the cell from lysis from its internal turgor (Vollmer and Bertsche, 2008).

1.3.3 Outer membrane

Above the periplasm is the OM, which is anchored to the underlying peptidoglycan by murein lipoprotein. The OM forms a selectively permeable barrier that prevents the entry of toxic molecules into the bacterial cell, ensuring their survival in diverse environments (Ruiz *et al.*, 2006). It is only found in Gram-negative bacteria; Gram-positive bacteria lack this organelle. The OM is a lipid bilayer; the inner leaflet consists of phospholipids and the outer leaflet consists of phospholipids and glycolipids, primarily lipopolysaccharide (LPS) (Silhavy *et al.*, 2010). LPS is highly conserved throughout Gram-negative bacteria where it plays a key role in maintaining the structural integrity of the OM. LPS is also one of the major virulence factors in Gram-negative bacteria. For pathogens like *S.* Typhimurium, LPS plays a vital role in facilitating infection as it provides protection against the host innate immune system (Shaio and Rowland, 1985). LPS-defective mutants of *S.* Typhimurium display increased OM permeability and hyper-susceptibility to antibiotics, dyes, and detergents (Vaara, 1993).

LPS is made up of a membrane anchor portion known as lipid A and a core oligosaccharide attached to a distal O-antigen that protrudes from the bacterial surface. The core oligosaccharide plays an essential role in OM stability, hence exhibits restricted structural diversity. For instance, 3-deoxy-D-manno-octulosonic acid is a sugar moiety of the core oligosaccharide found across all Gram-negative bacteria as it is essential for viability. On the other hand, the O-antigen is a highly variable region of LPS that can differ greatly in length and composition amongst Gram-negative bacteria (Raetz and Whitfield, 2002, Erridge *et al.*, 2002). In *Salmonella,* variation of the somatic O-antigen contributes to the myriad of *Salmonella* serovars (Brenner *et al.*, 2000). Lipid A is a highly conserved structure that anchors LPS to the OM. Its general structure comprises of a phosphorylated glucosamine disaccharide backbone, with

attached chains of long fatty acids (Raetz and Whitfield, 2002). Importantly, lipid A is responsible for the endotoxic activity of Gram-negative bacteria, including *Salmonella*, due to its ability to stimulate a strong innate immune response through the activation of Toll-like receptor 4 (Lien *et al.*, 2000).

Proteins constitute approximately 50% of the OM mass and can be classified as lipoproteins or β-barrel proteins. Lipoproteins in the OM do not span the entire membrane but instead are embedded in the inner leaflet of the OM through lipid moieties. The integral, transmembrane proteins of the OM assume a β-barrel conformation, a term used to describe β-sheets wrapped into a cylinder shape. β-barrel proteins are usually referred to as OMPs (outer membrane proteins) and in *Salmonella,* includes porins, such as OmpA and OmpC, that are vital for efficient nutrient uptake and waste excretion (Nikaido, 1992, Koebnik *et al.*, 2000, Ruiz *et al.*, 2006). Porins can be classified as general or specialised depending on their channel specificity. Enterobacteriaceae, including *Salmonella*, have general porins, such as OmpA, OmpC and OmpF, that form non-specific diffusion channels that allow passage of various small molecules (Vergalli *et al.*, 2020). By contrast, *Pseudomonas aeruginosa* has multiple specialised porins that only permit entry of certain molecules. For example, the *P. aeruginosa* porins OprB and OprP specifically transport glucose and phosphates, respectively (Hancock *et al.*, 1992, Wylie and Worobec, 1995).

1.4 Treatment and prevention of *Salmonella* infections

In healthy individuals, *Salmonella* infections are normally self-limiting and do not require treatment in most cases. When treatment is required, it depends on the severity of the disease. National Institute for Health and Care Excellence (NICE) does not recommend antibiotic

therapy for non-severe forms of gastroenteritis caused by NTS (BNF, 2021). Antibiotic therapy in healthy adults and children with non-severe forms of NTS infections does not confer any clinical benefit, and in fact appears to increase the incidence of adverse effects and prolong faecal shedding of *Salmonella* (Onwuezobe *et al.*, 2012). However, older people, immunocompromised individuals and patients with cardiac abnormalities are at an increased risk of developing systemic infections and hence may benefit from early intervention (Hsu and Lin, 2005). For these patients, the NICE recommends ciprofloxacin or cefotaxime treatment, but only once *Salmonella* is confirmed as the causative agent from microbiological testing (BNF, 2021). Compared to NTS infections, enteric fever caused by typhoidal *Salmonella* is usually rare in the UK due to clean water supplies, adequate sanitation, and routine vaccination of new-born babies; however, individuals returning from visiting high-risk areas sometimes contract enteric fever. Due to the increasing global prevalence of multi-drug resistant (MDR) *S.* Typhi and *S.* Paratyphi strains, ampicillin, trimethoprim-sulfamethoxazole, and chloramphenicol are no longer used as first-line treatments. Hence, fluoroquinolones are currently the recommended treatment option, although susceptibility to these antibiotics has also dwindled due to increasing usage fuelling resistance (Pieters *et al.*, 2018). Therefore, where fluoroquinolones fail to treat enteric fever, cefotaxime or ceftriaxone is routinely employed as a first-line treatment (BNF, 2021). Worryingly, there are now reports of large-scale emergence and spread of fluoroquinolone and third-generation cephalosporin-resistant *S.* Typhi clones in Pakistan (Klemm *et al.*, 2018). Hence, one of the few remaining effective treatment options for typhoid fever is azithromycin, however, there are now reports of efflux-mediated resistance to azithromycin in *S.* Typhi isolates in Bangladesh and Nepal (Hooda *et al.*, 2019, Duy *et al.*, 2020). Extensively drug-resistant *S.* Typhi is now endemic in Bangladesh, India, and Pakistan (Nabarro *et al.*, 2022). For Enterobacteriaceae, extensive drug resistance is defined as non-

susceptibility to at least one antibiotic in all but two or fewer class of antibiotics (Magiorakos *et al.*, 2012).

Vaccines are important tools to curb the growth and spread of AMR (Micoli *et al.*, 2021). For example, routine vaccination against *Haemophilus influenzae* type b and *Streptococcus pneumoniae* have significantly reduced disease burden and the incidence of resistant strains (Wellcome Trust and The Boston Consulting Group, 2018). Vaccines can reduce antibiotic consumption and hence selection pressure on bacterial pathogens (Micoli *et al.*, 2021). Currently, there are only two available vaccines licensed for use against *Salmonella* in humans (Fraser *et al.*, 2007). However, neither are used routinely at the country level due to their poor immunogenicity in young children. Additionally, both vaccines are targeted against *S.* Typhi, with no vaccine currently available against key NTS serovars, such as Enteriditis and Typhimurium (MacLennan *et al.*, 2014). By contrast, vaccines against key NTS serovars are available for chickens and have been used to effectively reduce NTS colonisation. For example, the Megan Vac 1 vaccine is effective against colonisation of *S.* Typhimurium, *S.* Enteritidis, and *S.* Heidelberg in the internal organs of vaccinated chickens (Hassan and Curtiss, 1994, Dorea *et al.*, 2010). In the UK, routine poultry vaccination has resulted a significant reduction in the incidence of NTS infections. Between 1993–1996, incidence of NTS in the community was 2.2 cases per 1,000 person years, but by 2008-2009 this had fallen to 0.7 cases per 1,000 person years. Moreover, between 1992 and 2008, reported foodborne *Salmonella* outbreaks fell from nearly 150 per year to just over 20 annually (O'Brien, 2013). However, vaccines are still urgently needed for NTS serovars for use in humans, especially in less economically developed countries, where there is often inadequate sanitation and a lack of access to clean water.

1.5 Antibiotic resistance

The first modern antibacterial agent arsphenamine was discovered in 1909 by Paul Ehrlich and his team, which was found to be an effective treatment for syphilis (Williams, 2009). Since then, antibiotics have saved countless lives by enabling the prevention and treatment of formerly deadly bacterial infections. Consequently, antibiotics have become a cornerstone of modern medicine, allowing many complex medical procedures, such as transplant surgery, cancer chemotherapy and cardiac surgery, to be carried out safely. Unfortunately, bacterial resistance has been observed to all available antibiotics developed so far, which jeopardises the medical response to bacterial diseases (Ventola, 2015). The latest systemic analysis of the global burden of AMR has estimated 4.95 million deaths associated with bacterial AMR in 2019 (Murray *et al.*, 2022). Excessive antibiotic consumption has been shown in multiple studies to correlate with increasing rates of antibiotic resistance across diverse settings, such as communities, hospitals, and nursing homes (Klein *et al.*, 2018). The Joint Interagency Antimicrobial Consumption and Resistance Analysis Report found a positive correlation between antibiotic consumption and resistance for cephalosporins and fluoroquinolones in *Escherichia coli* isolates in Europe between 2013 and 2015. In addition, a strong correlation was documented between antibiotic consumption and resistance for carbapenems and polymyxins in *Klebsiella pneumoniae* isolates within the same time period (European Centre for Disease Prevention and Control and European Food Safety Authority and European Medicines, 2017).

Extensive use of antibiotics in agriculture is another major contributor to the growing problem of antibiotic resistance. Most estimates highlight that on a global scale, far more antibiotics are used for animals than for humans; for instance, 70% of all medically important antibiotics sold

in the USA are used on farm animals (O'Neill, 2016). This is mainly due to their widespread use in intensive farming systems, wherein antibiotics are not only used to treat infections in livestock, but also for prophylaxis (preventative use), metaphylaxis (mass treatment of a group of animals after one animal becomes sick) and growth promotion (McEwen and Fedorka-Cray, 2002). Thus, uncontrolled use of antibiotics in food producing animals has contributed to the emergence of MDR bacteria. For example, a study conducted on 480 broiler chicken carcasses in the USA reported that more than 84% were positive for *Salmonella,* of which more than half were resistant to three or more antibiotics, including tetracycline, ampicillin, ceftiofur and streptomycin (Parveen *et al.*, 2007). Another study determined that MDR *S.* Typhimurium isolates from swine were resistant to a range of clinically relevant antibiotics, such as ampicillin, chloramphenicol, streptomycin, kanamycin, and tetracycline (Gebreyes and Altier, 2002). Worryingly, these resistant pathogens have the potential to be transferred through the food chain to humans (Economou and Gousia, 2015). For example, an outbreak of MDR *Salmonella* infections involving 192 patients in 2015 was traced back to pork consumption (Kawakami *et al.*, 2016).

Owing to their broad host range, NTS infections are generally considered to be zoonotic. Hence, one of the biggest sources of drug-resistant NTS is food products of animal origin, such as beef, chicken, eggs, milk, and pork, but also increasingly fruit and vegetables (Feasey *et al.*, 2012). In sub-Saharan Africa where invasive NTS is prevalent, in addition to contaminated food products, humans have also been found to be a significant reservoir of drug-resistant invasive NTS (Post *et al.*, 2019). By contrast, the typhoidal *Salmonella* serovars *S.* Typhi and *S.* Paratyphi are human-restricted pathogens that cause systemic disease. In a significant proportion of patients (1–6%), systemic illness progresses to an asymptomatic chronic carrier

state. In endemic countries, drug-resistant *S.* Typhi and *S.* Paratyphi can be transmitted through contaminated food or water (Gibani *et al.*, 2018).

Bacteria can become resistant to antibiotics in two ways: spontaneous mutations in the genes encoding protein target of antibiotics; and transfer of resistance genes through horizontal gene transfer. Many antibiotics target bacterial proteins that are essential for the survival of bacteria, hence mutations in the gene encoding the protein target can reduce or prevent the binding of antibiotics to their target (Blair *et al.*, 2015c). Fluoroquinolones, such as ciprofloxacin and levofloxacin, bind to DNA gyrase to inhibit DNA replication, however mutations in the *gyrA* gene encoding DNA gyrase subunit A can confer resistance to fluoroquinolones (Redgrave *et al.*, 2014). Although resistance genes are found on the bacterial chromosome, they are also found on mobile genetic elements, such as plasmids. Through horizontal gene transfer, plasmids containing resistance genes can be transferred amongst bacteria, resulting in the spread of MDR (Normark and Normark, 2002). A well-known example is the global dissemination of *bla*$_{\text{CTX–M}}$ extended-spectrum β-lactamase genes that confer resistance to a range of β-lactam antibiotics. Originating from the soil bacteria *Kluyvera*, these genes are now prevalent in a wide range of Enterobacteriaceae, including numerous *Salmonella* serovars, due to horizontal gene transfer (Canton *et al.*, 2012). Aside from genetic changes, bacteria can also display phenotypic resistance to antibiotics without any genetic changes. As non-inherited mechanisms of resistance, tolerance and persistence can contribute to and result in clinically relevant resistance (Brauner *et al.*, 2016). In *P. aeruginosa* biofilm infections, persister cells can survive following antibacterial therapy and re-establish biofilms, resulting in chronic infections that cannot be eradicated (Lewis, 2008, Bjarnsholt, 2013).

1.5.1 Mechanisms of antibiotic resistance

Bacteria utilise several different molecular mechanisms to resist the effects of antibiotics: 1) direct inactivation of the antibiotic molecule through hydrolysis or modification; 2) modification and/or protection of the antibiotic target; 3) decreased antibiotic penetration due to changes in the cell wall; 4) metabolic bypass; and 5) increased export of the antibiotic by the action of efflux pumps (Fig. 1.1) (Blair *et al.*, 2015c, Munita and Arias, 2016).

The best characterised example of antibiotic inactivation is the hydrolysis of β-lactams, such as penicillins, cephalosporins and carbapenems, by β-lactamase enzymes that cleave the functional β-lactam ring to abolish their antibacterial activity. For example, New-Delhi metallo-β-lactamases (NDM) are a versatile group of enzymes capable of inactivating virtually all β-lactams, including carbapenems, which are considered to be the last resort antibiotics against MDR bacteria (Zmarlicka *et al.*, 2015). NDM-1 containing *S. enterica* isolates have been previously reported to exhibit clinical resistance to a wide range of β-lactams, including cephalosporins and carbapenems (Huang *et al.*, 2013). Besides direct destruction of the antibiotic molecule, the other mechanism of antibiotic inactivation is through modification of the antibiotic molecule by an enzyme, which prevents the binding of the antibiotic to its target. For example, aminoglycoside modifying enzymes include nucleotidyltransferases, phosphotransferases and acetyltransferases, that catalyse the transfer of chemical moieties to aminoglycoside antibiotics to prevent their binding to the 30S subunit of the bacterial ribosome (Ramirez and Tolmasky, 2010). In *S.* Typhimurium, a type Ib extended-spectrum aminoglycoside acetyltransferase has been reported to confer clinical resistance to gentamicin, amikacin, netilmicin and tobramycin (all MICs ≥16 μg/mL) (Casin *et al.*, 2003).

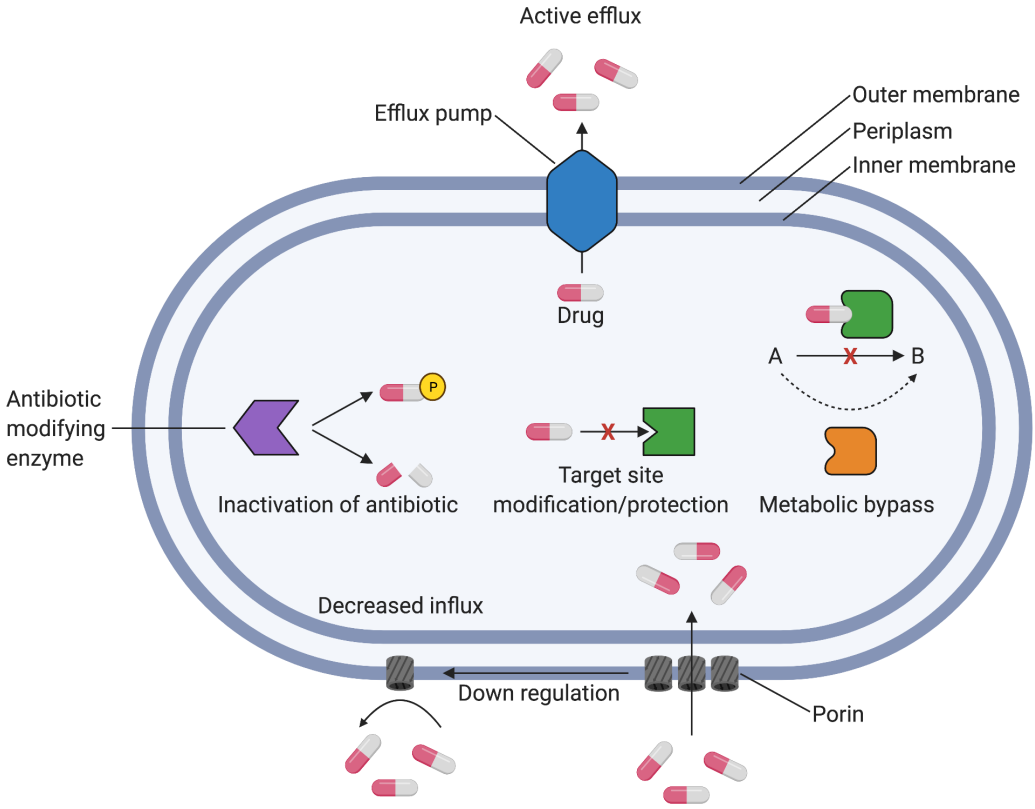


Figure 1.1. Schematic diagram of the main mechanisms of antibiotic resistance in bacteria.

Active efflux is the extrusion of drugs by efflux pumps out of the bacterial cell to the external environment to reduce their intracellular concentration. Drug inactivation is mediated by enzymes that act to destroy or modify the drug. Target site modification involves changes in the 3D structure of the protein target of the drug or modification of the protein target to prevent drug binding. It can also involve target protection proteins that displace or prevent binding of the drug to its target. Metabolic bypass is whereby the function of the drug target is accomplished by a new target that is not inhibited by the drug, hence, the drug becomes redundant. Decreased influx is primarily due to the downregulation of porins that are responsible for drug uptake but can also involve changes in the physiology of the bacterial cell wall. Created with BioRender.com.

Many antibiotics interact with and inhibit bacterial proteins that carry out essential processes, therefore another common mechanism of resistance is target site modification. This largely involves mutations in the gene encoding for the antibiotic target that alters the 3D structure of the protein and prevent binding of the antibiotic molecule (Blair *et al.*, 2015c). For example, fluoroquinolones are a class of clinically important antibiotics that work by inhibiting DNA gyrase to prevent bacterial DNA replication, resulting in cell death. Multiple studies have demonstrated that mutations in the *gyrA* gene, which encodes DNA gyrase subunit A, can prevent binding of fluoroquinolones, hence conferring fluoroquinolone resistance (Redgrave *et al.*, 2014). For instance, *S.* Typhimurium clinical isolates with *gyrA* mutations have been reported to exhibit a high degree of fluoroquinolone resistance, including ciprofloxacin (MIC of 32 μg/mL) (Heisig, 1993). More recently, *S. enterica* isolates from slaughtered pigs in Thailand were found to exhibit fluoroquinolone resistance due to mutations in the topoisomerase genes *parC* or *gyrA* (Poomchuchit *et al.*, 2021). Target site alteration can also involve enzymatic modification of the antibiotic target to prevent the binding of the antibiotic (Blair *et al.*, 2015c). Macrolides are an important class of clinically relevant antibiotics that inhibit protein synthesis by binding to the bacterial ribosome. The erythromycin ribosomal methylase enzyme, encoded by the *erm* class of genes, methylate an adenine residue at the macrolide binding site on the 50S ribosomal subunit, which prevents the binding of macrolides, resulting in resistance (Weisblum, 1995). Besides direct modification of the antibiotic target site, the antibiotic target can also be protected by a resistance protein to rescue it from antibiotic-mediated inhibition. In essence, target protection proteins physically bind to the antibiotic target and sterically remove or prevent binding of the antibiotic to its target (Wilson *et al.*, 2020). For example, TetM is a target protection protein that binds to the ribosome and displaces the tetracycline molecule, thereby relieving the ribosome of tetracycline-inhibition. The TetM

protein then dissociates from the ribosome, allowing protein synthesis to continue unhindered (Dönhöfer *et al.*, 2012).

Metabolic bypass is a strategy used by bacteria to replace or bypass the protein target of the antibiotic. Bacteria can evolve new targets that achieve the same function as the original target but are not inhibited by the antibiotic molecule (Munita and Arias, 2016). Target replacement is a common resistance mechanism to β-lactams in methicillin-resistant *Staphylococcus aureus*. Acquisition of the *mecA* gene, which encodes PBP2a (penicillin-binding protein 2a), allows *S. aureus* to resist the activity of most β-lactams as PBP2a has a low affinity for all β-lactams (Katayama *et al.*, 2000, Wielders *et al.*, 2002).

To exert their antibacterial activity, most antibiotics must penetrate the cell wall to enter bacteria to interact with their intracellular target. Antibiotics can enter bacteria in two main ways; hydrophobic antibiotics enter through a lipid-mediated pathway, and hydrophilic antibiotics enter through general diffusion porins (Prajapati *et al.*, 2021). As such, bacteria can modify these pathways to decrease the influx of antibiotics (Delcour, 2009). For example, in *E. coli*, negative regulation of *lamB*, which encodes a porin involved in antibiotic uptake, has been shown to confer resistance to fluoroquinolones and chlortetracycline (Lin *et al.*, 2014). In *S. enterica* isolates, loss of porins OmpC and OmpF have been reported to confer a high degree of resistance to cephalosporins and chloramphenicol, respectively (Medeiros *et al.*, 1987, Toro *et al.*, 1990). The loss of OmpC and OmpD porins have also been reported in carbapenem resistant *S.* Typhimurium isolates during treatment (Su *et al.*, 2012).

1.5.2 Efflux-mediated antibiotic resistance

Just as antibiotics enter bacterial cells, they can also be extruded by active efflux. Active efflux is driven by efflux pumps, which are membrane-bound transport proteins that export toxic compounds from within cells into the extracellular environment in an energy-dependent manner (Paulsen *et al.*, 1996). In essence, the efflux of an antibiotic molecule reduces its intracellular concentration, thus allowing bacteria to survive a higher concentration of the antibiotic. In terms of specificity, some efflux pumps can transport a particular type of substrate, whilst others can transport a range of structurally distinct compounds, including antibiotics from different classes; such efflux pumps can give rise to MDR (Du *et al.*, 2018). Efflux pumps are ubiquitous amongst bacteria and are thought to have evolved as a detoxification mechanism to cope with environmental stresses (Sun *et al.*, 2014). Genes encoding efflux pumps are mainly found on the bacterial chromosome, however they can also be found on plasmids (Kim *et al.*, 2009, Lv *et al.*, 2020). Under laboratory conditions, efflux pumps are expressed at low levels in bacteria, thereby providing intrinsic levels of resistance to a specific substrate or class of substrates. However, disruption of the regulatory networks that modulate efflux pump expression can result in increased efflux pump expression, leading to high levels of resistance (Piddock, 2006b, Li and Nikaido, 2009, Blair *et al.*, 2015a).

Multiple studies have now established that increased efflux pump expression contributes to the growing problem of antibiotic resistance in many clinical pathogens (Piddock, 2006a). For example, the efflux genes *adeB*, *abeM* and *abeS* were reported to be overexpressed in 21 MDR clinical *Acinetobacter baumannii*; furthermore, a pan drug-resistant isolate had increased expression of five of the eight efflux genes measured (Lin *et al.*, 2017). In another study involving 450 ticarcillin-resistant clinical *P. aeruginosa* isolates, it was found that 46% over-

expressed *mexB* and 58% over-expressed *mexX*, whilst more than a quarter (28%) simultaneously overexpressed both (Hocquet *et al.*, 2007). Efflux pump overexpression has also been reported in clinical *S.* Typhimurium isolates; a study reported increased expression of *acrB* in three clinical isolates, which was associated with reduced susceptibility to several antibiotics, including chloramphenicol, erythromycin, nalidixic acid and tetracycline (Piddock *et al.*, 2000).

Efflux pumps implicated in antibiotic resistance can be classified into six families: ATP-binding cassette (ABC) superfamily, multidrug and toxin extrusion (MATE) family, major facilitator superfamily (MFS), proteobacterial antimicrobial compound efflux (PACE) family, resistance-nodulation-division (RND) superfamily and small multidrug resistance (SMR) family. Apart from the ABC superfamily, which are primary active transporters that utilise energy from ATP hydrolysis, all other efflux pump families are secondary active transporters that drive efflux through energy generated from the proton/sodium motive force (Du *et al.*, 2018). In Gram-negative bacteria, the RND superfamily efflux pumps play a significant role in conferring clinically relevant levels of antibiotic resistance (Colclough *et al.*, 2020, Zwama and Nishino, 2021).

1.6 The RND superfamily of efflux pumps

The RND superfamily are a diverse group of transport proteins found across all major kingdoms of life, including archaea, eukaryotes, and prokaryotes (Nikaido, 2018). Based on phylogenetic analyses, RND transporters can be sub-divided into nine families, of which the heavy metal efflux (HME), hydrophobe/amphiphile efflux-1 (HAE-1), nodulation factor exporter (NFE) and aryl-polyene pigment extrusion (APPE) families are found mainly in Gram-negative bacteria (Nikaido, 2018). HME transporters are involved in extruding heavy metals, such as copper,

cobalt, silver and zinc, out of bacterial cells (Nies, 2003). NFE transporters are involved in transporting signalling molecules that initiate nodule formation on the roots of leguminous plants and are found primarily in nitrogen-fixing bacteria, such as Rhizobia (Saier *et al.*, 1994). The APPE family are a group of small transporters that export pigments; in *Xanthomonas oryzae*, these pumps play a role in exporting aryl polyene pigments, such as xanthomonadin (Goel *et al.*, 2002). The HAE-1 family comprises the largest number of RND transporters in Gram-negative bacteria and includes the most clinically relevant multidrug efflux pumps (Saier *et al.*, 2021).

In Gram-negative bacteria, RND-transporters function with two other proteins: a periplasmic adaptor protein (PAP) and outer membrane factor (OMF), to form a tripartite complex (Fig. 1.2) (Alav *et al.*, 2021). The RND-transporter itself spans the inner membrane and is bound to a PAP, which is also bound to an OMF that spans the outer membrane; the whole complex spans the double membrane of Gram-negative bacteria. This allows Gram-negative bacteria to export substrates directly to the external environment (Neuberger *et al.*, 2018). The *S. enterica* genome contains genes that encode five RND efflux systems: AcrAB, AcrAD, AcrEF, MdtABC and MdsABC (Table 1.1) (Nishino, 2016). All the RND efflux systems rely on TolC as an OMF to drive efflux, except for MdsABC, which can function with either MdsC or TolC (Nishino *et al.*, 2006). The AcrAB and AcrEF efflux systems possess very similar substrate profiles, with the latter postulated to compensate for the loss of function of AcrAB due to mutations (Nishino *et al.*, 2006). AcrD has been reported to exhibit a narrow substrate specificity, consisting of anionic antibiotics (β-lactams, fusidic acid and novobiocin), detergents and possibly metals (copper and zinc) (Yamasaki *et al.*, 2011, Nishino *et al.*, 2007). In *E. coli*, AcrD has also been reported to be involved in aminoglycoside efflux, however, this has not

been confirmed in *S. enterica* (Rosenberg *et al.*, 2000). Much like AcrD, MdtABC also has a narrow substrate profile, comprised of just one antibiotic (novobiocin), a few detergent molecules, and metals (copper and zinc) (Nishino *et al.*, 2006, Nishino *et al.*, 2007). MdsABC is a *Salmonella*-specific RND system, which confers resistance to several antibiotics and dyes, as well as gold (Nishino *et al.*, 2006, Pontel *et al.*, 2007, Conroy *et al.*, 2010). In addition, plasmid encoded RND efflux pumps in *S.* Typhimurium have also been reported. The earliest reported plasmid encoded RND efflux system in *S. enterica* was SilABC, an HME family transporter encoded on the pMG101 silver resistance plasmid. SilABC belongs to Group 4 of the HME family-like CusABC of *E. coli*, and exports monovalent silver ions (Gupta *et al.*, 1999, Nies, 2003). More recently, a plasmid-encoded RND efflux pump OqxAB-TolC, which exports fluoroquinolones, chloramphenicol, and olaquindox, has been identified in *S.* Typhimurium isolates from food producing animals (Li *et al.*, 2013).

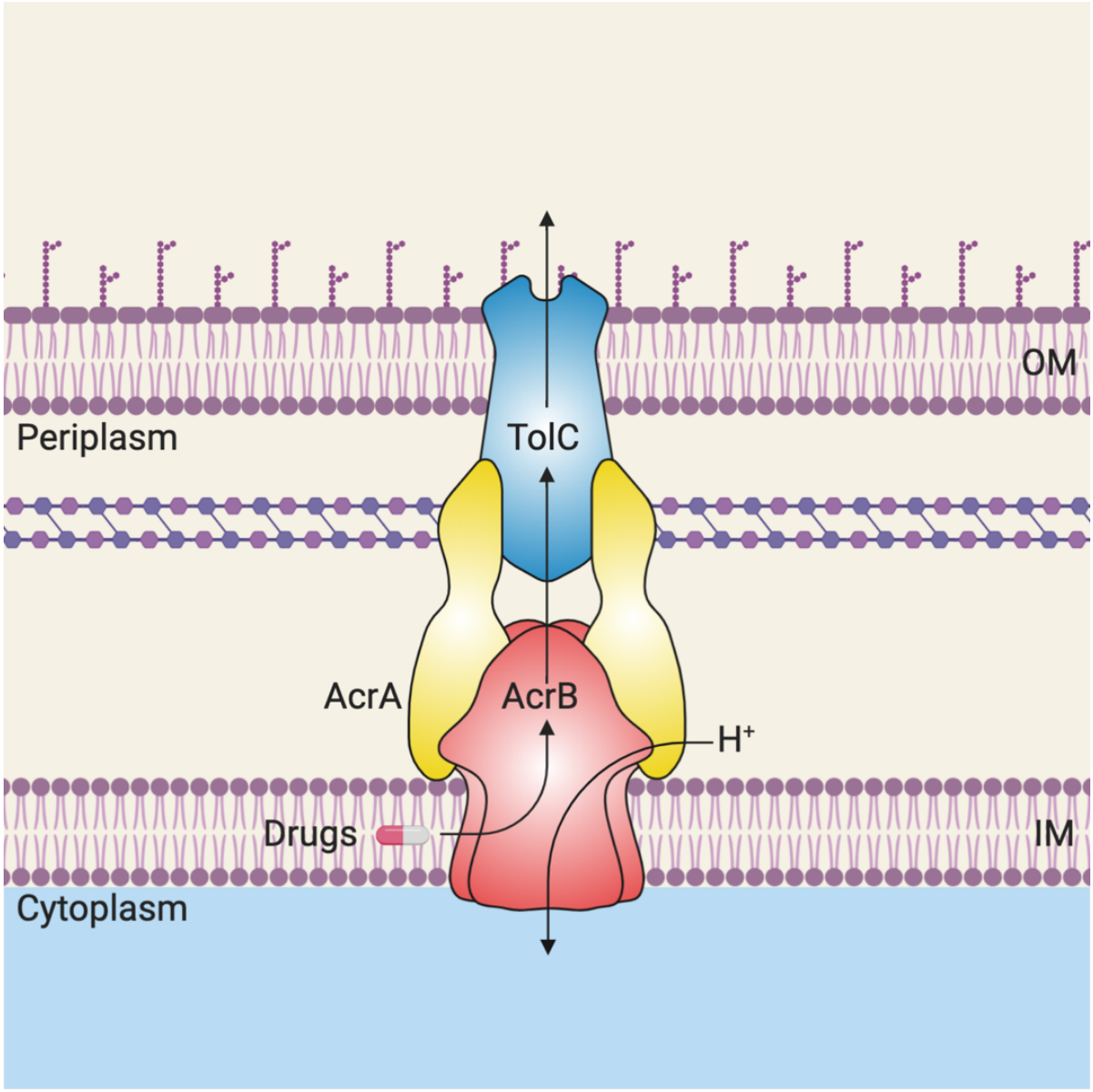


Figure 1.2. A schematic diagram of a tripartite RND efflux pump.

The AcrAB-TolC efflux complex consists of the inner-membrane transporter AcrB (red), the periplasmic adaptor protein AcrA (yellow), and the outer membrane factor TolC (blue). The pump uses the proton motive force to export drugs out of cells. Substrates can enter AcrB through multiple substrate channels. Lipophilic drugs can diffuse through the inner membrane and enter AcrB through one of the entry channels open to the inner membrane. Lipophobic drugs can enter from the substrate entry channel which is open to the periplasm. There are currently no studies to verify that substrates can enter AcrB from the cytoplasm. IM, inner membrane; OM, outer membrane. Created with BioRender.com.

Table 1.1. Substrate profiles of the five characterised RND efflux pumps in *Salmonella enterica.*

Efflux system	Substrates	References
AcrAB-TolC	ACR, BZK, BL, CHL, CHO, CV, DOC, DOX, EtBr, ERY, FQ, FA, LZD, MB, NOV, R6G, RIF, SDS, TET, TPP, TRI, TR	Nishino *et al.* (2003, 2006)
AcrAD-TolC	AZM, CAR, CLX, DOC, FA, NAF, NOV, OXA, SDS, SUL	Nishino *et al*. (2003, 2006, 2007) Yamasaki *et al.* (2011)
AcrEF-TolC	ACR, BL, CHL, CHO, CV, DOX, EtBr, ERY, FA, FQ, LZD, MB, NOV, R6G, SDS, TET, TPP, TRI, TRX	Nishino *et al.* (2003, 2006)
MdsABC/TolC	ACR, Au^{3+}, BAC, BL, CHL, CV, EtBr, MB, NOV, R6G, TPP	Nishino *et al.* (2003, 2006), Pontel *et al.* (2007), Conroy *et al.* (2010)
MdtABC-TolC	CHO, Cu^{+}, NOV, SDS, Zn^{+}	Nishino *et al.* (2006, 2007)

Drug abbreviations: ACR, acriflavine; Au, gold; AZM, aztreonam; BZK, benzalkonium chloride; BL, β-lactams; CAR, carbenicillin; CHL, chloramphenicol; CHO, cholate; CLX, cloxacillin; Cu, copper; CV, crystal violet; DOC, deoxycholate; DOX, doxorubicin; EtBr, ethidium bromide; ERY, erythromycin; FQ, fluoroquinolones; FA, fusidic acid; LZD, linezolid; MB, methylene blue; NAF, nafcillin; NOV, novobiocin; OXA, oxacillin; R6G, rhodamine 6G; RIF, rifampicin; SDS, sodium dodecyl sulphate; SUL, sulbenicillin; TET, tetracycline; TPP, tetraphenylphosphonium; TRI, triclosan; TRX, Triton X-100; Zn, zinc.

1.7 Physiological roles of RND efflux pumps

Genes encoding for RND pumps are evolutionarily ancient and ubiquitous throughout Gram-negative bacteria, indicating that RND pumps evolved before the advent of antibiotics to treat human infections (Brooks *et al.*, 2018). Therefore, the high level of evolutionary conservation of RND pumps supports a wider physiological role (Teelucksingh *et al.*, 2020). Although the role of RND pumps in efflux-mediated resistance has been extensively studied, their physiological role in bacteria remains poorly understood in comparison. However, there is now increasing evidence to suggest a role for RND pumps in several bacterial behaviours and processes, including biofilm formation, detoxification, quorum sensing and virulence (Piddock, 2006b, Alav *et al.*, 2018, Teelucksingh *et al.*, 2020).

1.7.1 Biofilm formation

Biofilms are aggregates of microbial cells that are irreversibly attached to a surface and encapsulated in a self-produced matrix of extracellular polymeric substances (EPS). Cells within a biofilm exhibit altered phenotype with respect to growth rate and gene transcription compared to planktonic cells, reflective of the biofilm lifestyle (Flemming *et al.*, 2016). The EPS comprises amino acids, lipids, nucleic acids, polysaccharides, and abiotic materials, such as clay, mineral crystals, and silt. Together, the EPS components maintain the structural integrity of biofilms and facilitate attachment to surfaces (Flemming and Wingender, 2010). Biofilm formation is regulated by QS in response to several different factors, including subinhibitory antibiotic exposure, nutritional and metabolic cues, and host-derived signals (Karatan and Watnick, 2009). Notably, biofilms afford bacteria greater protection against external insults, such as antimicrobials, biocides, and host immune responses. This is especially problematic in clinical settings, where pathogenic bacteria colonise and form biofilms on

indwelling medical devices and living tissue. Biofilms on medical devices can promote the dissemination of infection to other sites within the body and lead to chronic infections. Furthermore, biofilms on living tissue can trigger prolonged host inflammatory responses, impair wound healing and contribute to the pathogenesis of chronic wounds (Bjarnsholt, 2013). RND pumps have been reported in several studies to play a role in the biofilm formation of important pathogenic species, including *E. coli* and *S. enterica* (Alav *et al.*, 2018).

One of the earliest studies to identify a link between efflux pumps and biofilm formation was by Kvist *et al.* (2008) who reported significant overexpression of efflux pump genes during biofilm growth of several different *E. coli* strains. They also showed that mutant strains lacking either one of the two most highly upregulated efflux genes, *aaeX* and *yqgA*, exhibited significantly impaired biofilm formation. Importantly, the addition of efflux inhibitors thioridazine or phenylalanine-arginine β-naphthylamide (PAβN) was shown to reduce biofilm formation in *E. coli* and *K. pneumoniae* up to 80% compared to controls without EI (Kvist *et al.*, 2008). Shortly after, it was shown that the proton motive force inhibitor carbonyl cyanide-*m*-chlorophenylhydrazone (CCCP) significantly impaired *P. aeruginosa* biofilm development in several unrelated epidemiological isolates (Ikonomidis *et al.*, 2008). The role of RND efflux pumps in biofilm formation was demonstrated later by Matsumura *et al*. (2011), who investigated the effects of deleting various multidrug efflux pump genes on *E. coli* biofilm formation. They reported that *acrD*, *acrE*, *acrF*, *mdtE*-deleted mutant strains displayed extremely reduced biofilm formation. To a lesser extent, *acrA*, *acrB*, *mdtA*, *mdtB*, *mdtC* and *mdtF*-deleted strains also displayed impaired biofilm formation (Matsumura *et al.*, 2011). Baugh *et al.* (2012) observed that in *S.* Typhimurium 14028S, mutant strains lacking *tolC, acrB*, *acrD*, *acrEF*, *mdtABC* or *mdsABC* were significantly compromised in their ability to form

biofilms, which was linked to reduced curli gene (*csgB* and *csgD*) transcription (Baugh *et al.*, 2012). Curli are extracellular proteinaceous structures that are involved in cell adhesion to surfaces, cell aggregation and biofilm formation. In *E. coli*, curli-deficient mutant strains have been shown to display compromised biofilm architecture lacking structural integrity and distinct water channels (Kikuchi *et al.*, 2005). Therefore, reduced curli gene expression in *S.* Typhimurium efflux mutant strains is likely to result in impaired biofilm formation. In agreement with Kvist *et al.* (2008), the addition of efflux inhibitors, including chlorpromazine, CCCP and PAβN, at concentrations lower than the MIC of each efflux inhibitor impeded biofilm formation by *S.* Typhimurium cells (Baugh *et al.*, 2012). Despite the reported importance of RND efflux pumps in biofilm formation, their exact role remains to be elucidated.

1.7.2 Virulence

To infect and invade host cells, pathogenic bacteria, including *S. enterica*, must possess the ability to subvert the various host defence mechanisms (Anderson and Kendall, 2017). The host environment, which can be challenging for the survival of invading pathogens, comprises various antimicrobial compounds, such as bile salts, fatty acids, and peptides, which act to kill or inhibit the growth of invading bacteria (Gasteiger *et al.*, 2017). Therefore, to survive within their host, pathogenic bacteria employ various mechanisms to avoid killing by host cells, including efflux-mediated resistance to host produced antimicrobial compounds (Joo *et al.*, 2016). In the same way that RND efflux pumps expel antibiotics out of bacterial cells, they have also been reported in several studies to confer protection against bile salts, and antimicrobial fatty acids and peptides. Additionally, RND efflux pumps contribute to the infection process by exporting toxins and virulence factors to damage the host tissue (Bina *et al.*, 2008, Horiyama and Nishino, 2014). Importantly, the inactivation of RND efflux genes has

been shown to attenuate the virulence of several different Gram-negative bacteria in different host infection models (Alav *et al.*, 2021).

As the archetypal RND efflux pump across members of the Enterobacteriaceae, AcrAB-TolC has been shown to be involved in the efflux of bile salts and fatty acids (Thanassi *et al.*, 1997, Warner and Levy, 2010, Lennen *et al.*, 2013), and in *K. pneumoniae*, antimicrobial peptides, such as polymyxin B and defensin HBD-1 (Padilla *et al.*, 2010). In *S. enterica*, inactivation or deletion of genes coding for the AcrAB-TolC pump results in significantly reduced virulence in human epithelial cells, murine macrophages, *Galleria mellonella,* mice and chicken infection models (Lacroix *et al.*, 1996, Nishino *et al.*, 2006, Buckley *et al.*, 2006, Wang-Kan *et al.*, 2017, McNeil *et al.*, 2019). Other RND efflux pumps required for the virulence of *S. enterica* in mice include AcrEF-TolC, MdtABC and MdsABC. Deletion of the *acrD* gene had no significant effect on the virulence of *S. enterica* in mice (Nishino *et al.*, 2006). However, Buckner *et al.* (2016) reported that inactivation of *acrD* in *S. enterica* resulted in the reduced expression of 13 genes involved in virulence, mostly found on the *Salmonella* pathogenicity island 1 (SPI-1). The deletion of *acrAB* or *tolC* in *S. enterica* also leads to reduced SPI-1 expression (Webber *et al.*, 2009). Interestingly, in the *acrD*-inactivated mutant strain, reduced expression of virulence genes was not found to correlate with reduced virulence in Caco-2 polarised epithelial cells (Buckner *et al.*, 2016). A recent study also reported that the deletion of *acrD* in *S.* Enteriditis did not impact virulence in Caco-2 cells. However, it was found that the *acrD*-deleted mutant strain was unable to adhere to and invade Caco-2 cells in egg white filtrate, suggesting an important role for the AcrD-transporter in the survival of *S.* Enteriditis in eggs (Qin *et al.*, 2021).

1.7.3 Quorum sensing

Quorum sensing (QS) is a process of bacterial communication that allows bacteria to regulate gene expression according to their local cell population density. QS is driven by small signalling molecules called autoinducers (AI) that are used by bacteria to monitor changes in the cell population density. QS is involved in regulating several different bacterial behaviours, including biofilm formation, sporulation, motility, swarming and virulence (Bassler and Losick, 2006). RND efflux pumps have been suggested in several studies to be involved in the export of AI molecules in some species and in regulating QS by modulating the concentration of AI precursor molecules within the cells (Alav *et al.*, 2018).

Gram-negative bacteria mainly synthesise and utilise *N*-acyl homoserine lactones (AHLs) as their AI molecule. Both *E. coli* and *Salmonella* can detect QS molecules, such as AHLs produced by other species, but cannot synthesise their own AHLs (Michael *et al.*, 2001). Therefore, owing to its extensive QS network, much of the work on the relationship between efflux pumps and QS has been carried out in *P. aeruginosa.* One of the earliest studies reported that treatment of *P. aeruginosa* cells with azide, a proton gradient inhibitor, led to a strong intracellular accumulation of AHLs. Furthermore, a mutant strain lacking the *mexAB-oprM*-encoded RND efflux pump was found to accumulate AHLs similar to those of azide-treated wild type cells, suggesting a role for the MexAB-OprM efflux pump in AI transport (Pearson *et al.*, 1999). In *Burkholderia pseudomallei*, the export of AHLs has been suggested to be dependent on the activity of the RND efflux pump BpeAB-OprB (Chan *et al.*, 2007b). Other studies have suggested that RND efflux activity can influence QS by modulating levels of AHL precursor molecules. For instance, MexAB-OprM overexpressing *P. aeruginosa* strains exhibit

impaired AHL production and QS response due to the limited availability of octanoate, an AHL precursor molecule (Alcalde-Rico *et al.*, 2020).

1.8 Regulation of RND efflux pumps

Expression of RND efflux pumps is tightly regulated through complex and interconnected regulatory systems, consisting of local and global transcriptional regulators, that function to maintain baseline expression and inducible expression of RND efflux pumps (Colclough *et al.*, 2020). These regulators respond to various environmental signals, such as antibiotic exposure and iron limitation, to upregulate RND efflux pump expression. However, perturbations in regulatory networks, such as mutations in transcriptional regulators, can also result in the overexpression of efflux pumps giving rise to multidrug resistance (Blair *et al.*, 2015c).

AcrAB are both are encoded in the *acrRAB* operon, and are regulated at multiple levels by local and global regulators (Fig. 1.3) (Du *et al.*, 2018). The divergently oriented *acrR* gene encodes a local TetR-family transcriptional regulator (TFTR). Structurally, the TFTRs consist of an N-terminal DNA binding domain, which recognises and binds to a palindromic DNA sequence located in the intergenic region between the regulator and the regulated gene, and a larger C-terminal domain, which is responsible for the ligand-binding (Colclough *et al.*, 2019). Functioning as a dimer, TFTRs act to locally repress the expression of the efflux genes (Cuthbertson and Nodwell, 2013). AcrR directly represses the expression of *acrAB*, as well as its own expression (Olliver *et al.*, 2004). The binding of AcrB ligands, such as rhodamine 6G, to AcrR can cause conformation changes, inhibiting AcrR from being able to bind and repress the *acrAB* promoter (Su *et al.*, 2007). There have been several reports of clinical and veterinary isolates of *S.* Typhimurium with mutations in *acrR* that result in the derepression of *acrAB*,

leading to the overexpression of AcrAB-TolC and decreased antibiotic susceptibility (Olliver *et al.*, 2004, Shen *et al.*, 2017, Elnekave *et al.*, 2018). The expression of *acrEF*, which encodes the AcrEF pump, is repressed by its local repressor AcrS (EnvR) and the histone-like nucleoid structuring (H-NS) protein; however, AcrS can also repress *acrAB* expression (Hirakawa *et al.*, 2008, Nishino *et al.*, 2009). Unlike *acrAB*, which is expressed constitutively at basal levels, *acrEF* expression is silenced under laboratory conditions due to global repression by the H-NS protein (Nishino and Yamaguchi, 2004). However, deletion or loss of *acrA* has been shown to select for resistance through *acrE* overexpression to compensate for the loss of *acrA* (McNeil *et al.*, 2019). This was shown to be due to a 36-base pair (bp) duplication within the *ramR* gene, thereby inactivating it. RamR is a transcription factor that negatively regulates expression of the global regulator RamA (Fig. 1.3). The inactivation of *ramR* was found to result in *ramA* overexpression, which triggered the overexpression of the *acrEF* operon (McNeil *et al.*, 2019). Another study found that fluoroquinolone selected *acrB*-deleted *S.* Typhimurium mutants can trigger *acrEF* overexpression through insertion of IS1 and IS10 promoter sequences upstream of the *acrEF* operon (Olliver *et al.*, 2005). Hence, expression of *acrEF* or possibly other efflux pumps may be induced by the overexpression of global regulators or through changes in the promoter site.

Activators of *acrAB* expression in *Salmonella* include the global regulators MarA, RamA, Rob and SoxS, and the QS regulator SdiA (Fig. 1.3) (Rahmati *et al.*, 2002, Nikaido *et al.*, 2008, Eaves *et al.*, 2004, Bailey *et al.*, 2008). Although *tolC* is not clustered with the RND efflux pump genes, its expression is also regulated by global regulators MarA, Rob and SoxS (Du *et al.*, 2018). The expression of the global regulators MarA, RamA and SoxS are regulated by their own local repressors MarR, RamR and SoxR, respectively (Fig. 1.3). Therefore, the global

regulators are expressed when there is derepression. Mutations in the local repressors of global regulators can lead to efflux pump overexpression. For example, in *S.* Typhimurium, mutations in *ramR* lead to increased *ramA* and *acrAB* expression, which results in AcrAB-TolC overexpression and decreased antibiotic susceptibility (Abouzeed *et al.*, 2008). The global regulators MarA, RamA and SoxS also regulate genes relevant to biofilm formation and virulence, hence, efflux activity is linked to other phenotypes (Holden and Webber, 2020). The expression of the global regulators is further modulated by the selective ATP-dependent Lon protease. Lon protease is expressed in response to stress, such as heat shock, and is involved in the regulation of the SOS response in *E. coli* (Takaya *et al.*, 2003, Nicoloff and Andersson, 2013). In *S.* Typhimurium, Lon protease has been reported to recognise the N-terminus of RamA and target it for degradation (Ricci *et al.*, 2014).

In addition to the canonical transcriptional regulation, *acrAB* expression is also regulated by post-transcriptional regulation and two-component systems (TCS). One mechanism of post-transcriptional regulation is through the action of RNA-binding proteins, which are seen as increasingly important modulators of protein function (Holmqvist and Vogel, 2018). The RNA-binding protein CsrA (Carbon Storage Regulator A) acts as a global regulator of a wide range of genes. Ricci *et al.* reported that CsrA binds to and stabilizes *acrAB* mRNA, presumably by preventing the formation of repressive RNA structures that hinder ribosome binding. Furthermore, deletion or mutagenesis of *crsA* was shown to decrease the production of AcrAB. Therefore, CsrA may be involved in facilitating the efficient translation of AcrAB (Ricci *et al.*, 2017). The TCS EvgAS in *E. coli* has been demonstrated to regulate the expression of *acrAB*, *emrKY*, *mdtEF* and *tolC,* which encode AcrAB-TolC, EmrKY-TolC and MdtEF-TolC pumps, respectively (Eguchi *et al.*, 2003).

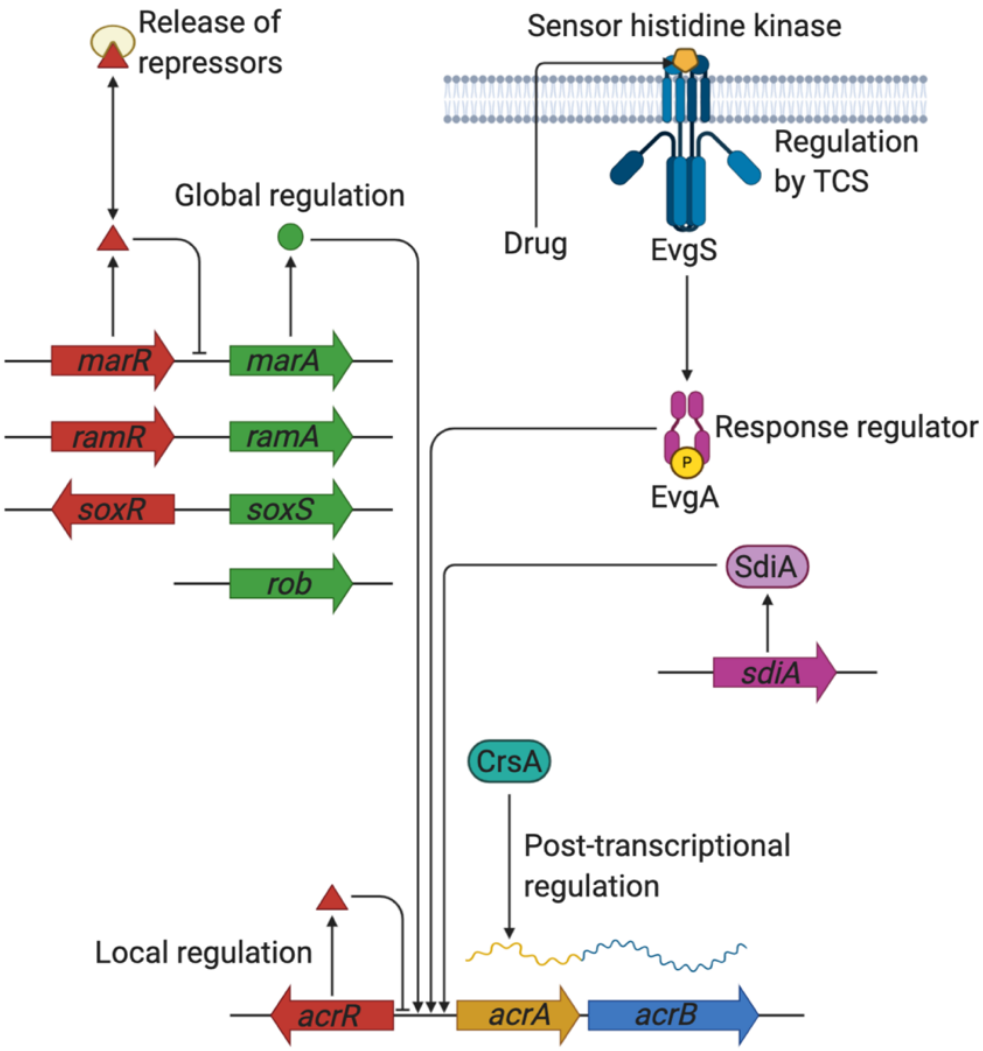


Figure 1.3. Schematic diagram of the different mechanisms of RND efflux pump expression.

Local regulation usually involves a TetR family transcriptional regulator, such as AcrR, that act to locally repress efflux gene expression and maintain basal levels of expression. Global regulation generally involves AraC/XylS family transcriptional regulators, like MarA, RamA and SoxS, that activate efflux pump gene expression. These global regulators themselves are locally regulated by their own TetR family transcriptional regulators, such as MarR, RamR and SoxR. The presence of antibiotics or other external stressors can release these repressors to allow activation of efflux gene expression. Other types of regulators, such as the quorum-sensing regulator SdiA, can also activate efflux gene expression. Two-component systems (TCS) consist of a sensor histidine kinase (EvgS) that detects external stimuli, such as drugs and phosphorylate a response regulator (EvgA), which becomes activated to trigger efflux pump gene expression. Post-transcriptional regulation includes RNA-binding proteins, like CrsA, that stabilize efflux gene mRNA to promote efficient efflux protein translation. Figure created with Biorender.com.

The role of efflux pumps in antibiotic resistance has been widely studied, however, their importance and expression in different environments and conditions remain poorly understood. RNA-seq and transcriptomic studies has provided some insight into the expression of efflux pumps in different hosts and niches. To cause infection, *Salmonella* must be able to invade and colonise the epithelial cells of the small intestine in many different hosts. However, host-derived antimicrobial compounds, such as bile, in the gut function to inhibit and kill invading pathogens (Hofmann and Eckmann, 2006). It has been shown that the expression of *acrAB* and *tolC* are significantly upregulated in the presence of bile (Nikaido *et al.*, 2008, Nikaido *et al.*, 2011), suggesting that AcrAB-TolC provides protection against bile. As an intracellular pathogen, *S.* Typhimurium is adapted to surviving within host macrophages. RNA-seq of the intra-macrophage *S.* Typhimurium 4/74 transcriptome in murine macrophage-like cells found that expression of *acrA*, *acrB* and *tolC* were significantly upregulated compared to early stationary phase (Srikumar *et al.*, 2015). Another study reported that *S.* Typhimurium 14028s infection of murine macrophages resulted in the upregulation of the *mdsABC* efflux genes (Song *et al.*, 2015). RNA-seq analysis of *S.* Typhimurium 4/74 grown in 22 different conditions found that of the RND efflux pumps, only *acrAB* and *tolC* were consistently expressed across all conditions. Interestingly, *acrD* was found to be expressed in low iron shock but the significance of this has not been investigated (Kroger *et al.*, 2013). Chaudhuri *et al.* (2013) screened pools of random insertion mutants of *S.* Typhimurium SL1344 in chickens, pigs, and cattle by transposon-directed insertion-site sequencing. It was found that importance of efflux pumps varied between hosts. For example, disruption of *acrE* attenuated fitness in cattle, whereas *acrF* disruption attenuated fitness in pig. Disruption of *tolC* was found to attenuate fitness in cattle and mouse (Chaudhuri *et al.*, 2013). NTS serovars also frequently contaminate food products. RNA-seq analysis of *S.* Typhimurium SL1344 inoculated into black pepper, chocolate, and

powdered milk found that the expression of *acrA* was significantly downregulated after 24 and 72 hours compared to control. Interestingly, the expression of *mdsABC* was upregulated after 24 and 72 hours for all three food products compared to control (Crucello *et al.*, 2019). These studies suggest that efflux pump expression can vary depending on the strain and environment of *Salmonella*.

1.9 The AcrAB-TolC multidrug efflux pump

AcrAB-TolC is the primary efflux system in some members of the Enterobacteriaceae, which includes *S. enterica*. Structurally, it comprises three components: the PAP AcrA, the RND transporter AcrB and the OMF TolC (Tikhonova and Zgurskaya, 2004) (Fig. 1.4). The structural stoichiometry of the AcrB-AcrA-TolC complex has been of great debate, with studies positing both 3:3:3 and 3:6:3 models. *In vivo* cross-linking experiments to investigate the interactions between AcrA and AcrB have reported a 1:1 stoichiometry for AcrA-AcrB (Symmons *et al.*, 2009). Furthermore, *in vivo* cross-linking experiments between AcrA and TolC have also suggested a 1:1 stoichiometry (Lobedanz *et al.*, 2007). AcrA-AcrB fusion proteins with 1:1 stoichiometries have been reported to display functional efflux activity through ethidium bromide efflux assays and antibiotic susceptibility testing. Furthermore, in *acrAB*-deficient and *acrAB acrEF* double-deficient strains, the AcrA-AcrB fusion proteins displayed efflux activity without the help of free AcrA or AcrE (Hayashi *et al.*, 2016). Therefore, a 3:3:3 stoichiometry of AcrA:AcrB:TolC seems to be functional. Contrastingly, surface plasmon resonance studies have provided evidence for the existence of AcrA as a dimer (Ge *et al.*, 2009). For example, the soluble AcrA variant, which lacks the N-terminal lipid modification required for dimerisation, was shown to bind to AcrB with a significantly lower affinity than a native lipid-modified AcrA protein. Additionally, it was found that the higher

affinity of the native AcrA protein to AcrB was due to the stabilisation of the membrane-proximal domain and oligomerisation of AcrA (Tikhonova *et al.*, 2011). In agreement, the cryo-electron microscopy structure of the whole AcrAB-TolC complex has revealed a 3:6:3 stoichiometry of AcrB:AcrA:TolC (Du *et al.*, 2014). Electron microscopy images of AcrAB-TolC using an AcrB-AcrA-AcrA link protein with TolC have also offered support for a 3:6:3 stoichiometric model (Kim *et al.*, 2015). The 3:6:3 model has also been reported in other homologous tripartite RND efflux systems. For example, the crystal structure of the CusA-CusB heavy metal efflux system of *E. coli* has a 3:6 stoichiometry (Su *et al.*, 2011). The recent structure of the tripartite MexAB-OprM efflux pump of *P. aeruginosa* has also been reported to have a 3:6:3 stoichiometry (Tsutsumi *et al.*, 2019). Earlier models postulated that AcrB and TolC may directly interact with each other, hence the upper part of AcrB had been tentatively named the TolC docking domain (Murakami *et al.*, 2002, Symmons *et al.*, 2009). However, in the 3:6:3 model, there is no direct contact between AcrB and TolC, instead, the two components are bridged across the periplasm by AcrA. Experimental *in vivo* cross-linking experiments and isothermal titration calorimetric assays have shown that AcrA interacts with AcrB and TolC independently, with no direct interaction between AcrB and TolC (Touze *et al.*, 2004). Accordingly, the crystal structure of the MexAB-OprM pump has also revealed that there is no interaction between the OMF OprM and the RND transporter MexB (Tsutsumi *et al.*, 2019). The prevailing model of AcrAB-TolC assembly in the literature seems to be the 3:6:3 stoichiometric model (Fig. 1.4), as demonstrated by more recent high-resolution cryo-electron microscopy and *in situ* electron cryo-tomography structures of AcrAB-TolC (Wang *et al.*, 2017, Shi *et al.*, 2019, Chen *et al.*, 2021). Hence, the 3:6:3 stoichiometric model of the AcrAB-TolC pump will be used as the basis for the work conducted in this study.

The AcrAB-TolC pump exhibits a remarkably broad substrate profile and can export structurally diverse substrates (Table 1.1). Importantly, it can export multiple classes of clinically relevant antibiotics, including β-lactams (e.g., carbenicillin, cefotaxime and oxacillin etc.), fluoroquinolones (e.g., ciprofloxacin and norfloxacin etc.), macrolides (e.g., erythromycin) and tetracyclines (e.g., doxycycline and tetracycline etc.). It can also export several other types of unrelated substrates, including detergents (e.g., sodium dodecyl sulphate), disinfectants (e.g., benzalkonium chloride and triclosan) and dyes (e.g., crystal violet and ethidium bromide) (Nishino, 2016, Li *et al.*, 2015). Owing to its broad substrate profile, the AcrAB-TolC pump confers intrinsic resistance to clinically relevant antibiotics in Gram-negative bacteria (Poole, 2005). In addition, overexpression of the AcrAB-TolC pump has been demonstrated in multiple studies to drive clinically relevant levels of resistance to antibiotics, such as fluoroquinolones and tetracycline (Piddock *et al.*, 2000, Oethinger *et al.*, 2000, Baucheron *et al.*, 2004). Multiple studies have also demonstrated that *S. enterica* mutant strains lacking one or more components of the AcrAB-TolC pump display increased susceptibility to antibiotics. Mutant strains lacking *acrB* have been reported to be more susceptible to a range of antibiotics, including chloramphenicol, erythromycin, novobiocin, norfloxacin and tetracycline (Nishino *et al.*, 2006). In another study, mutant strains lacking a functional TolC were hyper-susceptible to a range of antibiotics, as well as several detergents and dyes (Buckley *et al.*, 2006).

In addition to its role in efflux-mediated resistance, the AcrAB-TolC pump is also linked to other antibiotic resistance determinants. In *E. coli*, higher *acrAB* expression has been shown to result in lower expression of the DNA mismatch repair gene *mutS*, reduced growth rates, and higher mutation frequencies (El Meouche and Dunlop, 2018). Similarly, in *S.* Typhimurium

cells, overexpression of *ramA*, and consequently *acrB*, has been shown to result in significantly higher mutation frequency and rate compared to wild type (Grimsey *et al.*, 2020b). In a different study, inactivation, or inhibition of AcrAB-TolC was shown to increase the resistance of carbapenemase-producing Enterobacteriaceae, including *S.* Typhimurium, to carbapenems (Saw *et al.*, 2016). Nolivos *et al.* (2019) found that the AcrAB-TolC pump is critical for the acquisition of resistance by horizontal gene transfer in the presence of translation-inhibiting antibiotics. The authors suggested that by reducing the intracellular levels of tetracycline, the AcrAB-TolC pump allows cells to synthesise plasmid-encoded resistance determinants, such as TetA, chloramphenicol acetyltransferase or aminoglycoside phosphotransferase. Cells lacking *acrA*, *acrB* or *tolC* failed to acquire resistance in the presence of tetracycline, demonstrating the role of AcrAB-TolC in protecting protein synthesis (Nolivos *et al.*, 2019). Therefore, it is evident that the AcrAB-TolC pump plays a wider role in antibiotic resistance than just active efflux.

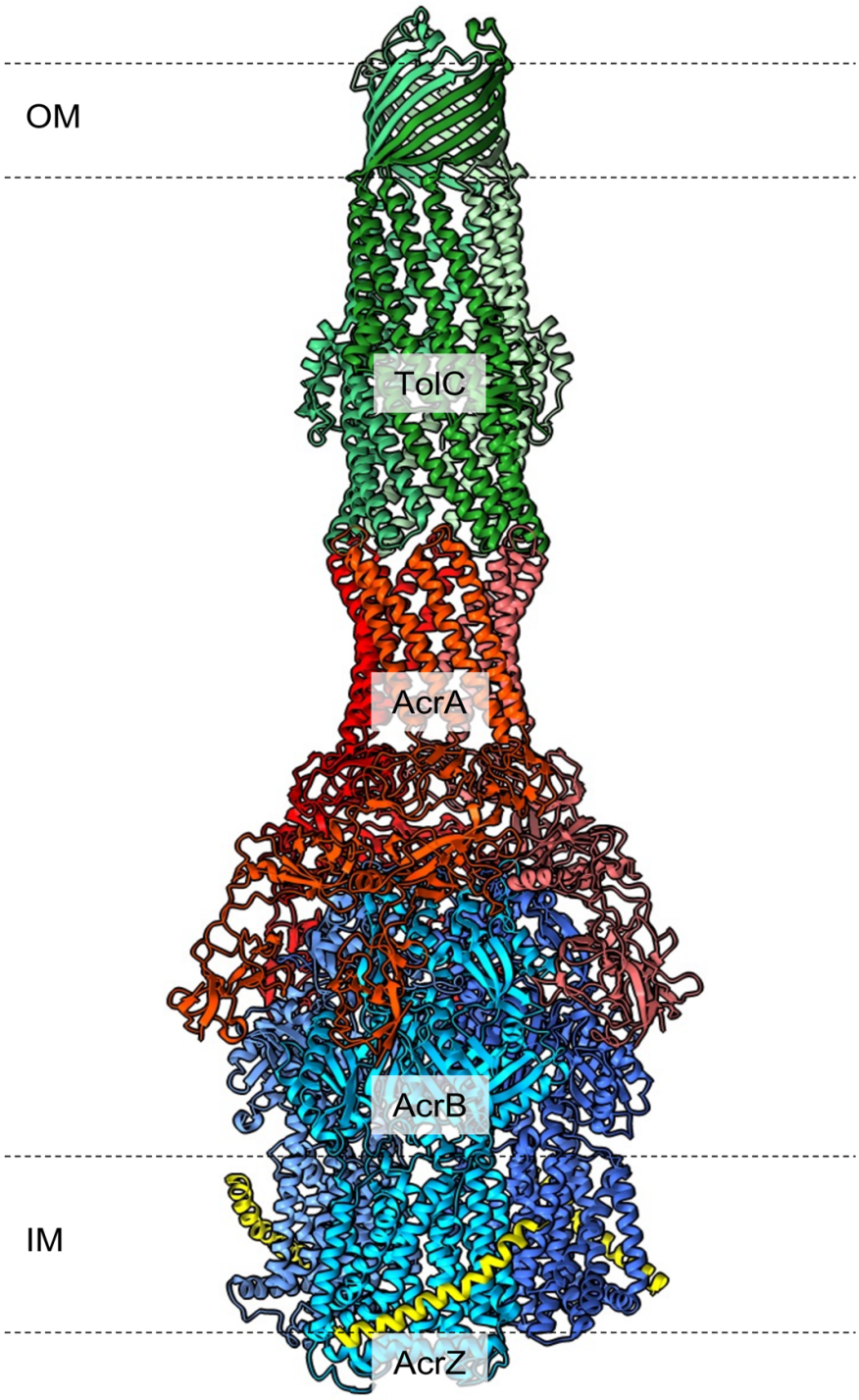


Figure 1.4. The structure of the AcrAB(Z)-TolC complex.

The 3:6:3 stoichiometric model is shown by the differently coloured protomers of each component. In this model, AcrB and TolC do not directly interact and are linked together by AcrA. The small protein AcrZ interacts with AcrB and is proposed to play a role in allosterically modulating the activity of AcrB. Structure of AcrAB(Z)-TolC from Wang *et al.* (2017). IM, inner membrane; OM, outer membrane. Figure created with UCSF ChimeraX (Pettersen *et al.*, 2021).

1.9.1 AcrB

1.9.1.1 Structure of AcrB

AcrB is the RND-transporter of the AcrAB-TolC efflux system, where it plays a crucial role in substrate recognition and energy transduction. Structurally, it is organised as a homotrimer, with each protomer comprising of a transmembrane domain (TMD), a pore domain and a so-called TolC docking domain (Fig. 1.5). The TMD consists of twelve transmembrane α-helices (TM1-12) organised into two pseudo-symmetric bundles consisting of TM1-6 and TM7-12, which are separated by an extra-membrane α-helix situated between TM6 and TM7 on the cytoplasmic side of the inner-membrane (Murakami *et al.*, 2002). Within each protomer, TM4 and TM10 are encircled by the other TM helices and possess key residues involved in proton translocation (Fig. 1.5). Residues D407 and D408 on TM4, K940 on TM10, and R971 and T978 on TM11 comprise the functionally critical protonation sites within AcrB. Studies have shown that substituting any of these residues with an alanine residue results in an inactive AcrB pump (Su *et al.*, 2006, Takatsuka and Nikaido, 2006). Together, these residues make up the putative proton relay network. The three TMDs of the protomers assume a ring-shaped structure with a central hole, which spans the inner membrane. The TMD is linked to the pore domain, which is in the periplasm and is divided into four subdomains: PN1, PN2, PC1 and PC2. The central pore is formed from the second helix of the PN1 subdomain of each protomer (Fig. 1.5). Linked to the pore domain is the TolC docking domain, which consists of two subdomains, DN and DC. The three TolC docking domains form a funnel-like structure, which narrows down to a central pore in the pore domain and the central cavity of the TMD. Additionally, there is a prominent opening, referred to as the vestibule, between the three protomers in proximity to the external surface of the outer leaflet of the inner membrane (Fig. 1.5) (Murakami *et al.*, 2002, Pos, 2009).

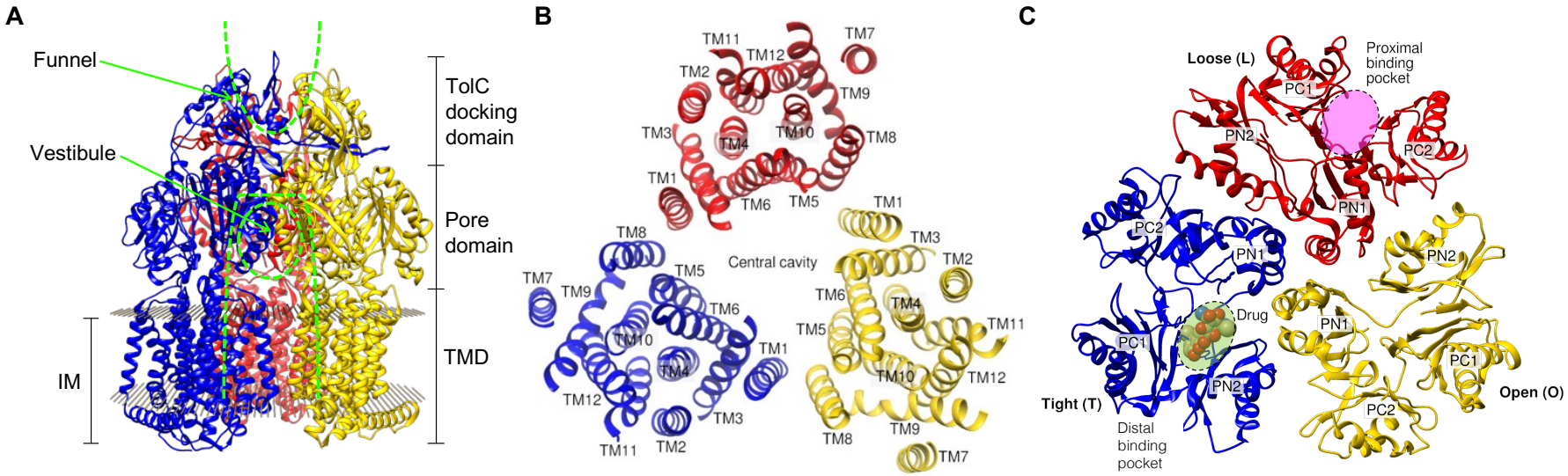


Figure 1.5. Structure of AcrB and top view of its transmembrane and pore domains.

A) Crystal structure of the asymmetric organisation of the AcrB trimer (PDB 5ENT). The three protomers are coloured individually (blue, red, and yellow). Each AcrB protomer consists of the TolC docking domain and the pore domain situated in the periplasm, and the transmembrane domain embedded within the inner membrane. **B)** Top view of AcrB onto the transmembrane domain. TM4 and TM10 are encircled by the other transmembrane helices. The central cavity is confined by the transmembrane helices of each AcrB protomer. **C)** Top view onto the pore domain, which consists of the PN1, PN2, PC1 and PC2 subdomains. The PN1 and PN2 subdomains originate from the N-terminal periplasmic loop between TM1 and TM2, and the PC1 and PC2 subdomains originate from the C-terminal periplasmic loop between TM7 and TM8. The distal binding pocket is located between the PC1 and PN2 subdomains of the tight conformer (green shading), illustrated here with the binding of minocycline (labelled 'Drug'). The proximal binding pocket (purple shading) is situated between the PC1 and PC2 subdomains of the loose conformer. High-molecular-mass drugs first bind to the proximal binding pocket and are then translocated to the distal binding pocket upon the functional rotation of the AcrB trimer. IM, inner membrane; TMD, transmembrane domain. Figures created with UCSF ChimeraX (Pettersen *et al.*, 2021).

1.9.1.2 Substrate recognition by AcrB

AcrB possesses two principal substrate binding sites located in its pore domain, the proximal binding pocket (PBP) located between the PC1 and PC2 subdomains of the loose (L) conformer, and the distal binding pocket (DBP) located between the PC1 and PN2 subdomains of the tight (T) conformer (Fig. 1.5). High-molecular-mass substrates, such as rifampicin and erythromycin, first bind to the PBP and are then translocated to the DBP by the peristaltic movement of the switch loop, a stretch of 11 residues situated between the PBP and the DBP (Eicher *et al.*, 2012). The flexibility of the switch loop is crucial for the ability of AcrB to transport large substrates. This was previously demonstrated by a G616N point mutation in the switch loop, which significantly reduced conferred resistance to high molecular mass substrates, such as erythromycin, rifampicin, and azithromycin (Wehmeier *et al.*, 2009, Cha *et al.*, 2014). In G614P-G621P and G616P-G619P point mutations, the movement of the F617 loop has been shown to be inhibited by the introduction of rigid proline residues, resulting in impaired growth under subinhibitory concentrations of erythromycin and doxorubicin (Nakashima *et al.*, 2011). Substitution of bulky residues of the switch loop, such as in F615A-F617A-R620A, has also been shown to dramatically impair tolerance to erythromycin (Ababou and Koronakis, 2016). Mutations in the PBP have also been reported in clinical *Salmonella* isolates. For instance, R717Q/L point mutations in AcrB have been documented in clinical azithromycin resistant *S.* Typhi isolates (MIC >32 μg/mL) (Hooda *et al.*, 2019). Low-molecular-mass substrates, such as chloramphenicol, linezolid and minocycline, bypass the PBP and the switch loop to directly bind to the DBP (Nakashima et al., 2011). The DBP largely consists of phenylalanine residues, as well as nonpolar residues such as glycine, alanine, isoleucine, and valine. Previous studies have highlighted the importance of the residues in the DBP on substrate susceptibility through site-directed mutagenesis. For example, F610A point

mutation in AcrB has been reported to significantly affect susceptibility to a broad range of substrates, underlining the important role of F610 in the transport of substrates (Bohnert *et al.*, 2008). A G288D substitution in the DBP of a clinical *S.* Typhimurium isolate has been shown to confer decreased fluoroquinolone sensitivity but increased doxorubicin and minocycline susceptibility (Blair *et al.*, 2015a). The hydrophobic nature of the DBP allows binding of all known AcrB substrates, however, changes in the residues of the DBP can alter substrate specificity. In addition to the PBP and DBP, an additional binding site located in a groove formed by the interface between TM1 and TM2 of the TMD has also been proposed. This binding site seems to be favoured by lipophilic carboxylated substrates, such as fusidic acid and carboxylated β-lactams (Oswald *et al.*, 2016).

Substrates can access AcrB through four different proposed channels, referred to as channels 1–4 (Fig. 1.6). The entrance of channel 1 and channel 2 is open to the periplasm and the outer leaflet of the inner membrane, respectively. Both channels converge at the PBP which leads to the DBP (Nakashima *et al.*, 2011). Therefore, high-molecular-mass substrates that enter AcrB through channel 1 or channel 2 first bind to the PBP to be translocated to the DBP by the action of the switch loop. Channel 3 has been shown to originate from the central cavity and is directly linked to the DBP, with substrate specificity favouring cationic, low molecular mass and planar compounds, such as acriflavine, ethidium bromide and rhodamine 6G (Zwama et al., 2018). The entrance of the recently proposed channel 4 is located between the groove formed by TM1 and TM2 of the TMD and leads to the DBP. This channel seems to be employed by AcrB for the transport of carboxylated low-molecular-mass substrates, such as fusidic acid, oxacillin, and piperacillin (Tam *et al.*, 2020).

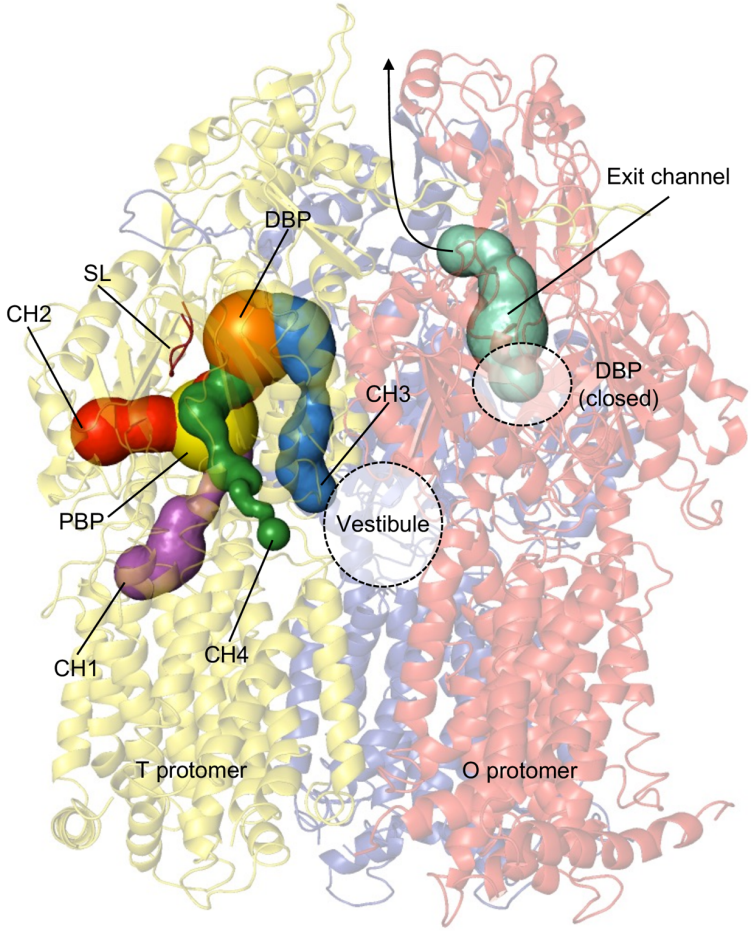


Figure 1.6. The asymmetric structure of AcrB showing its substrate entry channels and binding sites.

The entrance of channel 1 (CH1, purple) is located at the groove formed by TM7 and TM8 and is open to the outer leaflet of the inner membrane. Substrates entering CH1 are guided to the proximal binding pocket (PBP, yellow). The entrance of channel 2 (CH2, red) is situated at the cleft formed by the PC1/PC2 subdomains of AcrB and is open to the periplasmic space. High-molecular-mass drugs (HMMDs), such as erythromycin, preferentially enter through CH2 and bind to the PBP. The switch loop (SL, red) separates the PBP and the distal binding pocket (DBP, orange) and is important for the translocation of HMMDs from the PBP to the DBP. Low-molecular-mass drugs, such as chloramphenicol and linezolid, preferentially enter through CH1 and bypass the PBP and the SL and bind directly to the DBP. Channel 3 (CH3, blue) is open to the central cavity formed by the vestibules between the protomer interfaces. CH3 is preferentially used by planar aromatic cations, such as berberine, ethidium bromide and rhodamine 6G, for transport directly to the DBP. The entrance of channel 4 (CH4, green) is situated at the groove formed by TM1 and TM2 and leads directly to the DBP. CH4 is preferentially accessed by carboxylated drugs, such as β-lactams and fusidic acid. During the T to O transition, all substrate channels are closed, and an exit channel (teal) is created in the O protomer. The exit channel is connected to the closed DBP, allowing substrates to be exported. Figure created with PyMOL Version 2.5.2 (Schrödinger, 2022).

1.9.1.3 Transport mechanism of AcrB

Structural data from crystallographic studies have shown that AcrB exists in three different conformational states (Seeger *et al.*, 2006, Sennhauser *et al.*, 2007). Based on this observation, Murakami *et al.* (2006) proposed a functionally rotating transport mechanism, whereby AcrB transitions through three distinct conformational states, denoted as 'loose' (L), 'tight' (T) and 'open' (O), like the rotatory mechanism of the $(\alpha\beta)_3$-F_1-ATPase (Fig. 1.7). In the L (also called Access) state, the vestibule is open to the periplasm and the surface of the inner membrane, allowing potential substrates to access the vestibule, however, the binding pocket is contracted. In the T (also called Binding) state, the vestibule remains open, and the binding pocket is expanded to enable the binding of substrates. Hence, substrates enter the vestibule from the outer surface of the inner membrane, translocate through one of the uptake channels, and bind to the different sites within the voluminous substrate-binding pocket. In this state, the bound substrate is prevented from leaving the binding pocket as the exit is blocked by the central helix inclined from the O monomer. In the O (also called Extrusion) state, the vestibule is closed, and the central helix shifts away to unblock the exit. Next, the contraction of the binding pocket from the closing of PN1 and PC2 subdomains pushes the bound substrate out into the top funnel towards TolC (Fig. 1.7). Lastly, the O monomer switches back to the L conformation restarting the cycle of the functional rotation (Murakami *et al.*, 2006).

The functional rotation transport mechanism of AcrB is driven by the proton motive force, which is generated by proton translocation from the periplasm to the cytoplasm (Murakami *et al.*, 2002). The binding and release of protons occur in the TMD, specifically TM4, TM10 and TM11 (Fig. 1.5B), which contain critical residues involved in proton transport (D407, D408, K940, R971 and T978) (Guan and Nakae, 2001, Takatsuka and Nikaido, 2006). These charged

residues form and break salt bridges in the different conformational states of AcrB. Based on the binding change mechanism of ATP synthase, the conversion of the T monomer to the O monomer in AcrB is hypothesised to be the energy-dependent step of the rotating transport mechanism. Thus, it is likely that proton uptake from the periplasm occurs in the O monomer (Pos, 2009). The subsequent release of protons to the cytoplasm is expected in any of the three monomers, however, this has yet to be experimentally observed.

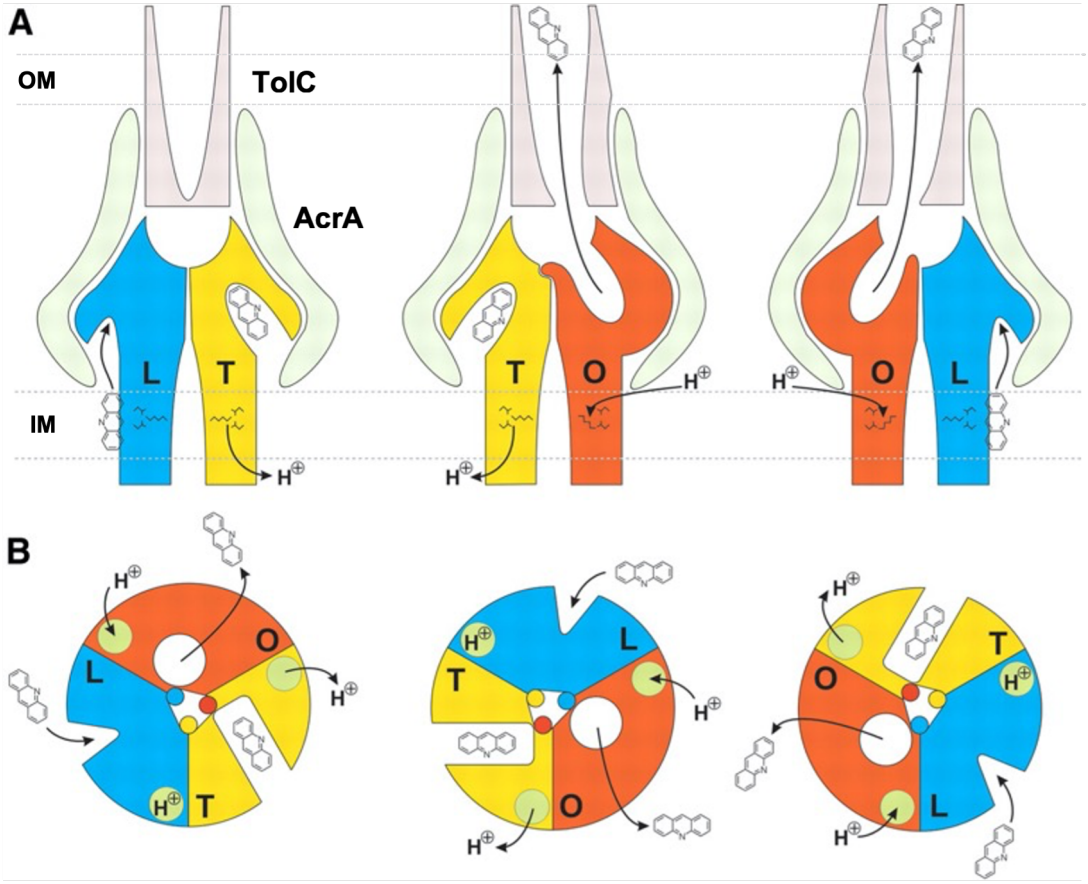


Figure 1.7. Schematic representation of the functional rotation mechanism of AcrB.

A) Side-view of the AcrAB-TolC complex during drug transport. The substrate depicted here is acridine. The proton translocation site is represented in the membrane section of each protomer. **B)** The substrate enters AcrB in its Loose (shown in blue and labelled as 'L') conformer and binds to the substrate-binding pocket in the Tight (shown in yellow and labelled as 'T') conformer and lastly exits AcrB in its Open (shown in orange and labelled as 'O') conformer to be thrust towards TolC. From Seeger et al. (2006). Reproduced and adapted with permission from AAAS (Order number: 4907701186519). IM, inner membrane; OM, outer membrane.

1.9.2 AcrA

1.9.2.1 Structure of AcrA

AcrA is the periplasmic adaptor protein (PAP) of the AcrAB-TolC efflux system (Zgurskaya and Nikaido, 1999), where it physically bridges the RND-transporter AcrB with the outer membrane factor (OMF) TolC to form a closed tunnel, thereby allowing substrates to be exported across the outer membrane (Xu *et al.*, 2011a). It also functions as a PAP for the RND-transporter AcrD, which is not encoded alongside its own PAP, to form a functional efflux system (Yamasaki *et al.*, 2011). AcrA is produced as a precursor protein with an N-terminal signal helix spanning residues 1-24, which is responsible for its localisation to the periplasm. Previously, C25A AcrA mutants have been shown to retain the N-terminal signal sequence on the cytoplasmic side of the inner membrane (Kawabe *et al.*, 2000). Structurally, AcrA is a lipoprotein that spans the periplasm and consists of four main domains: β-barrel domain, lipoyl domain and α-helical hairpin domain, and membrane-proximal domain (MPD) (Fig. 1.8). The β-barrel domain consists of six anti-parallel β-strands and a short α-helix. It is situated close to the inner membrane and is involved in the attachment of AcrA to the inner membrane through a lipid acylated cysteine (C25) residue. However, membrane attachment does not seem to be necessary for the functionality of AcrA; for example, in *E. coli*, soluble AcrA mutants have been demonstrated to display functional efflux activity (Zgurskaya and Nikaido, 1999, Mikolosko *et al.*, 2006). The β-barrel domain is linked to the coiled-coil α-helical domain by the central lipoyl domain (Mikolosko *et al.*, 2006). The α-helical hairpin domain interacts with the OMF TolC and plays a crucial role in maintaining the stability of the AcrAB-TolC pump; it has been shown that deleting all 74 residues of the α-helical domain results in a non-functional AcrAB-TolC pump (Stegmeier *et al.*, 2006). In addition to the three main domains, AcrA also has a proteolytically sensitive MPD that contains highly conserved residues. Previously, site-

directed mutagenesis was performed on 12 highly conserved residues in the MPD, of which a single G363C mutation was reported to significantly impair the efflux activity of AcrAB-TolC. Hence, the MPD also seems to play an essential role in the assembly and function of the AcrAB-TolC pump (Ge *et al.*, 2009). Each domain is linked to each other through flexible linkers made up of two anti-parallel sheets or turns. These flexible linkers are thought to be important for allowing optimal interactions with one another and with AcrB and TolC (Symmons *et al.*, 2015).

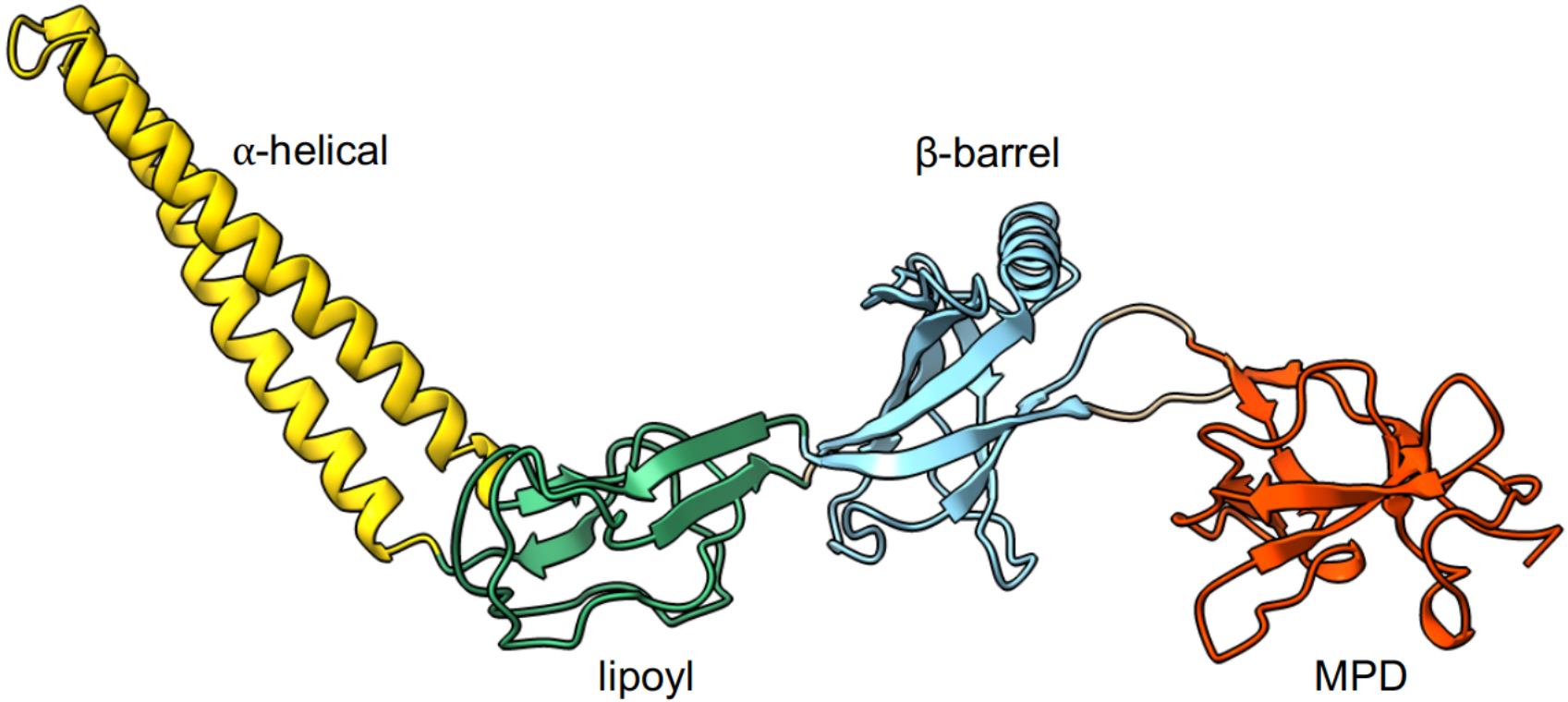


Figure 1.8. The structure of a single AcrA protomer labelled with its main domains.

Structure of AcrA (PDB ID 5O66) obtained from Wang *et al.* (2017). The α-helical domain is responsible for mediating interactions with the outer membrane factor TolC. The lipoyl domain is involved in the self-assembly of the AcrA protomers. The β-barrel domain and the membrane-proximal domain (MPD) are involved in interactions with the RND-transporter AcrB and will be the focus of this study. Figure created with UCSF ChimeraX (Pettersen *et al.*, 2021).

1.9.2.2 Function of AcrA

As an adaptor protein, AcrA interacts with AcrB and TolC to form a conduit for the transport of substrates across the outer membrane to the extracellular environment. Initial chemical cross-linking studies demonstrated that AcrA interacts with AcrB *in vivo* independently of efflux substrates and TolC (Zgurskaya and Nikaido, 2000, Kawabe *et al.*, 2000). Later, it was shown that AcrA interacts with TolC independently of efflux substrates and AcrB (Husain *et al.*, 2004). Touzé *et al*. (2004) demonstrated that AcrA cross-linked independently to AcrB and TolC *in vivo*, verifying the findings from the previous studies. Furthermore, they established that AcrA forms energetically favourable interactions with both AcrB and TolC, highlighting the important role of AcrA in the assembly of the AcrAB-TolC pump (Touze *et al.*, 2004).

Although it is known that AcrA interacts with AcrB and TolC to form a tripartite complex, the exact role of AcrA in the assembly of the AcrAB-TolC pump remains unclear. Several models have been posited to explain the role of AcrA. The first model postulated that AcrA interacts and forms bipartite complexes with AcrB and TolC. The AcrA-AcrB and AcrA-TolC complexes are then thought to assemble into a tripartite AcrAB-TolC complex. Evidence for this model stems from the tryptic profiles of AcrA. It was found that AcrA and bipartite complexes possessed unstructured membrane-proximal domains, which were readily cleaved by trypsin. Whereas, upon assembly of the tripartite AcrAB-TolC complex, the membrane-proximal domain was protected from trypsin cleavage (Ge *et al.*, 2009). Later, a different model was proposed, wherein AcrA-TolC, AcrA-AcrB and TolC-AcrB bipartite complexes assembled into a tripartite complex upon conformational changes in the membrane-proximal domain of AcrA. This was supported by surface plasmon resonance experiments that indicated that AcrA-TolC, AcrA-AcrB and TolC-AcrB were assembled with the same degree of high affinity.

Importantly, the opening of TolC is thought to reduce affinity to both AcrA and AcrB, thereby resulting in the disassembly of the complex and closing of TolC (Tikhonova *et al.*, 2011). In a more recent study, Shi *et al*. (2019) reported the first *in situ* structure of the AcrAB-TolC efflux pump and proposed a novel mechanism for the assembly of the complex. During *in vivo* assembly of AcrAB-TolC, AcrB is posited to associate with AcrA to form a bipartite complex AcrAB. This is hypothesised to be followed by conformational changes in AcrA to recruit TolC. The binding of TolC to the AcrAB complex is predicted to result in the complete assembly of the AcrAB-TolC efflux system (Shi *et al.*, 2019). Based on the postulated models, it is evident that AcrA plays a key role in the assembly of the AcrAB-TolC complex and could be considered the rate-limiting step of AcrAB-TolC complex formation.

1.9.2.3 Diverse roles of AcrA

In addition to its structural importance, there is growing evidence that AcrA also plays an active role in the efflux pump activity of AcrAB-TolC. Inactivation of *acrA* in *S.* Typhimurium has been reported to result in a distinct antibiotic susceptibility profile that differed from mutant strains lacking functional *acrB* or *tolC*. For instance, a mutant strain lacking *acrA* was found to be more susceptible to ciprofloxacin and triclosan than the *tolC* mutant strain (Blair *et al.*, 2009). Another study showed that out of the four identified PAPs in *S.* Typhimurium, only inactivation of *acrA* was shown to significantly increase susceptibility to substrates including acriflavine, chloramphenicol, ciprofloxacin, crystal violet, ethidium bromide, erythromycin, fusidic acid, methylene blue, novobiocin, oxacillin, tetracycline and rhodamine 6G (McNeil *et al.*, 2019). AcrA has also been shown to play a role in the virulence of *S.* Typhimurium. Inactivation of *acrA* alone has been shown to reduce the ability of *S.* Typhimurium cells to invade human intestinal cells and increase the survival of *Galleria* wax moth larvae in an

infection model (Blair *et al.*, 2009, McNeil *et al.*, 2019). A recent study reported that AcrA may also play a role in adaptive resistance, a phenomenon characterised by a rapid emergence of resistance and fast reversibility to a non-resistant phenotype when the antibiotic is removed (Motta *et al.*, 2015). Bhattacharyya *et al*. (2020) found that antibiotic-induced death of a sub-population of cells confers an advantage to the surviving cells by releasing AcrA. Reportedly, released AcrA from the dead cells interacts with the OMF protein TolC on the surface of surviving cells to facilitate drug efflux and induce efflux pump expression. This phenomenon has been termed 'necrosignalling', therefore, AcrA may also function as a necrosignalling protein in bacteria (Bhattacharyya *et al.*, 2020).

1.9.3 TolC

1.9.3.1 Structure of TolC

TolC spans almost 140 Å across the periplasm and outer membrane. Other species of Gram-negative bacteria also possess homologous OMF proteins, such as CmeC from *Campylobacter jejuni*, OprM from *P. aeruginosa* and MtrE from *N. gonorrhoeae*. Despite having very low sequence similarity, these OMF proteins share a high degree of structural similarity (Zgurskaya *et al.*, 2011). These homotrimeric OMF proteins, including TolC, consist of three domains: a transmembrane β-barrel domain, a periplasmic α-barrel domain and a mixed α/β equatorial domain (Fig. 1.9). The β-barrel domain is embedded in the outer membrane and consists of 12 β-strands formed by the three monomers. The α-barrel domain of each monomer extends 100 Å into the periplasm and comprises two long helices that span the entire length of the domain, and four shorter helices that are arranged into two long, pseudo-continuous helices, that also traverse the entire length of the α-helical domain. The mixed α/β equatorial domain is linked to

the α-barrel domain at the junction of the shorter helices (Fig. 1.9). The cavity of TolC is very large, capable of mediating the export of substrates up to 160 kDa in size.

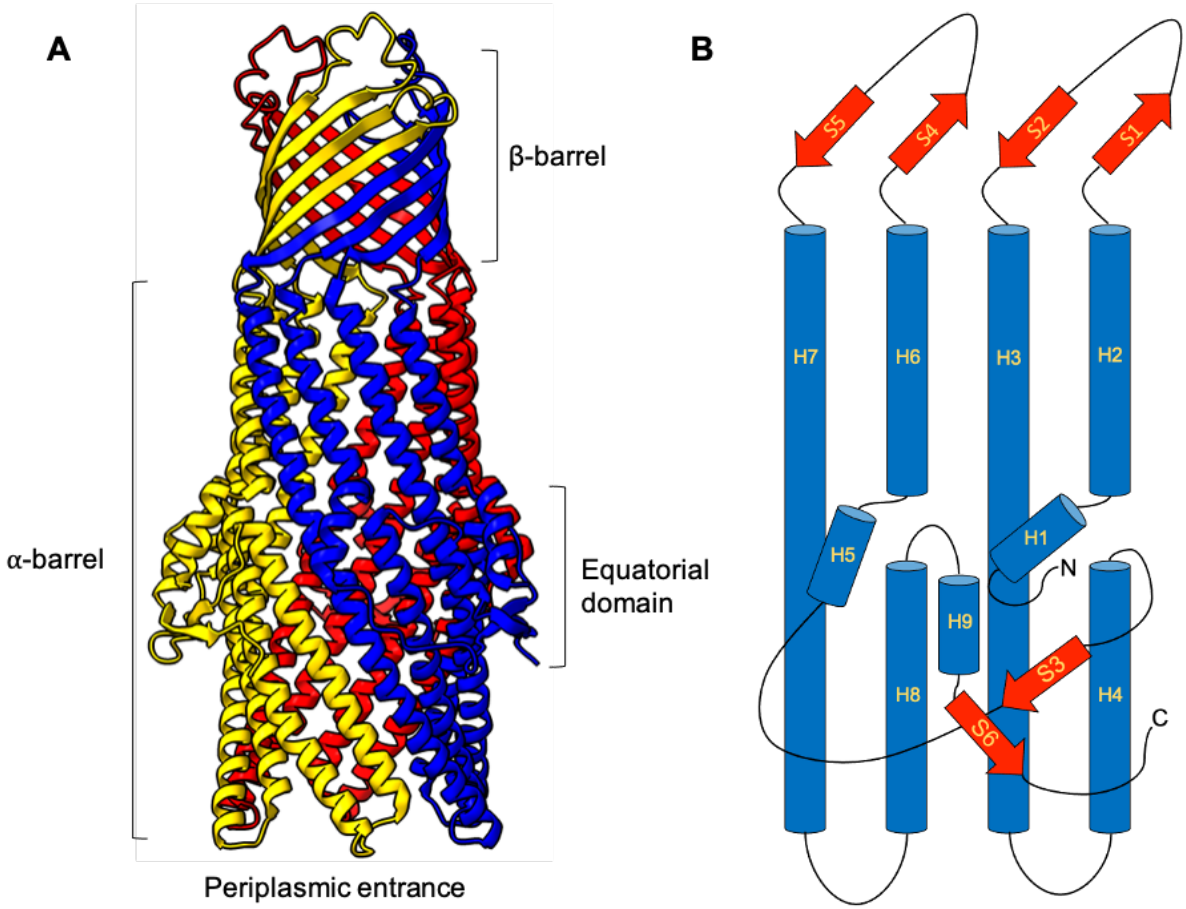


Figure 1.9. The structure of TolC labelled with its main domains.

A) The structure of the homotrimeric assembly of TolC (PDB 5O66, chains A, B and C) with each monomer coloured individually. The β-barrel domain is at the distal end and the α-barrel end is at the proximal end, where the periplasmic entrance is situated. Figure created with UCSF ChimeraX (Pettersen *et al.*, 2021). **B)** A schematic topology diagram of a single TolC monomer. The helices (H) are coloured in blue, and the β strands (S) are coloured in red. The β-barrel domain consists of S1, S2, S4 and S5. The α-helical domain consists of H2, H3, H4, H6, H7 and H8. The mixed α/β equatorial domain is made up of H1, H5, S3 and S6.

The apostate of TolC exists in a closed conformational state, wherein the periplasmic entrance is tightly closed. This closed conformation of the periplasmic entrance is maintained by a network of interprotomer hydrogen bonding between R367 in one protomer and T152, D153 and Y362 in the adjacent protomer (Andersen *et al.*, 2002, Augustus *et al.*, 2004, Bavro *et al.*, 2008). The inhibitor-bound structure of the AcrAB-TolC efflux pump has previously revealed that in the open state, the network of interprotomeric hydrogen bonds is broken and the periplasmic entrance fully opens through an 'iris-like' dilation (Wang *et al.*, 2017). The equatorial domain is necessary for TolC functionality; however, its exact function remains to be elucidated. Previously, Yamanaka *et al*. (2002) demonstrated that residues 50-60 of the C-terminal part of TolC, corresponding to the equatorial domain, is essential for the activity of TolC (Yamanaka *et al.*, 2001). In a follow-up study, it was shown that of these residues, L412 is specifically critical for the activity of TolC (Yamanaka *et al.*, 2002). Later, residues 198-214 within the equatorial domain were found to be involved in the pairing of the transporter-PAP with the OMF (Yamanaka *et al.*, 2007).

1.9.3.2 Function of TolC

TolC is an OMF protein that functions as the outer membrane channel of the AcrAB efflux system to enable the transport of substrates across the outer membrane. In addition to AcrAB, TolC functions as an outer membrane channel for all the other *S. enterica* RND pumps (AcrEF, AcrAD, MdtABC and MdsABC) and pumps from other families, such as MacAB and EmrAB of the ABC superfamily and the MFS, respectively (Horiyama *et al.*, 2010). In *E. coli*, TolC partners with additional efflux systems, such as EmrKY and MdtEF, which belong to the MFS and RND superfamilies, respectively (Nishino and Yamaguchi, 2002). TolC also functions as an outer membrane channel for the type 1 secretion system (T1SS) HlyBD, which is involved

in the secretion of the α-haemolysin toxin (Kim *et al.*, 2016). The tripartite ABC pump MacAB-TolC is also involved in the secretion of heat-stable enterotoxin II (Yamanaka *et al.*, 2008). Therefore, inactivation or deletion of *tolC* results in hyper susceptibility to a broad range of substrates, including antibiotics, biocides, dyes, and detergents, since most multidrug efflux systems rely on functional TolC to extrude substrates (Sulavik *et al.*, 2001). Additionally, TolC has been reported to be involved in the expulsion of excess metabolites, such as cysteine, glutathione, and porphyrins (Tatsumi and Wachi, 2008, Wiriyathanawudhiwong *et al.*, 2009, Dhamdhere *et al.*, 2010). Lastly, TolC not only functions as an export channel but can also be involved in the import of toxins. A recent study found that the bacteriocin klebicin C, a toxin produced by *K. pneumoniae*, binds TolC of a related species *Klebsiella quasipneumoniae* to transport itself across the outer membrane of target cells and block the efflux of drugs (Housden *et al.*, 2021).

1.9.4 AcrZ

AcrZ is a small membrane protein that is associated with the AcrAB-TolC pump in an AcrB-dependent manner. It affects the substrate specificity of the AcrAB-TolC pump. AcrZ is required for the efflux of some AcrB-substrates, such as chloramphenicol, puromycin, and tetracycline but not others, such as erythromycin and fusidic acid (Hobbs *et al.*, 2012). More recently, the cryo-EM structures of AcrB and the AcrBZ complex in lipid environments have been reported. The comparison of the two structures suggests that upon AcrZ binding, conformational confirmation changes occur in the substrate-binding pocket of AcrB. Hence, AcrZ and lipid have been suggested to allosterically modulate the activity of the AcrB-transporter (Du *et al.*, 2020).

1.9.5 Interactions between components of the AcrAB-TolC pump

1.9.5.1 AcrA and TolC interactions

The interaction between AcrA and TolC has been verified by both genetic and biophysical studies (Husain *et al.*, 2004, Gerken and Misra, 2004). The α-helical hairpin domain of AcrA and other PAPs play a key role in OMF recognition. This has been shown in RND efflux systems MexAB-OprM and MexEF-OprN of *P. aeruginosa*, wherein swapping of the α-helical hairpin domain of MexA for that of MexE enables the MexA-MexE hybrid to function with the OprM-MexF pump. Equally, the MexA-MexE hybrid construct is unable to function with OprN-MexF, and MexA proteins that possess the α-helical hairpin domain of MexE cannot form a functional complex with its cognate components OprM-MexB (Eda *et al.*, 2006). Likewise, swapping of the AcrA α-helical hairpin domain for that of MexA enables functional assembly of the chimeric AcrAB-OprM system (Stegmeier *et al.*, 2006).

There are two competing models to explain the nature of the AcrA-TolC interactions. The first model is known as the adaptor wrapping or the deep-interpenetration model, which posits a large binding interface between the PAP α-helical hairpin domain with the OMF helical-hairpin repeats of the α-barrel domain. This model stems from the 3:3:3 model of AcrAB-TolC assembly, which suggests a direct interaction between AcrB and TolC. In this model, AcrB and TolC interact tip-to-tip and AcrA 'wraps' around the outside of the AcrB-TolC complex. The α-helical hairpin domain of AcrA penetrates deep into the grooves formed by the α-barrel domain of TolC. Evidence for this model came from *in vivo* functional cross-linking and docking studies (Fernandez-Recio *et al.*, 2004, Tamura *et al.*, 2005, Stegmeier *et al.*, 2006, Lobedanz *et al.*, 2007, Symmons *et al.*, 2009, Janganan *et al.*, 2011).

The second model is referred to as the tip-to-tip or the cogwheel model. The tip-to-tip model was first conceived from a study that reported the crystal structure of the PAP MacA of the tripartite ABC efflux pump MacAB-TolC. In this study, it was found that MacA exhibits a tight hexameric assembly, in which the α-helical hairpin domains of MacA are organised into a funnel-like tubular structure that is very similar to the diameter of a fully dilated TolC channel (Yum *et al.*, 2009). In this arrangement, there are a limited number of contacts between the PAP and the OMF, mediated by the tip of the α-helical hairpin domain of the PAP and the tip of the α-barrel domain of the OMF (Fig. 1.10) (Xu *et al.*, 2010). Further evidence for the tip-to-tip model came from multiple crystallographic, cryo-EM and *in situ* cryo-ET studies of tripartite efflux assemblies (Yum *et al.*, 2009, Du *et al.*, 2014, Jeong *et al.*, 2016, Wang *et al.*, 2017, Tsutsumi *et al.*, 2019, Shi *et al.*, 2019, Glavier *et al.*, 2020). As a result of direct structural data, the tip-to-tip model has become the paradigm model of AcrAB-TolC assembly. In this model, H3, H4, H7 and H8 of the α-barrel domain of TolC interacts with the α-helical hairpins of AcrA (Fig. 1.10). Specifically, residue G365 in the conserved VGL/T motif of TolC interacts with K140 and S139 of AcrA. Residues N145 and T366 of TolC make direct contact with L132 of the conserved RLS motif of AcrA, as reported by *in vivo* cross-linking experiments and structural data (Fig. 1.10) (Xu *et al.*, 2011a, Wang *et al.*, 2017). The interaction between AcrA and TolC has also been shown to be highly dynamic, with a lifetime of seconds to minutes. However, the transient AcrA-TolC complex is formed with a high affinity, with a dissociation constant in the range of low nanomolar and micromolar (Tikhonova *et al.*, 2009).

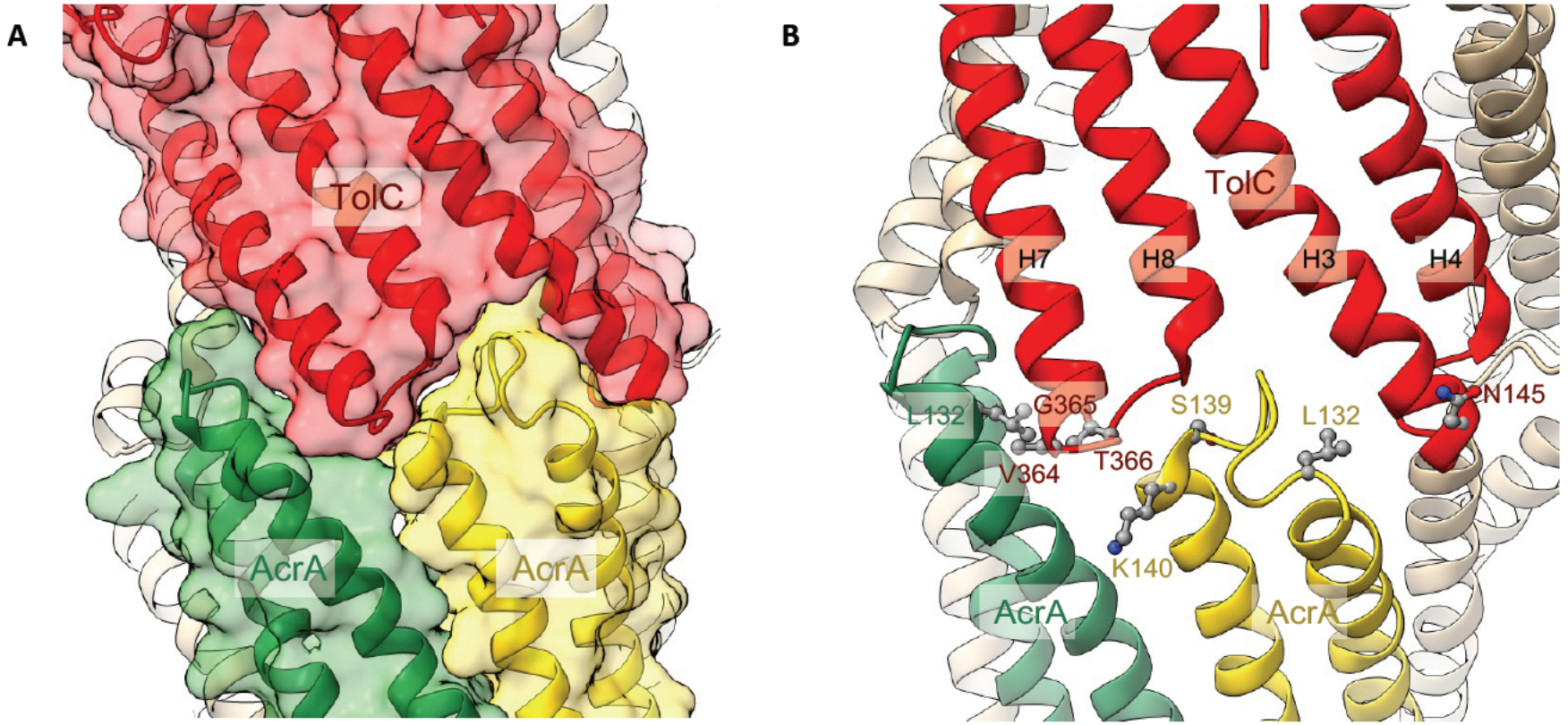


Figure 1.10. The interactions between AcrA and TolC.

A) Tip-to-tip interaction between a TolC protomer (red) and two α-helical hairpin domains of AcrA (green and yellow). **B)** Detailed view of the tip-to-tip interaction between AcrA and TolC. The VGL/T motif on helices 3, 4, 7 and 8 of TolC contacts the RLS motif at the tip of the α-helical domain of AcrA. Additional interactions are mediated by N145 of TolC and K140 of AcrA. Adjacent protomers are faded for clarity. Figure created with UCSF ChimeraX (Pettersen *et al.*, 2021).

1.9.5.2 AcrA and AcrB interactions

In the 3:6:3 stoichiometric model of AcrB:AcrA:TolC, AcrA interacts with each AcrB protomer as a dimer. In essence, AcrA interacts with AcrB in a 2:1 stoichiometry, wherein two AcrA protomers contact a single AcrB protomer in different locations. The two AcrA protomers interact with AcrB with slightly different affinities and specificities. In both AcrA protomers, the β-barrel and the membrane-proximal domains (MPD) are involved in binding with AcrB but at different sites on the AcrB surface (Fig. 1.11) (Ntreh *et al.*, 2016, Wang *et al.*, 2017). Wang *et al.* (2017) reported the near-atomic resolution cryo-EM structure of AcrAB-TolC, allowing an insight into the interactions between AcrA and AcrB. Specifically, the β-barrel domain of AcrA protomer-I docks onto the DN and DC subdomains of the funnel domain, while its MPD contacts the PC1 subdomain and the linker region between PC2 and DC subdomains (Fig. 1.11). On the other hand, the AcrA protomer-II makes fewer interactions with AcrB. The β-barrel domain of AcrA protomer-II contacts the crown of the DN subdomain, while its MPD is loosely associated with the PN2-DN linker region (Fig. 1.11) (Wang *et al.*, 2017). Despite the available structural data on AcrAB-TolC, the key residues involved in AcrA and AcrB interactions have remained poorly understood. Previous research in this laboratory with collaborators has predicted residues of AcrA involved in AcrB-binding. Work conducted in this thesis has validated which of these predicted residues are important and will be explored later in Chapter 3.

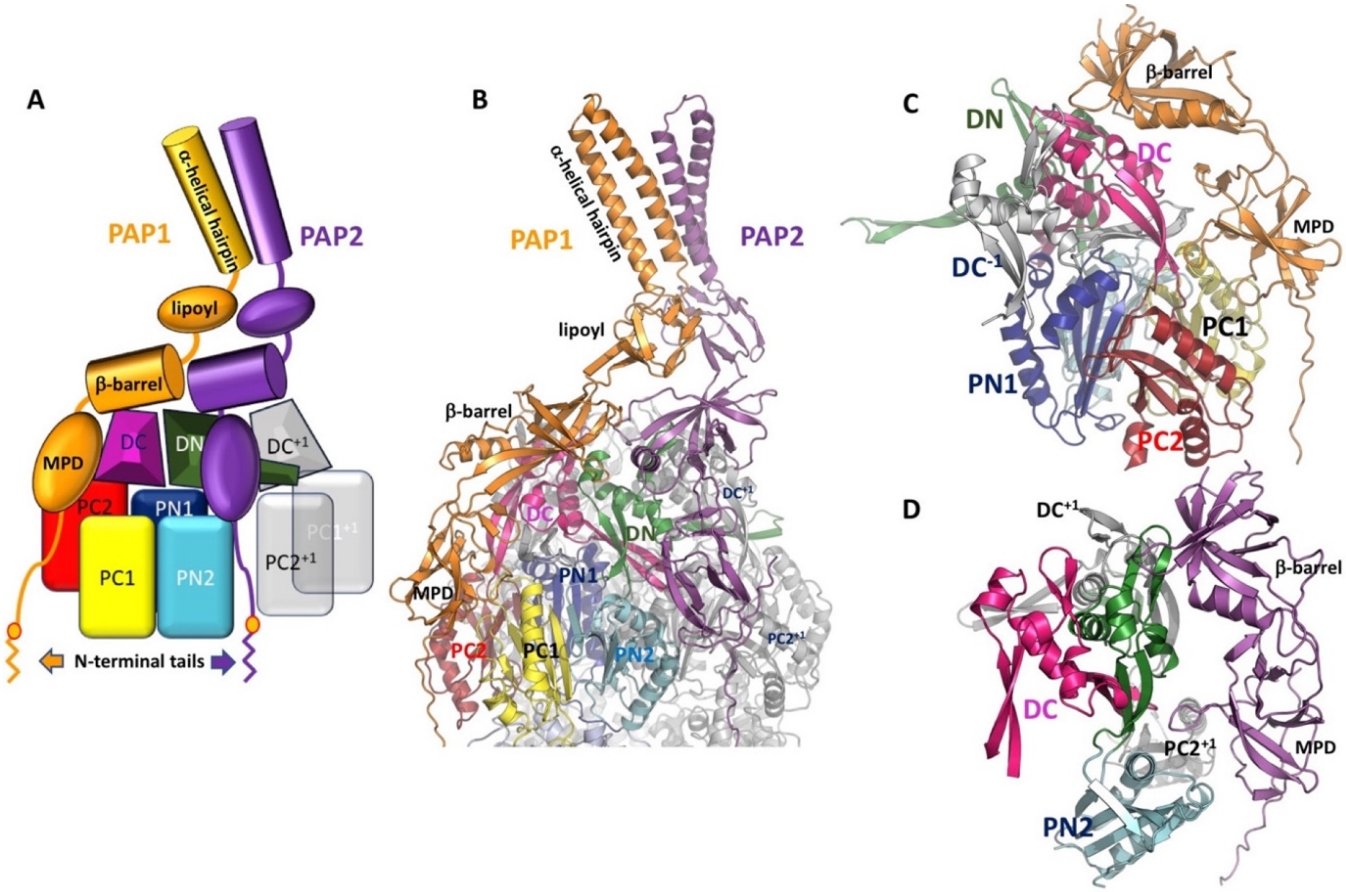


Figure 1.11. The interactions between AcrA and AcrB.

A) Schematic diagram showing the non-equivalent positioning of the two AcrA protomers (labelled 'PAP1' and 'PAP2') relative to the coloured subdomains of AcrB (PC1, PC2, PN1, PN2, DC and DN). The neighbouring AcrB protomer subdomains are coloured in grey. **B)** Cartoon representation of the same angle shown in **A)**. Isolated views of the interaction between **C)** PAP1 (orange) and **D)** PAP2 (purple) relative to the RND-transporter AcrB. The lipoyl and α-helical hairpin domains of AcrA have been removed for clarity as they do not contact AcrB. MPD, membrane-proximal domain. Figure reproduced from Alav *et al.* (2021).

1.10 PAP-RND transporter promiscuity

In *Salmonella*, there are four PAPs: AcrA, AcrE, MdtA and MdsA (Fig. 1.12) (Nishino *et al.*, 2006). Based on sequence analyses, AcrA and AcrE are the most closely related PAPs, with a protein sequence identity of 69.3% and a virtually identical secondary structure. On the other hand, MdtA and MdsA are more distantly related, with MdsA being the most divergent out of the four PAPs (McNeil *et al.*, 2019). As described previously, the PAP AcrA interacts with AcrB and TolC to form the AcrAB-TolC tripartite efflux pump. The PAP AcrE interacts with the RND transporter AcrF and the OMF TolC to form the AcrEF-TolC pump (Nishino, 2016). Although AcrA primarily functions with AcrB, it has been shown that AcrD also depends on AcrA and TolC to form a functional tripartite efflux pump since it lacks its own PAP encoded locus (Yamasaki *et al.*, 2011). In *E.* coli, AcrA has also been reported to function with the RND pumps AcrF and MdtF (Elkins and Nikaido, 2003, Kobayashi *et al.*, 2001). This promiscuity also exists with AcrE, which has been shown to function with the RND transporter AcrB (McNeil *et al.*, 2019). The remaining two RND pumps in *Salmonella* are MdtABC-TolC, which consists of the PAP MdtA; the RND transporter MdtBC; and the OMF TolC, and MdsABC, which consists of the PAP MdsA; the RND transporter MdsB; and the OMF MdsC or TolC (Nishino, 2016). Unlike AcrA and AcrE, which seem to be interchangeable, the PAPs MdtA and MdsA are unable to function with other RND pumps other than their own cognate RND pumps (McNeil *et al.*, 2019). The organisation of the five tripartite RND efflux systems found in *S. enterica* is illustrated in Figure 1.12.

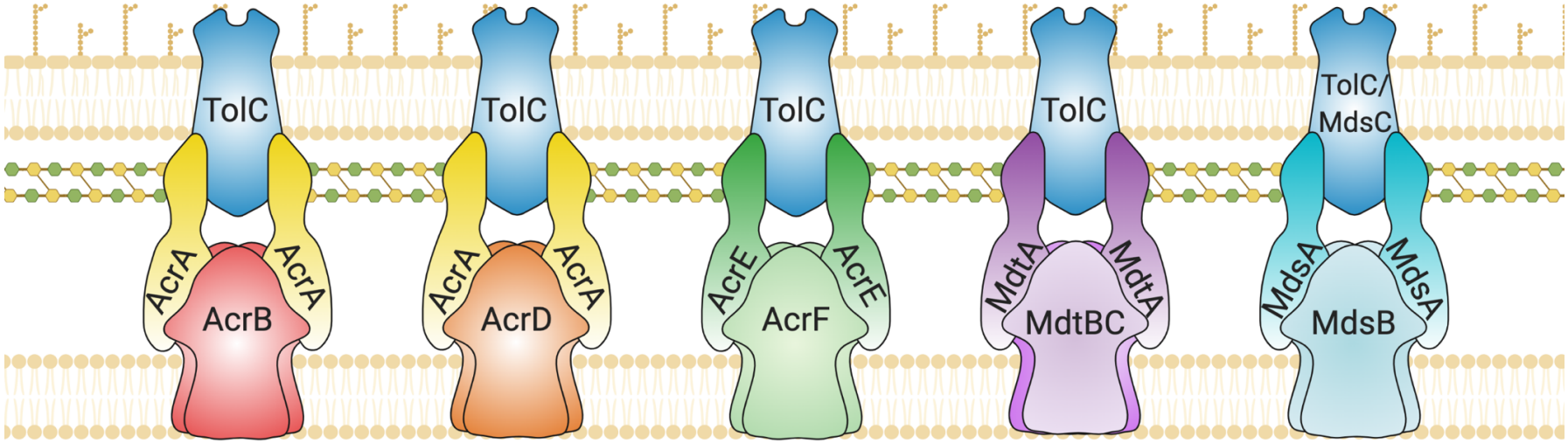


Figure 1.12. Schematic diagram of the five characterised tripartite RND efflux systems in *S. enterica*.

The inner membrane RND-transporters are AcrB, AcrD, AcrF, MdtBC, and MdsB. The MdtABC-TolC pump consists of two different RND-transporters, MdtB and MdtC, represented by different shades of purple. The RND-associated periplasmic adaptor proteins are AcrA, AcrE, MdtA and MdsA. All five RND pumps use TolC as an outer membrane factor. The MdsAB-MdsC/TolC pump has also been shown to use its cognate outer membrane factor MdsC (Nishino *et al.*, 2006). Figure created with Biorender.com

1.11 Efflux inhibitors

Efflux pump overexpression contributes to multidrug resistance, intrinsic resistance, selection of resistance, biofilm formation and virulence in Gram-negative bacteria. Therefore, efflux pumps are an attractive drug target for the development of compounds to inhibit their function. The activity and function of efflux pumps have been shown to be inhibited by compounds called efflux inhibitors (EIs) (Lomovskaya and Bostian, 2006). Although the term efflux pump inhibitor is widely used in the literature, some compounds may not directly interact to inhibit efflux pumps, therefore, the term EI is deemed a more accurate description. The primary rationale for using EIs is to restore the susceptibility of highly resistant bacteria to antibiotics by preventing their extrusion, thereby increasing intracellular concentrations of antibiotics. EIs could also be used to revive the effectiveness of antibiotics that have fallen out of use due to their loss of efficacy against bacteria that overproduce efflux pumps (Marquez, 2005). Furthermore, due to their reported roles in biofilm formation and virulence, EIs could also be deployed as anti-biofilm and anti-virulence agents. For a compound to be classified as an EI, it must fulfil several important criteria. Firstly, an EI should not exhibit antibacterial activity, but when used in tandem with an antibiotic, it should potentiate the activity of that antibiotic. Secondly, an EI should not possess activity against a strain that lacks the efflux pump that it is supposed to inhibit (Spengler *et al.*, 2017). Several EIs have been validated using *in vivo* mouse models but have been abandoned due to toxicity related issues (Opperman and Nguyen, 2015) In fact, the only EI to enter clinical trials was MP-601,20523, which entered phase 1 clinical trials in cystic fibrosis patients, but was suspended due to drug tolerability issues (Lomovskaya *et al.*, 2007, Springer, 2011). Consequently, no EI has been approved for clinical use to date. Studies have shown that EIs can exhibit different mechanisms of action (Fig. 1.13).

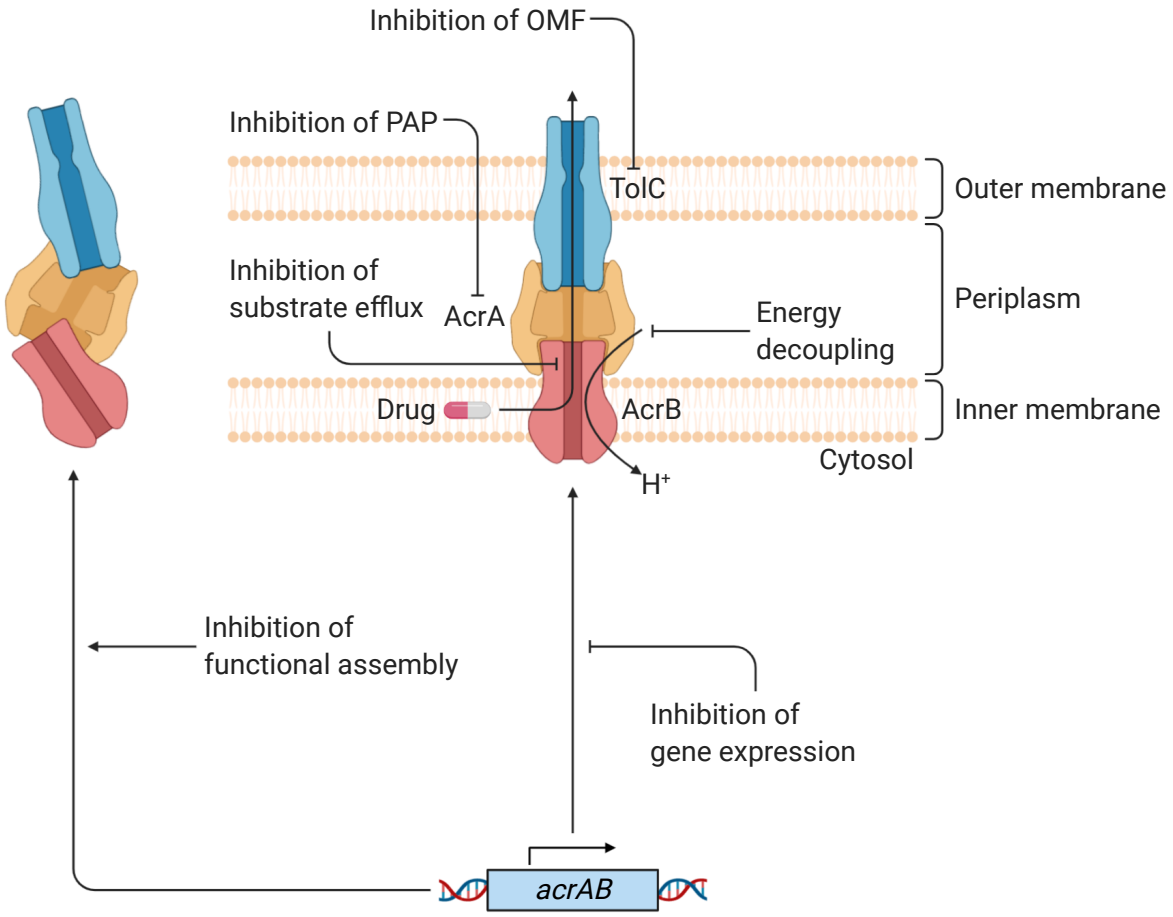


Figure 1.13. Schematic diagram of the different mechanisms of action of efflux inhibitors.

Inhibition of gene expression prevents transcription of efflux genes, thereby reducing efflux pump expression. Compounds that inhibit the functional assembly work by interfering with the interaction surfaces between the components of the tripartite efflux systems. Energy decoupling agents facilitate the flow of protons, thereby dissipating the electrochemical gradient, so that it cannot be exploited as an energy source by efflux pumps. Inhibitors of substrate efflux can work as a competitive inhibitor by actively competing with the binding site to prevent substrate binding or by blocking conformational change to prohibit enzymatic catalysis. Inhibitors of periplasmic adaptor proteins (PAP) are thought to work by preventing binding to the inner membrane transporter and by preventing the self-association of the PAP protomers. Outer membrane factor (OMF) inhibitors block the periplasmic entrance site to prevent translocation of substrates across the outer membrane. PAP, periplasmic adaptor protein; OMF, outer membrane factor. Figure created with BioRender.com

1.11.1 Targeting the inner membrane transporter

The inner membrane component of tripartite systems plays an important role in energy transduction, substrate recognition and uptake. Therefore, the majority of EIs described in the literature are posited to target the inner membrane transporter, such as AcrB. One of the first EIs to be characterized was phenylalanine-arginine β-naphthylamide (PAβN, 1; Fig. 1.14), a synthetic peptidomimetic inhibitor of the RND family tripartite efflux systems MexAB-OprM, MexCD-OprJ and MexEF-OprN of *P. aeruginosa* (Lomovskaya *et al.*, 2001). Since then, PAβN has been shown to be a broad-spectrum inhibitor of several different tripartite RND efflux systems in Gram-negative bacteria, including AcrAB-TolC from *S.* Typhimurium, and CmeABC from *C. jejuni* and *C. col*i (Hannula and Hanninen, 2008, Baucheron *et al.*, 2004). PAβN has been suggested to act as a competitive inhibitor of RND efflux systems by binding to the distal binding pocket, specifically the hydrophobic trap, to prevent the binding of substrates (Vargiu and Nikaido, 2012). Lamers *et al*. (2013) also reported that PAβN can permeabilize the outer membrane of Gram-negative, indicating an additional mechanism of action for PAβN (Lamers *et al.*, 2013). A recent study reported that PAβN exerts its EI activity in AcrB by restraining drug-binding pocket dynamics rather than acting as a competitive inhibitor. Computational and experimental data suggested that ciprofloxacin and PAβN bind to AcrB simultaneously at different subsites within the distal binding pocket and that PAβN inhibits efflux by perturbing the substrate translocation pathway (Reading *et al.*, 2020). PAβN was found to be cytotoxic *in vivo* so is unsuitable for clinical use (Lomovskaya and Bostian, 2006). However, it is still one of the most used inhibitors in laboratory assays to restore the activity of various antibiotics. One of the other early broad-spectrum EIs to be identified was the synthetic compound 1-(1-naphthylmethyl)-piperazine (NMP, 2; Fig. 1.14), which was shown to potentiate the activity of several antibiotics, including chloramphenicol, levofloxacin

and linezolid, in *E. coli* strains that were overexpressing *acrAB* or *acrEF* (Bohnert and Kern, 2005). In addition, NMP has been shown to potentiate the activity of antibiotics in several other Gram-negative bacteria, such as *A. baumannii, K. pneumoniae, Citrobacter freundii* and *Klebsiella aerogenes* (Schumacher *et al.*, 2006, Pannek *et al.*, 2006, Schumacher *et al.*, 2007). To date, the exact mechanism of action of NMP has not been elucidated. However, molecular dynamics simulations suggest that NMP binds to the outer face of the distal binding pocket to straddle the G-loop of AcrB, thereby reducing its flexibility and impairing the proper binding of substrates (Vargiu and Nikaido, 2012, Vargiu *et al.*, 2014). Further development of this compound was discontinued due to its low potency and structural similarity with serotonin agonists (Zechini and Versace, 2009). Another strategy to inhibit inner membrane transporters is by depleting the energy source required for efflux. Carbonyl cyanide *m*-chlorophenylhydrazone (CCCP, 3; Fig. 1.14) is a protonophore that dissipates the proton motive force, thus inhibiting all secondary active transporters. Due to its toxicity, CCCP has no therapeutic potential, however, it is a useful experimental tool as it is widely used in assays to measure efflux rate (Blair and Piddock, 2016).

Certain clinically approved drugs have also been reported to display EI activity. The psychotropic drug chlorpromazine (4; Fig. 1.14) has been reported to inhibit efflux in Gram-negative bacteria (Grimsey and Piddock, 2019). In *S.* Typhimurium and several other serovars, chlorpromazine was shown to significantly potentiate the activities of various antibiotics. In the same study, chlorpromazine was reported to repress *acrB* expression, suggesting that it may inhibit efflux by reducing efflux gene expression (Bailey *et al.*, 2008). Chlorpromazine can also affect cellular morphology and replication, membrane permeability, and energy generation, suggesting additional mechanisms of action (Grimsey and Piddock, 2019). A recent study has

shed some light on the mechanism of how chlorpromazine acts as an EI. Grimsey *et al.* (2020) reported chlorpromazine and amitriptyline to be substrates and inhibitors of the AcrB pump. Exposure to sub-inhibitory concentrations of chlorpromazine in *E. coli* and *S.* Typhimurium was found to select for *ramR*- and *marR*-mutants, which encode the regulators of the AcrAB-TolC system. Additionally, it was reported that when *S.* Typhimurium cells with a non-functional AcrB pump (D408A mutation) were exposed to sub-inhibitory chlorpromazine and amitriptyline concentrations, the D408A *acrB* mutants were found to revert to a wild type *acrB* allele, suggesting that both compounds act as substrates of AcrB. Lastly, molecular docking and dynamics simulations, and free energy calculations were shown to demonstrate that both chlorpromazine and amitriptyline bind to the hydrophobic trap within the distal binding pocket of AcrB (Grimsey *et al.*, 2020a).

Through high-throughput drug screening and rational drug design, newer and more potent EIs have been identified. A pyridopyrimidine (D13-9001, 5; Fig. 1.14) derivative acts as an inhibitor against the MexAB-OprM pump in *P. aeruginosa* (Yoshida *et al.*, 2007) and AcrAB-TolC of *E. coli* and was co-crystallized with AcrB (*E. coli*) and MexB (*P. aeruginosa*) (Nakashima *et al.*, 2013). This compound was shown to bind to the deep binding pocket area, which was designated the hydrophobic trap due to the enrichment of phenylalanine residues in this region. MBX2319 (6; Fig. 1.14) is another pyranopyridine inhibitor of the AcrAB-TolC system which was identified through high-throughput screening of 183,400 compounds. It was shown to potentiate the activity of multiple antibiotics against *E. coli* (Opperman *et al.*, 2014). Later, molecular docking studies led to the development of more potent derivatives of MBX2319, such as MBX3135 (7; Fig. 1.14). Pyranopyridine derivatives (MBX2319, MBX2931, MBX-3132 and MBX-3135) were found to be highly potent in the inhibition of

efflux pumps in *E. coli*, *K. aerogenes, K. pneumoniae* and *S. enterica* (Opperman *et al.*, 2014, Vargiu *et al.*, 2014, Aron and Opperman, 2018). Crystal structures of the MBX inhibitors (MBX2319, MBX2931, MBX-3132 and MBX-3135) were obtained with the soluble periplasmic domain of AcrB (AcrBper) and were found to bind in the proximity of the same region in the hydrophobic trap (Sjuts *et al.*, 2016). The inhibitory effect was suggested to be due to the competitive and overlapping binding of the inhibitors to the deep binding pocket of the T protomer and/or due to the tight interaction, possibly halting the conformational LTO cycling. Interestingly, single-particle Cryo-EM structures revealed an LTO trimeric setup in the presence of substrate (puromycin), whereas in the presence of MBX-3135, mostly particles in the TTT conformation were found (Du *et al.*, 2014, Wang *et al.*, 2017). A recent study reported the identification of 43 novel EIs of Gram-negative bacteria from a high-throughput drug screening of the Prestwick drug library and the proprietary compound library from Roche. It was found that the majority of identified EIs had specific EI-antibiotic combinations and/or species-specific synergy with antibiotics. Of the EIs identified, auranofin (8, Fig. 1.14), an antirheumatic agent, increased ethidium bromide accumulation and potentiated antibiotic activity in the checkerboard assays (Marshall *et al.*, 2020). While most drug screening efforts have focused on looking at inhibitors of RND inner membrane transporters, a recent study identified an inhibitor of the ABC type efflux pump MacAB in *S.* Typhimurium. Compound 9 (Fig. 1.14) was identified from screening a drug library for compounds that inhibited the growth of a *macAB*-overexpressing strain in the presence of erythromycin. It was reported to increase the susceptibility of this strain to several different macrolides, although its mechanism of action remains to be explored (Yamagishi *et al.*, 2020).

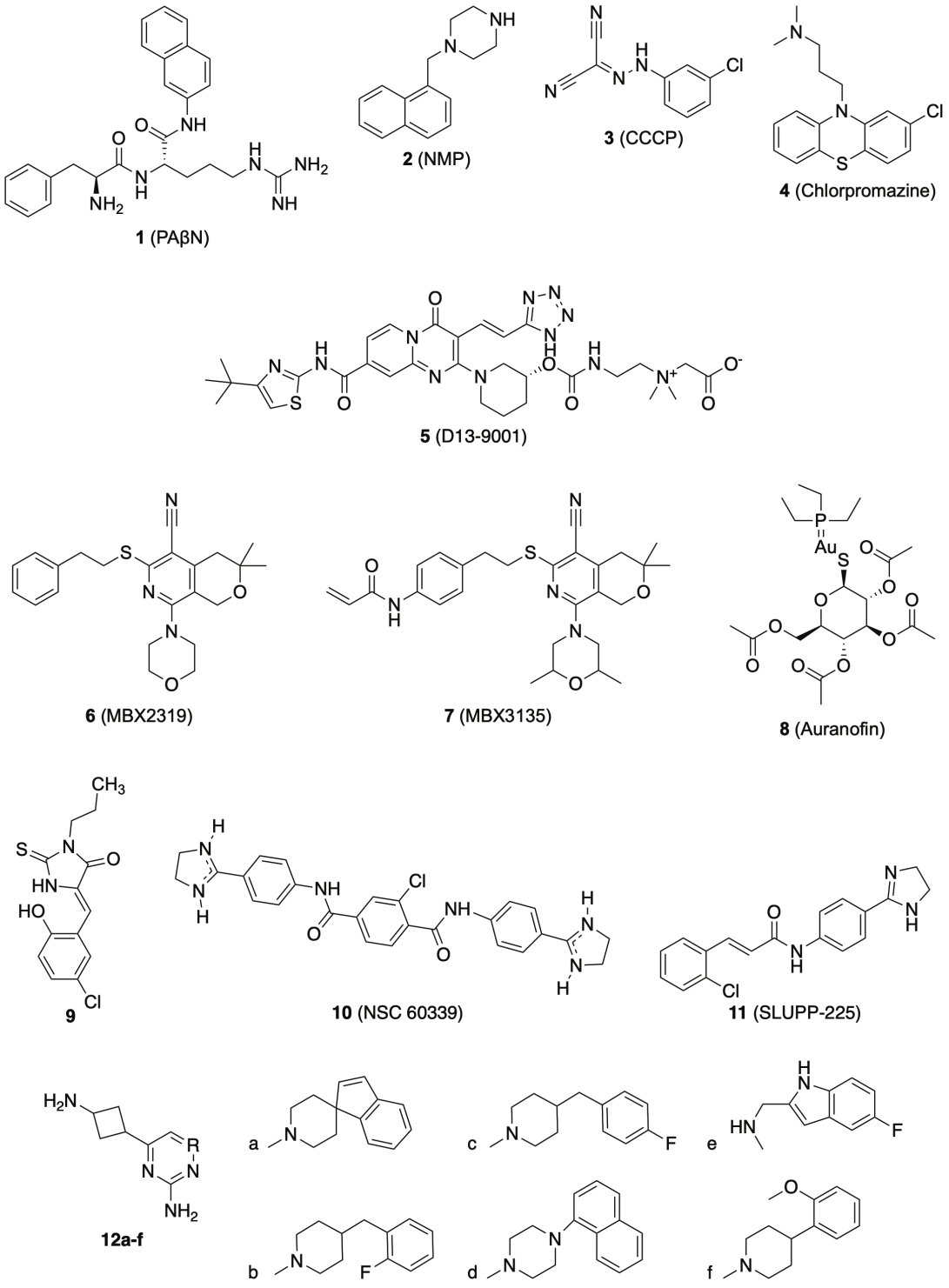


Figure 1.14. The structural formulae of representative efflux inhibitors that have been discussed in this section.

Efflux inhibitors possess broad structural diversity and originate from both natural and synthetic sources. Compounds 1–9 target the RND-transporter and compounds 10–12 target the periplasmic adaptor protein. Figure created using ChemDraw 20.0.

1.11.2 Targeting the outer membrane factor

The OMF component of tripartite efflux systems plays an important role in expelling substrates across the outer membrane to the external environment. As a paradigm OMF, TolC is rather promiscuous and functions with several different tripartite efflux systems, including T1SS, RND, ABC and MFS efflux systems. Despite being an attractive drug target, TolC inhibition is relatively under-researched. Higgins *et al*. (2004) reported the crystal structure of TolC in a complex with hexaamminecobalt (HC), a trivalent cation, and showed that it blocked the periplasmic entrance of TolC by forming salt bridges with D374 of each TolC monomer (Higgins *et al.*, 2004). Later, Gilardi *et al.* (2017) investigated the biophysical interaction of HC with TolC and found that it binds to TolC with a high affinity and fast association and dissociation rates. Furthermore, HC was found to not exhibit any intrinsic antimicrobial activity nor potentiate antibiotic activity in *E. coli* (Gilardi *et al.*, 2017). Thus, further research is required to identify more potent TolC inhibitors capable of inhibiting efflux and potentiating antibiotic activity. However, TolC inhibition may not be a good target for efflux inhibition in practice. Krishnamoorthy *et al*. (2013) found that the activity and assembly of the AcrAB-TolC complex in *E. coli* can tolerate substantial fluctuations in the amount of TolC available. Furthermore, they reported that only a small fraction of intracellular TolC is necessary for the efflux requirements of *E. coli* cells, indicating that significant depletion of TolC is well tolerated in bacterial cells (Krishnamoorthy *et al.*, 2013).

1.11.3 Targeting the periplasm adaptor protein

Although the majority of EIs described in the literature are reported to target inner membrane transporters, the PAP component of tripartite systems has also been shown to be a viable target for efflux inhibition. Abdali *et al.* (2017) carried out the parallel experimental and structure-

based screening of two drug libraries to identify inhibitors of AcrA, the PAP component of AcrAB-TolC. Several EIs were identified and shown to bind to AcrA, change its structure *in vivo*, and potentiate the activities of several antibiotics in *E. coli* and other Gram-negative bacteria. Additionally, the identified EIs, including NSC 60339 (10; Fig. 1.14) were found to require AcrA binding to inhibit efflux activity (Abdali *et al.*, 2017). Further optimization efforts of compound 10 lead to more potent derivatives, such as SLUPP-225 (11; Fig. 1.14), which was shown to penetrate the outer membrane of *E. coli* cells and exhibit a more potent efflux inhibition activity (Haynes *et al.*, 2017). Later, Darzynkiewicz *et al*. (2019) investigated the potential binding sites of compound 10 and found that it likely binds to a site situated between the lipoyl and β-barrel domain of AcrA (Darzynkiewicz *et al.*, 2019). The β-barrel domain of AcrA has been previously shown to be involved in RND binding and the lipoyl domain is involved in self-association, therefore, AcrA inhibitors may function to prevent the functional assembly of AcrAB-TolC (McNeil *et al.*, 2019). In a recent study, Green *et al.* (2020) searched the ZINC15 database for compounds with physicochemical properties matching those of existing EIs and Gram-negative antibiotics. Subsequently, compounds with the matching criteria were computationally docked onto AcrA of *E. coli* at the previously reported binding site of compound 10, as well as several other sites that when disrupted have been reported to disrupt efflux. The top thirty-four hits from all docking poses were then analysed using a combination of *in vitro* binding assays to measure binding affinity to AcrA and AcrB and *in vivo* antibiotic potentiation assays. They identified six compounds (12a-f; Fig. 1.14) with a shared scaffold that is bound to AcrA as verified by surface plasmon resonance. Promisingly, the six compounds also potentiated the activities of erythromycin and novobiocin in hyperporinated *E. coli* cells, as well as in wild-type *A. baumannii* and *K. pneumoniae* (Green *et al.*, 2020).

Several studies have also reported that targeting PAP expression can also potentiate antibiotic activity. Peptide-conjugated phosphorodiamidate morpholino oligomers (PPMOs) are an example of synthetic nucleotide oligomers that inhibit antisense mRNA translation. Ayhan *et al.* (2016) developed and identified an *acrA*-PPMO capable of increasing the efficacy of several antibiotics, such as cefotaxime, chloramphenicol, clindamycin and fusidic acid, by up to 40-fold and prevented AcrA protein translation in a dose-dependent manner in *E. coli*. Additionally, the *acrA*-PPMO was shown to be effective in *K. pneumoniae* and *S. enterica* by significantly increasing the activity of piperacillin-tazobactam (Ayhan *et al.*, 2016). More recently, an optimised *acrA*-PMMO was shown to potentiate the activity of azithromycin and levofloxacin in several clinical Enterobacteriaceae strains. Crucially, the *acrA*-PPMO was demonstrated to increase the efficacy of azithromycin *in vivo* in a *K. pneumoniae* septicaemia murine model. Inhibition of MexAB-OprM, the homologous RND system in *P. aeruginosa*, was also reported to enhance the efficacy of several antibiotics. PPMOs targeting *mexA* and *mexB* were found to enhance the activities of azithromycin, cefotaxime, and piperacillin-tazobactam by at least 4-fold in most tested clinical *P. aeruginosa* isolates (Sturge *et al.*, 2019). In a different study, antisense oligonucleotides were developed to inhibit the translation of the *cmeA* gene, which encodes for the PAP CmeA of CmeABC in *C. jejuni*. The *cmeA* antisense oligonucleotide was reported to sensitise *C. jejuni* cells to ciprofloxacin and erythromycin at very low concentrations (Oh *et al.*, 2014).

Although PAPs are good drug targets to inhibit efflux, PAPs also display promiscuity which can complicate their effectiveness. For instance, in *S.* Typhimurium, it has been demonstrated that inactivation of *acrE* alone had no phenotypic effect, however, inactivation of both *acrA*

and *acrE* had an additive effect, resulting in increased susceptibility to various drugs. The phenotypic defect in the *acrA acrE* mutant was rescued by complementation with either *acrA* or *acrE*, indicating redundancy between the two PAPs (Smith and Blair, 2014). Furthermore, McNeil *et al.* (2019) demonstrated that in *S.* Typhimurium, inactivation of AcrA results in AcrE compensating for its loss, indicating interchangeability between the two PAPs (McNeil *et al.*, 2019). Therefore, a successful PAP inhibitor would need to target both AcrA and AcrE in *S. enterica* to inhibit efflux. In this project, information about residues conserved between the PAPs will be used to identify residues that would be suitable for inhibition.

1.12 Hypotheses

- Disruption of predicted RND-binding residues in AcrA through site-directed mutagenesis will result in abrogated efflux
- The RND-binding residues are functionally conserved between AcrA and AcrE
- The periplasmic adaptor protein AcrE will function with the RND-transporter AcrD to form an efflux-competent pump

1.13 Aims and objectives

The aims of this project are:

- To use the information about residues conserved between AcrA and AcrE to identify RND-binding residues that would be suitable targets for inhibition
- To investigate whether AcrE can also function with AcrD to form a functional efflux pump

The objectives for this project are:

- Mutate the predicted RND-binding residues of AcrA and AcrE through site-directed mutagenesis
- Investigate the phenotypic impact of mutations in AcrA and AcrE
- Co-express *acrD* and *acrE* in a strain lacking functional RND-efflux to investigate whether AcrD and AcrE can function together

CHAPTER 2. Materials and Methods

2.1 Bacterial strains and growth conditions

All bacterial strains and plasmids used in this study are listed in Table 2.1. The wild-type strain used was *Salmonella enterica* serovar Typhimurium SL1344 (SE01), a pathogenic strain first isolated from an experimentally infected calf (Wray and Sojka, 1978). All other strains were constructed in this laboratory either previously or in this study. Unless stated otherwise, all strains were grown on Luria-Bertani (LB) agar (Sigma-Aldrich, Germany), with appropriate antibiotics where necessary, and incubated overnight at 37°C. Overnight cultures were grown in LB broth (Sigma-Aldrich, Germany), with appropriate antibiotics where necessary, and incubated at 37°C with aeration.

Table 2.1. List of strains used in this study.

Strain no.	Genotype	Resistance phenotype	Reference
Routinely used strains			
EC10	*Escherichia coli* BW1125 + pKD4	Amp^R, Kan^R	Datsenko & Wanner (2000)
EC112	*E. coli* ATCC 25922	None	ATCC®
EC157	*E. coli* TOP10 + pHSG398	Chl^R	Takara Bio Inc.
EC164	*E. coli* 1200 + pACYC177	Amp^R, Kan^R	ATCC®
EC216	*E. coli* TOP10 + pET-20b (+)	Amp^R	Novagen®
SE01	*Salmonella* enterica serovar Typhimurium SL1344	None	Wray & Sojka (1978)
SE10	SL1344 Δ*acrA* Δ*acrE* Δ*mdtA* Δ*mdsA* (Δ4PAP)	None	McNeil *et al.* (2019)
SE26	SL1344 Δ4PAP + pET-20b *acrA*	Amp^R	McNeil *et al.* (2019)
SE67	SL1344 + pSIM18	Hyg^R	Chan *et al.* (2007a)
SE141	SL1344 Δ*acrA* Δ*acrEF* Δ*mdtA* Δ*mdsA* (Δ4PAP Δ*acrF*)	None	McNeil *et al.* (2019)
SE143	SL1344 Δ*acrAB* Δ*acrE* Δ*mdtA* Δ*mdsA* (Δ4PAP Δ*acrB*)	None	McNeil *et al.* (2019)
SE160	SL1344 + pCP20	Amp^R	Datsenko & Wanner (2000)
SE566	SL1344 Δ4PAP Δ*acrB* + pET-20b *acrAB*	Amp^R	This study
SE599	SL1344 Δ4PAP Δ*acrF* + pTrcHis2 *acrE*	Amp^R	This study
AcrA mutations			
SE346	SL1344 Δ4PAP + pET-20b *acrA* (S220E)	Amp^R	McNeil *et al.* (2019)
SE347	SL1344 Δ4PAP + pET-20b *acrA* (T217F)	Amp^R	McNeil *et al.* (2019)
SE348	SL1344 Δ4PAP + pET-20b *acrA* (T270F–T271F)	Amp^R	McNeil *et al.* (2019)
SE349	SL1344 Δ4PAP + pET-20b *acrA* (E333F)	Amp^R	McNeil *et al.* (2019)
SE350	SL1344 Δ4PAP + pET-20b *acrA* (R315F)	Amp^R	McNeil *et al.* (2019)
SE351	SL1344 Δ4PAP + pET-20b *acrA* (G272P–S273P)	Amp^R	McNeil *et al.* (2019)

Table 2.1 (continued). List of strains used in this study.

Strain no.	Genotype	Resistance phenotype	Reference
SE352	SL1344 Δ4PAP + pET-20b *acrA* (R294F)	Amp^R	McNeil *et al.* (2019)
SE353	SL1344 Δ4PAP + pET-20b *acrA* (D250F)	Amp^R	McNeil *et al.* (2019)
SE354	SL1344 Δ4PAP + pET-20b *acrA* (G58F)	Amp^R	McNeil *et al.* (2019)
SE355	SL1344 Δ4PAP + pET-20b *acrA* (R318A)	Amp^R	McNeil *et al.* (2019)
SE356	SL1344 Δ4PAP + pET-20b *acrA* (F292G)	Amp^R	McNeil *et al.* (2019)
SE357	SL1344 Δ4PAP + pET-20b *acrA* (G363F)	Amp^R	McNeil *et al.* (2019)
SE358	SL1344 Δ4PAP + pET-20b *acrA* (R368D)	Amp^R	McNeil *et al.* (2019)
SE359	SL1344 Δ4PAP + pET-20b *acrA* (Q310F)	Amp^R	McNeil *et al.* (2019)
SE484	SL1344 Δ4PAP + pET-20b *acrA* (R59A)	Amp^R	This study
SE485	SL1344 Δ4PAP + pET-20b *acrA* (F292V)	Amp^R	This study
SE486	SL1344 Δ4PAP + pET-20b *acrA* (Q310P–Q311P)	Amp^R	This study
SE487	SL1344 Δ4PAP + pET-20b *acrA* (R318F)	Amp^R	This study
SE488	SL1344 Δ4PAP + pET-20b *acrA* (K366D)	Amp^R	This study
SE489	SL1344 Δ4PAP + pET-20b *acrA* (G272A–S273A)	Amp^R	This study
SE490	SL1344 Δ4PAP + pET-20b *acrA* (P317G)	Amp^R	This study
SE491	SL1344 Δ4PAP + pET-20b *acrA* (R368F)	Amp^R	This study
SE492	SL1344 Δ4PAP + pET-20b *acrA* (P317F)	Amp^R	This study
SE493	SL1344 Δ4PAP + pET-20b *acrA* (Q311F)	Amp^R	This study
SE494	SL1344 Δ4PAP + pET-20b *acrA* (Q365F)	Amp^R	This study
SE495	SL1344 Δ4PAP + pET-20b *acrA* (T270A)	Amp^R	This study
SE496	SL1344 Δ4PAP + pET-20b *acrA* (T270D)	Amp^R	This study
SE497	SL1344 Δ4PAP + pET-20b *acrA* (T271A)	Amp^R	This study
SE498	SL1344 Δ4PAP + pET-20b *acrA* (T271D)	Amp^R	This study
SE499	SL1344 Δ4PAP + pET-20b *acrA* (I343F–G344F)	Amp^R	This study

Table 2.1 (continued). List of strains used in this study.

Strain no.	Genotype	Resistance phenotype	Reference
SE503	SL1344 Δ4PAP + pET-20b *acrA* (D345A)	Amp^R	This study
SE504	SL1344 Δ4PAP + pET-20b *acrA* (K346A)	Amp^R	This study
SE505	SL1344 Δ4PAP + pET-20b *acrA* (R368A)	Amp^R	This study
SE600	SL1344 Δ4PAP + pTrcHis2 *acrA* (R59A)	Amp^R	This study
SE601	SL1344 Δ4PAP + pTrcHis2 *acrA* (T271D)	Amp^R	This study
SE602	SL1344 Δ4PAP + pTrcHis2 *acrA* (F292V)	Amp^R	This study
SE603	SL1344 Δ4PAP + pTrcHis2 *acrA* (Q311F)	Amp^R	This study
SE604	SL1344 Δ4PAP + pTrcHis2 *acrA* (Q310P-Q311P)	Amp^R	This study
SE605	SL1344 Δ4PAP + pTrcHis2 *acrA* (K366D)	Amp^R	This study
SE6365	SL1344 Δ4PAP + pTrcHis2 *acrA* (S273F)	Amp^R	This study
SE636	SL1344 Δ4PAP + pTrcHis2 *acrA* (I274D)	Amp^R	This study
AcrE mutations			
SE588	SL1344 Δ4PAP Δ*acrF* + pTrcHis2 *acrE* (G57F)	Amp^R	This study
SE589	SL1344 Δ4PAP Δ*acrF* + pTrcHis2 *acrE* (R58A)	Amp^R	This study
SE590	SL1344 Δ4PAP Δ*acrF* + pTrcHis2 *acrE* (T216F)	Amp^R	This study
SE591	SL1344 Δ4PAP Δ*acrF* + pTrcHis2 *acrE* (T270D)	Amp^R	This study
SE592	SL1344 Δ4PAP Δ*acrF* + pTrcHis2 *acrE* (F291G)	Amp^R	This study
SE593	SL1344 Δ4PAP Δ*acrF* + pTrcHis2 *acrE* (R293F)	Amp^R	This study
SE594	SL1344 Δ4PAP Δ*acrF* + pTrcHis2 *acrE* (G362F)	Amp^R	This study
SE595	SL1344 Δ4PAP Δ*acrF* + pTrcHis2 *acrE* (K365D)	Amp^R	This study
SE596	SL1344 Δ4PAP Δ*acrF* + pTrcHis2 *acrE* (R367D)	Amp^R	This study
SE626	SL1344 Δ4PAP Δ*acrF* + pTrcHis2 *acrE* (I273D)	Amp^R	This study
SE637	SL1344 Δ4PAP Δ*acrF* + pTrcHis2 *acrE* (S272F)	Amp^R	This study

Table 2.1 (continued). List of strains used in this study.

Strain no.	Genotype	Resistance phenotype	Reference
AcrAB mutations			
SE574	SL1344 Δ4PAP Δ*acrB* + p*acrA* (WT) *acrB* (A33W T37W N298W)	Amp^R	This study
SE587	SL1344 Δ4PAP Δ*acrB* + p*acrA* (K366D) *acrB* (A33W T37W N298W)	Amp^R	This study
SE631	SL1344 Δ4PAP Δ*acrB* + p*acrA* (WT) *acrB* (F380A)	Amp^R	This study
SE632	SL1344 Δ4PAP Δ*acrB* + p*acrA* (K366D) *acrB* (F380A)	Amp^R	This study
Chapter 6			
SE02	SL1344 Δ*acrB*	None	Eaves *et al.* (2004)
SE340	SL1344 Δ*acrAB*	None	This study
SE446	SL1344 Δ*acrB* + pHSG398	Chl^R	This study
SE449	SL1344 Δ*acrB* + pHSG398 *acrD*	Chl^R	This study
SE379	SL1344 Δ*acrD*	None	This study
SE381	SL1344 Δ*acrAB* Δ*acrD*	None	This study
SE502	SL1344 Δ*acrAB* Δ*acrD* Δ*acrEF* (Δ3RND)	None	This study
SE544	SL1344 Δ3RND + pHSG398	Chl^R	This study
SE545	SL1344 Δ3RND + pACYC177Kan^R	Kan^R	This study
SE507	SL1344 Δ3RND + p*acrD*	Chl^R	This study
SE510	SL1344 Δ3RND + pACYC177 *acrA*	Kan^R	This study
SE511	SL1344 Δ3RND + pACYC177 *acrE*	Kan^R	This study
SE506	SL1344 Δ3RND + pACYC177Kan^R with pHSG398	Chl^R, Kan^R	This study
SE548	SL1344 Δ3RND + pACYC177Kan^R with pHSG398 *acrD*	Chl^R, Kan^R	This study
SE508	SL1344 Δ3RND + pHSG398 *acrD* with pACYC177 *acrA*	Chl^R, Kan^R	This study
SE509	SL1344 Δ3RND + pHSG398 *acrD* with pACYC177 *acrE*	Chl^R, Kan^R	This study
SE546	SL1344 Δ3RND + pHSG398 with pACYC177 *acrA*	Chl^R, Kan^R	This study

Table 2.1 (continued). List of strains used in this study

Strain no.	Genotype	Resistance phenotype	Reference
SE547	SL1344 Δ3RND + pHSG398 with pACYC11 *acrE*	Chl^R, Kan^R	This study
SE553	SL1344 Δ3RND + pHSG398 with pACYC177 *acrA* (F292G)	Chl^R, Kan^R	This study
SE554	SL1344 Δ3RND + pHSG398 with pACYC177 *acrA* (G363F)	Chl^R, Kan^R	This study
SE554	SL1344 Δ3RND + pHSG398 with pACYC177 *acrE* (F291G)	Chl^R, Kan^R	This study
SE556	SL1344 Δ3RND + pHSG398 with pACYC177 *acrE* (G362F)	Chl^R, Kan^R	This study
SE557	SL1344 Δ3RND + pHSG398 *acrD* with pACYC177 *acrA* (F292G)	Chl^R, Kan^R	This study
SE558	SL1344 Δ3RND + pHSG398 *acrD* with pACYC177 *acrA* (G363F)	Chl^R, Kan^R	This study
SE559	SL1344 Δ3RND + pHSG398 *acrD* with pACYC177 *acrE* (F291G)	Chl^R, Kan^R	This study
SE560	SL1344 Δ3RND + pHSG398 *acrD* with pACYC177 *acrE* (G362F)	Chl^R, Kan^R	This study

Amp^R, ampicillin resistant; Chl^R, chloramphenicol resistant; Kan^R, kanamycin resistant; Hyg^R, hygromycin resistant; ATCC, American Type Culture Collection; WT, wild type

Table 2.2. List of plasmids used in this study.

Plasmid	Description	Resistance phenotype	Reference
pKD4	Template plasmid used to generate a PCR construct to disrupt the gene of interest	Amp^R, Kan^R	Datsenko & Wanner (2000)
pCP20	Temperature sensitive plasmid encoding FLP recombinase which removes FLT-flanked antibiotic resistance markers	Amp^R	Datsenko & Wanner (2000)
pSIM18	Plasmid encoding the lambda red recombination system to facilitate homologous recombination	Hyg^R	Chan *et al.* (2007a)
pHSG398	High-copy number cloning vector	Chl^R	Takara Bio Inc.
pET-20b (+)	High-copy number cloning vector for expressing proteins in the periplasm	Amp^R	
pHSG398 *acrD*	SL1344 *acrD* gene cloned into pHSG398	Chl^R	This study
pACYC177	Low-copy number cloning vector	Amp^R, Kan^R	ATCC®
pACYC177Kan^R	Low-copy number cloning vector	Kan^R	This study
pACYC177 *acrA*	SL1344 *acrA* gene cloned into pACYC177	Kan^R	This study
pACYC177 *acrE*	SL1344 *acrE* gene cloned into pACYC177	Kan^R	This study
pET-20b *acrA*	SL1344 *acrA* gene cloned into pET-20b (+)	Amp^R	McNeil *et al.* (2019)
pET-20b *acrAB*	SL1344 *acrA* and *acrB* genes cloned into pET-20b (+)	Amp^R	This study
pTrcHis2 *acrE*	SL1344 *acrE* gene cloned into pTrcHis2-TOPO	Amp^R	McNeil *et al.* (2019)
pTrcHis2 *acrA*	SL1344 *acrA* gene cloned into pTrcHis2-TOPO	Amp^R	McNeil *et al.* (2019)
pTrcHis2 *acrB*	SL1344 *acrB* gene cloned into pTrcHis2-TOPO	Amp^R	This laboratory

2.2 Molecular microbiology techniques

2.2.1 Preparation of bacterial lysates

A single bacterial colony was picked from a fresh plate and diluted in 100 µL of UltraPure™ DNase/RNase-free distilled water (Thermo Fisher Scientific, USA). The cell suspension was heated to 99°C for 10 minutes in a thermocycler. The resulting lysate was pelleted briefly at 10,000 × *g* to remove cellular debris before the removal of the supernatant. The supernatant was used as template for PCR reactions.

2.2.2 Routine PCR amplification primers and conditions

Primer numbers, their description and sequences are listed in Table 2.2. All oligonucleotides were obtained from Sigma-Aldrich (Germany) or Eurogentec (Belgium). PCR mixtures comprised of 0.5 µM of forward and reverse primer, 25 µL 2×MyTaq™ Red Mix (Bioline, UK), 1 µL template DNA, and DNase/RNase-free distilled water to 50 µL. Amplification was carried out in a Mastercycler® Nexus X2 (Eppendorf, Germany) thermal cycler. An initial denaturation at 95°C for 1 minute was followed by 35 cycles of denaturation at 95°C for 15 seconds, annealing at 51°C to 60°C for 15 seconds, and elongation at 72°C for 30 seconds to 3 minutes (30 seconds per kb of target product), with a final elongation step at 72°C for 10 minutes. PCR products and HyperLadder™ 1kb (Bioline, UK) molecular ladder were separated by electrophoresis on a 1% (w/v) agarose gel at 80-100 V and visualised with Midori Green Advance Nucleic Acid Stain (Geneflow, UK) using an Amersham Imager 680 (GE Life Sciences, UK) under UV light (312 nm). All PCRs included a negative control containing water but no template DNA. Where stated, amplified PCR products were purified after excision from the agarose gel using a QIAquick Gel Extraction Kit (Qiagen, Germany) according to the manufacturer's instructions. The concentration and quality of purified PCR products was

determined using Qubit™ dsDNA Broad Range Assay Kit (Invitrogen, USA) as per manufacturer's instructions.

Table 2.3. List of primers used for generating gene knockouts, checking sizes of genes and for cloning of inserts.

Primer no.	Description	Sequence (5'-3')
P1	T7 forward primer	TAATACGACTCACTATAGGG
P2	T7 terminal primer	TAGTTATTGCTCAGCGGTGG
P34	Upstream *acrE* check forward primer	GAAACATGCCAGGTTTTCAC
P36	Internal *aph* check forward primer	CGGTGCCCTGAATGAACTGC
P37	Internal *aph* check reverse primer	CGGCCACAGTCGATGAATCC
P38	pTrc forward primer for checking cloning insert in pTrcHis2-TOPO	GAGGTATATATTAATGTATCG
P39	pTrc reverse primer for checking cloning insert in pTrcHis2-TOPO	GATTTAATCTGTATCAGG
P32	*acrEF* inactivation forward primer	GGTTTTCACTCCTGCCCTCATTCATCATATTCTCTGCTGCGTGTAGGCTGGAGCTGCTTC
P47	*acrEF* inactivation reverse primer	AAGGCGTCCGAAGACGCCTCTGTTTACCGGTTAATCATGATGGCGATTAAATGGGAATT AGCCATGGTCCAT
P56	Forward primer for cloning *acrAB* into pET-20b (+) with the *Nde*I site	GGGGGGGGCATATGAACAAAAACAGAGGGTT
P66	Upstream *acrA* check forward primer	ACATCCAGGATGTGTTGTCG
P67	Downstream *acrA* check reverse primer	CAATCGTCGGATATTGCGCT
P81	Downstream *acrF* check reverse primer	CGAAGACGCCTCTGTTTACC
P82	Upstream *acrB* check forward primer	GCTCAGCCCAGGTCTTAACTT
P83	Downstream *acrB* check reverse primer	GCGGCCTTATCAACAGTGAG

Table 2.3 (continued). List of primers used for generating gene knockouts, checking sizes of genes and for cloning of inserts.

Primer no.	Description	Sequence (5'-3')
P256	*acrAB* inactivation forward primer	GTCACACTAAAAACGGAACCACTGCAAATCACAACTGAACGTGTAGGCTGGAGCTGCTTC
P257	*acrAB* inactivation reverse primer	GCTTGCGCGGCCTTATCAACAGTGAGCAAATCAGCGATGTGGGAATTAGCCATGGTCCAT
P305	Upstream *acrD* check forward primer	GCTTGCCGCTACAGTGAA
P306	Downstream *acrD* check reverse primer	CCAGAGGATATCGCAACA
P309	*acrD* inactivation forward primer	GGTGCTGGCTATCCTGTTGTGTCTGACAGGGGCGTTGTGTAGGCTGGAGCTGCTTC
P310	*acrD* inactivation reverse primer	AAGCGGCGACGTATCAGCACGAAAAACAGGGGTACAGGGAATTAGCCATGGTCCAT
P334	M13 forward primer for checking cloning insert in pHSG398	CAGGAAACAGCTATGAC
P335	M13 reverse primer for checking cloning insert in pHSG398	GTAAAACGACGGCCAGT
P336	Forward primer for cloning *acrD* into pHSG398 with the *Bam*HI site	CGCGGATCCCATTATCTCCTTTATTTCTCC
P337	Reverse primer for cloning *acrD* into pHSG398 with the *Sph*I site	CGCGCATGCTTATTTCGGGCGCGGCTTCAG
P340	Forward primer for cloning *acrA* into pACYC177 with the *Sca*I site	CGCAGTACTATGTCGGTGAATTTACAGGCG
P341	Reverse primer for cloning *acrA* into pACYC177 with the *Bam*HI site	CGCGGATCCGTCTTAACGGCTCCTGTTTAA
P342	Forward primer for cloning *acrE* into pACYC177 with the *trc* promoter and *Sca*I site	GCGCAGTACTGAGCTG**TTGACAATTAATCATCCGGCTCGTATAATG**TGTGGAATTTTAAG GAACAGTAATGACG

Table 2.3 (continued). List of primers used for generating gene knockouts, checking sizes of genes and for cloning of inserts.

Primer no.	Description	Sequence (5'-3')
P343	Reverse primer for cloning *acrE* into pACYC177 with the *Bam*HI site	GCGCGGATCCCCTTATTGCGCCGTTTTCGC
P451	Forward primer for checking the insert in pACYC177	CGGTTCGGTTTATTGACGAC
P452	Reverse primer for checking *acrA* in pACYC177	GCAGCAATGGGTTTAAGGAC
P453	Reverse primer for checking *acrE* in pACYC177	CTTACTGTCATGCCATCCG
P546	Reverse primer for cloning *acrAB* into pET-20b (+) with the *Bam*HI site	GGGGGGGATCCTCAGCGATGTTCTGTCGAAT
P666	Forward primer for sequencing the middle region of *acrB*	CCTGTTCCTGCAGAACTTC
P667	Reverse primer for sequencing the middle region of *acrB*	CAATAGTCGGAATCAACGTC
P668	Forward primer for sequencing the end region of *acrB*	TGGTCTTCGCCTTTAACCTG
P669	Reverse primer for sequencing the end region of *acrB*	AATCAACTCGAAGTCAAAGC

Sequences highlighted in yellow correspond to 20 bp of homology to the *aph* gene.
Sequence in bold corresponds to the *trc* promoter.

2.2.3 Plasmid purification

A single bacterial colony was picked from a fresh plate and inoculated into 5 mL LB broth supplemented with the appropriate antibiotics. The next day, cells were harvested by centrifugation at 4,000×*g* for 10 minutes. Plasmid was purified using the QIAprep Spin Miniprep Kit (Qiagen, Germany) according to the manufacturer's instructions. The quality and concentration of purified plasmids was determined using Qubit™ dsDNA Broad Range Assay Kit (Invitrogen, USA) as per manufacturer's instructions.

2.2.4 Preparation of electrocompetent cells

A single bacterial colony was inoculated into 5 mL LB broth supplemented with appropriate antibiotics where necessary and incubated overnight at 37°C with shaking. The next day, 4 mL of the overnight culture was inoculated into 50 mL of LB broth supplemented with appropriate antibiotics and incubated at 37°C with shaking for 2 hours until the optical density at a wavelength of 600 nm (OD_{600}) reached 0.6. Cells were harvested by centrifugation at 4,000 × *g* for 10 minutes at 4°C and re-suspended in 50 mL of 15% ice-cold glycerol to wash. The washing process was repeated twice and after the final centrifugation step, the cell pellet was re-suspended in 200 µL of 15% ice-cold glycerol and kept on ice for immediate use or stored at -80°C.

2.2.5 Electroporation

A 43 µL volume of competent cells and 2 µL of DNA (50-100 ng) was added to a pre-cooled 0.2 cm electroporation cuvette (Geneflow, UK). A negative control consisting of competent cells and no DNA was also prepared. Electroporation was carried out at 2.5 kV (25 µF, 200 Ω) using an Eppendorf Eporator (Thermo Fisher Scientific, USA). Immediately after

electroporation, 400 µL of pre-warmed LB broth was added to the cell mixture, which was incubated at 37℃ for 1 hour with aeration. Following incubation, 100 µL of the recovered cells was spread onto LB agar plates supplemented with appropriate antibiotics. The remaining cells were pelleted at 4,000 × *g* for 5 min and re-suspended in 100 µL of LB broth and spread onto an LB agar plate supplemented with appropriate antibiotics. The agar plates were incubated at 37℃ overnight and observed for growth the next day.

2.2.6 DNA sequencing of plasmids and PCR products

Purified plasmids and PCR products were sequenced by Eurofins Genomics (Eurofins Scientific, Germany). PCR products were prepared by diluting to a final concentration of 10 ng/µL in 15 µL of UltraPure™ DNase/RNase-free distilled water and containing 10 µM of either the forward or reverse check primer (Table 2.2). Plasmids were diluted in 15 µL of UltraPure™ DNase/RNase-free distilled water to a final concentration of 50-100 ng/µL and sequenced using standard sequencing primers available from Eurofins Genomics. The sequencing data were aligned to the wild-type SL1344 gene sequence using MEGA11 software (Tamura *et al.*, 2021).

2.2.7 Determination of antimicrobial susceptibility

The antimicrobial susceptibility of various antibiotics and dyes (Appendix I) was determined using the agar dilution method according to Clinical & Laboratory Standards Institute guidelines (CLSI, 2020). For every compound tested, fresh stock solutions were made on the day of use. Appropriate volumes of the compound stock solutions were pipetted into sterile universal containers, along with 20 mL of Iso-Sensitest agar (Oxoid, UK) cooled to 50°C. The compound and agar were mixed by gentle swirling, poured into labelled 100 mm square petri

dishes (Thermo Fisher Scientific, USA) and allowed to set. The plates were dried for 15 minutes at 60°C. Overnight cultures of the test strains were diluted 1:100 with LB to give appropriately 1×10^7 CFU/mL and a multipoint inoculator was used to print 1 μL onto each agar plate to give approximately 1×10^4 CFU/spot. The plates were allowed to dry at room temperature before being incubated overnight at 37°C. The minimum inhibitory concentration (MIC) was defined as the lowest concentration of a drug that inhibited visible growth of a micro-organism after overnight incubation. *E. coli* ATCC 25922 (Table 2.1) was used as a reference quality control strain. Data obtained from antimicrobial susceptibility experiments were only accepted if the MIC values for *E. coli* ATCC 25922 were within the range published by the European Committee on Antimicrobial Susceptibility Testing (EUCAST, 2021).

2.2.8 Growth kinetic assays

For each strain tested, a single colony was inoculated into 5 mL LB broth supplemented with appropriate antibiotics where necessary and incubated at 37°C overnight with aeration. The overnight cultures (~1×10^9 CFU/mL) were diluted 1:100 into LB broth with antibiotic to give approximately 1×10^7 CFU/mL of cells. 180 μL of LB broth with antibiotic was dispensed into the wells of a flat 96 well plate. A 20 μL volume of the diluted cultures were dispensed into the wells containing LB broth with antibiotic to give a final starting inoculum of approximately 10^6 CFU/mL. For each experiment, growth of each strain was also monitored in just LB broth without antibiotics. Growth was monitored by measuring the optical density at 600 nm every 10 minutes for 12 hours at 37°C with aeration in a FLUOstar OPTIMA plate reader (BMG Labtech, Germany). Each strain for a particular antibiotic was tested at least three times and each repeat included three technical replicates. To calculate the generation times, the OD_{600} values from the start and end of the exponential growth phase was multiplied by 1×10^6 to obtain

an estimate of the total number of bacteria per well. The following formula used to calculate generation times:

$$\text{Generation time (min)} = \frac{\text{Time interval from start to end of exponential phase}}{3.3 \times \log\left(\frac{\text{Number of bacteria at the end of exponential phase}}{\text{Number of bacteria at the start of exponential phase}}\right)}$$

2.3 Disruption of genes in *Salmonella* Typhimurium

Efflux genes of interest were disrupted using the protocol described by Datsenko & Wanner (2000) and Chan *et al*. (2007a). This method is used to disrupt chromosomal genes through homologous recombination with PCR products that contain the *aph* gene, which encodes a protein that confers resistance to kanamycin. The recombination step relies on the phage lambda red recombination system, which is encoded by pSIM18, an inducible and easily curable plasmid. Initially, the *aph* gene was amplified from the pKD4 plasmid using primers which had 40 bp of homology to the gene of interest. The recipient strain, containing the pSIM18 plasmid (Chan *et al.*, 2007a), was transformed with the PCR construct. The lambda red recombination system mediates homologous recombination to disrupt the chromosomal gene of interest with the *aph* gene. Mutants with the disrupted gene of interest are then screened by growing on LB agar containing 50 μg/mL kanamycin (Datsenko and Wanner, 2000).

2.3.1 Generation of the PCR product for gene inactivation

The pKD4 plasmid was purified from *E. coli* BW1125 pKD4 (EC10, Table 2.1) as described above in Section 2.2.3. PCR product was amplified using the pKD4 plasmid as template with an annealing temperature of 55°C, before being purified after excision from the agarose gel and quantified as described above in Section 2.2.2.

2.3.2 Transformation of *Salmonella* Typhimurium containing pSIM18 with the PCR construct

A single colony of the *S.* Typhimurium SL1344 strain containing the lambda red recombinase system on the pSIM18 plasmid (SE67, Table 2.1) was inoculated into 5 mL LB broth with 150 µg/mL hygromycin and incubated overnight at 30°C with aeration. The next day, 4 mL of the overnight culture was inoculated into 50 mL of LB broth supplemented with 150 µg/mL hygromycin and incubated at 30°C with shaking for 2 hours until OD_{600} reached 0.6. Cells were heat-shocked at 42°C for 15 minutes and then immediately cooled on ice for 10 minutes. Thereafter, electrocompetent cells were prepared as described in Section 2.2.4. The PCR product for gene inactivation was transformed into electrocompetent cells as described in Section 2.2.5 and selected on LB plates supplemented with 50 µg/mL kanamycin.

2.3.3 Verification of gene disruption in candidate colonies

Several candidate recombinant colonies were sub-cultured on LB agar plates supplemented with 50 µg/mL kanamycin and incubated overnight at 37°C. Bacterial cell lysates of the candidate recombinant colonies were prepared as described in Section 2.2.1. PCR was carried out to check the size of disrupted gene of interest and for the presence of the *aph* gene as described in Section 2.2.2, with an annealing temperature of 51°C. Recombinant colonies were verified by the presence of a PCR fragment corresponding to the size of the gene of interest with an *aph* insertion, which was purified after excision from the agarose gel and quantified as described in Section 2.2.2. Candidates with the correct sized PCR fragment were verified by sequencing the upstream and downstream regions of the disrupted gene as described in Section 2.2.6.

2.3.4 Removal of the *aph* gene using the pCP20 plasmid

The pCP20 plasmid was purified from the *S.* Typhimurium SL1344 with pCP20 strain (SE160, Table 2.1) as described in Section 2.2.3. Electrocompetent cells of the strain with the *aph* inactivated gene of interest was prepared as described in Section 2.2.4. Electroporation was carried out to transform pCP20 into electrocompetent cells as described in Section 2.2.5, using a recovery and incubation temperature of 30℃. Candidate colonies were sub-cultured on 50 μg/mL ampicillin LB agar plates. To cure the pCP20 plasmid, single colonies were inoculated into 10 mL of LB broth and grown overnight at 43℃ with shaking. A loop of overnight culture was streaked onto LB agar plates and incubated at 37℃. Colonies were screened for the loss of the *aph* gene and loss of the pCP20 plasmid by streaking onto plates of LB agar, LB agar with 50 μg/mL ampicillin, and LB agar with 50 μg/mL kanamycin. Candidates that only grew on LB were selected. Candidates were screened by PCR to confirm the loss of the *aph* cassette, and the size of the disrupted region as described in Section 2.2.3.

2.3.5 Disruption of multiple genes in *Salmonella* Typhimurium

Multiple gene knockouts were generated by transforming the pSIM18 plasmid into an existing knockout strain and repeating the methodology described above to produce double, triple, and quadruple gene knockouts. Previous knockouts were confirmed through PCR to ensure there was no reinsertion of the *aph* gene into an existing FRT scar.

2.4 Ethidium bromide efflux assay

Efflux of ethidium bromide (EtBr) was measured as described previously (Smith and Blair, 2014). For each strain tested, a single colony was inoculated into 5 mL LB broth supplemented

with appropriate antibiotics where necessary and incubated overnight at 37°C with aeration. The next day, overnight cultures were subcultured at 4% in 10 mL of fresh LB broth, with antibiotics where necessary, until OD_{600} reached 0.4. Cells were harvested by centrifugation at 3000 x *g* for 10 minutes at 23°C. The cell pellet was re-suspended in 20 mM potassium phosphate buffer (PPB) with 1 mM magnesium chloride, and the OD_{600} was adjusted to 0.2. 100 μM carbonyl cyanide 3-chlorophenylhydrazone (CCCP) and 50 μg/mL of EtBr was added to 10 mL of OD_{600} adjusted culture and incubated at 23°C for 1 hour. Following incubation, the bacterial suspensions were harvested by centrifugation and re-suspended in 10 mL of 20 mM PPB with 1 mM magnesium chloride and 190 μL was loaded into a black 96 well plate (Greiner, UK). The FLUOstar OPTIMA (BMG Labtech, Germany) was used to inject 10 μL of a 20% glucose solution into each test well (1% final concentration). Fluorescence intensity was measured over 2 hours at excitation and emission wavelengths of 544 and 590 nm, respectively. Each strain was tested in three biological replicates on separate occasions. The mean time taken for EtBr fluorescence to decrease by 25% was compared to the WT complement strain using one-way analysis of variance (ANOVA). Dunnett's test was used to correct for multiple comparisons. Only *P* values ≤0.05 were significant.

2.5 Doxorubicin efflux assay

Efflux of doxorubicin was measured as described previously (Nishino and Yamaguchi, 2001, Blair *et al.*, 2015a) with modifications. For each strain tested, a single colony was inoculated into 5 mL LB broth supplemented with appropriate antibiotics where necessary and incubated at 37°C overnight with aeration. The next day, overnight cultures were subcultured at 4% in 10 mL of fresh LB broth, with antibiotics where necessary, until OD_{600} reached 0.5-0.6. Cells were pelleted by centrifugation at 3,000 × *g* for 10 minutes at 23°C and re-suspended in 20 mM

PPB with 5 mM magnesium chloride. The wash step was repeated twice to remove residual salts from the LB broth. 100 μM CCCP and 20 μM of doxorubicin was added to 10 mL of cell suspension and incubated at 37°C for 1 hour with aeration. Following incubation, the cells were pelleted by centrifugation and re-suspended in 1 mL of 20 mM PPB with 5 mM magnesium chloride. The wash step was repeated twice to remove residual doxorubicin in the supernatant. 190 μL of cells was loaded into a black 96 well plate (Greiner, UK). The FLUOstar OPTIMA plate reader (BMG Labtech, Germany) was used to inject 10 μL of a 20% glucose solution into each test well (1% final concentration). Fluorescence intensity was measured over 30 minutes at excitation and emission wavelengths of 485 and 620-10 nm, respectively. Each strain was tested in three biological replicates on separate occasions.

2.6 Site directed mutagenesis (SDM)

Mutations in AcrA were generated in the plasmid pET-20b *acrA* (Table 2.2). Mutations in both AcrA and AcrB were generated in the plasmid pET-20b *acrAB* (Table 2.2.). Mutations in AcrE were generated in the plasmid pTrcHis2 *acrE* (Table 2.2). All site-directed mutagenesis (SDM) reactions were carried out using the QuikChange Lightning SDM Kit (Agilent, USA) according to the manufacturer's instructions. Primers were designed to incorporate the desired base changes in the middle of the primer with at least 8 non-overlapping bases at the 3' end (Appendix II).

The PCR cycling conditions consisted of initial denaturation at 95°C for 2 minutes, followed by 18 cycles of denaturation at 95°C for 20 seconds, annealing at 60°C for 10 seconds and elongation at 68°C for 3 minutes for AcrA and AcrE SDM and 8 minutes for AcrAB SDM, with a final elongation step at 68°C for 5 minutes. When the PCR cycle was complete, reactions

were cooled on ice before addition of 2 µL of *Dpn*I (Agilent, USA) and incubation at 37°C for 1 hour. A 5 µL volume of *Dpn*I-digested DNA was transformed into *E. coli* XL10-Gold® ultracompetent cells (Agilent, USA) according to the manufacturer's instructions. After recovery, 200 µL of cells were spread onto LB agar with 50 µg/mL ampicillin and incubated overnight at 37°C.

2.6.1 Validation of SDM

Approximately 100 colonies were obtained for each SDM reaction, of which four were picked for further analysis. Plasmids were purified and sequenced as described in Section 2.2.3 and Section 2.2.6, respectively. The sequencing data were aligned to the wild-type sequence using the MEGA11 software (Tamura *et al.*, 2021) to verify the desired point mutation and to ensure there were no unwanted secondary mutations.

2.7 Overexpression of *acrD* and *acrA* or *acrE* in the same *Salmonella* Typhimurium cell

To overexpress *acrD* in the same cell as either *acrA* or *acrE*, different cloning strategies were required. The pHSG398 (Fig. 2.1) and pACYC177 (Fig. 2.2) vectors were used to overexpress *acrD* and *acrA*, respectively, as described previously (Yamasaki *et al.*, 2011). pHSG398 is a high copy number plasmid used for the overexpression of genes under the control of the *lac* promoter (Takeshita *et al.*, 1987). pACYC177 is a low copy number plasmid used for gene expression with an ampicillin and a kanamycin resistance gene (Chang and Cohen, 1978). The *acrE* gene has been previously reported to be repressed by H-NS under basal conditions (Nishino *et al.*, 2009). Therefore, to clone *acrE* into pACYC177 and obtain sufficient expression, a forward primer (P342) was designed containing the *trc* promoter and the *acrE* ribosomal binding site (Table 2.2). The synthetic *trc* promoter is a hybrid derived from the *E.*

coli trp and *lac*UV5 promoters and it drives high level transcription (Tegel *et al.*, 2011). Both pHSG398 and pACYC177 can be co-transformed into a single cell since they have compatible origins of replication, thereby enabling co-expression of *acrD* with *acrA* or *acrE*.

2.7.1 Generating an *acrD* cloning amplicon

The *acrD* gene was amplified from the *S.* Typhimurium SL1344 genome by PCR using primers P336 and P337 (Table 2.3) to introduce *Bam*HI and *Sph*I restriction sites. The reactions consisted of 25 µL 2×Phusion High-Fidelity Master Mix with HF Buffer (New England BioLabs, USA), 0.5 µM P336 and P337 primers (Table 2.2), 1.5 µL DMSO (New England BioLabs, USA), 1 µL cell lysate, and UltraPure™ DNase/RNase-free distilled water to a final volume of 50 µL. The PCR cycling conditions consisted of initial denaturation at 98°C for 30 seconds, followed by 30 cycles of denaturation at 98°C for 10 seconds, annealing at 61°C for 30 seconds and elongation at 72°C for 3 minutes, with a final elongation step at 72°C for 10 minutes. The PCR product was separated on an agarose gel, and the fragment corresponding to the size of *acrD* was purified after excision from the agarose gel and quantified as described in Section 2.2.2. Purified *acrD* cloning amplicon was stored at -20°C.

2.7.2 Generating *acrA* and *acrE* cloning amplicons

The *acrA* gene was amplified from the *S.* Typhimurium SL1344 genome by PCR using primers P338 and P339 (Table 2.3) to introduce *Sca*I and *Bam*HI restriction sites. The PCR amplicon included 141 bp upstream of *acrA*, containing its native promoter, and 22 bp downstream of *acrA* (Hirakawa *et al.*, 2008). The *acrE* gene was amplified from *S.* Typhimurium SL1344 genome by PCR using the primers P340 and P341 (Table 2.3). The PCR amplicon included the *trc* promoter and a region 14 bp upstream to 2 bp downstream of *acrE*.

The PCR for generating the *acrA* and *acrE* cloning amplicons was prepared as described in Section 2.7.1 using primer pairs P338 and P339, and P340 and P341, respectively (Table 2.3). The cycling conditions were the same as Section 2.7.1 except that the annealing time was reduced to 15 seconds and the elongation time was reduced to 1 minute. PCR fragments corresponding to the size of *acrA,* and *acrE* was purified after excision from the agarose gel and quantified as described in Section 2.2.2.

2.7.3 Restriction digest reactions

FastDigest restriction enzymes (Thermo Fisher Scientific, USA) were used at a concentration of 10 U/µL, according to the manufacturer's instructions. Reactions consisted of 1 µg of plasmid DNA or cloning amplicon, 5 µL of 10×reaction buffer, 1 µL of each restriction enzyme, and UltraPure™ DNase/RNase-free distilled water to a final volume of 50 µL. Undigested and single digest plasmid controls were also included. Samples were incubated at 37°C for 1 hour. Plasmid DNA which had been digested with two enzymes was treated with 1 µL of calf intestinal phosphatase (New England BioLabs, USA) and incubated for a further hour at 37°C. After digestion, cloning amplicon was purified using a QIAquick PCR Purification Kit (Qiagen, Germany) and plasmid DNA was separated on a 1% (w/v) agarose gel by electrophoresis at 80 V for 1 hour and 30 minutes. The band corresponding to the double cut plasmid was purified after excision from the agarose gel and quantified as described in Section 2.2.2.

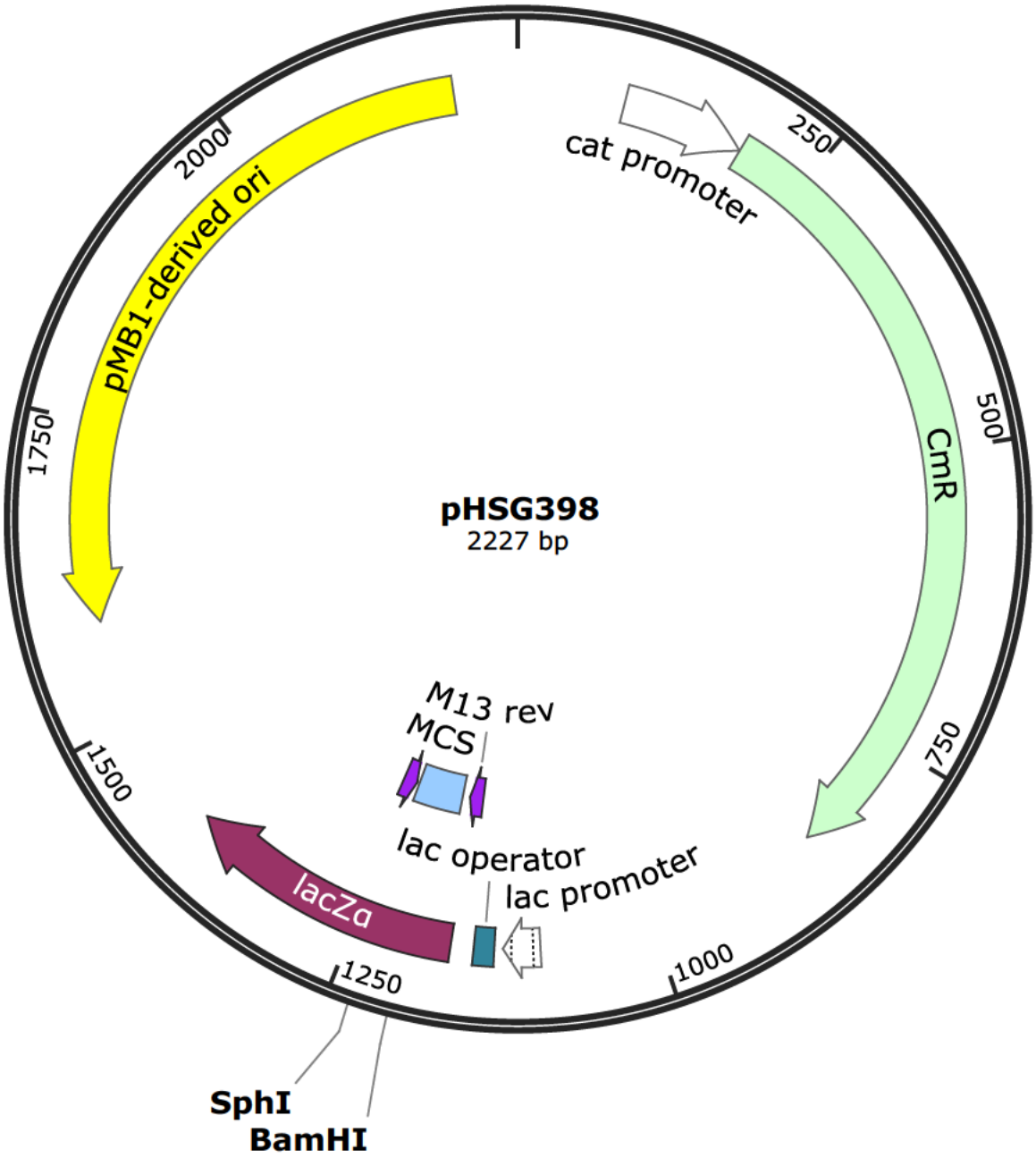


Figure 2.1. pHSG398 vector map.

The pHSG398 plasmid expresses inserted genes from the lac promoter. pMB1-derived ori, pMB1-derived origin of replication; CmR, chloramphenicol resistance gene; MCS, multiple cloning sites. Cloned genes can be sequenced using the M13 forward and reverse primers. Only Bam*HI* and Sph*I* restriction sites have been shown for clarity. Figure obtained from SnapGene® software (from GSL Biotech; available at snapgene.com)

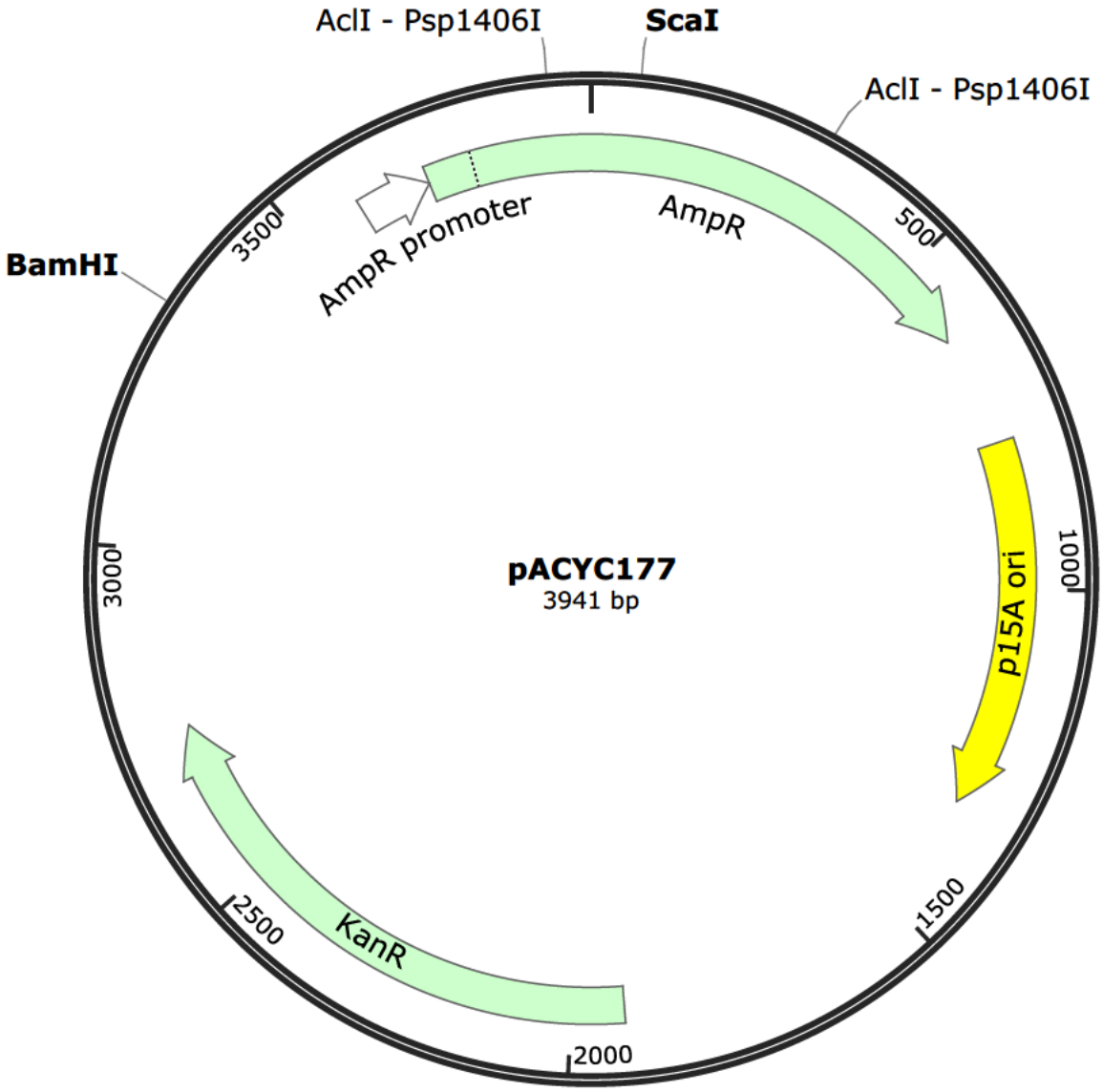


Figure 2.2. pACYC177 vector map.

The pACYC177 plasmid is a low copy number plasmid vector compatible for co-transformation with pHSG398. p15 ori, p15 origin of replication; AmpR, ampicillin resistance gene; KanR, kanamycin resistance gene. Only the restriction sites used in this study have been shown for clarity. Figure obtained from SnapGene® software (from GSL Biotech; available at snapgene.com).

2.7.4 Ligation reactions

To ligate the double cut plasmid and the cloning amplicon, a 3:1 ratio of insert to vector was used. Ligation reactions consisted of 1 µL T4 DNA ligase (New England BioLabs, USA), 2 µL of 10×T4 DNA ligase buffer, 3:1 ratio of insert to 20 ng vector, and UltraPure™ DNase/RNase-free distilled water to total volume of 20 µL. A background control of vector and no insert was also included. Samples were incubated overnight at 16°C. The next day, samples were heat inactivated at 65°C for 10 minutes. Samples were stored at -20°C until required for transformation reactions.

2.7.5 Transformation of ligation products

NEB® 5-alpha competent *E. coli* cells (New England BioLabs, USA) were transformed with 5 µL of each ligation reaction according to the manufacturer's instructions. Selection plates were warmed to 37°C and 100 µL of recovered cells were spread onto them and incubated at 37°C. Four colonies were randomly selected for verification of successful cloning.

2.7.6 Verification of cloning

Cloning candidates were checked for the gene of interest by colony PCR and sequencing. Bacterial cell lysates were prepared as described in Section 2.2.1. PCR was carried out to check for the insertion of *acrD,* and *acrA* or *acrE,* in the cloning site of pHSG398 and pACYC177, respectively, as described in Section 2.2.2. Plasmids were purified and sequenced as described in Sections 2.2.3 and 2.2.6, respectively. The sequencing data were aligned to the wild-type SL1344 *acrD*, *acrA* or *acrE* sequences to verify successful cloning and to ensure there were no mutations.

2.7.7 Generating the pACYC177Kan^R control plasmid

The pACYC177 plasmid has an ampicillin and kanamycin resistance marker. The *acrA* or *acrE* genes were cloned into a site within the ampicillin resistance gene, thereby inactivating it. Therefore, to obtain a control pACYC177 plasmid (pACYC177Kan^R) possessing solely a kanamycin resistance marker, the plasmid was cut at the two *Psp*1406I sites within the ampicillin resistance gene (Fig. 2.2) and self-ligated as described previously (Yamasaki *et al.*, 2011).

pACYC177 was purified from *E. coli* 1200 with pACYC177 (EC164, Table 2.1) as described in Section 2.2.3 before being digested with FastDigest *Psp*1406I (Thermo Scientific, USA), an isoschizomer of *Acl*I, as described above in Section 2.6.3. An uncut plasmid control was also included. The samples were separated on a 1% (w/v) agarose gel through electrophoresis at 80 V for 1 hour and 30 minutes. The *Psp*1406I enzyme was expected to cut pACYC177 at two sites to produce two fragments: 3568 bp and 373 bp. The larger fragment was purified after excision from the agarose gel and quantified as described in Section 2.2.2. Thereafter, the plasmid fragment was self-ligated using T4 DNA ligase and transformed into NEB® 5-alpha competent *E. coli* cells as described above in Sections 2.6.4 and 2.6.5, respectively. pACYC177Kan^R was purified and sequenced as described in Sections 2.2.3 and 2.2.6, respectively. The sequencing data were aligned to the sequence of the intact pACYC177 plasmid to verify the loss of a 373 bp chunk within the ampicillin resistance gene.

2.8 Cloning of *acrAB* into pET-20b (+)

The *acrAB* operon was amplified from the *S.* Typhimurium SL1344 genome by PCR using primers P56 and P546 (Table 2.2) to introduce flanking *Nde*I and *Bam*HI restriction sites. The

PCR for generating the *acrAB* cloning amplicon was prepared as described in Section 2.7. The cycling conditions were the same as Section 2.7.1 except that the annealing step was carried out at 55.7°C for 20 seconds and the extension step was increased to 4 minutes. PCR fragment corresponding to the size of *acrAB* was purified after excision from the agarose gel and quantified as described in Section 2.2.2. The *acrAB* cloning amplicon and the pET-20b (+) (Fig. 2.3) plasmid was digested with the *Nde*I and *Bam*HI restriction enzymes and ligated as described in Sections 2.7.3 and 2.7.4, respectively. The resulting ligation product was transformed into NEB® 5-alpha competent *E. coli* cells as described in Section 2.7.5. pET-20b *acrAB* was isolated from candidate colonies and sequenced using T7, T7 terminal, P666, P667, P668 and P669 primers (Table 2.3) as described in Sections 2.2.3 and 2.2.6, respectively.

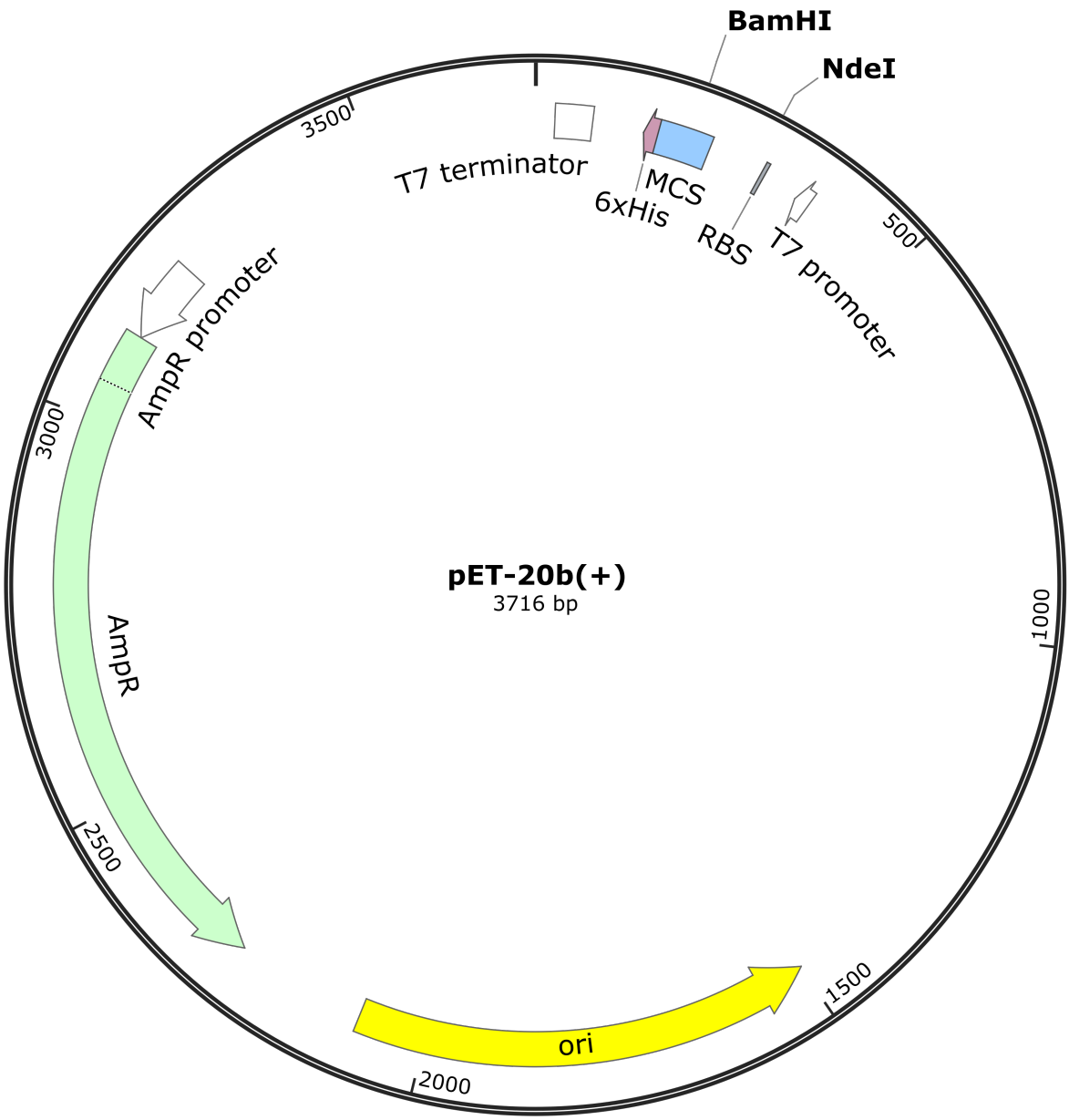


Figure 2.3. pET-20b (+) vector map.

The pET-20b (+) plasmid is a high copy number plasmid vector. AmpR, ampicillin resistance gene; MCS, multiple cloning site; ori, pBR322 origin of replication. Only the restriction sites used in this study have been shown for clarity. Figure obtained from SnapGene® software (from GSL Biotech; available at snapgene.com).

2.9 Western blotting

2.9.1 Preparation of membrane fractions

A single colony of each strain to be tested was inoculated into 5 mL LB broth supplemented with 50 µg/mL ampicillin and incubated overnight at 37°C with aeration. Next day, 50 mL LB broth supplemented with 50 µg/mL ampicillin was inoculated with 800 µL of overnight culture (4% inoculum) and grown to an OD_{600} of 0.5-0.6 without induction. Cells were pelleted at 3,000 × *g* for 10 minutes at 4°C and resuspended in 800 µL of ice-cold lysis buffer (10 mM Tris-HCl, 1 mM disodium EDTA (Sigma-Aldrich, Germany), pH 8.0, cOmplete™ EDTA-Free Protease Inhibitor Cocktail (Roche, Switzerland)). Lysozyme (Sigma-Aldrich, Germany) was added to cell suspension at a final concentration of 100 µg/mL and incubated on ice for 30 minutes. Cells were disrupted by sonication on ice; ten pulses of 10 seconds, with 30 seconds rest in between. Unbroken cells were pelleted by centrifugation at 2,500 × *g* for 5 minutes at 4°C. Supernatant containing total protein was pelleted at 22,500 × *g* for 1 hour at 4°C. The resulting pellet containing total membrane proteins was resuspended in 800 µL of ice-cold lysis buffer. Total protein concentration of each membrane preparation was determined using the Qubit™ Protein Assay Kit (Invitrogen, USA) on a Qubit 4 fluorometer (Invitrogen, USA) as per manufacturer's instructions.

2.9.2 Western blotting

Each membrane preparation was normalised to a concentration of 1 mg/mL in lysis buffer. For each sample, 20 µg of protein was mixed with 5 µL of 5×Protein Loading Buffer (National Diagnostics, USA) and boiled at 95°C for 10 minutes. A 25 µL volume of denatured protein samples were loaded onto an 12% SDS-PAGE gel for AcrA and AcrE or 8% SDS-PAGE gel for AcrB along with PageRuler™ Prestained Protein Ladder (Thermo Scientific, USA) as

molecular weight marker. Electrophoresis was carried out in Tris-Glycine-SDS running buffer (25 mM Tris, 192 mM glycine and 0.1% SDS, pH 8.6) (National Diagnostics, USA) at 140 V for 1 hour.

For Western blotting, proteins were transferred to a PVDF membrane (Roche, Germany) by electrophoresis at constant 320 mA for 25 minutes in a Mini Trans-Blot® cell unit (Bio-Rad, USA) filled with ice-cold transfer buffer (25 mM Tris, pH 8.3, 192 mM glycine, with 20% methanol) (National Diagnostics, USA). The membrane was blocked with PBST-M (phosphate-buffered saline, 0.05% Tween® 20 (Promega, UK), 5% w/v skimmed milk powder (Sigma-Aldrich, Germany)) for 1 hour at room temperature on a tube roller. After blocking, the membrane was incubated with anti-6x His tag HRP-conjugated monoclonal antibody (Invitrogen, USA) diluted 1:5000 in PBST-M for 1 hour at room temperature on a tube roller. The PVDF membrane was washed with PBST (phosphate-buffered saline, 0.05% Tween® 20) three times for 5 minutes at room temperature with gentle shaking. Following the last wash, the membrane was gently patted dry on a paper towel to remove excess PBST. To detect His-tagged proteins, the membrane was flooded with Clarity Western ECL Substrate (Bio-Rad, USA) and placed in a clear plastic film to prevent the membrane from drying out. The chemiluminescent signal was detected with the Amersham Imager 680 (Cytiva, USA) using the Chemiluminescence with colorimetric marker imaging method.

2.10 *Galleria mellonella* infection model of *in vivo* virulence

The larva of the greater wax moth *Galleria mellonella* was purchased from Livefood UK Ltd. Upon arrival, the larvae were checked for signs of melanisation, and any larvae with signs of visible melanisation were discarded. Discarded or deceased larvae were stored at -20℃ to

induce stupor and death. Thereafter, the dead larvae were disposed of as clinical waste. The larvae were stored at 15℃ in darkness and used within a week.

For each strain tested, a single colony was inoculated into 5 mL LB broth supplemented with appropriate antibiotics where necessary and incubated at 37℃ overnight with aeration. The next day, overnight cultures were diluted to an OD_{600} of 0.1 (~1×10^8 CFU) in 1 mL of sterile Dulbecco's phosphate-buffered saline (PBS) (Sigma-Aldrich, Germany). A volume of 50 µL from the 0.1 OD_{600} adjusted cells was dispensed into 950 µL of PBS to give approximately 5×10^6 CFU/mL.

The '*Galleria* Grabber', a wet sponge in a bulldog clip, was used to restrain the larvae and prevent movement during injection (Dalton *et al.*, 2017). Each larva was placed into the *Galleria* Grabber with its underside facing upwards. Each larva was injected in its third segment from the tail with a 20 µL volume of 5×10^6 CFU/mL cells using a 0.5 mL BD micro-fine 29G fixed 12.7 mm needle (BD, USA). This resulted in a final dose of 1×10^5 CFU/larva. As vehicle control, 20 µL of sterile PBS was injected. For each strain tested and the vehicle control, 15 larvae were injected and placed into a sterile petri dish filled with squares of white tissue as food and shelter. Plates were placed into a large secure plastic container with damp tissue to prevent the larvae from drying out. Plates were incubated at 37℃ and checked every 24 hours to see how many larvae were dead or alive. Dead larvae often displayed complete melanisation and cessation of movement. However, non-melanised larvae were also checked by gentle prodding using a sterile loop. Any larvae that displayed slight movement upon prodding were considered alive and any larvae that failed to display movement was considered dead.

CHAPTER 3. Defining the interactions between periplasmic adaptor protein AcrA and the RND-transporter AcrB in *Salmonella* Typhimurium

CHAPTER 3. Defining the interactions between periplasmic adaptor protein AcrA and the RND-transporter AcrB in *Salmonella* Typhimurium

3.1 Background

In tripartite RND efflux complexes, the role of the periplasmic adaptor protein (PAP) in the assembly of tripartite efflux complexes and the identities of specific residues involved in PAP-RND binding remain poorly understood. Recent high-resolution crystal structures of AcrAB-TolC and other tripartite RND pumps have allowed insight into the interactions between the inner membrane RND-transporter and the PAP. The PAPs bind to RND-transporters in a 2:1 stoichiometry, resulting in two PAP protomers binding to one RND-transporter (termed PAP1 and PAP2) at different semi-equivalent binding sites with slightly different specificities and affinities (Wang *et al.*, 2017, Shi *et al.*, 2019, Glavier *et al.*, 2020, Chen *et al.*, 2021). Work conducted in this laboratory in collaboration with Prof Vassiliy Bavro at the University of Essex used the high-resolution structures of tripartite efflux complexes to predict 3D sites on the PAP surface that are involved in PAP-RND binding (McNeil *et al.*, 2019). This prediction was based on the established promiscuity of AcrA and AcrE, which was used to look for conserved residues between the two PAPs that could drive this promiscuity. Multiple sequence alignment of the four *S.* Typhimurium SL1344 PAPs revealed that the four 3D sites are coded for by nine discrete linear binding sequences termed 'binding boxes' within each PAP sequence (Fig. 3.1). AcrA and AcrE are virtually identical across the identified binding boxes while MdsA and MdtA, which function with the significantly divergent RND-transporters MdsB and MdtB/C respectively, are substantially different within the predicted binding sites (McNeil *et al.*, 2019). Analysis of these binding sequences has enabled a predictive model of PAP-RND interaction, which could explain the promiscuity between AcrA and AcrE. Here, the role of binding boxes

in PAP-RND interaction will be investigated by site-directed mutagenesis. Subsequently, the impact of the mutations on efflux function will be measured using EtBr efflux assays and antimicrobial susceptibility.

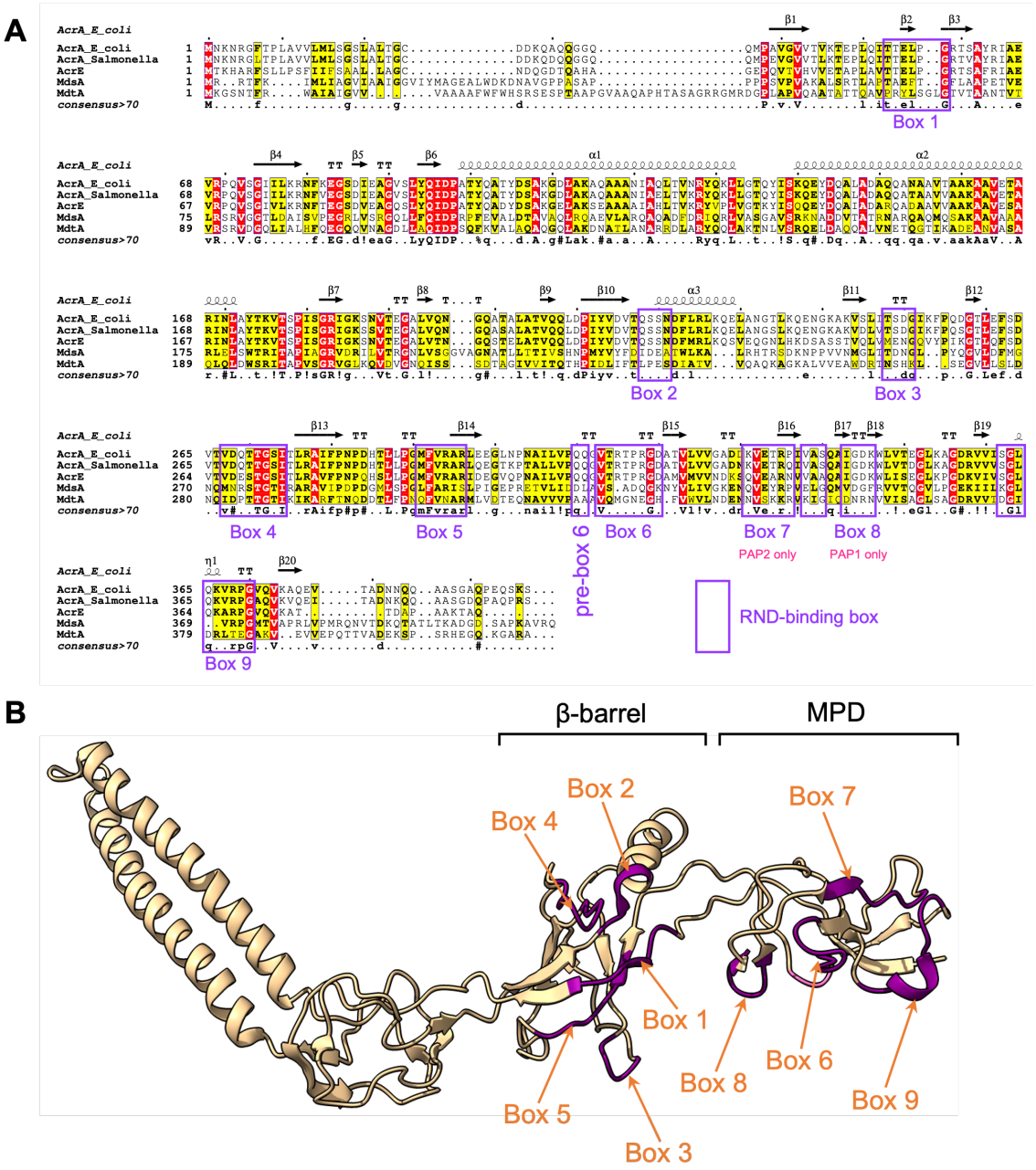


Figure 3.1. The predicted 3D binding sites of AcrA correspond to linear stretches of highly conserved residues.

A) Multiple sequence alignment of the four *Salmonella* Typhimurium SL1344 periplasmic adaptor proteins AcrA, AcrE, MdtA and MdsA with structural alignment of AcrA from *Escherichia coli* O157:H7 (PDB 5O66, chain G of AcrAB-TolC) (Wang *et al.*, 2017). The sequences of the periplasmic adaptor proteins are conserved within the *Salmonella* serovars. Conserved residues are highlighted in red. The predicted binding boxes are annotated from 1 to 9 and indicated with purple rectangles. **B)** Mapping of the predicted binding boxes onto the structure of AcrA (PDB 5O66, chain G). Chain G refers to one of the six identical AcrA protomers within the crystal structure of the AcrAB-TolC pump. MPD, membrane-proximal domain.

3.2 Aims

- To disrupt the predicted binding boxes of AcrA using disruptive site-directed mutagenesis.
- To test the phenotypic effects of the AcrA point mutations.
- To refine the binding box model by producing conservative mutations to identify the most critical PAP residues involved in RND-binding.
- To confirm that AcrA mutants are stably expressed by Western blotting.

3.3 Hypotheses

- Disruptive mutagenesis of PAP residues mapping to the binding boxes will disrupt RND-binding and result in impaired active efflux.
- Conservative mutations in the most critical residues will show a significant impairment of active efflux.

3.4 Defining the binding box model of PAP-RND interactions

Previously, analysis of cryo-EM data of the assembled AcrA-AcrB complexes has defined the possible PAP residues involved in interaction with RND-transporters. The regions of the PAP-RND transporter contact have been found to be compact and discrete. Homology modelling and sequence analysis of the four RND-associated PAPs in *S.* Typhimurium (AcrA, AcrE, MdtA and MdsA) has shown that these regions are highly conserved between AcrA and AcrE but divergent in both MdtA and MdsA.

To confirm that the predicted AcrA residues are indeed involved in binding to AcrB, the most conserved residues between AcrA and AcrE in each binding box (Fig 3.1) (McNeil *et al.*, 2019)

were selected for disruptive mutagenesis. Point mutations in AcrA were produced in pET-20b *acrA*, a high copy number plasmid allowing leaky expression of wild type *acrA* in *S.* Typhimurium cells (McNeil *et al.*, 2019). A set of 15 different AcrA point mutations in pET-20b *acrA* (gift from Dr Ricardo Corona Torres, University of Essex) mapping to binding boxes 1 to 9 was transformed individually into an *S.* Typhimurium strain in which all four PAPs had been deleted. This strain will be referred to as the Δ4PAP strain and lacks the four RND-associated PAPs (*acrA*, *acrE*, *mdtA* and *mdsA*), allowing the effect of the AcrA point mutations on AcrB-binding to be tested (McNeil *et al.*, 2019). These AcrA mutations were produced to target at least one residue in each of the 9 predicted binding boxes. Moreover, the point mutations were designed to be disruptive to interrupt any potential binding interactions between AcrA and AcrB.

The phenotypic impact of mutations was assessed by EtBr efflux assays and antimicrobial susceptibility testing. EtBr is a substrate of the AcrAB-TolC pump that fluoresces only when bound to DNA. Hence, its fluorescence is higher when intracellular than extracellular. Cells are preloaded with EtBr by temporarily inhibiting oxidative phosphorylation by the addition of carbonyl cyanide *m*-chlorophenyl hydrazone (CCCP) (Paixao *et al.*, 2009). CCCP is an ionophore that irreversibly binds to protons and dissipates the periplasmic proton gradient, thus depleting the proton motive force (PMF) (Mitchell, 2011). The PMF powers all RND efflux pumps, therefore CCCP can be used to arrest active efflux (Paulsen *et al.*, 1996). Following incubation with EtBr and CCCP, the CCCP is washed away, and the EtBr loaded cells are re-energised with glucose to resume efflux. The product of glucose metabolism is electron carrier molecules NADH and $FADH_2$, which feed into the electron transport chain. The movement of electrons through the electron transport chain is coupled to the flow of protons from the

cytoplasm to the periplasmic space, thus restoring the PMF (Kaila and Wikstrom, 2021). The active efflux of EtBr causes a decrease in EtBr fluorescence over time. The efflux efficiency of each strain was determined by calculating the time taken for peak EtBr fluorescence to decrease by 25%. Strains with efficient efflux are expected to export EtBr more quickly, whereas strains with impaired efflux would take longer to export EtBr.

In this study, the *S.* Typhimurium SL1344 strain was used because the role of RND efflux pumps in drug resistance phenotypes has been extensively studied (Eaves *et al.*, 2004, Buckley *et al.*, 2006, Blair *et al.*, 2009, Blair *et al.*, 2015b, Buckner *et al.*, 2016, Wang-Kan *et al.*, 2017). Moreover, *S.* Typhimurium SL1344 is a virulent strain (Wray and Sojka, 1978), thus allowing the effect of efflux on *in vitro* and *in vivo* virulence to be studied. The wild type (WT) SL1344 and the Δ4PAP (Δ*acrA* Δ*acrE* Δ*mdtA* Δ*mdsA*) strains were used as controls as they have defined efflux profiles. The WT strain possesses all RND efflux pumps, whereas the Δ4PAP strain lacks all four RND-associated PAPs and previous work has shown that strains lacking multiple PAPs have reduced efflux and are more susceptible to antimicrobials (McNeil *et al.*, 2019). In the WT strain, it took 4.6 minutes for the peak EtBr fluorescence to decrease by 25%, whereas the Δ4PAP strain took significantly longer (12.3 minutes) (Fig. 3.2). The Δ4PAP strain complemented with pET-20b *acrA* (WT AcrA complement) restored EtBr efflux level to that of the WT strain, indicating sufficient expression of *acrA* from the pET-20b vector. Compared to the WT complement, the G58F (box 1), T270F-T271F (box 4), G272P-S273P (box 4), F292G (box 5), R294F (box 5), and G363F (box 9) AcrA mutations significantly increased the time taken for EtBr to be exported (Fig. 3.2). Furthermore, antimicrobial susceptibility testing supported the EtBr efflux assay results; AcrA mutations that impaired EtBr efflux displayed greater than two-fold lower MIC values to AcrB-substrates, including acriflavine,

chloramphenicol, crystal violet, EtBr, erythromycin, fusidic acid, methylene blue, novobiocin and rhodamine 6G, compared to WT AcrA complement (Table 3.1). As a non-AcrB-substrate, streptomycin MIC values did not differ between the WT and the Δ4PAP strain (Table 3.1). These data show that mutations mapping to binding boxes 1, 4, 5 and 9 impact efflux, whereas mutations mapping to binding boxes 2, 3, 6, 7 and 8 did not alter efflux.

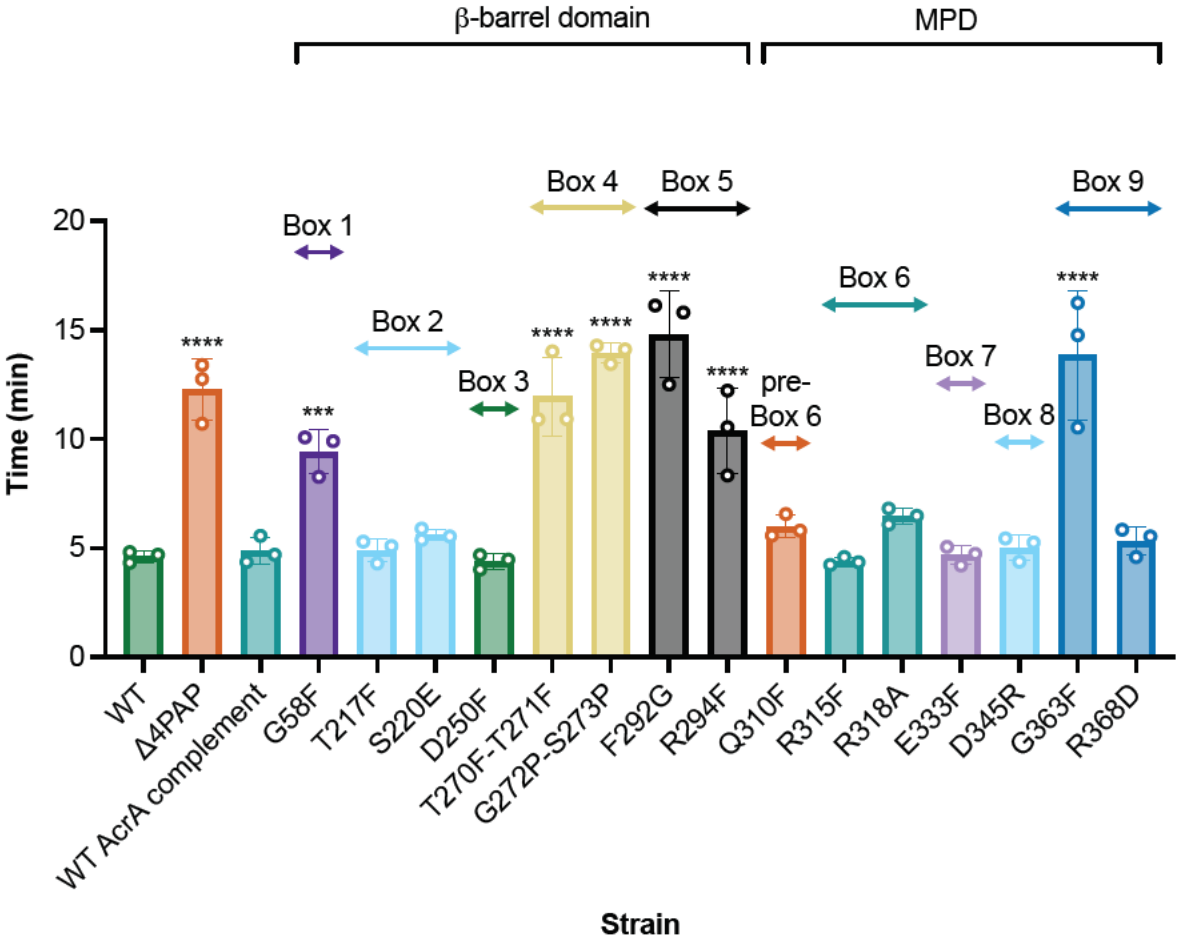


Figure 3.2. Efflux of ethidium bromide by the *Salmonella* Typhimurium SL1344 Δ4PAP strain carrying plasmid with different versions of AcrA.

Bacteria were treated with ethidium bromide and the proton-motive force dissipator CCCP for 1 hour and then re-energised with glucose. Annotation above indicates the mapping of each mutation to its binding box, as well as the domain mapping of respective boxes. All RND-binding boxes mapped to the β-barrel domain or the membrane proximal domain (MPD) since these are the only AcrA domains predicted to interact with AcrB. WT AcrA complement refers to the Δ4PAP complemented with pET-20b *acrA*. Data presented are the mean of three biological replicates and are shown as the time taken for the ethidium bromide fluorescence to decrease by 25% ± standard deviation. Each point mutation was compared to the WT AcrA complement using one-way ANOVA, followed by Dunnett's test to correct for multiple comparisons. Strains with significantly different efflux rates to the WT AcrA complement are indicated with *** ($P \leq 0.001$) or **** ($P \leq 0.0001$).

Table 3.1. Antimicrobial susceptibility of the *Salmonella* Typhimurium SL1344 Δ4PAP strain carrying plasmid with different versions of AcrA.

		MIC (μg/mL)									
Strain	**Box no.**	ACR	CHL	CV	EtBr	ERY	FA	MB	NOV	R6G	STR
WT		128	4	64	>1024	128	>1024	>1024	512	>1024	4
Δ4PAP		**16**	**1**	**4**	**32**	**16**	**8**	**16**	**2**	**8**	4
The following rows are Δ4PAP background strain + pET-20b carrying different versions of AcrA											
WT AcrA complement		64	4	16	512	128	512	256	128	256	4
G58F AcrA	**1**	**16**	**1**	**4**	**16**	**8**	**8**	**16**	**4**	**8**	4
T217F AcrA	2	64	4	16	512	128	512	256	256	256	4
S220E AcrA	2	64	2	16	512	128	512	256	128	256	4
D250F AcrA	3	64	4	16	512	128	512	256	128	256	4
T270F-T271F AcrA	**4**	**16**	**1**	**4**	**32**	**8**	**8**	**32**	**2**	**16**	4
G272P-S273P AcrA	**4**	**16**	**1**	**4**	**16**	**8**	**8**	**16**	**2**	**8**	4
F292G AcrA	**5**	**16**	**1**	**4**	**32**	**8**	**8**	**32**	**4**	**16**	4
R294F AcrA	**5**	**16**	**1**	**4**	**32**	**8**	**8**	**16**	**2**	**8**	4
Q310F AcrA	6	64	2	16	512	128	512	256	64	256	4
R315F AcrA	6	64	2	16	512	128	512	256	128	256	4
R318A AcrA	6	64	2	16	512	128	512	256	64	256	4
E333F AcrA	7	64	2	16	512	128	512	256	128	256	4
D345R AcrA	8	64	2	16	512	128	512	256	128	256	4
G363F AcrA	**9**	**16**	**1**	**4**	**64**	**8**	**8**	**32**	**4**	**16**	4
R368D AcrA	9	64	2	16	512	128	512	256	128	256	4

Underlined values highlight values for the Δ4PAP strain complemented with pET-20b *acrA* (WT AcrA complement). Box no. indicates the mapping of the mutation to its binding box. Bold values indicate two-fold or more differences compared to the parent strain. Strains coloured in red indicate AcrA mutations that caused impaired EtBr efflux. Drug abbreviations: ACR, acriflavine; CHL, chloramphenicol; CV, crystal violet; EtBr, ethidium bromide; ERY, erythromycin; FA, fusidic acid; MB, methylene blue; NOV, novobiocin; R6G, rhodamine 6G; STR; streptomycin.

3.5 Refining the binding box model of PAP-RND interactions

The initial set of AcrA mutants highlighted the importance of binding boxes 1, 4, 5 and 9 in RND-binding (Fig. 3.2). To narrow down which are the most critical residues within these boxes, more subtle and conservative mutations were produced to identify the PAP-residues most important for RND-binding. Specifically, residues that were previously shown to be important for RND-binding (Fig. 3.2) were mutated to residues with similar properties, while residues in binding boxes 6, 7 and 9, the previous mutation of which led to limited or no functional impact were subjected to more disruptive mutagenesis. The AcrA mutations produced for the refinement of the binding box model and the rationale for producing each mutation are listed in Table 3.2. The location of the residues mutated for the refinement of the binding box model is shown in Figure 3.3. The new set of mutated versions of AcrA was expressed in the Δ4PAP strain. The effect of the mutations on efflux function was assessed using EtBr efflux assays, antimicrobial susceptibility testing and the *Galleria mellonella* infection model.

Table 3.2. List of AcrA mutations produced for the refinement of the binding box model of PAP-RND interactions and the rationale for producing the mutations.

Mutation (s)	Rationale for mutation (s)
R59A	• R59 is conserved between AcrA and AcrE and is in proximity to Q797 of AcrB • Produce R59A to disrupt this interaction by replacing the positively charged and polar arginine residue with a nonpolar and aliphatic alanine residue
T270A, T270D, T271A, T271D	• T270F-T271F mapping to box 4 abrogated active efflux • Produce T270A and T271A as conservative mutations by replacing the slightly polar and uncharged threonine residues with nonpolar yet uncharged alanine residues • Produce T270D and T271D as disruptive mutations by replacing threonine with negatively charged aspartate residues
G272A-S273A	• G272P-S273P mapping to box 4 was disruptive due to rigidification of the flexible glycine-serine loop • Produce G272A-S273A as a conservative mutation by replacing the small glycine and serine residues with similar small alanine residues
G272F, S273F	• G272P-S273P double mutation separated into G272F and S273F as disruptive mutations to elucidate which of the two residues plays a more important role in efflux function • Produce G272F and S273F as disruptive mutations by replacing the small glycine and serine residues with bulky and hydrophobic phenylalanine residues
I274D	• I274 is highly conserved between AcrA, AcrE, MdtA and MdsA • Produce I274D as a disruptive mutation by replacing the aliphatic and hydrophobic isoleucine residue with a negatively charged and polar aspartate residue
F292V	• F292G mapping to box 5 was a disruptive mutation • Produce F292V as a conservative mutation by replacing the bulky and hydrophobic phenylalanine residue with a slightly smaller yet hydrophobic valine residue
Q310P-Q311P	• The β-hairpin of the AcrB protruding loop responsible for oligomerisation is encountering Q310-Q311 of AcrA • Produce Q310P-Q311P to disrupt the interaction by replacing the polar glutamine residues with small and hydrophobic proline residues
Q311F	• Q310P-Q311P abrogated efflux function • Produce Q311F as a disruptive mutation by replacing the polar glutamine residue with an aromatic and hydrophobic phenylalanine residue to elucidate which of Q310-Q311 is critical

Table 3.2 (continued). List of AcrA mutations produced for the refinement of the binding box model of PAP-RND interactions and the rationale for producing the mutations.

Mutation (s)	Rationale for mutation (s)
P317G, P317F, R318F	• Residues mapping to box 6 appear to make extensive contacts with the RND-transporter (McNeil *et al.*, 2019) • Produce P317G and P317F as disruptive mutations by replacing the small and rigid proline residue with a flexible glycine residue or a bulky and hydrophobic phenylalanine residue, respectively • Produce R318F as a disruptive mutation by replacing the positively charged and polar arginine residue with an aromatic and hydrophobic phenylalanine residue
I343F-G344F, K346A	• D345R mapping to box 8 did not impact efflux function • Produce I343F-G344F as a disruptive mutation by replacing the aliphatic isoleucine and glycine residues with aromatic and bulky phenylalanine residues • Produce K346A as a disruptive mutation by replacing the positively charged and polar lysine residue with an uncharged and nonpolar alanine residue
Q365F, K366D, R368F, R368A	• G363F mapping to box 9 impaired efflux function • Produce Q365F as a disruptive mutation by replacing the polar glutamine residue with an aromatic and hydrophobic phenylalanine residue • Produce K366D as a disruptive mutation by replacing the positively charged lysine residue with as a negatively charged aspartate residue • Produce R368F and R368A by replacing the positively charged and polar arginine residues with an aromatic and hydrophobic phenylalanine residue or an aliphatic and hydrophobic alanine residue

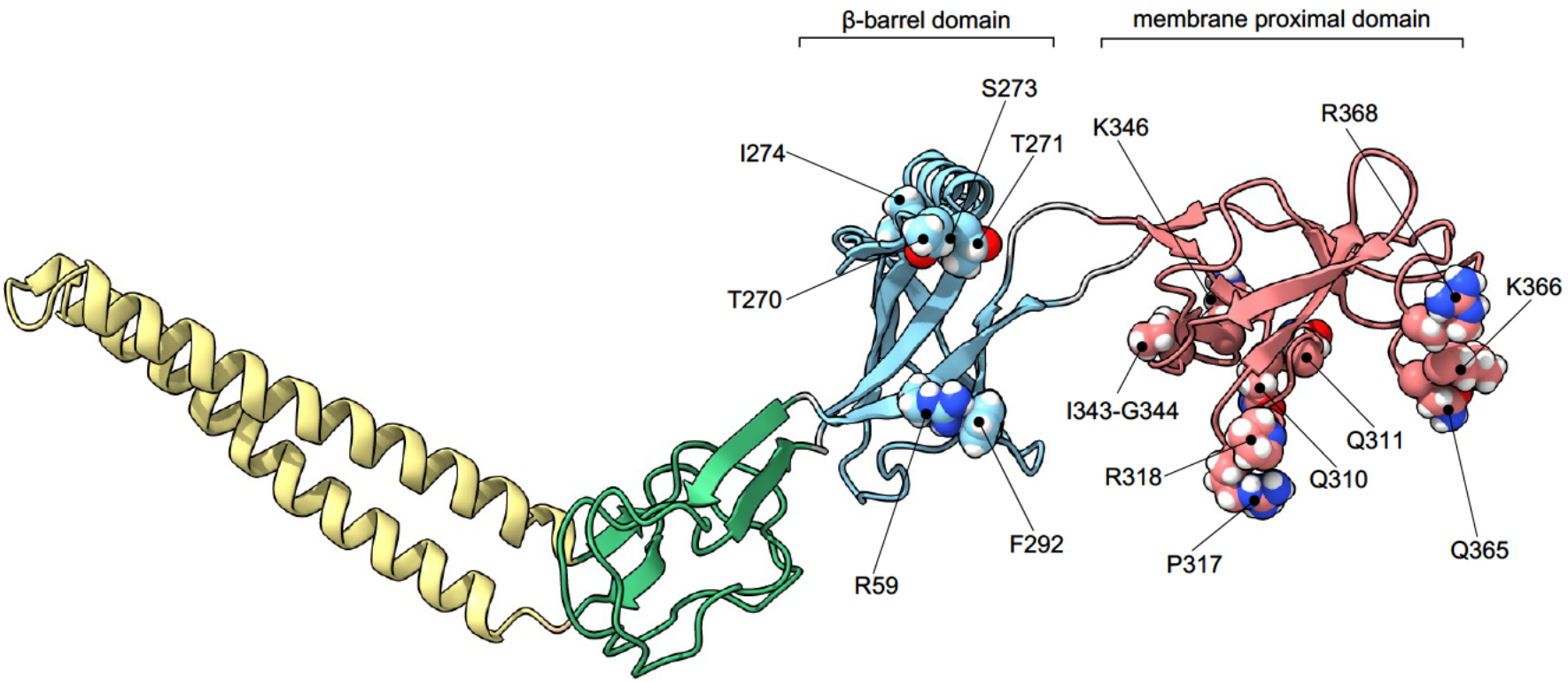


Figure 3.3. The structure of AcrA labelled with the residues selected for mutagenesis to refine the binding box model.

The colouring corresponds to the individual domains of AcrA: α-hairpin (yellow), lipoyl (green), β-barrel (turquoise), and membrane proximal (coral). The residues selected for mutagenesis are restricted to the β-barrel and membrane proximal domains. Figure produced using ChimeraX (Pettersen *et al.*, 2021).

3.5.1 Impact of disruptive mutations mapping to binding boxes 6, 7 and 9

The Q310-Q310 residues mapping to box 6 of PAP1 form a loop that is predicted to interact with the protruding loop of AcrB. In Section 3.4, the Q310F mutation did not have an observable effect on efflux function (Fig. 3.2 and Table 3.1), therefore, Q311F was produced and tested. Glutamine is a polar residue, so a radical replacement with the aromatic and hydrophobic phenylalanine residue is likely to disrupt interactions mediated by glutamine (Betts and Russell, 2003). However, the Q311F mutation had no impact on efflux function. Considering that both Q310-Q311 may interact with the protruding loop of AcrB, the Q310P-Q311P double mutant was produced to disrupt this interaction by replacing the polar glutamine residues with hydrophobic and rigid proline residues (Table 3.2). Compared to the WT AcrA complement, the Q310P-Q311P mutation significantly impaired active efflux (Fig. 3.4) and increased susceptibility to AcrB-substrates (Table 3.4). This data indicated that both Q310 and Q311 appear to play an important role in RND-binding.

The spatial arrangement of AcrA and AcrB in the crystal structure of AcrAB-TolC (Wang *et al.*, 2017) suggest that residues mapping to binding box 6 make extensive contacts with AcrB. However, the initial R315F and R318A mutations had no observable effect on efflux function (Fig. 3.2 and Table 3.1). Therefore, further disruptive mutations mapping to box 6 were produced to investigate whether other residues play a role in the efflux function of AcrA. However, the P317G, P317F and R318F mutations did not affect efflux function compared to WT AcrA complement (Fig. 3.4 and Table 3.3). Likewise, further disruptive mutations mapping to box 8 had no effect on efflux function (Fig. 3.4 and Table 3.3), suggesting that both boxes 6 and 8 are not critical for RND-binding. The G363F mutation mapping to box 9 was shown to significantly impair efflux function, therefore, further disruptive mutations mapping to box 9

were produced. However, the Q365F, K366D, R368F and R368A mutations did not have a significant impact on efflux function or antimicrobial susceptibility (Fig. 3.4 and Table 3.3). Interestingly, the impact of the K366D mutation was substrate dependent. The K366D AcrA mutation did not affect EtBr efflux (Fig. 3.4) nor susceptibility to tested dyes, including acriflavine, crystal violet, EtBr, methylene blue and rhodamine 6G (Table 3.3). However, the K366D AcrA mutation conferred a two-fold or more decrease in MIC values to other AcrB-substrates, such as clindamycin, doxorubicin, erythromycin, fusidic acid and novobiocin (Table 3.3). The significance of this surprising result will be further explored in Chapter 4. The data here suggest that residues mapping to binding boxes 6, 7 and 9 do not play an active role in RND-binding.

3.5.2 Impact of mutations mapping to binding boxes 1, 4 and 5

Like G58F, the R59A mutation mapping to box 1 displayed intermediate impairment of EtBr efflux and increased susceptibility to AcrB-substrates (Fig. 3.4 and Table 3.3). This indicated that box 1 plays a critical role in the efflux function of AcrA. The disruptive T270F-T271F double mutation mapping to box 4 was separated to identify which of the residues was critical for efflux function. The T270A and T270D mutations had no effect on EtBr efflux or antimicrobial susceptibility (Fig. 3.4 and Table 3.3). However, the conservative T271A mutation displayed mild impairment of EtBr efflux and the disruptive T271D mutation completely abolished EtBr efflux (Fig. 3.4 and Table 3.3). This highlighted the critical role of T271 in efflux function. The conservative G272A-S273A double mutation mapping to box 4 had no effect on EtBr efflux or antimicrobial susceptibility, however, the previous G272P-S273P mutation had a significant impact on efflux function (Fig. 3.4 and Table 3.3). Hence, the G272P-S273P mutation was separated into G272F and S273F mutations to identify which of

the two residues were critical for efflux function. The G272F mutation had no observable effect on efflux function, however, the S273F mutation abrogated EtBr efflux and significantly increased susceptibility to AcrB-substrates (Fig. 3.4 and Table 3.3). This indicated that S273 plays a critical role in efflux function, whereas G272 had no major role. The I274D mutation mapping to box 4 also completely abolished EtBr efflux and increased susceptibility to AcrB-substrates (Fig. 3.4 and Table 3.3). These data showed that mutations mapping to box 4 severely abrogated efflux function, highlighting the critical role of T271, S273 and I274 in the function of AcrA. Compared to the disruptive F292G mutation, the conservative F292V mutation mapping to box 5 still abolished EtBr efflux and significantly increased susceptibility to AcrB-substrates (Fig. 3.4 and Table 3.3), highlighting the critical role of F292. Taken together, the data here suggest that residues mapping to binding boxes 1, 4 and 5 play an important role in the efflux function of AcrA.

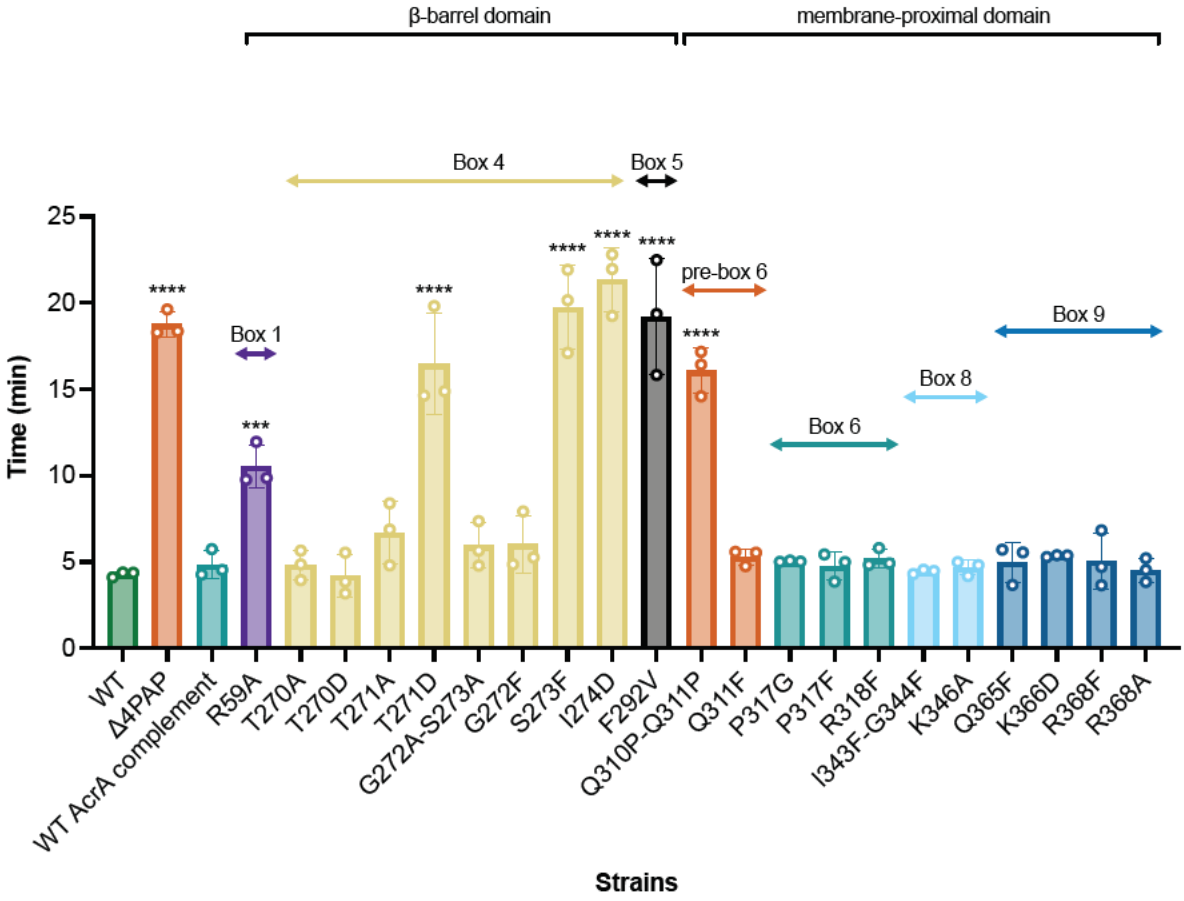


Figure 3.4. Refinement of the RND-binding box model to identify the most critical AcrA residues.

Bacteria were treated with ethidium bromide and the proton-motive force dissipator CCCP for 1 hour and then re-energised with glucose. Annotation above indicates the mapping of each mutation to its binding box, as well as the domain mapping of respective boxes. All RND-binding boxes map to either the β-barrel domain or the membrane proximal domain as these are the only AcrA domains predicted to interact with AcrB. WT AcrA complement refers to the Δ4PAP complemented with pET-20b *acrA*. Data presented are the mean of three biological replicates and are shown as the time taken for ethidium bromide fluorescence to decrease by 25% ± standard deviation. Each point mutation was compared to the WT AcrA complement using one-way ANOVA, followed by Dunnett's test to correct for multiple comparisons. Strains with significantly efflux rates to the WT AcrA complement are indicated with *** ($P \leq 0.001$) or **** ($P \leq 0.0001$).

Table 3.3. Antimicrobial susceptibility of the *Salmonella* Typhimurium SL1344 Δ4PAP strain carrying plasmid with different versions of AcrA to refine the binding box model.

		MIC (μg/mL)										
Strain	**Box no.**	ACR	CLI	CV	DOX	EtBr	ERY	FA	MB	NOV	R6G	STR
WT		256	256	64	512	>1024	128	1024	>1024	512	>1024	8
Δ4PAP		16	2	2	2	16	2	4	8	1	8	4
The following rows are Δ4PAP background strain + pET-20b carrying different versions of AcrA												
WT AcrA complement		64	128	16	64	128	64	256	128	128	128	4
R59A AcrA	1	**16**	**2**	**2**	**2**	**32**	**2**	**4**	**16**	**2**	**16**	8
T270A AcrA	4	64	128	16	64	128	64	256	128	128	128	4
T270D AcrA	4	64	128	16	64	128	64	256	128	128	128	4
T271A AcrA	4	64	16	8	32	64	**8**	**64**	**32**	**8**	**32**	8
T271D AcrA	4	**16**	**2**	**2**	**2**	**16**	**2**	**4**	**8**	**1**	**8**	4
G272A-S273A AcrA	4	64	128	16	64	128	64	256	128	128	128	4
G272F AcrA	4	64	128	16	64	128	64	256	128	128	128	8
S273F AcrA	4	**16**	**2**	**2**	**2**	**16**	**2**	**4**	**8**	**2**	**8**	4
I274D AcrA	4	**16**	**2**	**2**	**2**	**16**	**4**	**4**	**8**	**1**	**8**	4
F292V AcrA	5	**16**	**2**	**2**	**2**	**16**	**2**	**4**	**8**	**1**	**8**	4
Q310P-Q311P AcrA	6	**16**	**2**	**2**	**2**	**16**	**2**	**4**	**8**	**1**	**8**	8
Q311F AcrA	6	64	128	16	64	64	64	128	128	64	128	4
P317G AcrA	6	64	128	16	64	64	64	128	128	128	128	4
P317F AcrA	6	64	128	16	64	128	64	256	128	128	128	8
R318F AcrA	6	64	128	16	64	128	64	256	128	128	128	4
I343F-G344F AcrA	8	64	128	16	64	128	64	256	128	128	128	4
K346A AcrA	8	64	128	16	64	128	64	256	128	128	128	4
Q365F AcrA	9	64	128	16	64	128	64	256	128	128	64	4
K366D AcrA	9	64	**16**	16	**16**	64	**16**	**16**	128	**16**	64	4
R368F AcrA	9	64	128	16	64	128	64	256	128	128	128	4

Underlined values highlight values for the Δ4PAP strain complemented with pET-20b *acrA* (WT AcrA complement). Box no. indicates the mapping of the mutation to its binding box. Bold values indicate two-fold or more differences compared to the parent strain. Strains coloured in red indicate AcrA mutations that caused impaired EtBr efflux. Drug abbreviations: ACR, acriflavine; CLI, clindamycin; CV, crystal violet; DOX, doxorubicin; EtBr, ethidium bromide; ERY, erythromycin; FA, fusidic acid; MB, methylene blue; NOV, novobiocin; R6G, rhodamine 6G; STR, streptomycin.

3.6 Effect of AcrA point mutations on the *in vivo* virulence of *Salmonella* Typhimurium SL1344

The AcrAB-TolC efflux pump has been shown in multiple studies to play a role in the virulence of *S.* Typhimurium. Inactivation or deletion of *acrA*, *acrB* or *tolC* has been reported to significantly attenuate the pathogenesis and virulence of *S.* Typhimurium in both *in vitro* and *in vivo* models of infection (Buckley *et al.*, 2006, Nishino *et al.*, 2006, Blair *et al.*, 2009, Wang-Kan *et al.*, 2017, McNeil *et al.*, 2019). Based on the established importance of the AcrAB-TolC efflux pump in the virulence of *S.* Typhimurium SL1344, the effect of several AcrA mutations on *in vivo* virulence was assessed using the *Galleria mellonella* infection model. The larva of the greater wax moth *G. mellonella* has been used and validated in numerous studies as an experimental model to study host-pathogen interactions (Pereira *et al.*, 2020). Importantly, the *G. mellonella* infection model has been used to study the *in vivo* virulence of *S.* Typhimurium (Viegas *et al.*, 2013, Bender *et al.*, 2013, McNeil *et al.*, 2019). Compared to mice or chicken, *G. mellonella* lacks an adaptive immune system (Tsai *et al.*, 2016). Hence, the *G. mellonella* infection model does not provide information on the impact of *S.* Typhimurium infection on adaptive immunity. However, *G. mellonella* possesses an innate immune response remarkably like that of humans, consisting of hemocytes (phagocytes of invertebrates), opsonins, and antimicrobial peptides (Tsai *et al.*, 2016). Furthermore, it is cheap, relatively high-throughput, and requires no ethical approval (Tsai *et al.*, 2016).

Initially, a dose of 1×10^4 colony forming units (CFU) per larvae was used to test the virulence of WT, Δ4PAP and WT AcrA complement *S.* Typhimurium SL1344 cells. As a vehicle control, 20 μL of sterile PBS was injected per larvae. Consistent with previous work, the Δ4PAP strain killed significantly fewer larvae after 3 days compared to the WT strain, confirming that a

functional AcrAB-TolC pump is required for virulence (Fig. 3.5A) (McNeil *et al.*, 2019). However, the Δ4PAP strain complemented with WT AcrA (WT AcrA complement) was not significantly different to the Δ4PAP, indicating a lack of phenotypic rescue (Fig. 3.5A). Therefore, the dose was increased to 1×10^6 CFU/larvae, however, this proved to be lethal as all larvae were dead after one day for all three strains tested (data not shown). Next, a dose of 1×10^5 CFU/larvae were tested to see if there was a difference between the Δ4PAP and WT AcrA complement strains. At this dose, the WT strain killed all the larvae after one day (Fig. 3.5B). However, the Δ4PAP strain killed significantly fewer larvae compared to WT AcrA complement after three days of incubation (Fig. 3.5B). Therefore, the effect of AcrA mutations was assessed using a dose of 1×10^5 CFU/larvae.

Since a functional AcrAB-TolC pump is required for the virulence of *S.* Typhimurium, the impact of several AcrA mutations on *in vivo* virulence was tested. The F292V and G363F mutations were selected as representative efflux defective AcrA mutations (Fig. 3.4 and Fig. 3.2, respectively). The Q311F and K366D mutations were selected as representative neutral AcrA mutations as they did not affect EtBr efflux (Fig. 3.4). Due to the high number of larvae required to test each strain per biological replicate, not all efflux impaired mutations could be tested. Compared to the WT AcrA complement strain, the Δ4PAP strain complemented with AcrA with the F292V and G363F AcrA point mutations killed significantly fewer larvae at the end of 3 days, indicating reduced virulence (Fig. 3.5C). This corroborated the EtBr efflux and antimicrobial susceptibility data, showing that mutations that interfere with the binding of AcrA to AcrB also altered the ability of *S.* Typhimurium to cause infection (Fig. 3.5C). Accordingly, the Δ4PAP strain complemented with AcrA with the Q311F and

K366D mutations were not significantly different to the WT AcrA complement strain in the *Galleria mellonella* infection model (Fig. 3.5C), indicating a lack of impact on virulence.

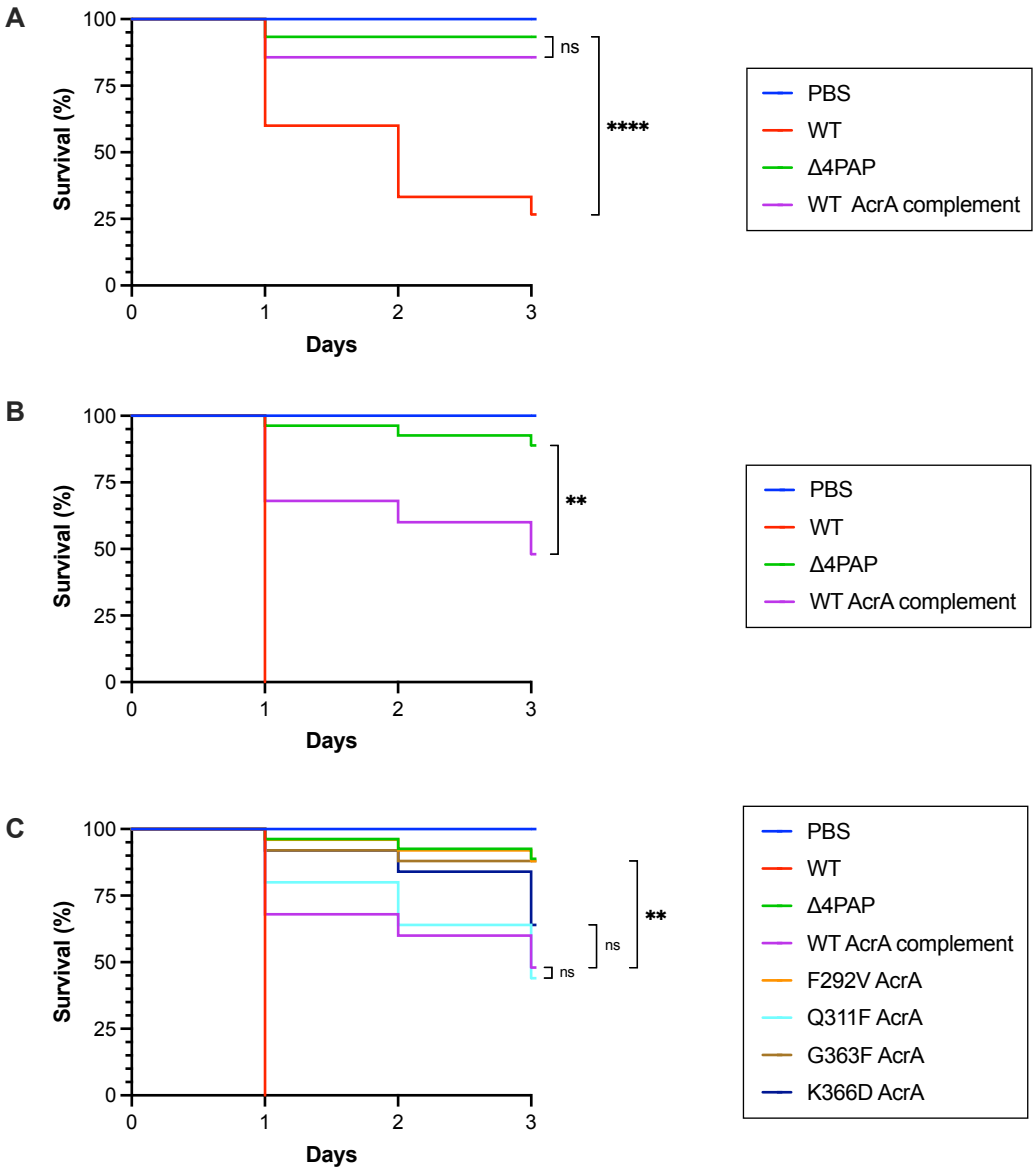


Figure 3.5. Effect of *Galleria mellonella* infection by different *Salmonella* Typhimurium SL1344 strains.

A) Kaplan-Meier survival curve of larvae after infection with *S.* Typhimurium wild type, Δ4PAP and WT AcrA complement with a dose of 1×10^4 CFU. WT AcrA complement refers to the Δ4PAP complemented with pET-20b *acrA*. **B)** Kaplan-Meier survival curve of larvae after infection with *S.* Typhimurium wild type, Δ4PAP and WT AcrA complement cells with a dose of 1×10^5 CFU. **C)** Kaplan-Meier survival curve of larvae after infection with *S.* Typhimurium Δ4PAP carrying plasmid with different versions of AcrA with a dose of 1×10^5 CFU. The results represent three independent experiments. Data were analysed using Logrank test to determine significance between pairs of strains and corrected for multiple comparisons using the Bonferroni method. Significantly different strains are indicated with ** ($P \leq 0.01$) or **** ($P \leq 0.0001$). ns, not significant.

3.7 Western blotting of AcrA mutant proteins

The stability of the AcrA mutations with impaired efflux were confirmed by Western blotting to ensure that the observed phenotypic impact was because of the mutations and not due to changes in protein expression or stability. Although the phenotypic assays were carried out using pET-20b *acrA*, the AcrA protein levels were quantified in the Δ4PAP strain with pTrcHis2 *acrA*, a high-copy number plasmid expressing the *acrA* gene with a C-terminal His-tag, thereby allowing detection with an anti-His (C-terminal)-HRP conjugated antibody. The expression of *acrA* from pET-20b is under the control of the T7 promoter, however, *S.* Typhimurium SL1344 lacks T7 RNA polymerase to drive high level of expression. Hence, expression of *acrA* from pET-20b was leaky but sufficient to restore efflux activity (Fig. 3.2 and Fig. 3.4). On the other hand, the expression of *acrA* from pTrcHis2 is driven by the *trc* promoter allowing high-level expression (Amann *et al.*, 1983, Smith and Blair, 2014). This was necessary to enable sufficient AcrA protein production for detection as leaky expression from pET-20b *acrA* was insufficient to allow detection with the anti-His (C-terminal)-HRP conjugated antibody. In agreement with previous studies (Ge *et al.*, 2009, McNeil *et al.*, 2019), the presence of a C-terminal His-tag did not affect the function of the AcrA protein as verified by antimicrobial susceptibility testing (Appendix III).

Membrane fractions of AcrA expressing cells were harvested and run on a 12% SDS-PAGE gel (20 µg protein) and transferred to a PVDF membrane. The membrane was blocked with skimmed milk, incubated with anti-His (C-terminal)-HRP conjugated antibody and imaged using chemiluminescence. The size of the *S.* Typhimurium SL1344 AcrA protein in pTrcHis2 *acrA* is ~46 kDa (kilodaltons), which was observed as a band between the 40 and 55 kDa marker bands (Fig. 3.6). The efflux impaired AcrA mutant proteins R59A, T271D, S273F, I274D,

F292V and Q310P-Q311P, all produced a band between the 40 and 55 kDa markers, confirming their stable expression (Fig. 3.6). Furthermore, the phenotypically neutral Q311F and K366D AcrA proteins also showed stable expression (Fig. 3.6). All the mutant AcrA proteins were expressed at least 92% of the level of WT AcrA, indicating their stable expression (Fig. 3.6).

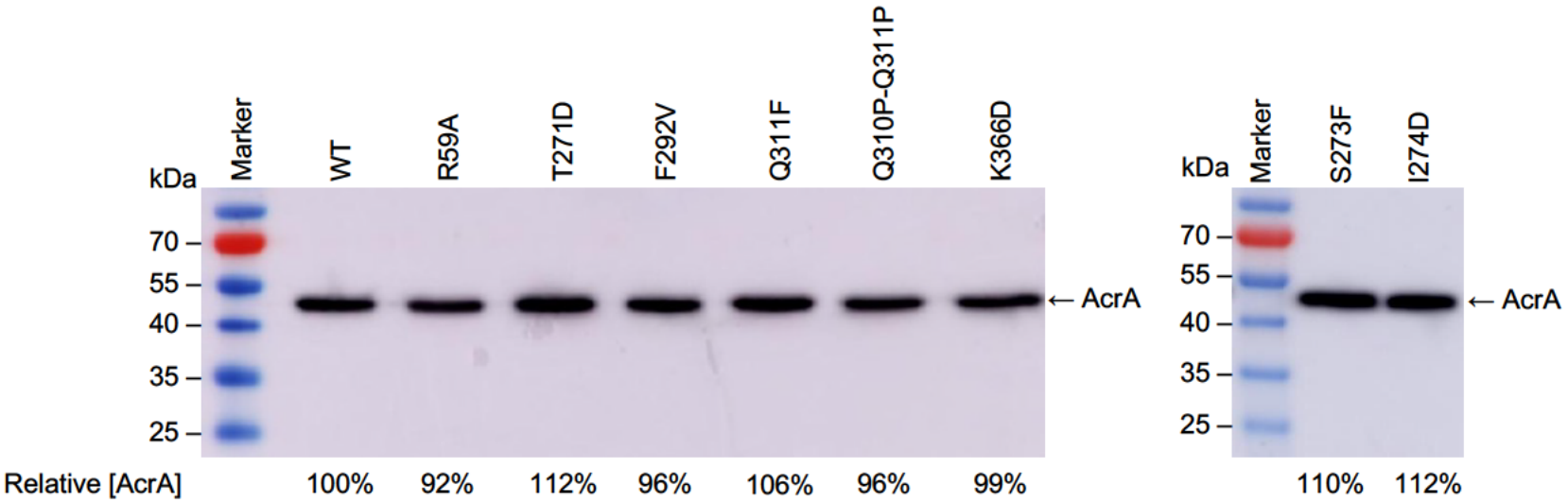


Figure 3.6. Western blotting of mutant AcrA.

Wild type and mutant AcrA were expressed in the *Salmonella* Typhimurium SL1344 Δ4PAP strain from pTrcHis2 *acrA* plasmids. Membrane fractions of AcrA expressing cells were harvested and separated on a 12% SDS-PAGE gel (20 µg protein) and transferred to a PVDF membrane. Western blotting was performed using an anti-His antibody, HRP-conjugated and imaged using chemiluminescence. The PageRuler Prestained Protein Ladder was used as a molecular weight marker. Band intensity was determined using ImageJ Version 2.1 (Schindelin *et al.*, 2012), which was used to assign a relative concentration of AcrA to each band, expressed in percentage of WT AcrA protein.

3.8 Discussion

The advances in structural understanding of the AcrAB-TolC pump have enabled insight into the complete assembly of tripartite efflux systems. Structures, such as the engineered *E. coli* AcrAB-TolC complex (Du *et al.*, 2014), disulphide-stabilised AcrAB-TolC complex (Wang *et al.*, 2017), and the recent *in situ* structure of AcrAB-TolC at subnanometer resolution (Chen *et al.*, 2021) have provided near-atomic resolution of the interactions within the pump. Importantly, these advances have allowed elucidation of the protein-protein interactions underlying the assembly of tripartite pumps. However, the specific residues involved in the interaction between the PAP and the RND-transporter have remained poorly understood.

Previous work conducted in this laboratory predicted four 3D sites involved in PAP-RND binding within each PAP protomer, which correspond to nine discrete linear binding sequences within the PAP sequence (McNeil *et al.*, 2019). The PAPs bind to RND-transporters in a 2:1 stoichiometry. This results in two protomers of the PAP binding to one protomer of the transporter at different semi-equivalent binding sites with slightly different specificities. Here, the two different PAP positions are referred to as PAP 1 and PAP2 (Fig. 3.7A) (Tikhonova *et al.*, 2011). Firstly, to corroborate the binding box model, several residues that were highly conserved between the four *Salmonella* PAPs mapping to each of the nine binding boxes of AcrA were mutated and the phenotypic impact of the mutations was tested in the Δ4PAP strain. Mutations mapping to binding boxes 1 (G58F), 4 (T270F-T271F and G272P-S273P) and 5 (F292G and R294F) were found to significantly impair efflux function (Fig. 3.8). This revealed that the binding site on the surface of the β-barrel domain of AcrA is critical for efflux function (Fig. 3.7B), which is consistent with the spatial arrangement of AcrA and AcrB in the crystal structures of the AcrAB-TolC complex (Chen *et al.*, 2021, Wang *et al.*, 2017).

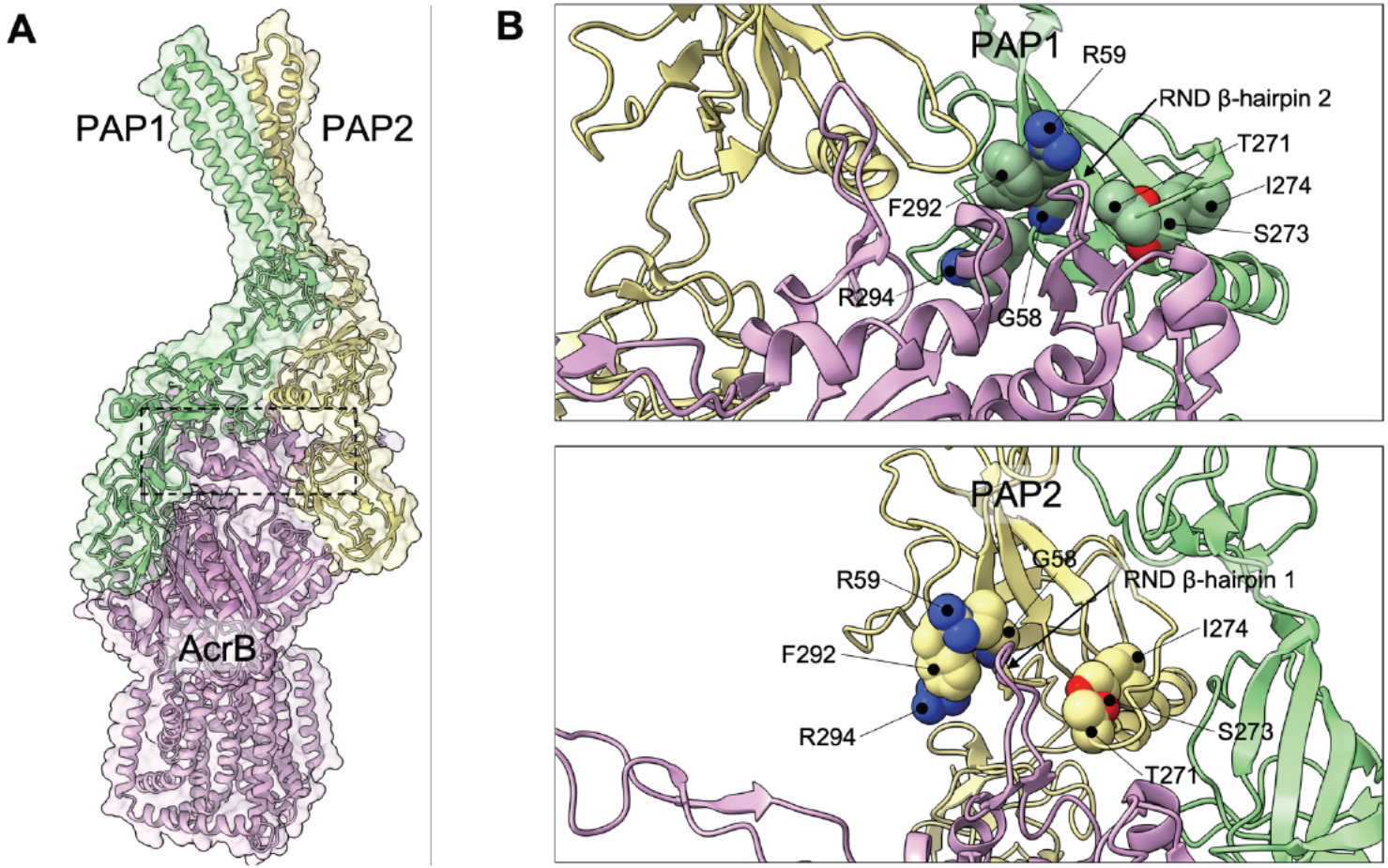


Figure 3.7. Interaction between the AcrA β-barrel domain with AcrB.

A) Position of the two AcrA protomers (PAP1 and PAP2) relative to a single AcrB protomer. The interaction between the β-barrel domain of PAP1 and PAP2 with AcrB is delineated by a box with dashed lines. **B)** Zoomed in view of the RND-binding residues (spheres) mapping to the β-barrel domains of (top) PAP1 (green) and (bottom) PAP2 (yellow), which interact with the RND-transporter β-hairpin (purple) in a pincer-like fashion. Figure produced using ChimeraX (Pettersen *et al.*, 2021).

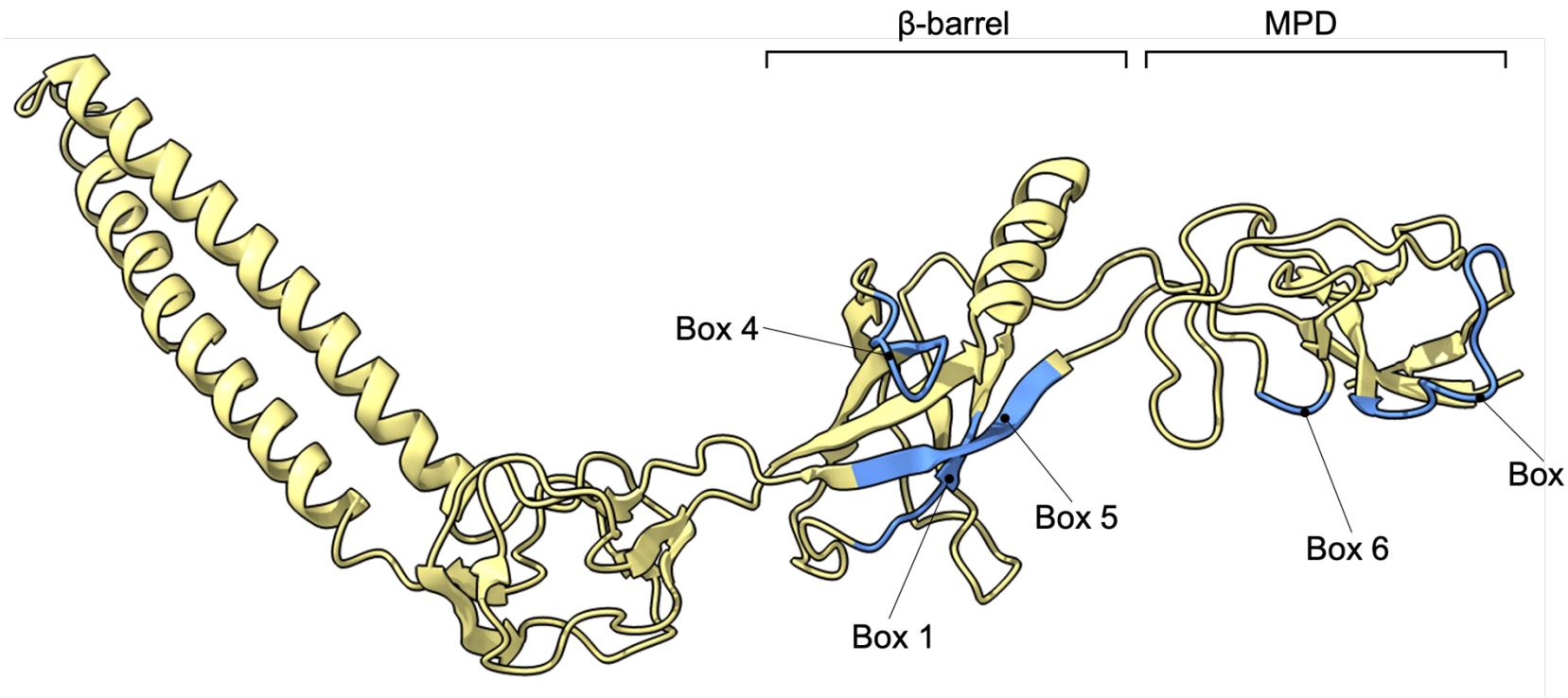


Figure 3.8. Structure of AcrA labelled with the important RND-binding boxes.

Binding boxes 1, 4 and 5 map to the β-barrel domain and binding boxes 6 and 9 map to the membrane-proximal domain (MPD). Figure produced using ChimeraX (Pettersen *et al.*, 2021).

After identifying the important binding boxes, further mutations mapping to binding boxes were produced to refine the model and identify the most critical residues. Mutations mapping to box 1 (R59A), box 4 (T271D, S273F and I274D), box 5 (F292V), and box 6 (Q310P-Q311P) significantly impaired the efflux function of AcrA (Fig. 3.3 and Table 3.3). Western blotting confirmed that the observed effects of the mutations were not due to changes in protein stability or expression levels (Fig. 3.6). The refinement narrowed the most critical residues down to a region clustering around the β-barrel domain of PAP1 and PAP2, and the MPD of PAP1. The residues mapping to binding boxes 1, 4 and 5 of PAP1 and PAP2 provide binding to AcrB in a pincer-like fashion around each hairpin (Fig. 3.7B). This is consistent with previous studies highlighting the importance of the PAP β-barrel domain in RND-binding of homologous efflux systems. In the MexAB-OprM pump of *P. aeruginosa*, mutating T256 or H279 MexA (corresponding to T271 or R294 AcrA, respectively) has been shown to impair efflux function by disrupting the MexA-MexB interaction (Nehme *et al.*, 2004). In another study, mutating V259 of MexA (corresponding to I274 AcrA) was also found to impair the efflux function of the MexAB-OprM pump (Nehme and Poole, 2005).

In addition to the β-barrel domain, mutations mapping to binding boxes 6 and 9 of the MPD also affected efflux function (Fig. 3.8). The Q310P-Q311P mutation mapping to box 6 had a significant impact on efflux function. In the MPD of PAP1, Q310-Q311 appear to make multiple contacts with the residues of the protruding loop of the adjacent RND-transporter (Fig. 3.9A). The protruding loop of AcrB has only been reported to be involved in AcrB trimerisation (Fang *et al.*, 2013). However, given the proximity of Q310-Q311 AcrA to the protruding loop of AcrB (Fig. 3.9A), it may also act as a point of interaction with AcrA. The G363F mutation mapping to box 9 in the membrane-proximal domain also significantly impaired efflux function

(Fig. 3.8). In PAP1, G363 appears to make multiple contacts with K659 and D660 of AcrB (Fig. 3.9B). In agreement with the data here, Ge *et al.* (2009) reported the importance of G363 in the C-terminal of AcrA in the assembly and function of the AcrAB-TolC complex (Ge *et al.*, 2009).

In this study, the impact of the AcrA mutations mapping to the predicted binding boxes was measured by EtBr efflux assays. This assumed that the residues that were selected for mutagenesis were involved in binding to the RND-transporter based on sequence analysis and homology modelling (McNeil *et al.*, 2019). Therefore, one limitation of this study was the lack of biophysical analysis of the impact of the AcrA mutations on AcrB-binding. It is possible that some of the mutations may exert other effects on the structure and function of AcrA to impact EtBr efflux. For instance, some AcrA mutations may have impacted the intramolecular interactions within AcrA or affected the relaying of information from AcrA to TolC (Weeks *et al.*, 2010). Another possibility is that very minor alterations in RND-binding could not be detected by measuring function and so the effect of some mutations on RND-binding may have been missed.

Mutations mapping to binding boxes 2, 3, 7 and 8 did not have any observable impact on RND-binding (Fig. 3.2 and Table 3.1), despite being in sufficient proximity to AcrB to make direct contact. This could be because these binding boxes are not critical for the assembly of the AcrAB-TolC pump or that their impact on RND-binding is minor and so not detected using phenotypic assays. The impact of these mutations may be detectable using more sensitive assays that measure the binding affinity between AcrA and AcrB.

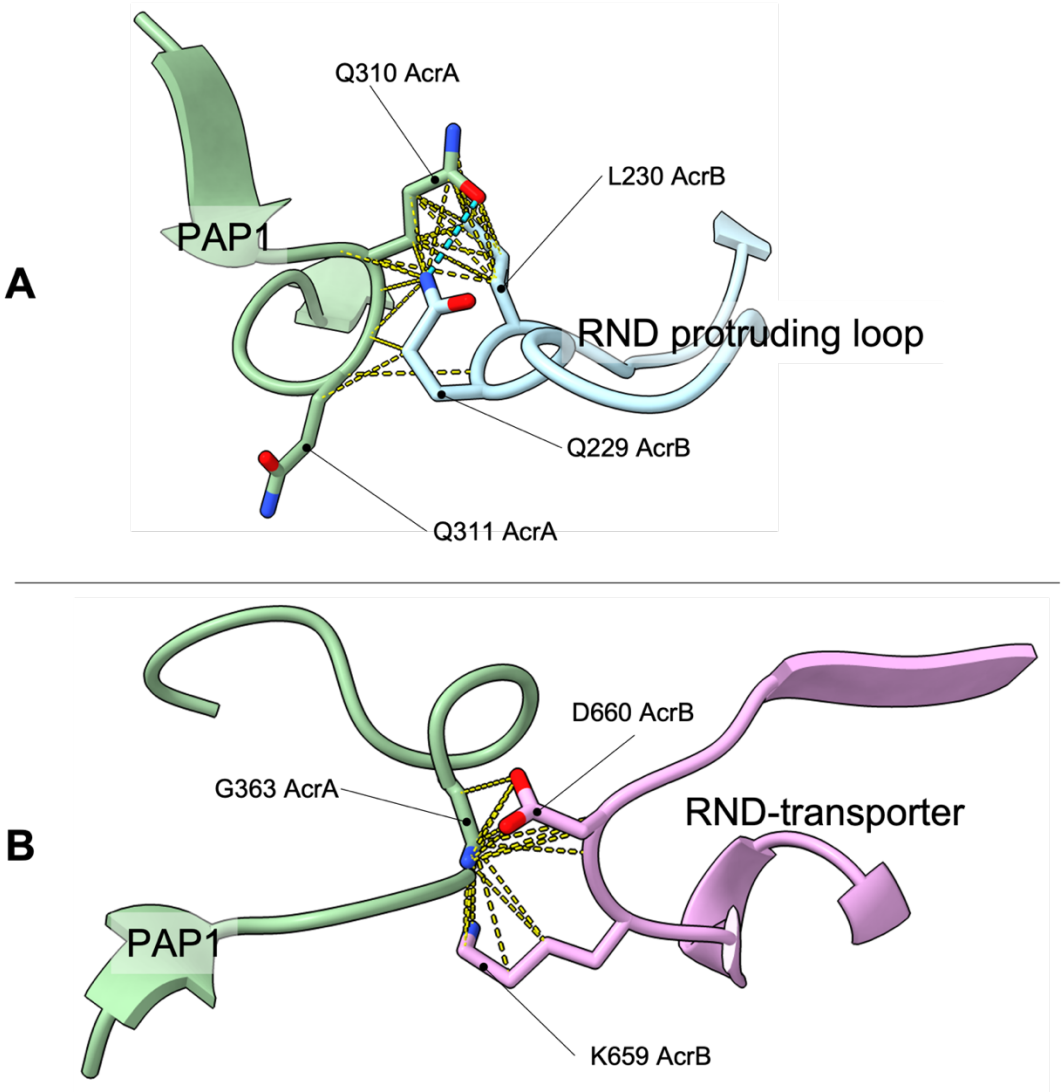


Figure 3.9. Interaction between the AcrA membrane-proximal domain with AcrB.

A) The Q310-Q311 residues mapping to box 6 of PAP1 interact with the protruding loop of the neighbouring RND-transporter. Specifically, Q310 AcrA forms a hydrogen bond (blue dashed line) with Q229 of AcrB, and both Q310-Q311 make multiple polar and apolar contacts with Q229 and L230 of AcrB (dashed yellow lines). **B)** The highly conserved G363 residue mapping to box 9 of PAP1 makes multiple contacts (dashed yellow lines) with the K659 and D660 residues of the RND-transporter. Only regions of interest are displayed for clarity. Figure produced using ChimeraX (Pettersen *et al.*, 2021).

Efflux has been found to have different effects on the phenotype of *S.* Typhimurium, including virulence (Buckley *et al.*, 2006, Nishino *et al.*, 2006, Wang-Kan *et al.*, 2017). Therefore, the impact of selected mutations on the *in vivo* virulence of *S.* Typhimurium was also tested. In agreement with previous studies, the efflux-deleted Δ4PAP strain, which lacks all four RND-associated PAPs, was avirulent in the *G. mellonella* infection model (Blair *et al.*, 2009, McNeil *et al.*, 2019). The WT AcrA complement strain was significantly more virulent compared to the Δ4PAP strain (Fig. 3.5). However, complementation with pET-20b *acrA* did not restore virulence fully. One reason for this might be due to the expression levels of *acrA* from the pET-20b vector, which provides leaky low-level expression in *S.* Typhimurium cells (McNeil *et al.*, 2019). Hence, there might have been insufficient *acrA* expression to fully restore virulence. Another reason may have been the absence of the *acrE*, *mdtA* and *mdsA* genes in the Δ4PAP strain, which encode the PAP components of the AcrEF-TolC, MdtABC and MdsABC RND pumps, respectively. Previously, the AcrEF, MdtABC and MdsABC efflux pump have also been shown to be important for the *in vivo* virulence of *S.* Typhimurium (Nishino *et al.*, 2006). Therefore, complementing the Δ4PAP strain with WT *acrA* may be insufficient to restore *in vivo* virulence fully. The efflux impaired F292V and G363F mutants displayed significantly attenuated virulence, whilst the neutral mutants Q311F and K366D had no detrimental effect on virulence compared to WT complement. The role of tripartite efflux pumps in virulence is not fully understood. However, studies suggest several possible roles, including export of virulence factors and toxins (Yamanaka *et al.*, 1998, Horiyama and Nishino, 2014) and defence against antimicrobial host-derived molecules, such as bile salts, fatty acids and hormones (Thanassi *et al.*, 1997, Elkins and Mullis, 2006, Lennen *et al.*, 2013). The innate immune response of *G. mellonella* consists of hemocytes (phagocytes of invertebrates), opsonins, and antimicrobial peptides (Tsai *et al.*, 2016). The AcrAB-TolC pump of *S.* Typhimurium has been

shown to be important for survival in macrophages, but the identity of the substrates have not been elucidated (Buckley *et al.*, 2006). The AcrAB-TolC has also been suggested to play a role in acquired resistance to antimicrobial peptides, such as 4DK5L7 and seg5D, in *S.* Typhimurium (Kapach *et al.*, 2020). Hence, it is possible that in the *G. mellonella* infection model, the *S*. Typhimurium SL1344 strains with efflux-impaired mutations are unable to efflux host-derived antimicrobial peptides or survive within the hemocytes. Recently, an untargeted metabolomics study by Wang-Kan *et al.* (2021) has shown that *S.* Typhimurium SL1344 cells with non-functional AcrB accumulated significantly more metabolite classes implicated in the virulence of *S*. Typhimurium (Wang-Kan *et al.*, 2021). Therefore, the efflux impaired F292V and G363F AcrA mutations may also impair the export of necessary factors required for virulence.

Here, the most critical residues of AcrA involved in RND-binding were elucidated. This has important implications for the development of efflux inhibitors targeting the assembly of tripartite efflux pumps. The majority of efflux inhibitor molecules reported in the literature target AcrB (Vargiu *et al.*, 2014, Opperman and Nguyen, 2015, Sjuts *et al.*, 2016), however, the PAP component of tripartite efflux pumps has also been demonstrated to be a feasible drug target to inhibit the function of AcrAB-TolC pump (Abdali *et al.*, 2017, Darzynkiewicz *et al.*, 2019). Therefore, the RND-binding residues of AcrA identified in this study could be potential drug target sites for the development of efflux inhibitors to disrupt the assembly of the AcrAB-TolC pump. Importantly, this can restore the efficacy of antibiotics that have lost their efficacy against multidrug-resistant isolates and reduce the *in vivo* virulence of *S.* Typhimurium.

3.9 Key findings

- Discrete stretches of residues in the PAP sequence termed ‘binding boxes’ control interactions with the RND-transporter.
- The binding box model was validated by site-directed mutagenesis to produce disruptive mutations mapping to the nine predicted binding boxes
- Mutations mapping to binding boxes 1, 4, 5, 6 and 9 impaired EtBr efflux and increased antimicrobial susceptibility.
- The most critical RND-binding residues in the binding boxes was determined by producing more conservative mutations and testing their phenotypic effects.
- AcrA mutations that conferred impaired efflux also attenuated *in vivo* virulence in the *Galleria mellonella* infection model.
- All the efflux impaired AcrA mutant proteins were stably expressed compared to WT AcrA protein.

3.10 Future work

The current work highlights critical residues of AcrA that are predicted to be involved in RND-binding. As mentioned previously, one limitation of this study has been the use of antimicrobial susceptibility testing and EtBr efflux assays to infer the impact of AcrA mutations on RND-binding. However, the role of these residues should be verified using a biophysical technique, such as isothermal titration calorimetry or surface plasmon resonance, to determine the binding affinity between wild type AcrB and the efflux impaired AcrA mutants. This would allow measurement of whether the AcrA mutations affect the physical binding with AcrB.

The RND-binding residues identified in this study could be used as drug target sites to search for inhibitors of AcrA capable of preventing the assembly of the AcrAB-TolC pump. Firstly, *in silico* screening methods, such as ensemble docking, should be used to identify potential compounds that bind to the critical RND-binding residues of AcrA. The top hits should be tested for their ability to inhibit efflux using phenotypic assays, such as EtBr efflux assays and antimicrobial susceptibility testing. Lastly, to verify the binding of candidate AcrA inhibitors to the RND-binding residues, the binding affinity between the compound and the AcrA protein should be tested using isothermal titration calorimetry or surface plasmon resonance.

CHAPTER 4. A potential role for periplasmic adaptor protein AcrA in vetting substrate channel access to the RND transporter AcrB

Chapter 4. A potential role for periplasmic adaptor protein AcrA in vetting substrate channel access to the RND-transporter AcrB

4.1 Background

In Chapter 3, the refinement of the binding box model of PAP-RND interaction led to the discovery of an AcrA mutation with a peculiar phenotype. The K366D AcrA mutation mapping to binding box 9 of the membrane-proximal domain (MPD) did not impact efflux of or susceptibility to EtBr but showed a distinct profile of susceptibility to some of the other antimicrobials tested. The MPD of RND-associated PAPs is critical for the assembly and function of AcrAB-TolC in *E. coli* and *S. enterica* (Elkins and Nikaido, 2003, Ge *et al.*, 2009, McNeil *et al.*, 2019). In the PAPs ZneB and CusB of the tripartite ZneCAB and CusABC RND efflux pumps, respectively, the MPD appears to play an important role in substrate acquisition and presentation to the metal pumping RND-transporters (De Angelis *et al.*, 2010, Chacon *et al.*, 2014). Additionally, in the related ABC-transporter-associated PAP MacA, the MPD has been demonstrated to be involved in direct binding of possible pump substrates (Lu and Zgurskaya, 2013) and has been suggested to be involved in the substrate vetting (Symmons *et al.*, 2015). This suggested that the K366D AcrA mutation may impact the access of certain substrates to the RND-transporter AcrB. Here, the impact of the K366D AcrA mutation on the substrate profile of the AcrAB-TolC pump will be determined using more sensitive assays using specific drugs. Additionally, the impact of the K366D AcrA mutation on the AcrB-transporter substrate channels will be investigated.

4.2 Aims

- To determine the impact of the K366D AcrA mutation on the substrate profile of the AcrAB-TolC pump concerning the physicochemical properties of substrates.
- To investigate how the K366D AcrA mutation affects the access of substrates to the AcrB-transporter with respect to the substrate entry channels.

4.3 Hypotheses

- The K366D AcrA mutation does not affect the efflux of planar aromatic cations using channel 3 of the AcrB-transporter.
- The K366D AcrA mutation affects the efflux of high-molecular-mass drugs using channel 2 of the AcrB-transporter.

4.4 Effect of the K366D AcrA mutation on the antimicrobial susceptibility of the AcrAB-TolC pump

In Chapter 3, complementation with the K366D AcrA mutant did not restore the susceptibility phenotype of the Δ4PAP strain in the same manner as complementation with WT AcrA (Table 3.3). Furthermore, complementation of the Δ4PAP strain with the K366D AcrA mutation had no impact on susceptibility to the tested substrate dyes of AcrB (acriflavine, crystal violet, EtBr, methylene blue, and rhodamine 6G). However, complementation of the Δ4PAP strain with the K366D AcrA mutation conferred increased susceptibility to other AcrB-substrates (erythromycin, fusidic acid, novobiocin etc.) relative to complementation with WT AcrA. Interestingly, the dyes tested share a similar chemical scaffold because they all consist of multiple planar aromatic rings and a cationic moiety. Owing to this, the dyes have been previously referred to as planar aromatic cations (PACs) (Zwama *et al.*, 2018). On the other

hand, the substrates affected by the K366D AcrA mutation were generally non-planar and uncharged. These substrates were further categorised as either a low-molecular-mass drug (*M* <500 Da) or a high-molecular-mass drug (*M* >500 Da) (Zwama *et al.*, 2018). The structural formulae of representative planar aromatic cations, low-molecular-mass drugs and high-molecular-mass drugs are shown in Appendix IV. The impact of the K366D AcrA mutation on the antimicrobial susceptibility of the AcrAB-TolC pump for further planar aromatic cations, low-molecular-mass drugs and high-molecular-mass drugs was tested to validate the findings observed in Chapter 3. The F292V and Q311F AcrA mutations were used as positive and negative controls, respectively because the F292V AcrA mutation had no impact on EtBr efflux and increased susceptibility to AcrB-substrates, whereas Q311F was a neutral mutation with no impact on efflux activity on the AcrAB-TolC pump.

In agreement with the findings in Chapter 3, the complementation of the Δ4PAP strain with the K366D AcrA mutation caused two-fold or lower MIC values for high-molecular-mass drugs (erythromycin, doxorubicin, fusidic acid, and novobiocin) and low-molecular-mass drugs (chloramphenicol, clindamycin, minocycline, and linezolid) compared to Δ4PAP complemented with WT AcrA (WT AcrA complement) (Table 4.1). Furthermore, the K366D AcrA mutation did not impact MIC values for planar aromatic cations (acriflavine, benzalkonium chloride, berberine, crystal violet, EtBr, methylene blue, and rhodamine 6G) compared to the WT AcrA complement (Table 4.1). The efflux impaired F292V AcrA mutant resulted in two-fold or lower MIC values to all AcrB-substrates tested (Table 4.1). This indicated that the F292V mutation disrupted the function of AcrA, resulting in a non-functional AcrAB-TolC pump. The Δ4PAP strain complemented with the neutral Q311F AcrA mutation did not have any impact on susceptibility of the to the tested AcrB-substrates compared to the

WT AcrA complement (Table 4.1). This indicated that the Q311F mutation did not alter the function of AcrA and hence the function of the AcrAB-TolC pump in exporting substrates. This data verified that the K366D AcrA mutation had no impact on susceptibility to planar aromatic cations, but increased susceptibility to high-molecular-mass drugs and low-molecular-mass drugs of the AcrB-transporter.

Table 4.1. Antimicrobial susceptibility of the *Salmonella* Typhimurium SL1344 Δ4PAP strain carrying plasmid with the F292V, Q311F or K366D AcrA mutations to drugs with different physicochemical characteristics.

	MIC (μg/mL)														
	HMMD				LMMD				PAC						
Strain	ERY	DOX	FA	NOV	CHL	CLI	MIN	LZD	ACR	BZK	BER	CV	EtBr	MB	R6G
WT	128	1024	1024	512	4	512	2	512	256	64	>1024	64	1024	1024	1024
Δ4PAP	**4**	**2**	**8**	**2**	**0.5**	**4**	**0.25**	**16**	**16**	**4**	**128**	**2**	**16**	**8**	**4**
The following rows are Δ4PAP background strain + pET-20b carrying different versions of AcrA															
WT AcrA complement	64	64	256	64	4	128	1	128	64	32	>1024	16	128	128	128
F292V AcrA	**4**	**2**	**8**	**2**	**0.5**	**4**	**0.25**	**16**	**16**	**4**	**128**	**2**	**16**	**8**	**4**
Q311F AcrA	64	64	256	64	4	128	1	128	64	32	>1024	16	64	128	128
K366D AcrA	**16**	**16**	**32**	**16**	**1**	**32**	**0.25**	**16**	64	32	>1024	16	64	128	64

Underlined values highlight values for WT AcrA complement (Δ4PAP with pET-20b *acrA*). Bold values are two-fold or more different than the parent strain. HMMDs, high-molecular-mass drugs; ERY, erythromycin; DOX, doxorubicin; FA, fusidic acid; NOV, novobiocin; LMMDs, low-molecular-mass drugs; CHL, chloramphenicol; CLI, clindamycin; MIN, minocycline; LZD, linezolid; PACs, planar aromatic cations; ACR, acriflavine; BZK, benzalkonium chloride; BER, berberine; CV, crystal violet; EtBr, ethidium bromide; MB, methylene blue; R6G, rhodamine 6G.

4.5 Probing the impact of the K366D AcrA mutation on AcrB substrate channels

Previous studies have shown that the molecular mass of the substrate influences which channel molecules use to enter the RND pump and which binding pocket they interact with (Nakashima *et al.*, 2011, Schuster *et al.*, 2016, Zwama *et al.*, 2018, Tam *et al.*, 2021). The RND-transporter AcrB has four substrate entry channels (Murakami *et al.*, 2002, Nakashima *et al.*, 2011, Zwama *et al.*, 2018) (Fig. 4.1). Low-molecular-mass drugs have been proposed to preferentially enter through channel 1, whilst high-molecular-mass drugs are reported to enter AcrB through channel 2 (Murakami *et al.*, 2002, Murakami *et al.*, 2006, Zwama and Yamaguchi, 2018). The cleft entrance of channel 2 has been previously suggested to be impacted by the membrane-proximal domain (MPD) of AcrA, where the K366D mutation is located (Zwama *et al.*, 2018). This is seen in cryo-EM structures of the AcrAB-TolC complex, which show that AcrA interacts with the PC1 and PC2 subdomains on the surface of the AcrB-transporter (Du *et al.*, 2014, Daury *et al.*, 2016, Wang *et al.*, 2017). Planar aromatic cations on the other hand are preferentially taken up through channel 3, which starts from the vestibule formed by the central cavity of the three AcrB protomers and leads directly to the distal binding pocket (DBP) (Zwama *et al.*, 2018). The entrance of the recently proposed channel 4 is in the groove formed by TM1 and TM2 of AcrB and leads to the DBP (Tam *et al.*, 2020). The location of channel 3 and channel 4 within AcrB suggests that the MPD of AcrA, where K366 is located, should not have a direct steric impact on the drug access (Fig. 4.1).

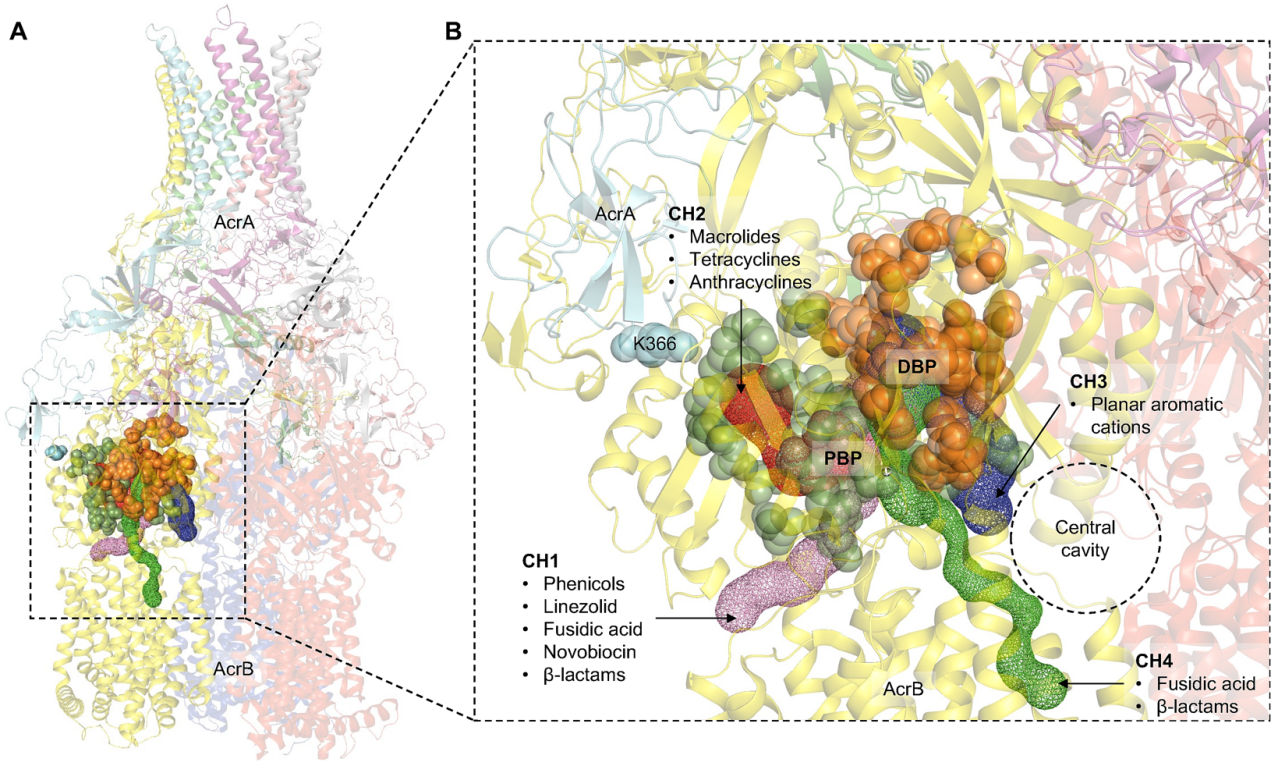


Figure 4.1. The structure of the trimeric AcrB transporter and the hexameric AcrA assembly (TolC not shown for clarity).

A) The different substrate entry pathways are shown as coloured channels, and the binding pockets are indicated by coloured spheres. **B)** Zoomed-in view of the substrate channels and the binding pockets relative to K366 of AcrA. The green and orange spheres correspond to the space-fill representation of the residues lining the proximal binding pocket (PBP) and the deep binding pocket (DBP), respectively. K366 is in the membrane-proximal domain of AcrA and impacts the residues lining the PBP and the entrance of channel 2 (CH2, red). Channel 1 (CH1, magenta) also feeds into the PBP, so is likely to be impacted by changes in K366. Channel 3 (CH3, blue) starts from the central cavity and leads to the DBP. Similarly, channel 4 (CH4, green) starts from the groove formed by TM1/TM2 and leads to the DBP. Therefore, CH3 and CH4 are unlikely to be directly impacted by K366 substitutions. Figure created with PyMOL Version 2.5.2 (Schrödinger, 2022).

To understand how the K366D AcrA mutation affects the susceptibility of the Δ4PAP strain to high-molecular-mass drugs and low-molecular-mass drugs, but not to planar aromatic cations, more sensitive assays using specific drug screens were used to be able to better differentiate the usage of the access channels by respective substrates and the impact of the K366D mutation on specific substrate channels. Doxorubicin has been reported to use channel 2 of the AcrB-transporter (Nakashima *et al.*, 2011, Tam *et al.*, 2021). Therefore, the effect of the K366D AcrA mutation on doxorubicin efflux was measured. Doxorubicin is a fluorescent substrate of the AcrAB-TolC pump that exhibits higher fluorescence when extracellular as it cannot fluoresce when inside cells (Nakashima *et al.*, 2011). Therefore, doxorubicin fluorescence can be used to establish the rate of efflux by bacterial cells. Like the EtBr efflux assay, cells are preloaded with doxorubicin by dissipating the proton motive force through the addition of CCCP. Doxorubicin preloaded cells are re-energised with glucose causing an increase in doxorubicin fluorescence over time due to active efflux of doxorubicin (Nishino and Yamaguchi, 2001). To analyse the data, the area under the curve (AUC) for the doxorubicin fluorescence was calculated for each strain and compared to one another using one-way ANOVA. Strains with more efficient doxorubicin efflux have a higher AUC value, whereas strains with impaired doxorubicin efflux have a lower AUC value.

In agreement with the antimicrobial susceptibility data, the Δ4PAP strain displayed impaired doxorubicin efflux compared to WT (Fig. 4.2A). This is due to the lack of the *acrA* gene in the Δ4PAP strain, which encodes the PAP AcrA required for the function of the AcrAB-TolC pump to export doxorubicin (Murakami *et al.*, 2006). The WT strain showed very high fluorescence levels due to the efficient efflux of doxorubicin (Fig. 4.2A). Therefore, the WT strain was shown separately with a different axis scale to allow for better visualisation of the Δ4PAP strain

complemented with mutated versions of AcrA (Fig. 4.2B). The complementation of the Δ4PAP strain with pET-20b *acrA* (WT AcrA complement) significantly rescued doxorubicin efflux (Fig. 4.2C). Compared to the WT AcrA complement, the efflux impaired F292V AcrA mutation caused a significant impairment of doxorubicin efflux, whereas the neutral Q311F mutation had no significant impact on doxorubicin efflux (Fig. 4C). Importantly, the K366D AcrA mutation caused a significant impairment of doxorubicin efflux compared to WT AcrA complement (Fig. 4C). This data provided further evidence that the K366D AcrA mutation impacts the entry of substrates through channel 2 of the AcrB-transporter.

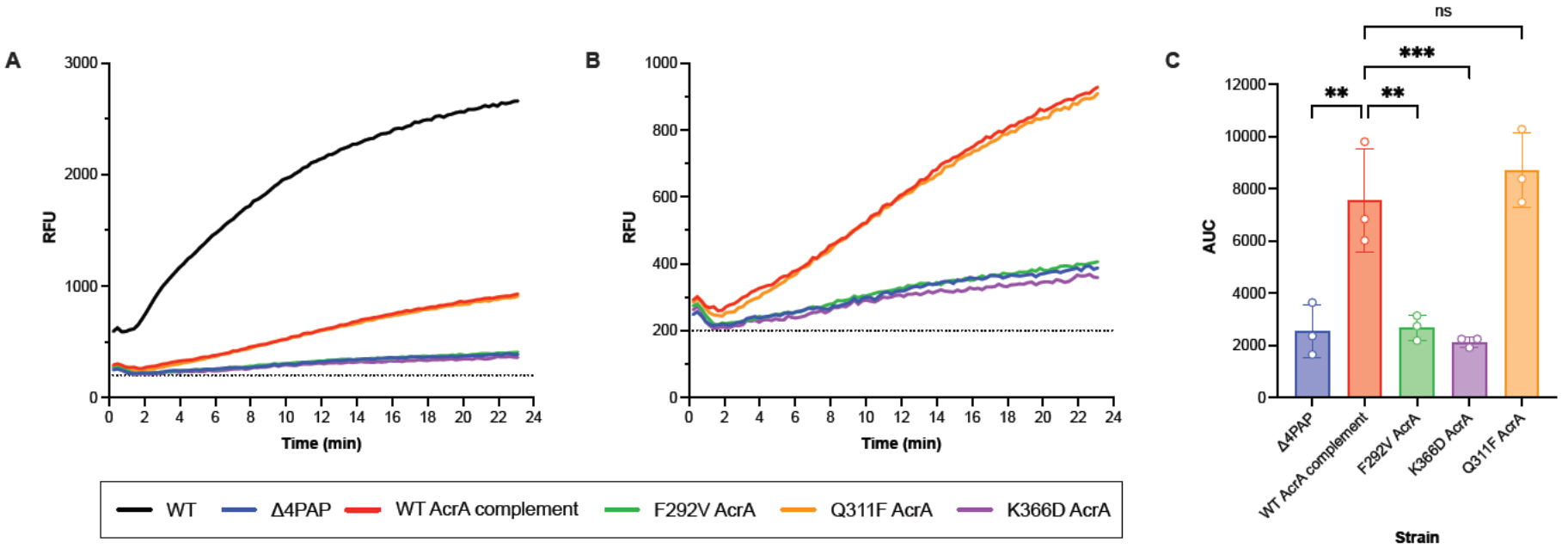


Figure 4.2. Efflux of doxorubicin by the *Salmonella* Typhimurium SL1344 Δ4PAP strain carrying plasmid with different versions of AcrA.

A) Efflux of doxorubicin over time in *Salmonella* Typhimurium WT and the Δ4PAP strain carrying plasmid with different versions of AcrA. WT AcrA complement refers to the Δ4PAP complemented with pET-20b *acrA*. Bacteria were treated with doxorubicin and the proton-motive force dissipater CCCP for 1 hour and then re-energised with glucose. Efflux was monitored by increasing RFU due to extracellular doxorubicin. presented are the mean of three biological replicates. Error bars omitted for clarity. **B)** Efflux of doxorubicin over time in Δ4PAP strain carrying plasmid with different versions of AcrA. The data shown is identical to A) with WT strain data omitted. Error bars were omitted for clarity. **C)** Area under curve (AUC) analysis for doxorubicin efflux over time. Data shown are the mean AUC values of the three biological replicates shown in panel B ± standard deviation. A baseline of 200 RFU was used for AUC analysis (dashed line in panel B). Data were analysed by one-way ANOVA, followed by Dunnett's test to correct for multiple comparisons. Strains with a significantly different AUC are indicated with ** ($P \leq 0.01$) or *** ($P \leq 0.001$). ns, not significant.

Of the channel 2-substrates tested, doxorubicin was the only one for which it was possible to measure efflux as it was the only substrate that has fluorescence properties to allow measurement of efflux. Therefore, to further clarify the impact of the K366D AcrA mutation on transport through specific AcrB channels, the growth of the Δ4PAP strain complemented with AcrA with the K366D mutation was monitored in the presence of efflux-substrates at 0.25×MIC. The list of AcrB-substrates with their predicted substrate channel preference are listed in Table 4.2. The efflux impaired F292V AcrA and the phenotypically neutral Q311F AcrA mutations were used as controls. All strains grew well in LB broth without additional drugs/dyes (Fig. 4.3) and did not have significantly different mean generation times compared to WT (Appendix V), indicating that the plasmids did not impact fitness. Consistent with the antimicrobial susceptibility data, the Δ4PAP strain was unable to grow in the presence of any AcrB-substrate compared to WT (Fig. 4.3). This is due to the lack of the *acrA* and *acrE* genes in the Δ4PAP strain, which encode the PAP components required for the function of the AcrAB-TolC and AcrEF-TolC pumps to export substrates, respectively (McNeil *et al.*, 2019). The Δ4PAP strain complemented with WT AcrA grew well in the presence of all AcrB-substrates (Fig. 4.3). The Δ4PAP strain complemented with AcrA with the F292V mutation was unable to grow in the presence of any AcrB-substrate like the Δ4PAP strain, which matched the antimicrobial susceptibility data (Fig. 4.3). Hence, the mean generation times of the Δ4PAP strain complemented with AcrA with the F292V mutation could not be calculated as it had no observable exponential phase (Appendix V). The Δ4PAP strain complemented with AcrA with the Q311F mutation grew well in the presence of any AcrB-substrate (Fig. 4.3) and its mean generation times were not significantly different compared to the WT AcrA complement (Appendix V). The K366D AcrA mutation caused a channel-specific effect concerning growth. Consistent with the antimicrobial susceptibility data, the Δ4PAP strain complemented with

AcrA with the K366D mutation grew well in the presence of channel 3-substrates EtBr or rhodamine 6G (Fig. 4.3) and its mean generation time in the presence of EtBr or rhodamine 6G was not significantly different to the WT AcrA complement (Appendix V). However, when grown in the presence of channel 2-substrates, including clindamycin, erythromycin, doxorubicin, or minocycline, the K366D AcrA mutation caused poor growth compared to the WT AcrA complement (Fig. 4.3). The Δ4PAP strain complemented with AcrA with the K366D mutation had a significantly longer mean generation time in the presence of clindamycin compared to WT complement (Appendix V). For the other channel 2-substrates, the Δ4PAP strain complemented with AcrA with the K366D mutation did not have an observable exponential phase to allow calculation of mean generation times (Appendix V). Interestingly, the K366D AcrA mutation also caused diminished growth in the presence of channel 1-substrates, such as novobiocin, chloramphenicol or fusidic acid (Fig. 4.3). Compared to the WT AcrA complement, the Δ4PAP strain complemented with AcrA with the K366D mutation had a significantly longer mean generation time in the presence of chloramphenicol, fusidic acid and novobiocin (Appendix V). These data provided further evidence for the effect of the K366D AcrA mutation on channel 2- and possibly channel 1-substrate entry.

Table 4.2. List of AcrB-substrates with their predicted channel preference (s).

Substrate	Predicted channel (s) preference	Reference (s)
Chloramphenicol	CH1	Tam *et al.* (2021)
Fusidic acid	CH1 and CH4	Tam *et al.* (2021)
Linezolid	CH1	Tam *et al.* (2021)
Novobiocin	CH1	Tam *et al.* (2021)
Clindamycin	CH2	Tam *et al.* (2021)
Doxorubicin	CH2	Nakashima *et al.* (2011)
Erythromycin	CH2	Nakashima *et al.* (2011)
Acriflavine	CH3	Zwama *et al.* (2018)
Minocycline	CH2	Nakashima *et al.* (2011)
Benzalkonium chloride	CH3	Zwama *et al.* (2018)
Berberine	CH3	Zwama *et al.* (2018)
Crystal violet	CH3	Zwama *et al.* (2018)
Ethidium bromide	CH3	Zwama *et al.* (2018)
Methylene blue	CH3	Zwama *et al.* (2018)
Rhodamine 6G	CH3	Zwama *et al.* (2018)

CH1, channel 1; CH2, channel 2; CH3, channel 3; CH4, channel 4.

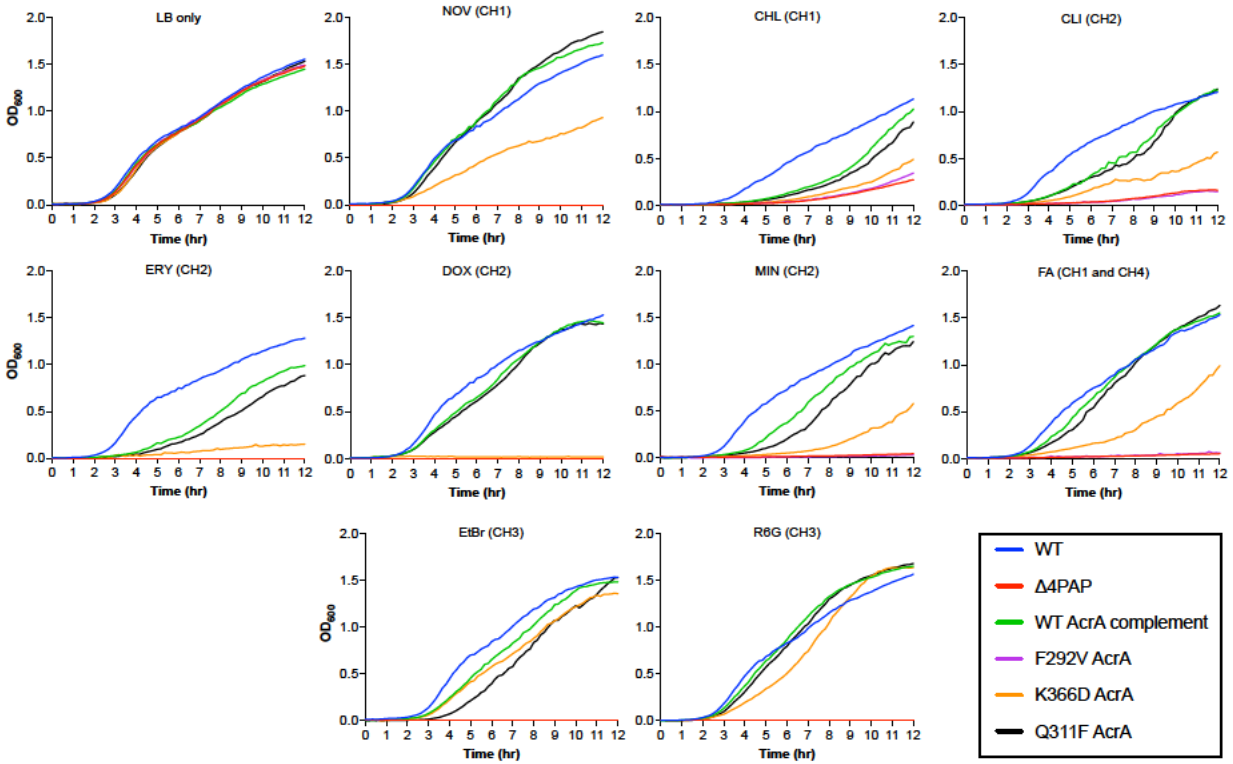


Figure 4.3. Growth kinetics of the *Salmonella* Typhimurium SL1344 Δ4PAP strain carrying plasmid with different versions of AcrA in the presence of AcrB-substrates.

Overnight bacterial cultures were diluted to a starting OD_{600} of 0.01 in a flat bottom clear 96-well plate. Bacteria were grown at 37°C with shaking in a plate reader. The OD_{600} readings of the wells was taken at 10-minute intervals for 12 hours. The data shown are the mean OD_{600} values of three biological replicates. WT AcrA complement refers to Δ4PAP strain complemented with pET-20b *acrA*. Error bars omitted for clarity. All mean generation times are listed in Appendix V. Abbreviations and concentrations of drugs used: CHL, 0.5 µg/mL chloramphenicol; CLI, 8 µg/mL clindamycin; DOX, 4 µg/mL doxorubicin; EtBr, 16 µg/mL ethidium bromide; ERY, 4 µg/mL erythromycin; FA, 8 µg/mL fusidic acid; MIN, 0.25 µg/mL minocycline; NOV, 4 µg/mL novobiocin; R6G, 16 µg/mL rhodamine 6G. Brackets indicate the preferred channel utilised by the substrate: CH1, channel 1; CH2, channel 2; CH3, channel 3; CH4, channel 4.

4.6 The impact of the K366D AcrA mutation on channel 3 of the AcrB-transporter

The evidence from the EtBr efflux assay, antimicrobial susceptibility, and growth kinetics data strongly suggested that the K366D AcrA mutation does not impact the entry of planar aromatic cations through channel 3 of the AcrB-transporter. Therefore, to further increase assay sensitivity and avoid interference from AcrB-substrates that use channel 1, channel 2 and channel 3 promiscuously, such as EtBr, an AcrB mutation that impacted channel 3 function was required (Zwama *et al.*, 2018). The channel 3 AcrB mutation would be expected to result in the intermediate impairment of EtBr efflux as it would be unable to use channel 3 but would be able to enter through the unaffected channel 1 and channel 2. Consequently, combining the channel 3 AcrB mutation with the K366D AcrA mutation, which impacts channel 1 and channel 2, it was hypothesised that EtBr efflux would be impaired completely due to impacted channel 1, channel 2 and channel 3.

To produce mutations in both AcrA and AcrB proteins, the SL1344 *acrAB* operon was cloned into the high-copy number plasmid pET-20b as described in Section 2.8 to allow for the leaky expression of both *acrA* and *acrB* efflux genes. The cloning of *acrAB* into pET-20b was verified by PCR as described in Section 2.7.6. The *acrAB* insert was checked using primers P1 (T7 primer) and P2 (T7 terminal primer) (Table 2.1) that annealed upstream and downstream of the cloning insert in pET-20b, respectively. The plasmid map of the cloned *acrAB* insert in pET-20b is shown in Figure 4.4A. As shown in Figure 4.4B, candidate 7 produced an amplicon corresponding to the size of the *acrAB* insert (4563 bp). The correct sequence of candidate 7 was verified by Eurofins Genomics using the check primers P1, P2, P666, P667, P668 and P669 (Table 2.1) that provided sequencing coverage of the entire *acrAB* insert.

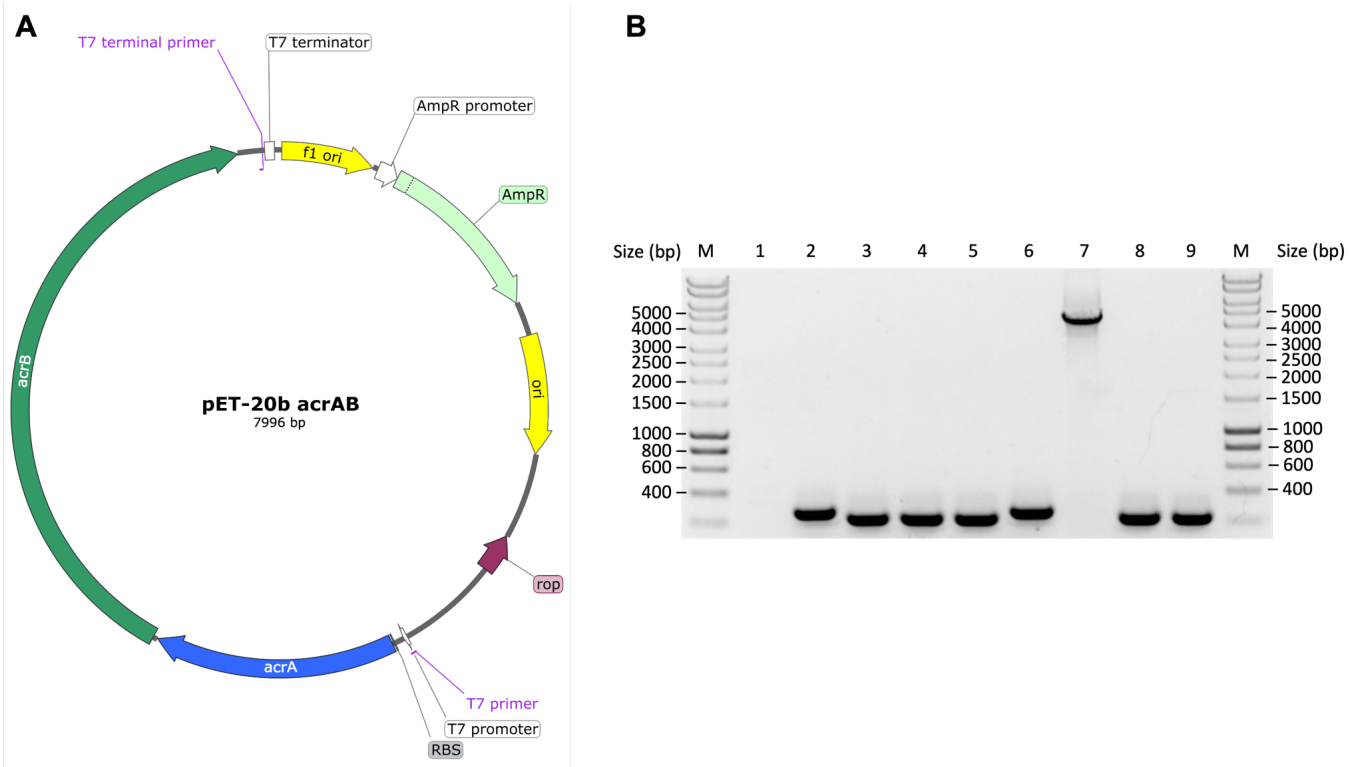


Figure 4.4. PCR check of the *acrAB* cloning insert.

A) The plasmid map of pET-20b *acrAB*. The T7 and T7 terminal primers used for checking the size of the *acrAB* insert in pET-20b anneal upstream of *acrA* and downstream of the *acrB* inserts to produce a product of 4563 bp. Figure obtained from SnapGene® software (from GSL Biotech; available at snapgene.com). **B)** Agarose gel electrophoresis of PCR amplified products using T7 and T7 terminal primers to check for the *acrAB* insert in cloning candidates. Negative control contained no template DNA.
Lane M: HyperLadder 1kb molecular weight ladder
Lane 1: negative control
Lane 2-9: cloning candidates

The expression of the resulting pET-20b *acrAB* plasmid was verified by transforming it into the Δ4PAP Δ*acrB* strain, which lacks the genes encoding the four RND-associated PAPs, including AcrA, and the AcrB-transporter needed for the function of the AcrAB-TolC pump (McNeil *et al.*, 2019). Since AcrAB-TolC is the principal efflux pump of *S*. Typhimurium, complementation of the Δ4PAP Δ*acrB* strain with pET-20b *acrAB* was expected to restore the efflux defect. The complementation of the Δ4PAP Δ*acrB* strain with pET-20b *acrAB* (WT AcrAB complement) restored EtBr efflux and antimicrobial susceptibility defects, confirming the expression of pET-20b *acrAB* (Fig. 4.5 and Table 4.3).

Zwama *et al*. (2018) first identified channel 3 of the AcrB-transporter and showed that it is preferentially used by planar aromatic cations for efflux (Zwama *et al.*, 2018). In their study, they substituted the A33, T37 and N298 AcrB residues in the entrance of channel 3 with bulky tryptophan residues to impact the entry of planar aromatic cations into the AcrB-transporter (Zwama *et al.*, 2018). The A33W T37W N298W mutation in AcrB (channel 3 AcrB mutation) was produced in the pET-20b *acrAB* plasmid by site-directed mutagenesis. The resulting plasmid referred to as the channel 3 AcrB mutation expressed WT AcrA protein, but an AcrB protein with channel 3 mutated. The plasmid expressing the channel 3 AcrB mutation was transformed into the Δ4PAP Δ*acrB* strain to verify its effect on EtBr efflux. In agreement with Zwama *et al*. (2018), the channel 3 AcrB mutation resulted in significantly more EtBr accumulation compared to complementation with the WT AcrAB, but not significantly more than the efflux-deficient Δ4PAP Δ*acrB* strain, indicating intermediate impairment of EtBr efflux (Fig. 4.5).

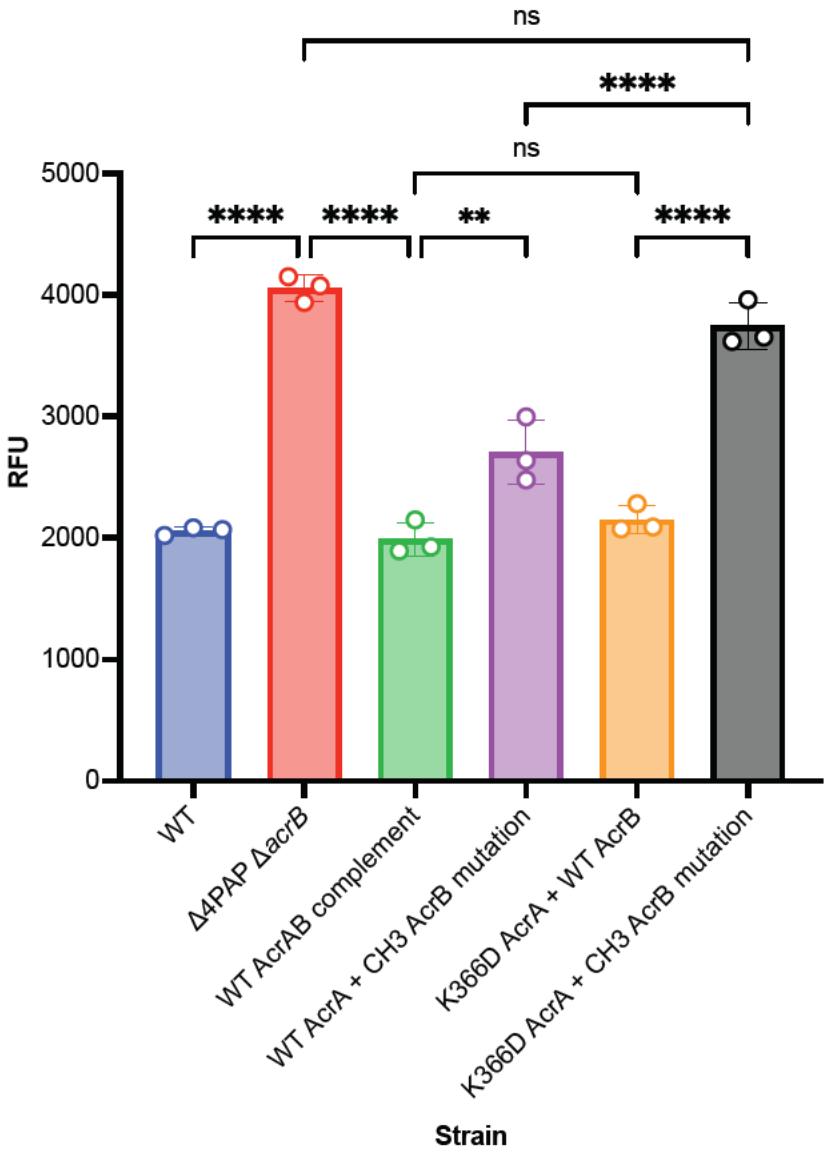


Figure 4.5. Accumulation of ethidium bromide in the *Salmonella* Typhimurium SL1344 Δ4PAP Δ*acrB* strain carrying the plasmid with the K366D AcrA and channel 3 AcrB (A33W T37W N298W AcrB) mutations.

Bacteria were grown to early exponential phase and then diluted to an OD_{600} of 0.2 in buffer. Cells were loaded into a flat bottom black 96-well plate and injected with ethidium bromide immediately. Fluorescence of ethidium bromide was measured over 30 minutes. Data shown are the mean of three biological replicates showing maximum relative fluorescence unit (RFU) values at the end of 30 minutes of ethidium bromide exposure ± standard deviation. Data were analysed by one-way ANOVA and corrected for multiple comparisons using Tukey's test. WT AcrAB complement refers to Δ4PAP Δ*acrB* strain complemented with pET-20b *acrAB*. Strains with significantly different intracellular ethidium bromide accumulation are indicated with ** ($P \leq 0.01$) or **** ($P \leq 0.0001$). ns, not significant.

Next, the K366D AcrA mutation was produced in the plasmid with the channel 3 AcrB mutation to obtain a plasmid with the combined K366D AcrA + channel 3 AcrB mutation. The rationale was that the K366D AcrA mutation would alter the efflux of EtBr through channel 1 and channel 2 if channel 3 is impacted. The plasmid with the K366D AcrA + channel 3 AcrB mutation was transformed into the Δ4PAP Δ*acrB* strain for phenotypic assessment. The K366D AcrA + channel 3 AcrB mutation had an additive effect on EtBr efflux impairment (Fig. 4.5). Compared to the K366D AcrA or the channel 3 AcrB mutations acting alone, the Δ4PAP Δ*acrB* strain carrying the plasmid with the K366D AcrA + channel 3 AcrB mutation accumulated significantly more EtBr (Fig. 4.5). Furthermore, the combined K366D AcrA + channel 3 AcrB mutation was not significantly different to the efflux-defective Δ4PAP Δ*acrB* strain, indicating complete impairment of EtBr efflux (Fig. 4.5). The antimicrobial susceptibility data also supported the EtBr accumulation data. The channel 3 AcrB mutation caused two-fold or more reduced MIC values to planar aromatic cations, including acriflavine, benzalkonium chloride, EtBr, methylene blue and rhodamine 6G, compared to WT AcrAB complement (Table 4.3). The Δ4PAP Δ*acrB* strain carrying the plasmid with the K366D AcrA mutation caused two-fold or more reduced MIC values to high-molecular-mass drugs, including doxorubicin, erythromycin, fusidic acid and novobiocin, but no impact on susceptibility to planar aromatic cations, compared to complementation with the WT AcrAB (Table 4.3). The combined K366D AcrA + channel 3 AcrB mutation caused further increased susceptibility to all AcrB-substrates, like that of the Δ4PAP Δ*acrB* strain (Table 4.3). Together these data show that the channel 3 AcrB disruption has a clearly pronounced additive effect compared to K366D AcrA mutation acting on its own, consistent with the role of the membrane-proximal domain of the PAP in the control of channel 1- and channel 2-substrates. These data further support the essential role that K366, and the MPD in general, plays in the transport of channel 1- and channel 2-substrates.

Table 4.3. The antimicrobial susceptibility of the *Salmonella* Typhimurium SL1344 Δ4PAP Δ*acrB* strain carrying the plasmid with the K366D AcrA and channel 3 (A33W T37W N298W) AcrB mutations.

	MIC (μg/mL)									
	HMMD				PAC					
Strain	DOX	ERY	FA	NOV	ACR	BZK	CV	EtBr	MB	R6G
WT	1024	128	1024	512	256	64	64	>1024	1024	>1024
Δ4PAP Δ*acrB*	2	4	4	1	8	2	2	8	8	8
The following rows are Δ4PAP Δ*acrB* background strain + pET-20b carrying different versions of AcrAB										
WT AcrAB complement	64	64	128	64	128	32	16	256	256	128
WT AcrA + CH3 AcrB mutation	32	16	32	16	32	8	8	32	32	32
K366D AcrA + WT AcrB	16	16	16	16	128	32	16	128	128	64
K366D AcrA + CH3 AcrB mutation	**2**	**4**	**4**	**1**	**8**	**2**	**2**	**8**	**8**	**8**

Underlined values highlight values for the Δ4PAP Δ*acrB* strain complemented with pET-20b *acrAB* (WT AcrAB complement). Bold values highlight the MIC values of the Δ4PAP Δ*acrB* strain carrying the plasmid with the K366D AcrA + channel 3 (CH3) AcrB mutations compared to its single mutation parent strains. HMMD, high-molecular-mass drugs; DOX, doxorubicin; ERY, erythromycin; FA, fusidic acid; NOV, novobiocin; PAC, planar aromatic cation; ACR, acriflavine; BZK, benzalkonium chloride; CV, crystal violet; EtBr, ethidium bromide; MB, methylene blue; R6G, rhodamine 6G.

4.7 Western blotting of AcrB proteins

The stability of the channel 3 AcrB mutant was confirmed by Western blotting to ensure that the observed phenotypic impact was because of its effect on channel 3 and not due to changes in protein stability. The AcrB protein levels were quantified in the Δ4PAP Δ*acrB* strain with pTrcHis2 *acrB*, a high-copy number plasmid expressing the *acrB* gene with a C-terminal His-tag, thereby allowing detection with an anti-His (C-terminal)-HRP conjugated antibody. Membrane fractions of AcrB expressing cells were harvested and run on an 8% SDS-PAGE gel (20 µg protein) and transferred to a PVDF membrane. The membrane was blocked with skimmed milk, incubated with anti-His (C-terminal)-HRP conjugated antibody and imaged using chemiluminescence.

The size of the *S.* Typhimurium SL1344 AcrB protein in pTrcHis2 *acrB* is ~117 kDa, which was observed as a band between the 100 and 130 kDa marker bands (Fig. 4.6). The channel 3 AcrB mutant protein produced a band of similar density between the 100 and 130 kDa markers (Fig. 4.6). Compared to the WT AcrB protein, the channel 3 AcrB mutant protein was expressed at a level of 98%, indicating stable expression. This agreed with the previous observation by Zwama *et al.* (2018).

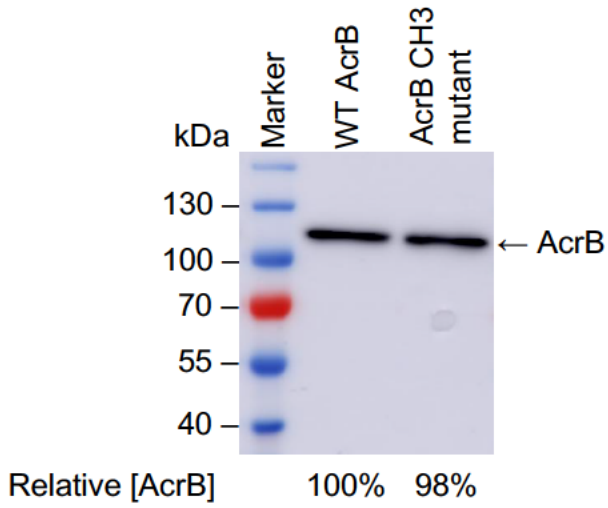


Figure 4.6. Western blotting of the channel 3 AcrB mutant protein.

Wild type and the CH3 AcrB (A33W T37W N298W) mutant were expressed in the *Salmonella* Typhimurium Δ4PAP Δ*acr*B strain from pTrcHis2 *acrB* plasmids. Membrane fractions of AcrB expressing cells were harvested and separated on an 8% SDS-PAGE gel (20 µg protein) and transferred to a PVDF membrane. Western blotting was performed using an anti-His antibody, HRP-conjugated and imaged using chemiluminescence. The PageRuler Prestained Protein Ladder was used as a molecular weight marker. Band intensity was determined using ImageJ Version 2.1 (Schindelin *et al.*, 2012), which was used to assign a relative concentration of AcrB to each band, expressed in percentage of WT AcrB protein.

4.8 The impact of the K366D AcrA mutation on channel 1 of the AcrB-transporter

The growth kinetics data suggested that the K366D AcrA mutation may also impact the entry of channel 1-substrates into AcrB, such as chloramphenicol, fusidic acid and linezolid (Tam *et al.*, 2021). Therefore, to assess the impact of the K366D AcrA mutation on substrates using channel 1, its growth in the presence of a range of linezolid concentrations was monitored. The K366D AcrA mutation conferred a clearly pronounced concentration-dependent effect, which was most pronounced at 8 μg/mL linezolid and above (Fig. 4.7). Compared to growth in LB only, the mean generation times of the Δ4PAP strain complemented with AcrA with the K366D mutation in the presence of 2 or 4 μg/mL linezolid was significantly longer (Appendix VI). The mean generation times in the presence of 8 or 16 μg/mL linezolid could not be calculated because there was no observable exponential phase at these concentrations (Appendix VI). This data supported the idea that the K366D AcrA mutation impacted the access of linezolid to channel 1 of AcrB.

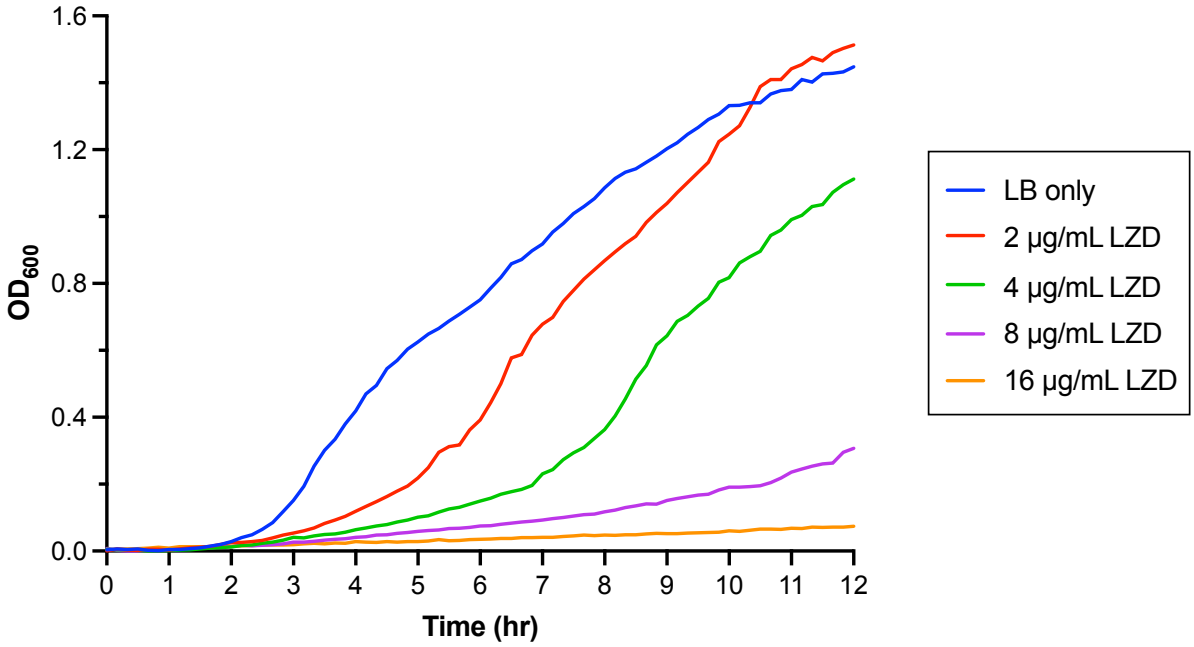


Figure 4.7. Growth kinetics of the *Salmonella* Typhimurium SL1344 Δ4PAP strain carrying plasmid with the K366D AcrA mutation in the presence of different concentrations of linezolid (LZD), a channel 1-substrate of AcrB.

Overnight bacterial cultures were diluted to a starting OD_{600} of 0.01 in a flat bottom clear 96-well plate. Bacteria were grown at 37°C with shaking in a plate reader. The OD_{600} readings of the wells was taken at 10-minute intervals for 12 hours. The data shown are the mean OD_{600} values of three biological replicates. Error bars omitted for clarity. All mean generation times are listed in Appendix VI.

The antimicrobial susceptibility and growth kinetics data showed that the K366D AcrA mutation affects the efflux of fusidic acid by the AcrB-transporter (Fig. 4.3 and Table 4.1). However, fusidic acid has been reported to use both channel 1 and channel 4 of AcrB (Fig. 4.1). Therefore, the effect of the K366D AcrA mutation on fusidic acid efflux was investigated using a channel 4 AcrB mutation. The F380A AcrB (channel 4 AcrB mutation) mutation has been previously reported to affect the access of channel 4 substrates, such as β-lactams and fusidic acid (Tam *et al.*, 2020, Tam *et al.*, 2021). Firstly, the channel 4 AcrB mutation was produced in the pET-20b *acrAB* plasmid by site-directed mutagenesis. The resulting plasmid encoding WT AcrA and the channel 4 AcrB mutation was transformed into the Δ4PAP Δ*acrB* strain to assess its phenotypic impact. The growth of the Δ4PAP Δ*acrB* strain carrying the plasmid with the channel 4 AcrB mutation was monitored in the presence of a range of fusidic acid concentrations. Compared to the WT AcrAB complement, the channel 4 AcrB mutation did not alter growth in the presence of 4, 8 or 16 μg/mL fusidic acid (Fig. 4.8). This was supported by the fact that the channel 4 mutation did not confer significantly different mean generation times compared to WT AcrAB complement (Appendix VII). This was presumably because fusidic acid was using the unaffected channel 1 (Tam *et al.*, 2021). Since the K366D AcrA mutation impacts the access of channel 1-substrates to the AcrB-transporter, it was hypothesised that combining the K366D AcrA and channel 4 AcrB mutations would impair fusidic acid efflux further. Hence, the K366D AcrA mutation was produced using the plasmid with the channel 4 AcrB mutation as a template to obtain a plasmid with the combined K366D AcrA + channel 4 AcrB mutation. Consistent with this prediction, the Δ4PAP Δ*acrB* strain complemented with the K366D AcrA + channel 4 AcrB mutation was unable to grow in the presence of 8 or 16 μg/mL fusidic acid more than the K366D AcrA or the channel 4 AcrB mutations acting alone

(Fig. 4.8). These data suggest that the K366 AcrA mutation is also involved in either active substrate vetting or surveillance of the substrate-bound state of the AcrB-transporter.

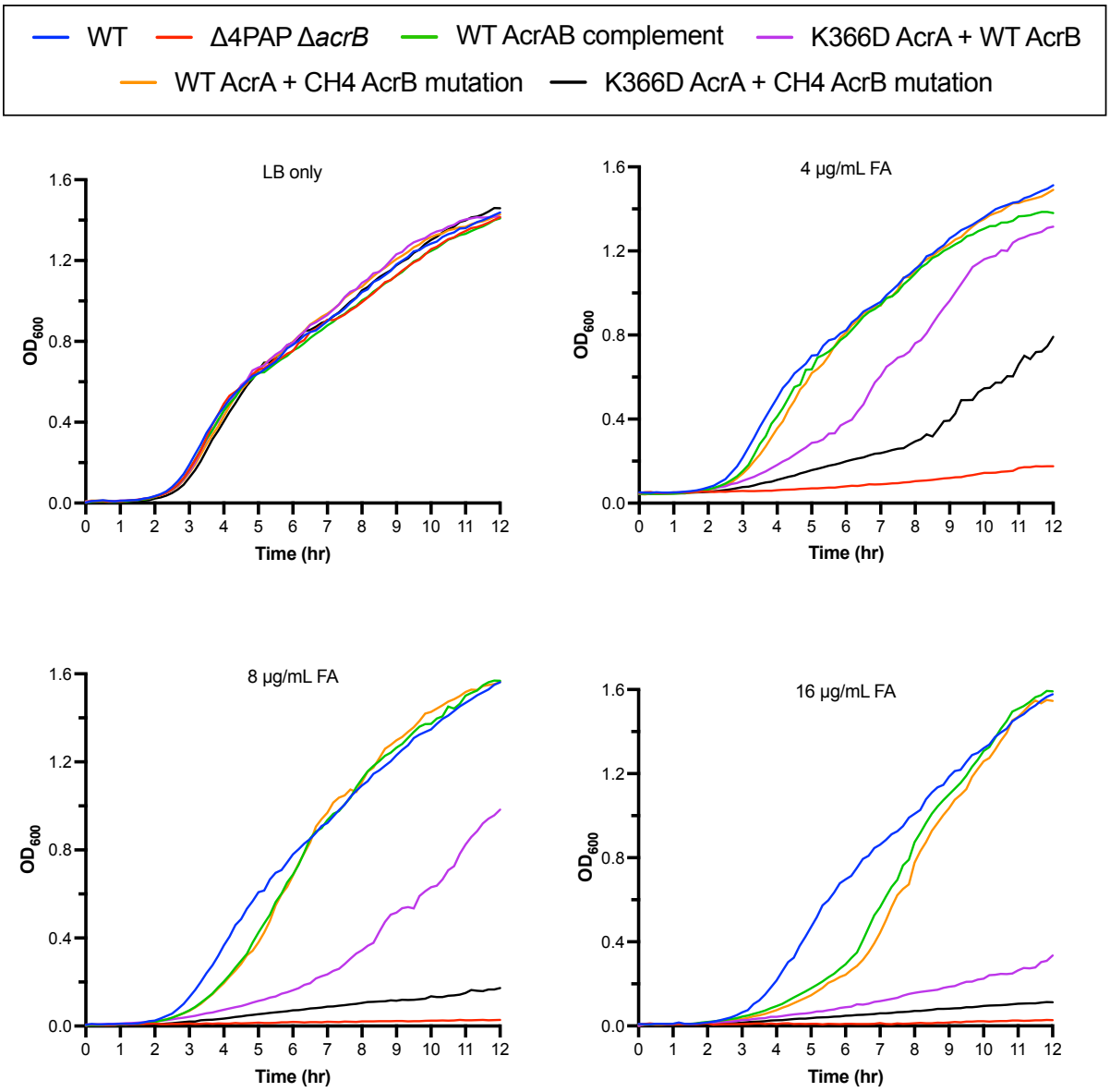


Figure 4.8. Growth kinetics of the *Salmonella* Typhimurium SL1344 Δ4PAP Δ*acrB* strain carrying the plasmid with the K366D AcrA and channel 4 (F380A) AcrB mutations in the presence of fusidic acid (FA), a channel 1- and channel 4-substrate of AcrB.

Overnight bacterial cultures were diluted to a starting OD_{600} of 0.01 in a flat bottom clear 96-well plate. Bacteria were grown at 37°C with shaking in a plate reader. The OD_{600} readings of the wells was taken at 10-minute intervals for 12 hours. WT AcrAB complement refers to the Δ4PAP Δ*acrB* strain complemented with pET-20b *acrAB*. The data shown are the mean OD_{600} values of three biological replicates. Error bars omitted for clarity. All mean generation times are listed in Appendix VII.

4.9 Discussion

During efforts to identify the critical PAP residues involved in RND-binding, the K366D mutation mapping to the MPD of AcrA showed peculiar results concerning antimicrobial susceptibility. In this section, the impact of the K366D AcrA mutation on the antimicrobial susceptibility of the Δ4PAP strain with respect to the substrate channel preference was investigated. The data indicated that the K366D AcrA mutation impacted the efflux of substrates entering AcrB through channel 1 and channel 2 but not channel 3 and channel 4 (Fig. 4.3), suggesting a role for the PAP in altering substrate specificity. The involvement of the PAPs in modulating substrate specificity is poorly understood, however studies on non-cognate PAP complementation suggest a role. Krishnamoorthy *et al.* (2008) found a change of substrate profile brought by the complementation analysis of AcrA interactions with the MexB-transporter of *P. aeruginosa*. In the chimeric complex, AcrA was reported to confer near WT resistance to EtBr, novobiocin and SDS, but not to other MexB-substrates, such as erythromycin, lincomycin and nalidixic acid. Furthermore, single point mutations in AcrA were found to be sufficient to increase the efflux activity of the MexB-transporter. This suggested that the change of the PAP component (MexA to AcrA) altered the substrate specificity of the MexB-transporter (Krishnamoorthy *et al.*, 2008). The MFS-associated PAP EmrA of the EmrAB-TolC complex has been reported to bind substrates CCCP and nalidixic acid (Borges-Walmsley *et al.*, 2003). This suggests that EmrA may capture substrates from the periplasm to present to the EmrB-transporter or receive substrates from the transporter to transfer to the outer membrane channel TolC (Zgurskaya *et al.*, 2009).

The available data does not provide a definitive answer as to how the MPD of the PAP may impact the apparent substrate preference and selection. However, the analysis of the available

PAP-RND complex structures (Glavier *et al.*, 2020, Wang *et al.*, 2017, Tsutsumi *et al.*, 2019) (Fig. 4.1), provides hints to the possible mechanism of the K366 action. One straightforward possibility, based on the location of K366 near the suggested entry of channel 2 (Zwama *et al.*, 2018), and the flexibility of its side-chain is that it may affect channel 2 substrate access and kinetics by playing the role of a "cap" on the tunnel entrance, possibly sensing, and even partially coordinating the incoming substrate. However, the effect of the K366D AcrA mutation also extends to channel 1-substrates, such as linezolid and chloramphenicol, while K366 is located too far away from the suggested channel 1 entry points to be directly involved in any active substrate vetting. Therefore, it may be that K366, and the MPD may be involved in more generalised sensing of the substrate occupied state of the PBP, which is the convergence of channel 1 and channel 2 (Fig. 4.1) (Sennhauser *et al.*, 2007, Nakashima *et al.*, 2011). The recent *in-situ* structure of the AcrAB-TolC complex unambiguously identified the location of the C-terminal helices and the membrane-associated N-terminal tails of the PAP AcrA (Chen *et al.*, 2021). These appear to occupy a crevasse on the surface of AcrB that may also plausibly account for channel 1 effects reported here, possibly providing additional sensory or allosteric input. Such sensory input may be allosterically conveyed to the engagement of the OMF TolC during the initial assembly of the tripartite complex, or possibly provide directionality of the L-T-O transition during the efflux cycle, which is compatible with the mechanistic model of RND pump cycling suggested recently (Alav *et al.*, 2021).

In this chapter, the effect of the K366D AcrA mutation on the AcrB substrate channels was explored. Through phenotypic assessment of the K366D AcrA mutation, a potential role for the PAP membrane-proximal domain in modulating substrate access to the RND-transporter was identified. This provides further support for the increasingly important role of the PAP in the

assembly, structure, and function of tripartite efflux pumps. Owing to their crucial role in tripartite efflux pumps, PAPs are attractive drug targets for efflux inhibition to combat the growing threat of AMR.

4.10 Key finding

- The K366D AcrA mutation impacts the efflux of substrates that enter the AcrB-transporter through channel 1, channel 2 but not channel 3 or channel 4.
- This study provides evidence for the role of the PAP in substrate vetting.

4.11 Future work

The K366D mutation was a radical replacement, wherein the positively charged lysine residue was replaced by a negatively charged aspartate residue. Therefore, K366 could be subjected to conservative replacement with an uncharged yet polar residue, such as serine or threonine. This would allow investigation of the importance of the positive moiety at position 366 for substrate access to the AcrB-transporter.

Previous studies have employed molecular dynamics to study the effect of mutations on PAPs and the binding of ligands to RND-transporters of the tripartite efflux assemblies (Vargiu and Nikaido, 2012, Johnson *et al.*, 2020, Cacciotto *et al.*, 2022). Therefore, molecular dynamic simulations could be used to investigate the impact of the K366D AcrA mutation on the dynamics of the AcrAB-TolC pump. Using the available tripartite structures of the AcrAB-TolC pump (Du *et al.*, 2014, Wang *et al.*, 2017), the K366D mutation could be generated in AcrA and its effect on AcrB could be studied *in silico*. This could provide insight into how the K366D mutation alters the access of substrates to the channels of AcrB. Experimentally, the

effect of the K366D AcrA mutation on AcrB substrate channel access should be investigated by *in vivo* crosslinking. The N-terminal tail of AcrA, where K366 is located, should be crosslinked *in vivo* to AcrB using a crosslinker with a long spacer arm, such as DSP (dithiobis (succinimidyl propionate)). This could allow to see impact of changes in the N-terminal tail of AcrA on channel 1 and channel 2 substrate access.

The F380A AcrB mutation has been previously shown to be stable in *E. coli* (Tam *et al.*, 2021), however, it could not be blotted in *S.* Typhimurium. Therefore, the F380A AcrB mutation should be blotted in *S.* Typhimurium to ensure that its additive effect on fusidic acid efflux is not due to changes in protein expression or stability.

CHAPTER 5. Functional validation of the conserved binding box boxes in the related periplasmic adaptor protein AcrE of *Salmonella* Typhimurium

CHAPTER 5. Functional validation of the conserved binding boxes in the related periplasmic adaptor protein AcrE of *Salmonella* Typhimurium

5.1 Background

In *S.* Typhimurium, the PAPs AcrA and AcrE are closely related with an amino acid sequence identity of 69.3%, and a virtually identical secondary structure compared to the experimentally determined structure of AcrA from *E. coli* (McNeil *et al.*, 2019). In addition to its cognate RND-transporter AcrF, AcrE has also been shown to function with the non-cognate RND-transporter AcrB (Elkins and Nikaido, 2003, McNeil *et al.*, 2019). Likewise, AcrA has been shown to function with the non-cognate RND-transporter AcrF (Elkins and Nikaido, 2003). In Chapter 3, the binding box model of PAP-RND interactions was validated for AcrA in AcrB-binding. Specifically, mutations in residues mapping to boxes 1, 4, 5 and 9 of AcrA were found to impair efflux function by disrupting its interaction with AcrB. The residues mapping to the binding boxes of AcrA and AcrE are identical in *S.* Typhimurium, potentially explaining the observed interchangeability between the PAPs (Smith and Blair, 2014, McNeil *et al.*, 2019). Here, the functional role of binding boxes 1, 4, 5 and 9 of AcrE in AcrB-binding will be investigated. To validate their functional role, site-directed mutagenesis will be used to mutate the residues corresponding to the most critical binding box residues previously identified in AcrA – namely G57, R58, T270, S272, I273, F291, R293 and G362. Subsequently, the phenotypic effects of the AcrE mutations will be assessed by measuring the intracellular accumulation of EtBr and antimicrobial susceptibility.

5.2 Aims

- To mutate the residues of AcrE corresponding to the most critical binding box residues previously identified in AcrA.
- To test the phenotypic effects of AcrE mutations by measuring the intracellular accumulation of EtBr and antimicrobial susceptibility
- To confirm the stable expression of AcrE mutants by Western blotting.

5.3 Hypothesis

- AcrA and AcrE bind to RND-transporters in the same way using equivalent residues

5.4 Investigating the functional role of the binding box model in AcrE

The functional role of the binding boxes in AcrE was investigated by site-directed mutagenesis to mutate the residues previously identified as important for AcrA binding to AcrB from Chapter 3 – namely G57, R58, T270, S272, I273, F291, R293 and G362. The leaky expression of *acrE* from pET-20b has been previously shown to be insufficient for phenotypic rescue in *S.* Typhimurium SL1344 (Smith and Blair, 2014, McNeil *et al.*, 2019). Therefore, mutations in AcrE were produced in pTrcHis2 *acrE*, a high copy number plasmid expressing WT *acrE* with a C-terminal His-tag (McNeil *et al.*, 2019). The C-terminal His-tag is in the membrane proximal domain of AcrE, facing away from the RND-transporter, therefore, it is unlikely to affect the stability of the complex. Moreover, the C-terminal His-tag has been shown to have no impact on the function of *acrE* (McNeil *et al.*, 2019). The effect of AcrE mutations was assessed by measuring the intracellular accumulation of EtBr and antimicrobial susceptibility in the SL1344 Δ4PAP Δ*acrF* strain (McNeil *et al.*, 2019). This strain lacks all four RND-associated PAPs and the cognate RND-transporter AcrF, thereby allowing the effect of AcrE mutations on AcrB-

binding to be determined. The effect of AcrE mutations was tested for AcrB-binding and not AcrF-binding. This is because the AcrF-transporter is expressed at very low levels under standard laboratory conditions (Nishino *et al.*, 2006), therefore, the impact of AcrE mutations on AcrF-binding would not produce an observable phenotypic effect.

Compared to the WT strain, the Δ4PAP Δ*acrF* strain accumulated significantly more EtBr and displayed increased susceptibility to AcrB-substrates (Fig. 5.1 and Table 5.1). This is because the Δ4PAP Δ*acrF* strain lacks the genes encoding for the PAPs AcrA and AcrE necessary to form efflux competent RND pumps with AcrB and TolC (McNeil *et al.*, 2019). The lack of the gene encoding for the AcrF-transporter in the Δ4PAP Δ*acrF* strain did not result in any differences in antimicrobial susceptibility compared to the Δ4PAP strain because the lack of PAPs in the latter strain has already rendered any RND pump non-functional (McNeil *et al.*, 2019).

Complementation of the Δ4PAP Δ*acrF* strain with pTrcHis2 *acrE* (WT AcrE complement) significantly reduced EtBr accumulation and susceptibility to AcrB-substrates (Fig. 5.1 and Table 5.1). This verified the previously reported functionality of AcrE with the RND-transporter AcrB (McNeil *et al.*, 2019). The Δ4PAP Δ*acrF* strain carrying plasmid with the AcrE mutations in the critical residues of AcrA (AcrE G57F, R58A, T270D, S272F, I273D, F291G, R293F and G362F) resulted in significantly more EtBr accumulation compared to complementation with the WT AcrE (Fig. 5.1). The mutations which increased EtBr accumulation also reduced MIC values by at least two-fold to AcrB-substrates (Table 5.1). Consistent with this, the mutation of residues shown to be phenotypically neutral in AcrA, corresponding to the AcrE T216F, K365D and R367D mutations respectively, had no impact

on EtBr accumulation (Fig. 5.1) or antimicrobial susceptibility (Table 5.1). Unexpectedly, the K365D AcrE mutation, which corresponds to the substrate channel specific K366D AcrA mutation, did not affect the efflux of substrates using channel 1 (ciprofloxacin, chloramphenicol, fusidic acid and novobiocin) or channel 2 (clindamycin, doxorubicin, erythromycin, and minocycline) (Table 5.1). These data indicated the conservation of function of the binding boxes between AcrA and AcrE, which explains their interoperability in conjunction with AcrB to form an efflux-competent pump.

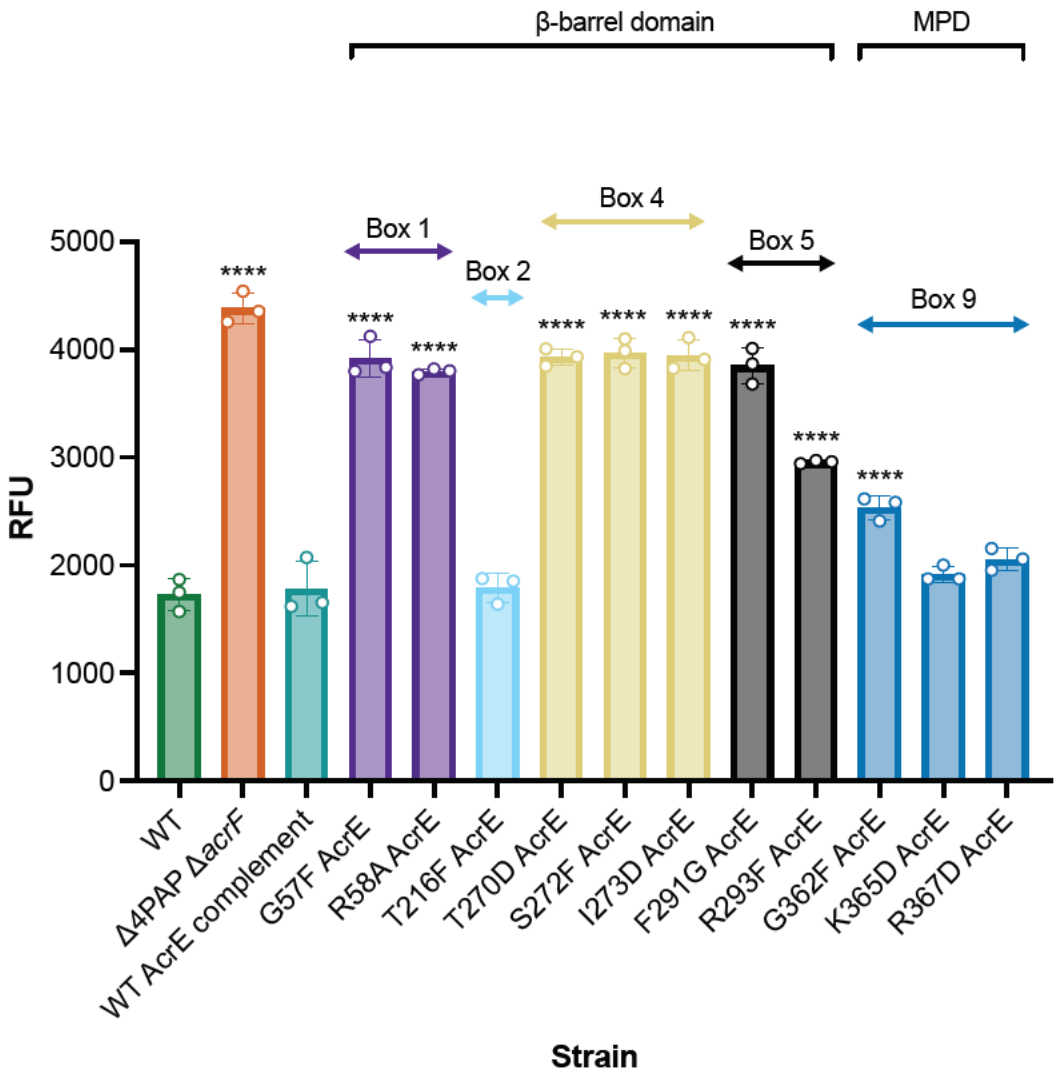


Figure 5.1. Accumulation of ethidium bromide in the *Salmonella* Typhimurium SL1344 Δ4PAP Δ*acrF* strain carrying plasmid with different versions of AcrE.

Bacteria were grown to early exponential phase, diluted to an OD_{600} of 0.2 in buffer. Cells were loaded into a flat bottom black 96-well plate and injected with ethidium bromide immediately. Fluorescence of ethidium bromide was measured over 30 minutes. WT AcrE complement refers to the Δ4PAP Δ*acrF* strain with pTrcHis2 *acrE*. Annotation above indicates the mapping of each mutation to its binding box, as well as the domain mapping of respective boxes. Data shown are the mean of three biological replicates showing maximum relative fluorescence unit (RFU) values at the end of 30 minutes of ethidium bromide exposure ± standard deviation. Each point mutation was compared to the WT AcrE complement using one-way ANOVA, followed by Dunnett's test to correct for multiple comparisons. Strains with significantly different ethidium bromide accumulation to WT AcrE complement are indicated with **** ($P \leq 0.0001$). MPD, membrane-proximal domain.

Table 5.1. Antimicrobial susceptibility of the *Salmonella* Typhimurium SL1344 Δ4PAP Δ*acrF* strain carrying plasmid with different versions of AcrE.

	MIC (μg/mL)													
Strain	ACR	BZK	CHL	CIP	CLI	CV	DOX	EtBr	ERY	FA	MB	MIN	NOV	R6G
WT	256	64	4	0.015	512	64	1024	>1024	64	1024	1024	1	512	>1024
Δ4PAP Δ*acrF*	16	4	0.5	0.008	1	2	2	16	4	4	8	0.25	1	8
The following rows are Δ4PAP Δ*acrF* background strain + pTrcHis2 carrying different versions of AcrE														
WT AcrE complement	256	64	4	0.015	256	32	512	>1024	64	512	1024	1	512	>1024
G57F AcrE	**16**	**4**	**0.5**	**0.008**	**4**	**1**	**2**	**16**	**4**	**4**	**8**	**0.25**	**2**	**8**
R58A AcrE	**16**	**4**	**0.5**	**0.008**	**4**	**1**	**2**	**16**	**4**	**4**	**8**	**0.25**	**2**	**8**
T216F AcrE	256	64	4	0.015	128	32	512	1024	64	1024	1024	1	512	1024
T270D AcrE	**16**	**4**	**0.5**	**0.008**	**4**	**1**	**2**	**16**	**4**	**8**	**8**	**0.25**	**1**	**8**
S272F AcrE	**16**	**4**	**1**	**0.008**	**4**	**4**	**4**	**32**	**2**	**4**	**16**	**0.25**	**1**	**8**
I273D AcrE	**16**	**4**	**1**	**0.008**	**4**	**4**	**2**	**32**	**2**	**4**	**16**	**0.25**	**1**	**8**
F291G AcrE	**16**	**4**	**0.5**	**0.008**	**4**	**2**	**2**	**16**	**4**	**8**	**8**	**0.25**	**1**	**8**
R293F AcrE	**16**	**8**	**0.5**	**0.008**	**8**	**2**	**8**	**64**	**4**	**32**	**64**	**0.25**	**16**	**64**
G362F AcrE	**32**	**8**	**0.5**	**0.008**	**16**	**2**	**8**	**64**	**4**	**32**	**128**	**0.25**	**16**	**64**
K365D AcrE	128	64	4	0.015	256	16	512	1024	64	512	1024	1	256	1024
R367D AcrE	256	64	4	0.015	256	32	512	1024	64	512	1024	1	256	1024

Underlined values highlight values for the Δ4PAP Δ*acrF* strain complemented with pTrcHis2 *acrE* (WT AcrE complement). Bold values indicate at least two-fold or more difference compared to the parent strain. Strains coloured in red indicate AcrE mutations with impaired ethidium bromide efflux. Drug abbreviations: ACR, acriflavine; BZK, benzalkonium chloride; CHL, chloramphenicol; CIP, ciprofloxacin; CLI, clindamycin; CV, crystal violet; DOX, doxorubicin; EtBr, ethidium bromide; ERY, erythromycin; FA, fusidic acid; MB, methylene blue; MIN, minocycline; NOV, novobiocin; R6G, rhodamine 6G.

5.5 Western blotting of AcrE mutant proteins

The protein expression and stability of the AcrE mutants with impaired efflux were confirmed by Western blotting. The AcrE protein levels were quantified in the Δ4PAP Δ*acrF* strain with pTrcHis2 *acrE*, a high-copy number plasmid expressing the *acrE* gene with a C-terminal His-tag, thereby allowing detection with an anti-His (C-terminal)-HRP conjugated antibody. Membrane fractions of AcrE expressing cells were harvested and run on a 12% SDS-PAGE gel (20 μg protein) and transferred to a PVDF membrane. The membrane was blocked with skimmed milk, incubated with anti-His (C-terminal)-HRP conjugated antibody, and visualised using chemiluminescence.

The size of the *S.* Typhimurium SL1344 AcrE protein in pTrcHis2 *acrE* is ~45 kDa, which was seen as a band between the 40 and 55 kDa marker bands (Fig. 5.2). The efflux impaired AcrE point mutants R58A, T270D, S272F, I273D, F291G, R293F and G362F, all produced a band between the 40 kDa and 55 kDa marker that corresponded to broadly similar expression level as WT AcrE protein. The G57F AcrE mutant produced a band with weaker intensity, which corresponded to an expression level of 55% compared to WT AcrE protein. The phenotypically neutral T216F, K365D and R367D AcrE proteins also showed stable expression with similar expression levels to that of WT AcrE protein. This verified that the effect of all the mutations, except for G57F, were not likely to be due to changes in protein expression or stability.

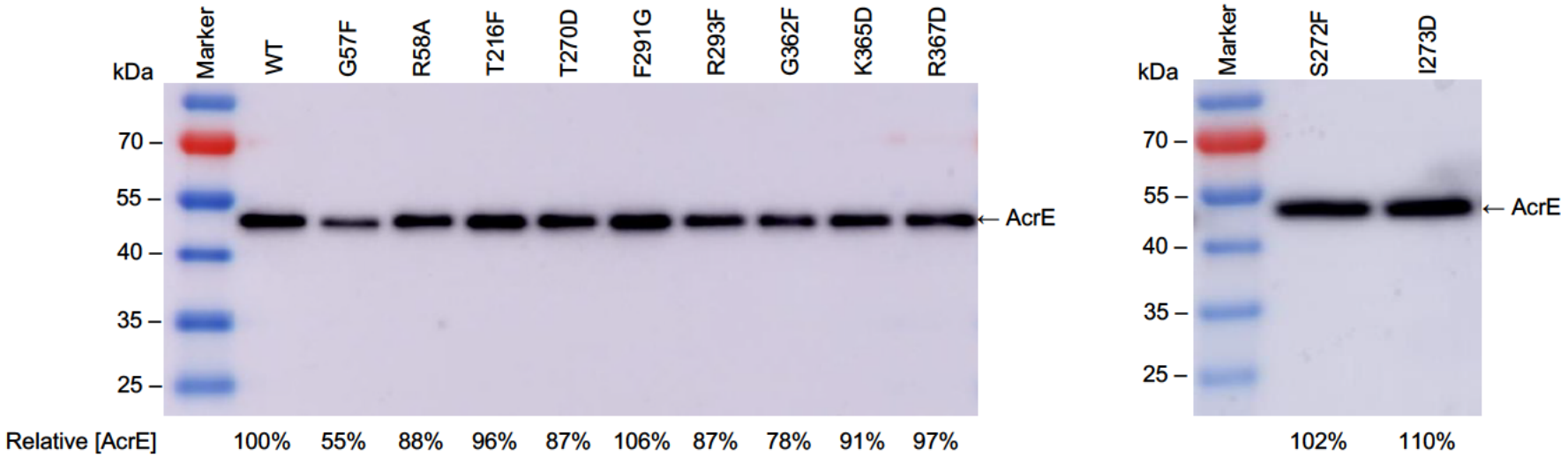


Figure 5.2. Western blotting of mutant AcrE.

Membrane fractions of AcrE expressing *Salmonella* Typhimurium SL1344 Δ4PAP Δ*acrF* cells were harvested and separated on a 12% SDS-PAGE gel (20 µg protein) and transferred to a PVDF membrane. Western blotting was performed using an anti-His antibody, HRP-conjugated and imaged using chemiluminescence. The PageRuler Prestained Protein Ladder was used molecular weight marker. Band intensity was determined using ImageJ Version 2.1 (Schindelin *et al.*, 2012), which was used to assign a relative concentration of AcrE to each band, expressed in percentage of WT AcrE protein.

5.6 Discussion

AcrA and AcrE are closely related PAPs and share an almost identical secondary structure (McNeil *et al.*, 2019). Furthermore, AcrA and AcrE have been shown in multiple studies to be interchangeable (Kobayashi *et al.*, 2001, Elkins and Nikaido, 2003, Smith and Blair, 2014, McNeil *et al.*, 2019). Their cognate RND-transporters AcrB and AcrF are also very similar with an amino acid sequence similarity of 90.4% (Blair *et al.*, 2015b), hence the AcrA and AcrE RND-binding residues were expected to be similar. However, the molecular determinants that drive this interoperability have not been studied in detail. In Chapter 3, the binding box model of PAP-RND interactions was defined to elucidate the most critical residues of AcrA involved in binding to its cognate RND-transporter AcrB. These were limited to binding boxes 1, 4, 5 and 9. Using the defined binding box model from Chapter 3, the role of AcrE RND-binding residues in AcrB-binding was investigated.

The AcrE residues corresponding to the most critical binding box residues previously identified in AcrA (Chapter 3) were mutated and their phenotypic effect was assessed. The AcrE mutations mapping to binding boxes 1 (G57F and R58A), 4 (T270D, S272F and I273D), 5 (F291G and R293F) and 9 (G362F) were found to significantly impair efflux function (Fig. 5.1 and Table 5.1). This validated the conservation of function of the binding boxes between AcrA and AcrE, explaining their interoperability with AcrB. Consistent with this, the mutation of phenotypically neutral residues in AcrA, corresponding to the AcrE T216F, K365D and R367D, also had no impact on efflux function (Fig. 5.1 and Table 5.1). The binding boxes between AcrA and AcrE are virtually identical, whilst differing significantly in MdtA and MdsA. Additionally, AcrA and AcrE share a virtually identical structure in binding regions and are therefore interoperable with the AcrB-transporter. On the other hand, MdtA and MdsA have a

markedly different structure and therefore cannot function with non-cognate RND-transporters. Although there is no structural information available for AcrE, due to its high level of similarity with AcrA, homology modelling can be used to make accurate structural predictions. As shown in Figure 5.3, the critical RND-binding residues in AcrE map to identical regions as in AcrA. As with AcrA, the critical binding box residues of AcrE mapping to the β-barrel domain form a pincer-like interface that presumably provides an interaction site with the RND-transporter. Similarly, the conserved G362 residue mapping to the MPD is presumably involved in multiple interactions with the RND-transporter. Although further work is necessary due to the lack of an assembled structure with AcrE, some of the binding residues have been defined in this study. Interestingly, the K365D AcrE mutation, which corresponds to the K366D AcrA mutation discussed in Chapter 4, did not impact the efflux of substrates that enter AcrB through channel 1 or channel 2 (Table 5.1). This suggests that even though AcrA and AcrE share functionally conserved RND-binding residues, there may be subtle differences in their MPD. This may account for the observed lack of impact of the K365D AcrE mutation on substrate channel vetting.

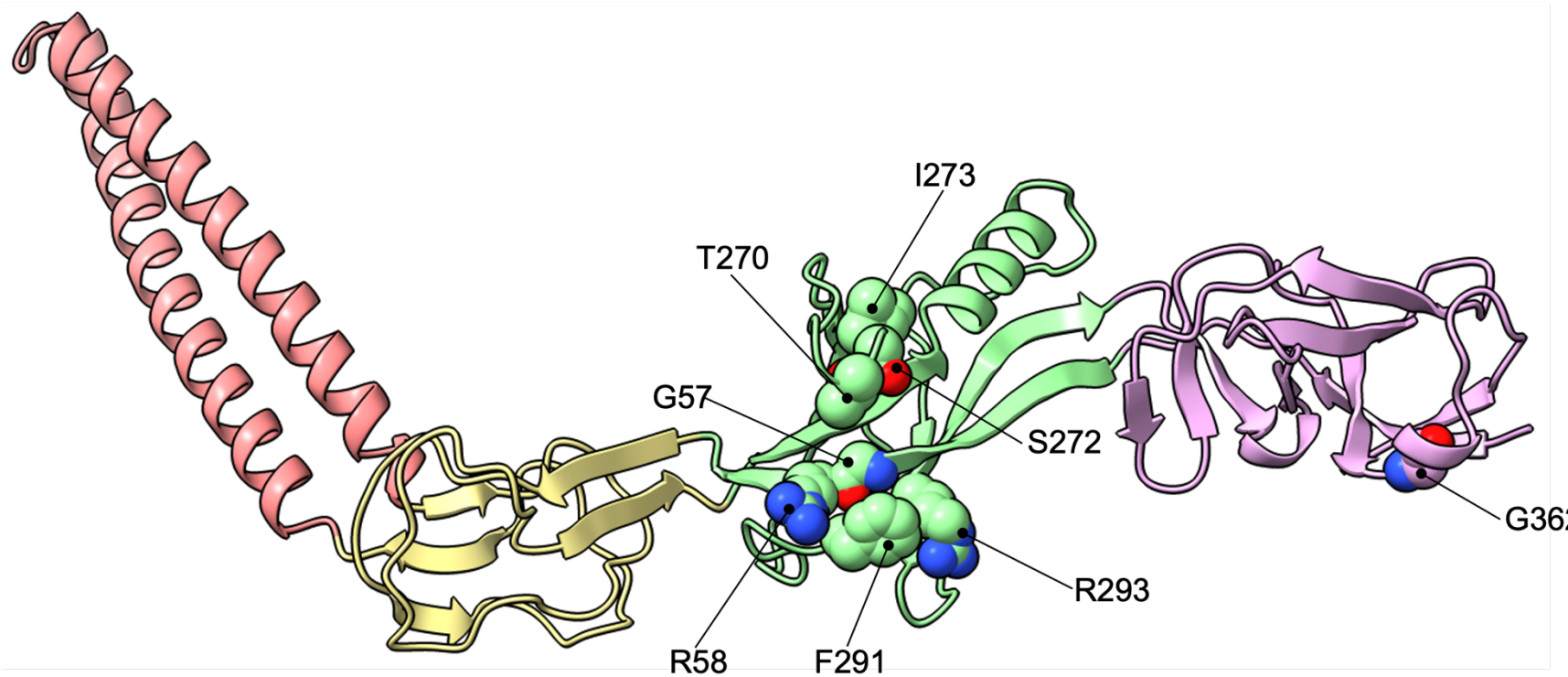


Figure 5.3. The predicted structure of AcrE.

The critical RND-binding residues are labelled and denoted by spheres. The colouring highlights the domain arrangement of AcrE: α-hairpin (coral), lipoyl (yellow), β-barrel (green), and membrane-proximal (purple) domains. The structural prediction of AcrE was made using AlphaFold Monomer v2.0 (Jumper *et al.*, 2021, Varadi *et al.*, 2021).

Here, the RND-binding residues of AcrA and AcrE were shown to be identical, explaining their interoperability with the RND-transporter AcrB. This has important implications for the development of efflux inhibitors. Previously, targeting AcrA has been shown to be a viable strategy for the inhibition of the AcrAB-TolC pump (Abdali *et al.*, 2017, Darzynkiewicz *et al.*, 2019). However, any potential PAP inhibitor would need to target both AcrA and AcrE to be effective due to their interchangeability. If the function of AcrA alone was inhibited, AcrE would be able to carry out the function of AcrA, thereby rendering AcrA inhibition redundant. Hence, the conserved RND-binding residues identified in this study could be potential drug target sites for the development of efflux inhibitors capable of inhibiting both AcrA and AcrE.

5.7 Key findings

- Mutations mapping to binding boxes 1, 4 and 5 of the β-barrel domain and box 9 of the MPD of AcrE significantly increased EtBr accumulation and increased susceptibility to AcrB-substrates.
- With a possible exception for G57F, the efflux impaired AcrE mutants were stably expressed compared to WT protein.
- The function of the critical RND-binding boxes is conserved between AcrA and AcrE.

5.8 Future work

The current work demonstrates that AcrA and AcrE share highly conserved binding boxes with respect to AcrB-binding. Since AcrA and AcrE can also function with the RND-transporters AcrD and AcrF, the role of the critical binding boxes of AcrA and AcrE should be investigated for AcrD- and AcrF-binding. This would provide insight into the PAP regions that drive the promiscuity between AcrA and AcrE. Importantly, if the shared binding boxes of AcrA and

AcrE are shown to be important for binding to other RND-transporters, targeting these residues with an efflux inhibitor could prevent the assembly of all RND pumps that rely on AcrA or AcrE. This would provide a broader range of inhibition of tripartite RND pumps that are important mediators of AMR. Lastly, to verify the impact of the AcrE mutations on AcrB-binding, the physical binding affinity between the WT AcrB and the AcrE mutant proteins should be measured using isothermal titration calorimetry or surface plasmon resonance.

CHAPTER 6. Investigating the interchangeability of periplasmic adaptor proteins AcrA and AcrE in forming functional efflux pumps with AcrD in *Salmonella* Typhimurium

CHAPTER 6. Investigating the interchangeability of periplasmic adaptor proteins AcrA and AcrE in forming functional efflux pumps with AcrD in *Salmonella* Typhimurium

6.1 Background

The RND-transporter AcrD does not have its own PAP. It has been previously shown that AcrD depends on the PAP AcrA to form a functional tripartite efflux system in *S.* Typhimurium (Yamasaki *et al.*, 2011). Indeed, AcrA has been reported to also function with AcrF in *E. coli* and recently, AcrE has been demonstrated to function with AcrB in *S.* Typhimurium (Kobayashi *et al.*, 2001, McNeil *et al.*, 2019). The major RND-transporter binding residues of AcrA have been highlighted by cryogenic electron microscopy structural studies and validated by mutagenesis in this study. Comparative analysis of *Salmonella* PAPs demonstrated that these critical residues fall within a discrete number of linear sequence sites, which was termed RND-binding boxes (Chapter 3). These are shared between AcrA and AcrE, potentially explaining their interchangeability. However, MdtA and MdsA are not interchangeable and cannot function with non-cognate RND-transporters and correspondingly are significantly different within RND-binding boxes. Although AcrA and AcrE have been shown to be largely interchangeable, the ability of AcrE to function with AcrD remains unknown.

6.2 Aims

- To investigate whether the periplasmic adaptor protein AcrE can support function through the RND-transporter AcrD.
- To test whether the same residues are important for this as for AcrA-AcrB interactions.

6.3 Hypotheses

- Co-expression of *acrD* and *acrE* in the Δ3RND strain will decrease susceptibility to AcrD-substrates, indicating functionality of AcrE with AcrD.
- Disruption of the RND-binding residues in AcrA or AcrE will impair AcrD-mediated efflux of substrate drugs.

To test these hypotheses, the antimicrobial susceptibility of the mutant strains to AcrD-substrates and AcrB-substrates was determined by agar dilution.

6.4 Construction of the *acrAB*, *acrD* and *acrEF*-deletion *Salmonella* Typhimurium mutant strain

To test whether the PAP AcrE can support function through the RND-transporter AcrD, a basal strain lacking the *acrAB*, *acrD* and *acrEF* efflux genes was constructed. The *acrAB* and *acrEF* genes encode the AcrAB and AcrEF RND pumps, respectively. The AcrAB and AcrEF pumps can export most AcrD-substrates (Nishino *et al.*, 2006). Therefore, background efflux of AcrD-substrates was eliminated by deleting the *acrAB*, *acrD* and *acrEF* genes. The *mdtABC* and *mdsABC* genes encoding for the MdtABC and MdsABC RND pumps, respectively, were not deleted as they are not expressed under laboratory conditions and do not export AcrD-substrates (Nishino *et al.*, 2006, McNeil *et al.*, 2019). Firstly, the *acrAB* operon was inactivated and deleted as described in Section 2.3. Thereafter, the pSIM18 plasmid was transformed into the Δ*acrAB* strain, and the process was repeated to delete the *acrD* gene and then finally the *acrEF* operon.

6.4.1 Verification of gene deletion

To verify the deletion of all three RND efflux systems, PCR was carried out to check for the size of the *acrAB*, *acrD* and *acrEF* genes. The size of the *acrAB* operon was checked by using primers P66 and P83 (Table 2.2), which bind upstream of the *acrA* and downstream of the *acrB* genes, respectively. The size of the *acrD* gene was checked by using primers P305 and P306 (Table 2.2), which bind upstream and downstream of the *acrD* gene. The size of the *acrEF* operon was checked by using primers P34 and P81 (Table 2.2), which bind upstream of the *acrE* and downstream of the *acrF* genes, respectively. Furthermore, PCR was carried out after each gene deletion to ensure that the *aph* cassette was not re-inserted at previous FRT scar sites. As shown in Figure 6.1, the final Δ*acrAB* Δ*acrD* Δ*acrEF* *Salmonella* Typhimurium SL1344 strain produced amplimers of approximately 500, 550 and 200 bps for the *acrAB*, *acrD* and *acrEF* check primers, respectively. This suggested the successful deletion of the RND efflux genes. The correct sequence of the amplicons was verified by Eurofins Genomics, confirming successful deletion of the *acrAB*, *acrD* and *acrEF* genes. The Δ*acrAB* Δ*acrD* Δ*acrEF* *Salmonella* Typhimurium SL1344 strain was designated SE502 (Table 2.1).

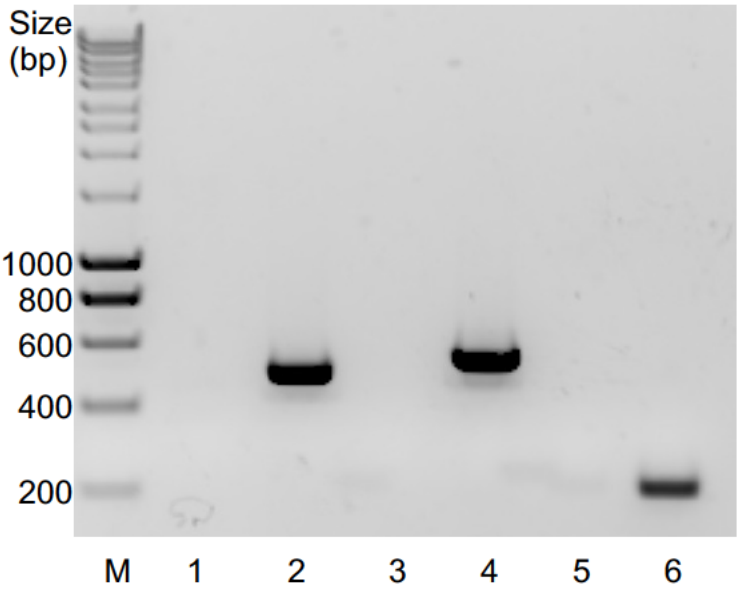


Figure 6.1. Agarose gel electrophoresis of PCR amplified products using check primers for *acrAB*, *acrD* and *acrEF* from *Salmonella* Typhimurium SL1344 Δ*acrAB* Δ*acrD* Δ*acrEF* (Δ3RND).

Negative controls contained no template DNA.
Lane M: HyperLadder 1kb molecular weight ladder.
Lane 1: *acrAB* negative control
Lane 2: *acrAB* amplicon
Lane 3: *acrD* negative control
Lane 4: *acrD* amplicon
Lane 5: *acrEF* negative control
Lane 6: *acrEF* amplicon

6.5 Verification of cloning

The *acrD* gene was cloned into pHSG398, a high copy number plasmid with a pMB1-derived origin of replication. The *acrA* or *acrE* genes were cloned into pACYC177, a low copy number plasmid with a p15 origin of replication. This allowed co-expression of *acrD* with *acrA* or *acrE* because pHSG398 and pACYC177 have compatible origins of replication. The cloning of *acrD*, *acrA* and *acrE* into their respective plasmids was verified by PCR as described in Section 2.7.6. The *acrD* insert was checked by using primers P334 and P335 that annealed to the upstream and downstream of the cloning insert in pHSG398. The *acrA* or *acrE* inserts were checked by using primers P338 and P339 that annealed to the upstream and downstream of the cloning insert in pACYC177. As shown in Figure 6.2, successful cloning candidates produced amplicons of 1345 bp, 1369 bp and 3299 bp for *acrA*, *acrE* and *acrD*, respectively. The predicted size of the cloned *acrD* insert in pHSG398 is shown in Figure 6.3, and the predicted sizes of the *acrA* or *acrE* insert in pACYC177 is shown in Figure 6.4. The correct sequence of the cloning candidates was verified by Eurofins Genomics.

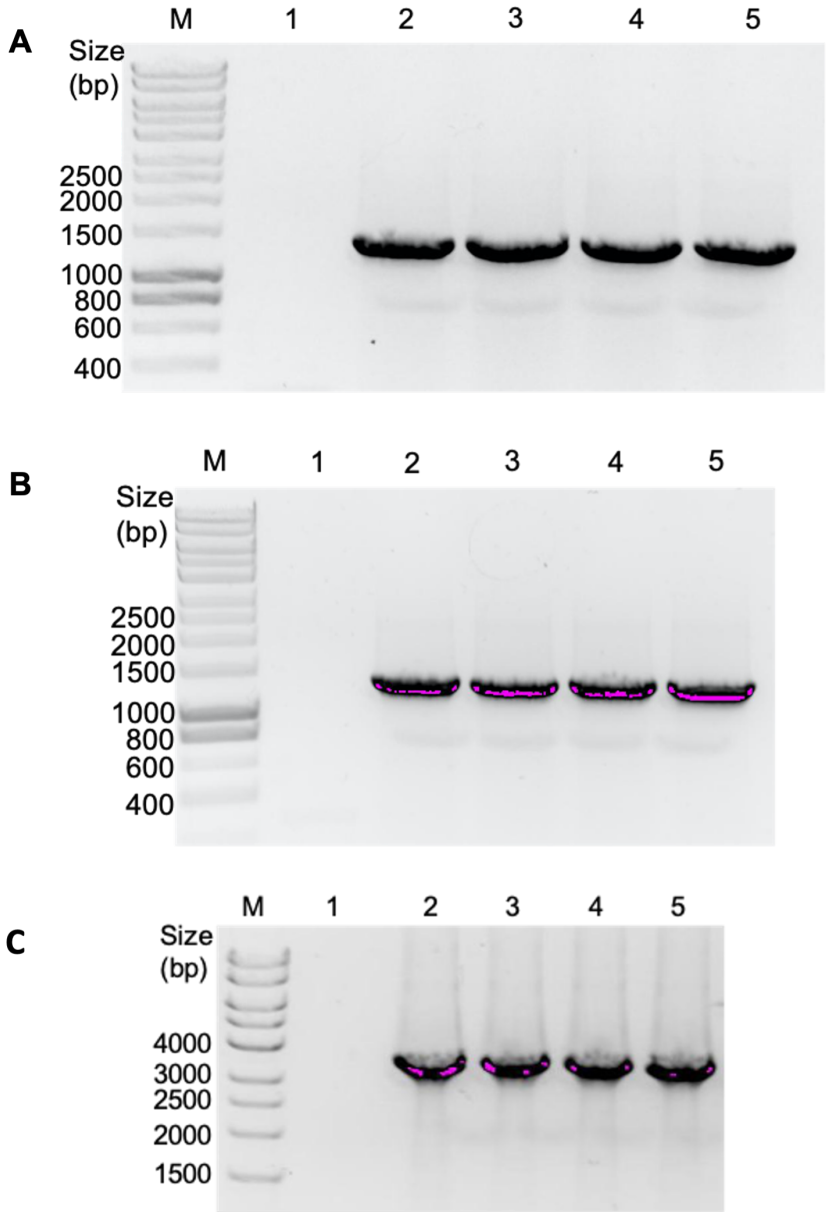


Figure 6.2. PCR check of the *acrA*, *acrE* and *acrD* cloning inserts.

Agarose gel electrophoresis of PCR amplified products using plasmid insert check primers for **A)** *acrA* (expected size 1345 bp), **B)** *acrE* (expected size 1369 bp) and **C)** *acrD* (expected size 3299 bp) in cloning candidates. Negative controls contained no template DNA.
Lane M: HyperLadder 1kb molecular weight ladder.
Lane 1: negative control
Lanes 2-5: cloning candidates
Lanes 2-5: cloning candidates

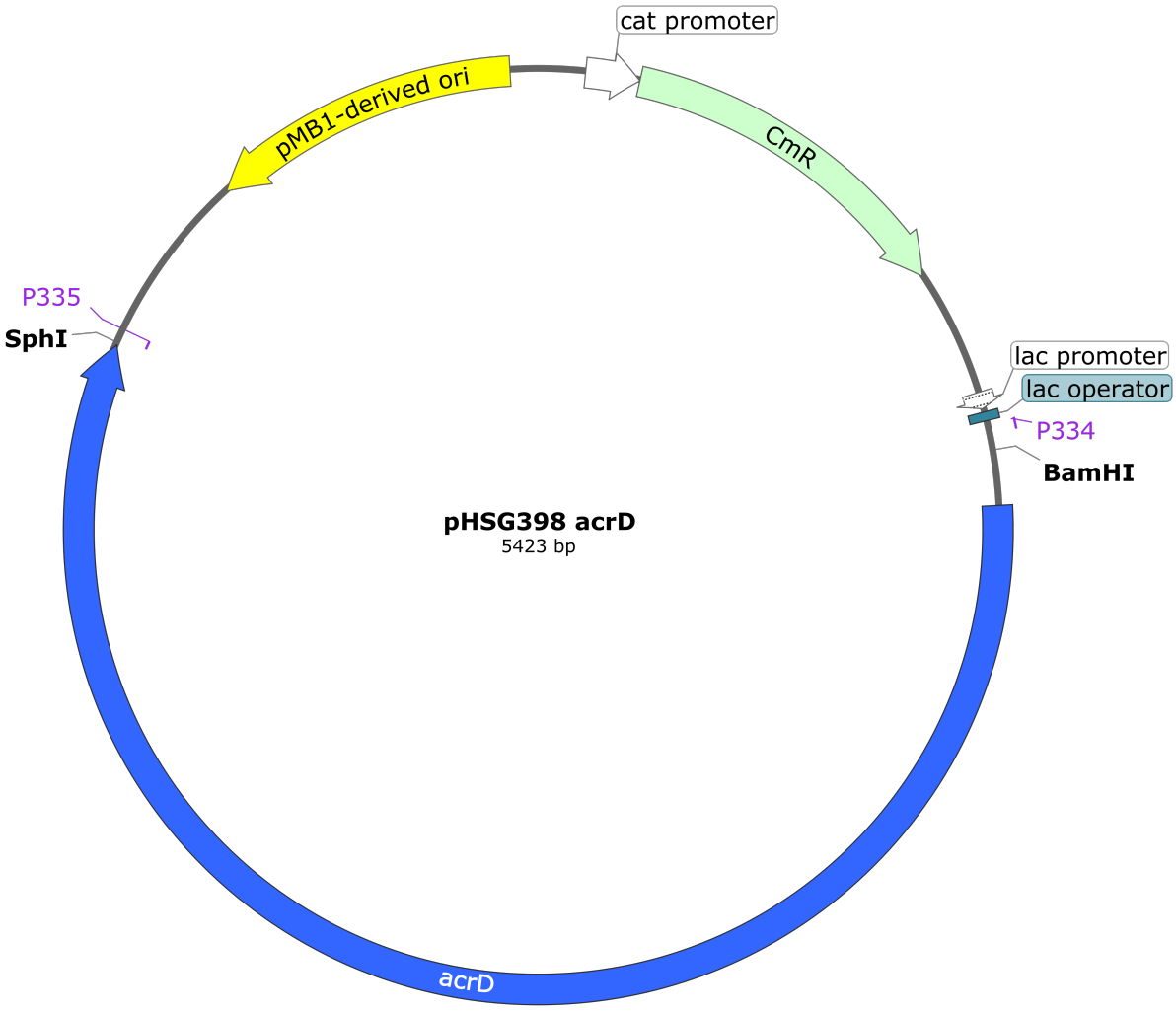


Figure 6.3. Map of pHSG398 containing an insert corresponding to a region 100 bp upstream to the stop codon of *acrD*.

The P334 and P335 primers used for checking the size of *acrD* in pHSG398 anneal upstream and downstream of the *acrD* insert, respectively, to produce a product of 3299 bp. Figure created with SnapGene® software (from GSL Biotech; available at snapgene.com).

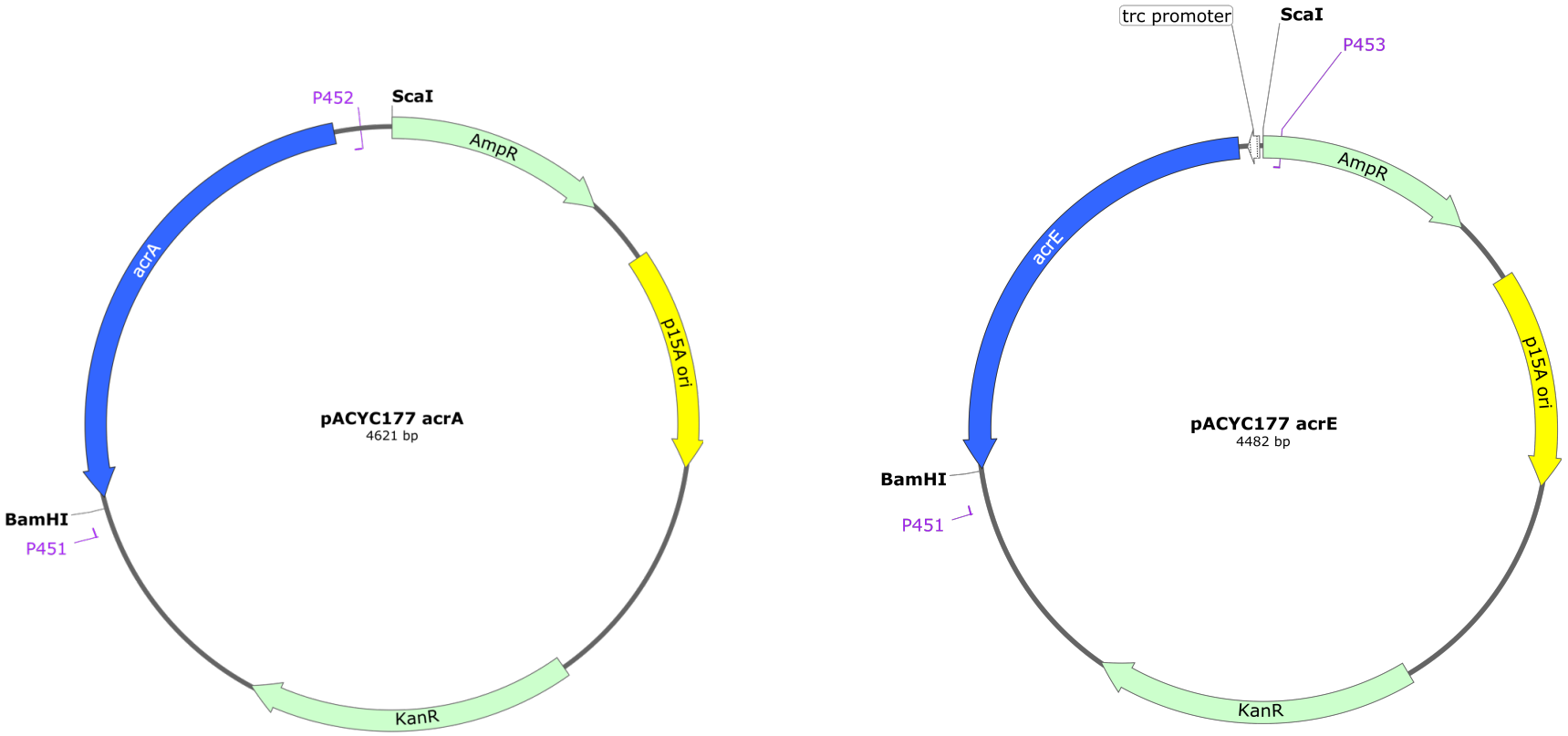


Figure 6.4. Maps of pACYC177 with an insert corresponding to a region 141 bp upstream to 22 bp downstream of *acrA* or 22 bp upstream to stop codon of *acrE*.

The P451 and P452 primers used for checking the size of *acrA* in pACYC177 anneal upstream and downstream of the *acrA* insert to produce a product of 1345 bp. The P451 and P453 primers used for checking the size of *acrE* in pACYC177 anneal upstream and downstream of the *acrE* insert to produce a product of 1369 bp. The ampicillin resistance (Amp^R) gene is non-functional because the *Sca*I restriction site cuts along the gene thereby interrupting it. The pACYC177 *acrA* and pACYC177 *acrE* plasmids solely possess the kanamycin resistance (Kan^R) marker. Figures created with SnapGene® software (from GSL Biotech; available at snapgene.com).

6.6 Verifying the expression of cloned genes

Before the plasmids were used for any further experiments, the expression of the cloned *acrA*, *acrE* and *acrD* genes was determined by MIC testing and/or EtBr efflux assays. The function of pHSG398 *acrD* was verified by transforming the plasmid into the SL1344 Δ*acrB* strain and determining its susceptibility to AcrD-substrates carbenicillin, nafcillin and oxacillin by broth MIC. The function of pHSG398 *acrD* could not be checked using the EtBr efflux assay as EtBr is not a substrate of the AcrD-transporter (Nishino *et al.*, 2006, Blair *et al.*, 2015b). The introduction of pHSG398 *acrD* into the Δ*acrB* strain significantly increased MIC values to carbenicillin, nafcillin and oxacillin compared to its parent strain (Table 6.1). This confirmed that the expression of *acrD* rescued phenotypic defect in the Δ*acrB* strain.

To verify the function of cloned *acrA* and *acrE* genes, the ability of pACYC177 *acrA* or pACYC177 *acrE* to complement the Δ4PAP strain was determined by MIC testing and EtBr efflux assays. The Δ4PAP strain displayed significantly slower EtBr efflux compared to the WT strain as it lacks all four RND-associated PAPs required for functional active efflux (Fig. 6.5). Complementing the Δ4PAP strain with pACYC177 *acrA* or pACYC177 *acrE* significantly reduced the time taken for the peak EtBr fluorescence to decrease by 25%, indicating rescue of efflux defect (Fig. 6.5). Furthermore, antimicrobial susceptibility testing showed that complementation of the Δ4PAP strain with pACYC177 *acrA* or pACYC177 *acrE* fully restored the antimicrobial susceptibility to that of the WT strain (Table 6.2). Taken together, the pACYC177 *acrA* and pACYC177 *acrE* plasmids were found to be fully functional. The level of rescue from pACYC177 *acrA* and pACYC177 *acrE* was comparable to the function of pET-20b *acrA* and pTrcHis2 *acrE* used in Chapter 3 and Chapter 5, respectively.

Table 6.1. The susceptibility of the *Salmonella* Typhimurium SL1344 Δ*acrB* strain complemented with pSHG398 *acrD* to AcrD-substrates.

	MIC (μg/mL)		
Strain genotype	CAR	NAF	OXA
WT SL1344	8	1024	512
Δ*acrB*	2	16	4
Δ*acrB* + pHSG398 *acrD*	**16**	**64**	**16**

Bold values indicate at least two-fold or more difference compared to the parent strain.
Drug abbreviations: CAR, carbenicillin; NAF, nafcillin; OXA, oxacillin.

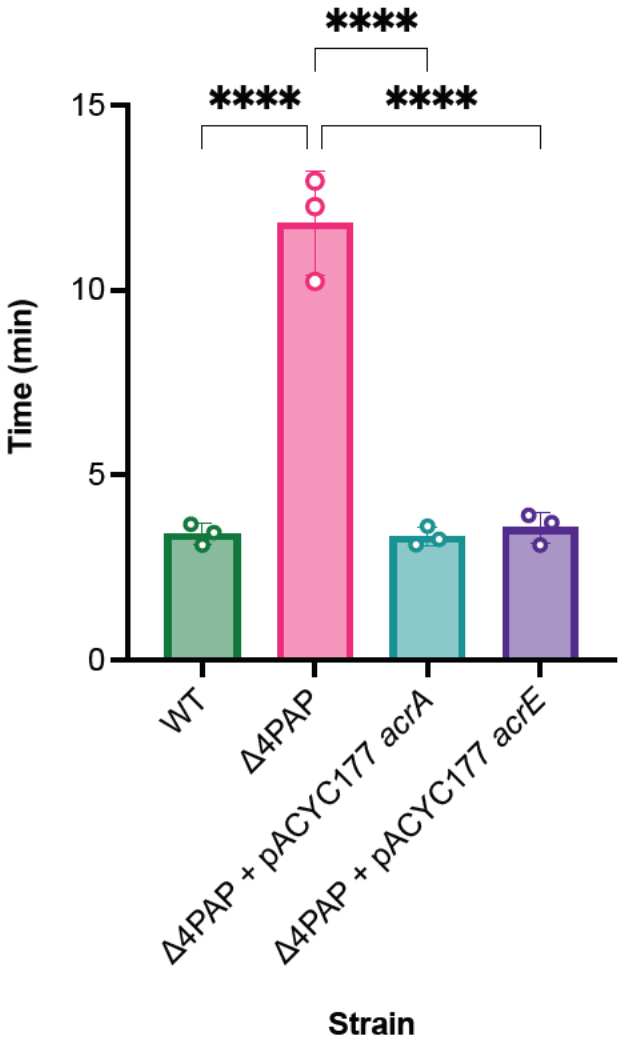


Figure 6.5. Efflux of ethidium bromide by the *Salmonella* Typhimurium SL1344 Δ4PAP strain complemented with pACYC177 *acrA* or pACYC177 *acrE*.

Bacteria were treated with ethidium bromide and the proton-motive force dissipator CCCP for 1 hour and then re-energised with glucose. Data presented are the mean of three biological replicates and are shown as the time taken for ethidium bromide fluorescence to decrease by 25% ± standard deviation. The mean of each strain was compared to that of the Δ4PAP strain using one-way ANOVA, followed by Dunnett's test to correct for multiple comparisons. Strains with significantly different efflux to the Δ4PAP strain are indicated by **** ($P \leq 0.0001$).

Table 6.2. The susceptibility of the *Salmonella* Typhimurium SL1344 Δ4PAP strain complemented with pACYC177 *acrA* or pACYC177 *acrE* to AcrB-substrates.

	MIC (μg/mL)			
Strain genotype	CAR	FA	NAF	NOV
WT SL1344	8	1024	1024	256
Δ4PAP	1	4	4	2
Δ4PAP + pACYC177 *acrA*	**8**	**1024**	**512**	**256**
Δ4PAP + pACYC177 *acrE*	**8**	**1024**	**512**	**256**

Bold values indicate two-fold or more differences compared to the parent strain.
Drug abbreviations: CAR, carbenicillin; FA, fusidic acid; NAF, nafcillin; NOV, novobiocin.

6.7 Substrate specificity of the AcrD-transporter in *Salmonella* Typhimurium SL1344

The inactivation of *acrD* did not alter the susceptibility of SL1344 to any of the antimicrobials tested (Table 6.3). As the loss of *acrD* function did not produce an observable phenotypic effect, the *acrD* gene was cloned into the high copy number plasmid pHSG398 to determine the phenotypic effect of *acrD* overexpression. The pHSG398 *acrD* plasmid was transformed into the Δ*acrB* strain, and the effect of *acrD* overexpression on antimicrobial susceptibility of the resulting transformant was determined. The MIC values for the empty vector control strain did not differ from its parent strain for all antimicrobials tested (Table 6.3). The Δ*acrB* + pHSG398 *acrD* strain displayed a greater than two-fold increase in MIC values to known AcrD-substrates aztreonam, carbenicillin, cloxacillin, fusidic acid, nafcillin, novobiocin, oxacillin and ticarcillin (Table 6.3). Surprisingly, the Δ*acrB* + pHSG398 *acrD* strain did not show any difference in susceptibility to aminoglycosides gentamicin, kanamycin, spectinomycin, streptomycin or tobramycin (Table 6.3). This was contrary to the previously reported role for AcrD as an aminoglycoside efflux pump in *E. coli* (Rosenberg *et al.*, 2000). The Δ*acrB* + pHSG398 *acrD* strain also did not show any difference in susceptibility to the following AcrB-substrates: acriflavine, crystal violet, EtBr, erythromycin, methylene blue, rhodamine 6G and tetracycline (Table 6.3). This verified that the AcrD-transporter cannot export AcrB-substrates, highlighting the substrate profile differences between the two RND-transporters.

6.8 Investigating the functionality of AcrE with AcrD

The RND-transporter AcrD does not possess its own PAP, however, previously it has been shown that AcrD depends on the PAP AcrA to form a functional efflux pump (Yamasaki *et al.*, 2011). Owing to the high similarity of the RND-binding sites between the PAPs AcrA and AcrE (Chapter 5), it was hypothesised that AcrE should also function with AcrD. This was tested by

co-expressing pACYC177 *acrE* and pHSG398 *acrD* in the Δ*acrAB* Δ*acrD* Δ*acrEF* (Δ3RND) strain.

The presence of the empty pHSG398 and pACYC177Kan^R plasmids alone, or their co-presence in the Δ3RND strain had no effect on its antimicrobial susceptibility (Table 6.4). The co-expression of pACYC177 *acrA* and pHSG398 *acrD* in the Δ3RND strain resulted in a greater than two-fold increase in MIC values to known AcrD-substrates aztreonam, carbenicillin, cloxacillin, fusidic acid, nafcillin, novobiocin, oxacillin and ticarcillin confirming that AcrA can function with AcrD (Table 6.4). Similarly, co-expression of pACYC177 *acrE* and pHSG398 *acrD* in the Δ3RND strain resulted in a greater than two-fold increase in MIC values to the AcrD-substrates, clearly showing that AcrE can support function through AcrD to form an efflux competent pump (Table 6.4). There was no difference in MIC values between co-expressing *acrD* with *acrA* or *acrE* (Table 6.4), indicating full interchangeability between AcrA and AcrE in supporting function of AcrD.

The co-expression of *acrD* with *acrE* or *acrA* in the Δ3RND strain did not increase MIC values to aminoglycosides (gentamicin, spectinomycin and streptomycin) or AcrB-substrates (i.e., acriflavine, crystal violet, EtBr, erythromycin, methylene blue, rhodamine 6G and tetracycline) (Table 6.4). This indicated that AcrA or AcrE were functioning specifically with AcrD because aminoglycosides and AcrB-substrates are not exported by AcrD.

Table 6.3. The antimicrobial susceptibility of *Salmonella* Typhimurium SL1344 Δ*acrB* complemented with pHSG398 *acrD*.

	MIC (μg/mL)																		
	Aminoglycosides					β-lactams						Dyes					Others		
Strain genotype	GEN	KAN	SPC	STP	TOB	AZT	CAR	CLX	NAF	OXA	TIC	ACR	CV	EtBr	MB	R6G	ERY	FA	NOV
WT SL1344	0.5	1	16	8	2	0.06	4	512	1024	512	8	128	64	1024	1024	1024	128	1024	512
Δ*acrB*	0.25	1	16	8	2	0.06	1	4	8	4	1	16	2	16	4	8	2	4	2
Δ*acrD*	0.5	1	16	4	2	0.06	4	512	1024	512	8	128	64	1024	1024	1024	128	1024	512
Δ*acrB* + pHSG398	0.25	1	16	4	2	0.06	1	4	8	2	1	8	2	32	2	8	1	4	2
Δ*acrB* + pHSG398 *acrD*	0.25	1	16	4	2	**0.25**	**8**	**16**	**64**	**16**	**16**	8	2	32	4	8	1	**64**	**8**

Bold values indicate two-fold or more differences compared to the parent strain. Drug abbreviations: GEN, gentamicin; KAN, kanamycin; SPC, spectinomycin; STP, streptomycin; TOB, tobramycin; AZT, aztreonam; CAR, carbenicillin; CLX, cloxacillin; NAF, nafcillin; OXA, oxacillin; TIC, ticarcillin; ACR, acriflavine; CV, crystal violet; EtBr, ethidium bromide; MB, methylene blue; R6G, rhodamine 6G; ERY, erythromycin; FA, fusidic acid; NOV, novobiocin.

Table 6.4. The antimicrobial susceptibility of the *Salmonella* Typhimurium SL1344 Δ*acrAB* Δ*acrD* Δ*acrEF* (Δ3RND) strain complemented with pHSG398 *acrD* and pACYC177 *acrA* or pACYC177 *acrE*.

	MIC (μg/mL)																
	Aminoglycosides			β-lactams						Dyes					Others		
Strain genotype	GEN	SPC	STP	AZT	CAR	CLX	NAF	OXA	TIC	ACR	CV	EtBr	MB	R6G	ERY	FA	NOV
WT SL1344	0.5	16	8	0.06	4	512	1024	512	4	128	64	1024	1024	1024	128	1024	512
Δ*acrAB* Δ*acrD* Δ*acrEF* (Δ3RND)	0.25	16	4	0.06	1	1	4	1	1	16	2	8	4	4	2	4	1
Δ3RND + pHSG398	0.25	16	4	0.06	0.5	1	4	1	1	8	4	16	2	4	1	4	1
Δ3RND + pACYC177Kan^R	0.5	16	4	0.06	1	1	2	1	1	16	2	16	2	4	2	4	1
Δ3RND + pHSG398 *acrD*	0.25	16	4	0.06	0.5	1	2	1	1	8	2	16	4	4	2	4	1
Δ3RND + pACYC177 *acrA*	0.5	16	4	0.06	1	1	2	1	1	16	2	16	4	4	2	4	1
Δ3RND + pACYC177 *acrE*	0.5	16	4	0.06	1	1	2	1	1	8	2	16	2	4	2	4	1
Δ3RND + pACYC177Kan^R with pHSG398	0.25	16	8	0.06	0.5	1	2	1	1	8	2	16	2	4	2	4	1
Δ3RND + pACYC177Kan^R with pHSG398 *acrD*	0.25	16	4	0.06	1	1	2	1	1	8	2	8	2	4	1	4	1
Δ3RND + pHSG398 *acrD* with pACYC177 *acrA*	0.5	16	4	**0.25**	**8**	**16**	**32**	**16**	**8**	8	2	16	4	4	2	**128**	**8**
Δ3RND + pHSG398 *acrD* with pACYC177 *acrE*	0.5	16	4	**0.25**	**8**	**16**	**32**	**16**	**8**	8	2	16	4	4	2	**128**	**8**
Δ3RND + pHSG398 with pACYC177 *acrA*	0.5	16	4	0.06	0.5	1	2	1	1	8	4	16	2	4	1	4	1
Δ3RND + pHSG398 with pACYC177 *acrE*	0.5	16	4	0.06	0.5	1	2	1	1	8	2	16	2	4	1	4	1
Δ3RND + pHSG398 with pACYC177 *acrA* (F292G)	0.5	16	4	0.06	0.5	1	2	1	1	8	2	16	2	4	1	4	1
Δ3RND + pHSG398 with pACYC177 *acrA* (G363F)	0.5	16	4	0.06	0.5	1	2	1	1	8	2	16	2	4	1	4	1
Δ3RND + pHSG398 with pACYC177 *acrE* (F291G)	0.5	16	4	0.06	0.5	1	2	1	1	8	2	16	2	4	1	4	1

The MIC values for the Δ*acrAB* Δ*acrD* Δ*acrEF* (Δ3RND) strain are underlined. Bold values indicate two-fold or more differences compared to the parent strain. Drug abbreviations: GEN, gentamicin; SPC, spectinomycin; STP, streptomycin; AZT, aztreonam; CAR, carbenicillin; CLX, cloxacillin; NAF, nafcillin; OXA, oxacillin; TIC, ticarcillin; ACR, acriflavine; CV, crystal violet; EtBr, ethidium bromide; MB, methylene blue; R6G, rhodamine 6G; ERY, erythromycin; FA, fusidic acid; NOV, novobiocin.

Table 6.4. (continued). The antimicrobial susceptibility of the *Salmonella* Typhimurium SL1344 Δ*acrAB* Δ*acrD* Δ*acrEF* (Δ3RND) strain complemented with pHSG398 *acrD* and pACYC177 *acrA* or pACYC177 *acrE*.

	MIC (μg/mL)															
	Aminoglycosides			β-lactams						Dyes					Others		
Strain genotype	GEN	SPC	STP	AZT	CAR	CLX	NAF	OXA	TIC	ACR	CV	EtBr	MB	R6G	ERY	FA	NOV
Δ3RND + pHSG398 with pACYC177 *acrE* (G362F)	0.5	16	4	0.06	0.5	1	2	1	1	8	2	16	2	4	1	4	1
Δ3RND + pHSG398 *acrD* with pACYC177 *acrA* (F292G)	0.5	16	4	0.06	0.5	1	2	1	1	8	2	16	2	4	1	4	1
Δ3RND + pHSG398 *acrD* with pACYC177 *acrA* (G362F)	0.25	16	4	0.06	1	1	2	1	1	8	2	16	2	4	1	4	1
Δ3RND + pHSG398 *acrD* with pACYC177 *acrE* (F291G)	0.25	16	4	0.06	0.5	1	2	1	1	8	2	16	2	4	1	4	1
Δ3RND + pHSG398 *acrD* with pACYC177 *acrE* (G362F)	0.25	16	4	0.06	1	1	2	1	1	8	2	16	2	4	1	4	1

Bold values indicate two-fold or more differences compared to the parent strain. Drug abbreviations: GEN, gentamicin; SPC, spectinomycin; STP, streptomycin; AZT, aztreonam; CAR, carbenicillin; CLX, cloxacillin; NAF, nafcillin; OXA, oxacillin; TIC, ticarcillin; ACR, acriflavine; CV, crystal violet; EtBr, ethidium bromide; MB, methylene blue; R6G, rhodamine 6G; ERY, erythromycin; FA, fusidic acid; NOV, novobiocin.

6.9 The role of RND-binding residues of AcrA and AcrE in forming functional tripartite efflux system with AcrD

The RND-binding residues of AcrA and AcrE were defined in Chapter 3 and Chapter 5, respectively. The residues mapping to binding boxes 1, 4, 5 and 9 of AcrA and AcrE when mutated were found to impair efflux function by disrupting their interaction with AcrB. This data indicated that the same RND-binding residues are critical for AcrA and AcrE in interacting with AcrB. The AcrD-transporter has been previously shown to depend on AcrA (Yamasaki *et al.*, 2011). In Section 6.8, AcrE was shown to support function through AcrD to form an efflux competent pump. Hence, it was hypothesised that the same RND-binding residues of AcrA and AcrE involved in AcrB-interactions was also important for their interaction with AcrD.

The mutations with the most pronounced phenotypic effect were selected to test their effect on AcrD interactions. For AcrA, the F292G and G363F, and for AcrE, the corresponding F291G and G362F, point mutations were selected to be produced in pACYC177 *acrA* and pACYC177 *acrE*, respectively. The mutated versions of AcrA or AcrE were co-expressed with pHSG398 *acrD* in the Δ3RND strain for phenotypic assessment. The co-expression of pHSG398 *acrD* with pACYC177 *acrA* (F292G) or pACYC177 *acrA* (G363F) in the Δ3RND strain did not have any effect on its susceptibility to the substrates tested (Table 6.5). Similarly, the co-expression of pHSG398 *acrD* with pACYC177 *acrE* (F291G) or pACYC177 *acrE* (G362F) in the Δ3RND strain did not have any effect on its susceptibility to any of the tested substrates (Table 6.5). This data indicated that the same residues of AcrA and AcrE that are critical for AcrB-binding are also critical for AcrD-binding.

6.10 Discussion

The substrate profile of the RND transporter AcrD in *S.* Typhimurium was characterised. In agreement with previous studies, the AcrD-transporter of *S.* Typhimurium was found export aztreonam, carbenicillin, cloxacillin, fusidic acid, nafcillin, novobiocin and oxacillin (Table 6.3) (Yamasaki *et al.*, 2011, Bernal *et al.*, 2021). Furthermore, ticarcillin was also found to be a novel AcrD-substrate (Table 6.3). The introduction of *acrD* into the Δ*acrB* (Δ*acrB* + pHSG398 *acrD*) strain did not result in a significant increase in MICs of the aminoglycosides kanamycin, gentamicin, spectinomycin or streptomycin (Table 6.3), implying that AcrD is not measurably contributing to aminoglycoside efflux. This is in contrast to the reported role of AcrD in the aminoglycoside resistance of *E. coli*, wherein deletion of *acrD* was shown to decrease aminoglycoside MICs by 2- to 8-fold (Rosenberg *et al.*, 2000) and expression of *acrD* from a plasmid in an *acrB::aph* Δ*acrD* strain increased aminoglycoside MICs by two-fold (Elkins and Nikaido, 2002). In agreement with the findings here, the AcrD efflux pump of the Gram-negative plant pathogen *Erwinia amylovora* has also been reported to not play a role in aminoglycoside resistance (Pletzer and Weingart, 2014).

A possible explanation for the differences in the substrate profiles of AcrD between *E. coli* and *S.* Typhimurium could be the observed discrepancy between the residues in their respective proximal and distal binding pockets (Fig. 6.6) (Ramaswamy *et al.*, 2017, Bernal *et al.*, 2021). Due to the lack of experimental AcrD structure, the functional significance of the residues of the respective drug-binding pockets of AcrD is inferred from their positional homology with corresponding AcrB residues, structures of which have been experimentally defined for both *E. coli*, and more recently for *Salmonella* (Johnson *et al.*, 2020). Specifically, the presence of a serine residue in the distal binding pocket of *S.* Typhimurium AcrD at position 610, which in

E. coli AcrD is occupied by an alanine, could possibly impact the previously described lipophilic character of the drug-binding cavity (Ramaswamy *et al.*, 2017). Recently, Bernal *et al*. (2021), reported that an S610A point mutation in AcrD of *S.* Typhimurium increased susceptibility to AcrD-substrates oxacillin and carbenicillin. However, aminoglycoside susceptibility was not tested.

There are two additional differences between the proximal binding pockets of AcrD between the two species. Position 663 in *S.* Typhimurium AcrD is occupied by a phenylalanine residue, whereas in *E. coli* AcrD it is occupied by an isoleucine residue. This difference is likely to cause steric hindrance of the proximal binding pocket (Kobayashi *et al.*, 2014, Ramaswamy *et al.*, 2017). Position 565 in *S.* Typhimurium AcrD is occupied by a glutamine residue, whereas in *E. coli* AcrD it is occupied by a leucine residue. This is also likely to impact the electrostatic environment of the proximal binding pocket (Kobayashi *et al.*, 2014, Ramaswamy *et al.*, 2017). These subtle differences may account for the notable differences in substrate recognition by AcrD between the two species.

The AcrD-transporter is not encoded with its own PAP but has been shown to rely on AcrA to function (Yamasaki *et al.*, 2011). Here, it was shown that either of the PAPs AcrA or AcrE can interact with AcrD to form a functional efflux pump in *S.* Typhimurium (Table 6.4). A possible explanation for the interoperability between AcrA and AcrE is that the latter may function as a backup PAP for when AcrA function is impaired or lost. This idea is supported by evidence from studies demonstrating that in *S.* Typhimurium, in the absence of *acrA*, it was possible to select for resistance through *acrE* overexpression (Zhang *et al.*, 2018, McNeil *et al.*, 2019). A different study demonstrated that in the absence of *acrA* and *acrE*, it was possible to restore the

phenotypic defect in active efflux by complementing with either *acrA* or *acrE* (Smith and Blair, 2014), highlighting their redundancy. There may have been a selection to maintain redundant tripartite efflux components so if one loses its function, there is another component to carry out the same function. This suggests a critical role for efflux pumps in the physiology of bacteria because they maintain multiple efflux systems encoded in their genome to possess efflux capacity in all scenarios (Alon Cudkowicz and Schuldiner, 2019, Henderson *et al.*, 2021).

Another advantage of possessing promiscuous tripartite efflux components, such as PAPs and OMFs, could be to provide flexibility in modulating the substrate profile of tripartite efflux pumps according to their environment. For example, the MexXY RND pump of *P. aeruginosa* can alter its substrate specificity depending on its OMF partner. When MexXY partners with OprM, it can export aminoglycosides, but when it partners with OprA, it can export anionic β-lactams, such as carbenicillin and sulbenicillin, but not aminoglycosides (Singh *et al.*, 2020). Similarly, the redundancy that exists between efflux pump components may confer an advantage to the different environments that *Salmonella* occupies, such as soil, food, water, different hosts, and organs within hosts. Therefore, it is possible that *acrE* is expressed under different environmental conditions to *acrA* and so provide the AcrD-transporter with the ability to efflux under different stress conditions. However, the expression of *acrEF* is repressed by the local regulator AcrS (EnvR) and the global regulator H-NS (Hirakawa *et al.*, 2008, Nishino *et al.*, 2009). Previous studies have shown that the overexpression of *acrEF* confers a similar effect to *acrAB* (Nishino et al., 2006). As *acrAB* is constitutively expressed in *S.* Typhimurium, the expression of *acrEF* is tightly repressed presumably to avoid the fitness cost associated with producing excess efflux pump proteins (Nishino *et al.*, 2009). Hence, the exact environmental conditions under which *acrEF* expression is triggered remains to be determined.

The RND-binding residues of AcrA and AcrE involved in their interaction with AcrB were defined in Chapter 3 and Chapter 5, respectively. Here, disruption of these RND-binding residues in AcrA or AcrE also impaired AcrD-mediated efflux of substrate drugs. Consistent with the data obtained in co-expression with AcrB (McNeil *et al.*, 2019), the disruption of F292 or G363 in AcrA resulted in impaired AcrD-mediated efflux of AcrD-substrates, confirming that the same residues required for binding of AcrA to AcrB are also required for its binding to AcrD (Table 6.4). To determine whether the corresponding residues in AcrE were also important for AcrD-binding, F291 and G362 were mutated. As expected, the F291G or G362F point mutations in AcrE also impaired AcrD-mediated efflux in the Δ3RND strain (Table 6.4). These data suggest that the PAP-RND binding sites previously identified based upon AcrA-AcrB interaction, are indeed both sequentially and functionally conserved between AcrA and AcrE and account for the productive recognition formation of functional tripartite pumps. This indicates that AcrA and AcrE share common RND-binding residues to recognise and interact with RND-transporters. Importantly, these residues could be ideal drug target sites for the development of efflux inhibitors to inhibit the assembly of tripartite RND efflux pumps. Preventing the functional assembly of RND efflux pumps could restore the activity of existing antimicrobials which have lost their efficacy due to overexpression of RND efflux pumps. Furthermore, disrupting the assembly of RND efflux pumps could attenuate the virulence of *S.* Typhimurium as a problematic animal and human pathogen.

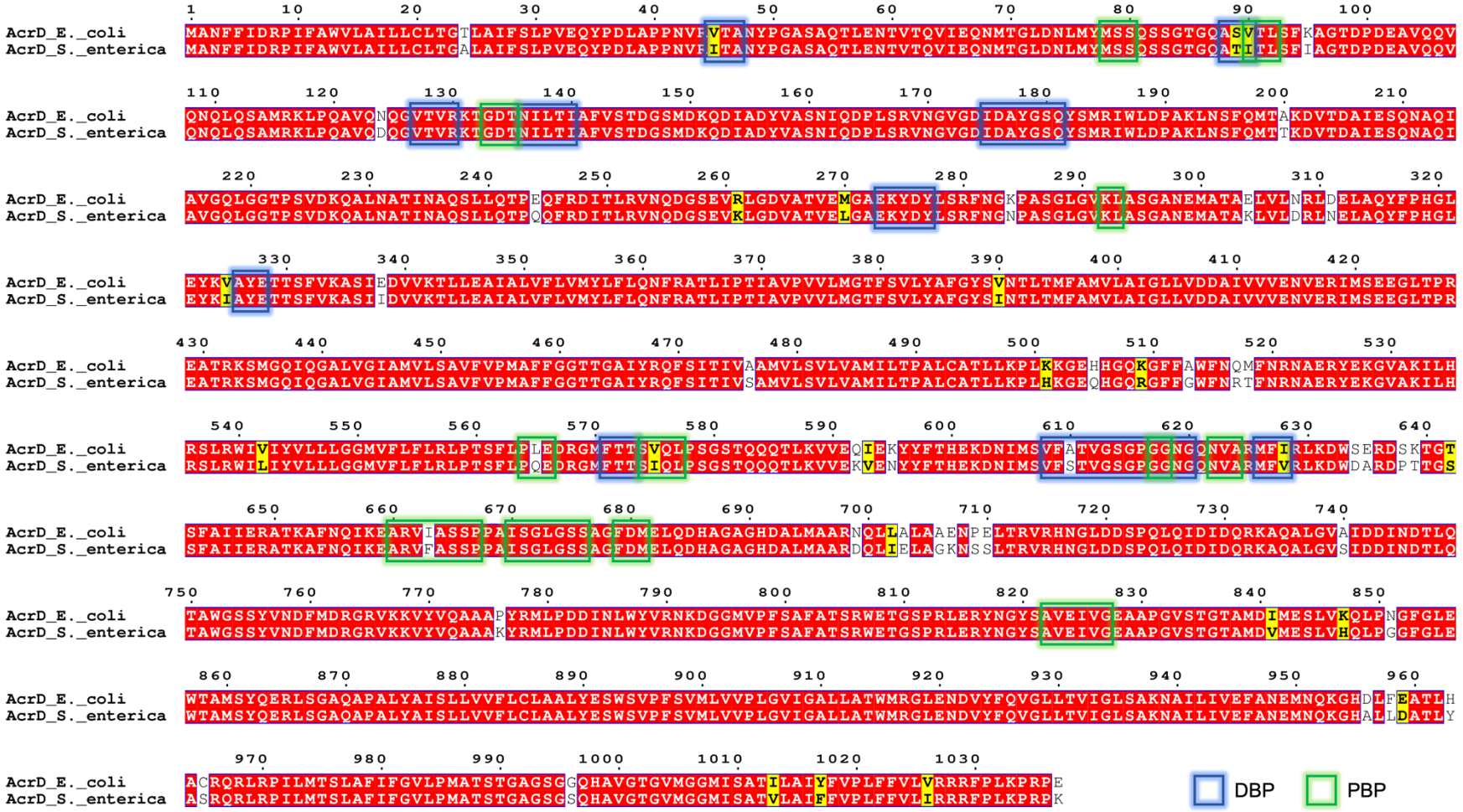


Figure 6.6. Pairwise sequence alignment of AcrD of *Escherichia coli* K-12 and AcrD of *Salmonella* Typhimurium SL1344.

Identical residues are highlighted in red, similar in yellow, while all others are mismatches. Green and blue boxes indicate residues mapping to the proximal binding pocket (PBP) and the distal binding pocket (DBP), respectively (Ramaswamy *et al.*, 2017).

6.11 Key findings

- The AcrD-transporter of *S.* Typhimurium SL1344 exports aztreonam, carbenicillin, cloxacillin, fusidic acid, nafcillin, oxacillin and ticarcillin, but not aminoglycosides.
- The AcrD-transporter of *S.* Typhimurium SL1344 can function with the PAPs AcrA or AcrE to form a functional tripartite efflux pump.
- The previously identified PAP-RND binding sites based upon AcrA-AcrB interaction, are also important for AcrD-binding in both AcrA and AcrE.

6.12 Further work

The substrate specificity of AcrD differs between *S.* Typhimurium and *E. coli*, with AcrD being able to export aminoglycosides in the latter organism. Although the amino acid sequence of AcrD is highly similar between the two species, there are several key differences in the proximal and distal binding pockets which may explain the substrate differences. To investigate the role of these discrepancies, the different residues in the binding pockets of *S.* Typhimurium AcrD could be mutated to those of *E. coli* AcrD. Subsequently, it can be expressed in the *S.* Typhimurium Δ*acrB* strain to determine its aminoglycoside susceptibility. Another experiment would be to express the *acrD* gene of *E. coli* K-12 in the *S.* Typhimurium SL1344 Δ*acrB* strain. Bernal *et al*. (2021) demonstrated heterologous expression of the *S.* Typhimurium *acrD* gene in *E. coli* (Bernal *et al.*, 2021), therefore it can be fair to assume heterologous expression of the *E. coli acrD* gene in *S.* Typhimurium due to their high similarity. This would allow to see whether the AcrD-transporter of *E. coli* K-12 can confer aminoglycoside efflux in *S.* Typhimurium SL1344. It was shown here that mutations in two of the residues in RND-binding boxes and 9 of AcrA and AcrE impaired AcrD-mediated efflux. Therefore, the role of

residues in the other RND-binding boxes identified in Chapter 3 could also be investigated. This would further strengthen the role of the binding box model in PAP-RND interactions.

CHAPTER 7. Overall Discussion and Conclusions

CHAPTER 7. Overall Discussion and Conclusions

7.1 Increased understanding of PAP-RND binding and the role of PAPs in substrate efflux

Tripartite efflux pumps belonging to the RND superfamily, such as AcrAB-TolC, contribute to the intrinsic and acquired MDR of Gram-negative bacteria, including *S.* Typhimurium (Okusu *et al.*, 1996, Piddock *et al.*, 2000, Baucheron *et al.*, 2002, Ni *et al.*, 2020). Hence, there is significant interest in identifying ways to inhibit the function of these tripartite efflux complexes to curb the growing threat of MDR bacteria (Lomovskaya and Bostian, 2006). However, to identify novel drug target sites for inhibition, a greater understanding of the structural organisation of tripartite efflux pumps is necessary (Opperman and Nguyen, 2015). The recent advances in structural biology have enabled an insight into the interactions between the components of tripartite RND pumps. Whilst there has been considerable effort to define the interactions between the PAP and the OMF components (Husain *et al.*, 2004, Gerken and Misra, 2004, Xu *et al.*, 2010, Kim *et al.*, 2010, Weeks *et al.*, 2010, Xu *et al.*, 2011b, Boyer *et al.*, 2022), the PAP-RND transporter interactions have remained poorly understood. Hence, knowledge of the exact PAP residues important for efflux complex recognition and assembly is limited. To address this problem, previous work in this laboratory has predicted residue ranges involved in the PAP-RND binding using the near-atomic resolution structures of the AcrAB-TolC pump (McNeil *et al.*, 2019). The regions of contact between the PAP and RND-transporter were found to be relatively compact, forming four homologous 3D binding sites within each PAP protomer, that corresponded to nine discrete linear binding boxes (Fig. 3.1). Multiple sequence alignments of the four *Salmonella* PAPs (AcrA, AcrE, MdtA and MdsA) revealed that these binding boxes are highly conserved between the interchangeable PAPs AcrA and AcrE, whilst differing substantially in the phylogenetically distant PAPs MdtA and MdsA that cannot function with non-cognate RND-transporters (McNeil *et al.*, 2019). The high degree of similarity between the

binding boxes of AcrA and AcrE suggested that these residues could be responsible for their ability to bind to the same RND-transporters.

In this study, using the AcrAB-TolC pump of *S.* Typhimurium, the functional role of the predicted RND-binding boxes was validated. The most important residues in RND-binding mapped to binding boxes 1, 4 and 5 of the β-barrel domain and binding boxes 6 and 9 of the MPD. In the homologous MexAB-OprM efflux pump of *P. aeruginosa*, the residues mapping to the β-barrel domain of the PAP MexA has been found to be important for binding to the RND-transporter MexB (Nehme *et al.*, 2004, Nehme and Poole, 2005, Nehme and Poole, 2007). This interaction has also been observed in the binding of the PAP CusB to the metal RND-transporter CusA, which are homologues of AcrA and AcrB, respectively (Su *et al.*, 2011, Long *et al.*, 2012). Additionally, the structural data of AcrAB-TolC show the MPD of AcrA interacting with the TolC docking domain and the top of the porter domain of the AcrB-transporter (Du *et al.*, 2014, Wang *et al.*, 2017, Chen *et al.*, 2021). These studies support the observed importance of RND-binding boxes identified in this study and demonstrate that the regions involved in PAP-RND binding are conserved between homologous tripartite RND efflux complexes.

AcrA and AcrE are closely related PAPs that share an almost identical secondary structure (McNeil *et al.*, 2019). Furthermore, the binding boxes between AcrA and AcrE are highly conserved in *S.* Typhimurium, potentially explaining their observed interchangeability with the AcrB-transporter (Elkins and Nikaido, 2003, Smith and Blair, 2014, McNeil *et al.*, 2019). The results from this study support this hypothesis as AcrA and AcrE were shown to share conserved RND-binding boxes and use the same residues to interact with the AcrB-transporter.

Furthermore, the interoperability of AcrA and AcrE was also shown to extend to the AcrD-transporter, which does not have its own cognate PAP but has been shown to depend on AcrA to form a functional efflux pump (Yamasaki *et al.*, 2011). Since AcrA and AcrE are interchangeable in supporting function through the AcrB- and AcrF-transporters (Elkins and Nikaido, 2003, Smith and Blair, 2014, McNeil *et al.*, 2019), it was hypothesised that AcrE should also form a functional efflux pump with the AcrD-transporter. Consistent with this prediction, the results in this study demonstrated that both AcrA and AcrE can support function through the AcrD-transporter to export AcrD-substrates. Importantly, AcrA and AcrE use the same residues to interact with the AcrD-transporter. This confirmed that the PAP-RND binding sites previously identified based upon AcrA-AcrB interaction are indeed both sequentially and functionally conserved between AcrA and AcrE and account for the productive recognition and formation of functional tripartite efflux pumps. This also provides an explanation as to why the divergent *Salmonella* PAPs MdtA and MdsA are not able to function with the AcrB-transporter as they have markedly different binding boxes and structures compared to AcrA and AcrE.

One explanation for the redundancy between AcrA and AcrE and the selection for RND-binding between the two PAPs to remain similar in *S. enterica* could be because *Salmonella* and other Gram-negative bacteria maintain promiscuous tripartite efflux components to have resilience against the loss of efflux function. If the function of one tripartite efflux component is compromised or lost, there is another component to carry out the same function. This points to an important role for efflux pumps in the physiology of bacteria because they maintain multiple efflux systems in their genomes to maintain efflux in all scenarios. This is supported by studies that suggest these efflux pumps are ancient and have remained stable throughout the

evolutionary history of Gram-negative bacteria (Gorecki and McEvoy, 2020, Teelucksingh *et al.*, 2020, Henderson *et al.*, 2021).

In this study, a potential role for the PAP in modulating substrate channel access to the RND-transporter was also identified. The K366D AcrA mutation mapping to the MPD differentially affected the export of substrates depending on their preferred AcrB channel access. Although the role of PAPs in substrate selectivity have not been widely studied, there are a few lines of evidence indicating a role for PAPs in active participation of transport activity. A previous study reported that single amino acid substitutions in the β-barrel domain AcrA were sufficient to confer efflux activity of the non-cognate RND-transporter MexB (Krishnamoorthy *et al.*, 2008). The MPD of the PAPs ZneB and CusB of the tripartite ZneCAB and CusABC heavy metal RND efflux pumps, respectively, have also been reported to play an important role in substrate acquisition and presentation to the metal pumping RND-transporters (De Angelis *et al.*, 2010, Chacon *et al.*, 2014). Overall, this study builds on existing evidence for the potential role for the PAP in modulating substrate access to the RND-transporter, highlighting the increasingly important role of the PAPs in the active efflux process of tripartite efflux complexes.

One limitation of this study has been the use of efflux assays to measure the effect of AcrA and AcrE mutations on RND-binding. This limited the sensitivity of measuring the impact of certain mutations because efflux assays only showed the biggest phenotypic differences. Furthermore, without biophysical analysis of the binding affinity between the PAP mutant proteins and the RND-transporter, it is difficult to verify whether the impact of the mutations is due to their effect on RND-binding. Therefore, future work should address the impact of the AcrA and AcrE mutant proteins on binding to the RND-transporter. This should be investigated using a

biochemical technique to identify protein-protein interactions, such as *in vivo* crosslinking. Previous studies have used DSP, a crosslinking agent with a long spacer arm, to crosslink AcrA and AcrB proteins within *E. coli* cells and verify their interaction (Zgurskaya and Nikaido, 2000, Tikhonova and Zgurskaya, 2004, Ge *et al.*, 2009). Despite the lack of data on the binding between mutant PAP proteins and the AcrB-transporter, this study bridges the available structural information with experimental functional validation to identify the specific RND-binding residues of AcrA and AcrE suitable for inhibition.

7.2 Targeting RND-binding residues to inhibit the function of PAPs

The development and potential use of efflux inhibitors to overcome efflux-mediated resistance has been of significant interest for some time (Lomovskaya *et al.*, 2001). Many potent efflux inhibitors targeting the RND-transporter of tripartite efflux complexes, such as AcrB and MexB, have been described in the literature (Yoshida *et al.*, 2007, Nakashima *et al.*, 2013, Sjuts *et al.*, 2016, Ple *et al.*, 2022). Some studies have also attempted to target the OMF component TolC (Higgins *et al.*, 2004, Gilardi *et al.*, 2017). However, these strategies have largely failed primarily due to the toxic effects at the concentrations essential for their activity, poor pharmacokinetic properties, or low *in vivo* efficacy (Lamut *et al.*, 2019). For example, the efflux inhibitor PAβN has been shown to be toxic to mice (LD_{50} < 25 mg/kg) (Renau *et al.*, 2003) and its further developed analogues, despite showing potent *in vivo* activity, were found to be nephrotoxic due to accumulation in lysosomes (Watkins *et al.*, 2003). The toxicity of some compounds has also stemmed from their structural similarity to clinically used drugs. For instance, the efflux inhibitor NMP is structurally like clinically used selective serotonin reuptake inhibitors and so displays various off-target effects *in vivo* (Kaatz *et al.*, 2003). Previous studies have demonstrated that targeting the PAP component of tripartite efflux pumps

is a good strategy to inhibit efflux-mediated resistance (Ayhan *et al.*, 2016, Abdali *et al.*, 2017, Darzynkiewicz *et al.*, 2019, Sturge *et al.*, 2019, Green *et al.*, 2020). Currently, the toxicity of these compounds has not been tested *in vitro* or *in vivo*.

Several previous studies and this study have demonstrated that the PAPs AcrA and AcrE are interchangeable in their ability to function with the RND-transporters AcrB, AcrD and AcrF (Elkins and Nikaido, 2003, Smith and Blair, 2014, McNeil *et al.*, 2019). Consequently, any inhibitor of AcrA would also need to inhibit AcrE to be an effective efflux inhibitor. The RND-binding residues identified in this study are functionally conserved between AcrA and AcrE since both PAPs use the same residues to interact with the AcrB- and AcrD-transporters. Hence, the critical RND-binding boxes identified in this study provide potential drug target sites for the development of efflux inhibitors capable of inhibiting the function of both AcrA and AcrE by preventing their binding to their RND-transporter partners. This would not only diminish the incidence of resistance to new antibiotics but also restore the activity of existing antibiotics that have lost their efficacy due to efflux pump overexpression (Lomovskaya and Bostian, 2006, Wang *et al.*, 2016).

Tripartite RND efflux pumps, including AcrAB-TolC and AcrEF-TolC, also play a role in the virulence of *S.* Typhimurium (Nishino *et al.*, 2006, Buckley *et al.*, 2006, Blair *et al.*, 2009, Wang-Kan *et al.*, 2017). In this study, targeting the critical RND-binding residues of AcrA also attenuated the *in vivo* virulence of *S.* Typhimurium in the *Galleria mellonella* infection model. Hence, targeting RND-binding residues of AcrA and AcrE could prevent the assembly of functional tripartite RND complexes, thereby impairing the efflux of molecules necessary to cause infection (Wang-Kan *et al.*, 2021), inhibiting survival of *S.* Typhimurium in phagocytes

(Srikumar *et al.*, 2015, Wang-Kan *et al.*, 2017) and preventing the efflux of host antimicrobial peptides (Kapach *et al.*, 2020). Accordingly, the disruption of the AcrAB-TolC pump in *S.* Typhimurium during *G. mellonella* infection may attenuate the survival of *S.* Typhimurium in hemocytes, prevent the efflux of molecules necessary to cause infection and increase susceptibility to *G. mellonella* antimicrobial peptides. This provides a rationale for targeting RND-binding residues to not only restore antibiotic efficacy but also to reduce the virulence of *S.* Typhimurium. This is supported by studies that have reported the ability of efflux inhibitors to reduce the virulence of pathogenic Gram-negative bacteria. The efflux inhibitors PAβN and MBX3132 have been shown to significantly reduce the association and invasion of *S*. Typhimurium SL1344 into INT-407 cells in a dose-dependent manner (Wang-Kan *et al.*, 2017). The efflux inhibitor PAβN has also been shown to reduce the *in vivo* virulence of *P. aeruginosa* in the *Galleria mellonella* infection model (Rampioni *et al.*, 2017). However, the impact of efflux inhibitors on the *in vivo* virulence of *S.* Typhimurium has not been studied yet. The findings in this study should be validated in a more complex *in vivo* model like the mouse model of *S.* Typhimurium infection (Wang-Kan *et al.*, 2017). Furthermore, the F292V, Q311F and K366D AcrA point mutations should be produced in the chromosome of *S*. Typhimurium SL1344 rather than relying on plasmid expression. This would circumvent the problem of using efflux-deleted mutant strains, which can sometimes upregulate other efflux systems to compensate (Blair *et al.*, 2015b). Targeting virulence could attenuate the ability of pathogenic bacteria from causing infection and also exert less evolutionary pressure towards the development of resistance (Rasko and Sperandio, 2010).

To identify an efflux inhibitor capable of targeting the conserved RND-binding residues of both AcrA and AcrE, a drug library should be screened using parallel experimental and structure-

based *in silico* screening techniques. Drug libraries that have been used to identify efflux inhibitors active against *S.* Typhimurium include the Maybridge HitFinder™ drug-diversity library (14,400 compounds) and the L. Hoffman La Roche™ compound library (47,168 compounds) (Reens *et al.*, 2018, Marshall *et al.*, 2020). Drug libraries that have been used to specifically screen for AcrA inhibitors include the National Cancer Institute (NCI) Diversity 5 set (1593 compounds), NCI Natural Product Set (117 compounds) (Abdali *et al.*, 2017) and the ZINC15 database (Green *et al.*, 2020). The experimental screen should involve growth inhibition assays, whereby a drug library could be screened for antibacterial activity in the presence of subinhibitory concentrations of an AcrB-substrate, such as erythromycin or novobiocin. The *in-silico* screen would involve using an ensemble docking approach to rank compounds in the drug library for their ability to bind to the different AcrA and AcrE conformers and the RND-binding sites identified in this study. The top hits from both the experimental and computational screens should be investigated further for their ability to inhibit efflux activity using EtBr efflux assays and checkerboard assays to identify multidrug potentiation. Promising candidates should be assessed for their ability to bind AcrA and AcrE using biophysical methods, such as surface plasmon resonance. This approach has been previously used to identify AcrA-inhibitors capable of binding to the hinge regions between the β-barrel domain and the membrane proximal domains (Darzynkiewicz *et al.*, 2019, Abdali *et al.*, 2017), which is in proximity to many of the RND-binding residues identified in this study. Therefore, the RND-binding residues are potentially druggable sites in AcrA and AcrE for the development of efflux inhibitors.

References

Ababou, A. & Koronakis, V. 2016. Structures of Gate Loop Variants of the AcrB Drug Efflux Pump Bound by Erythromycin Substrate. *PLoS One,* 11**,** e0159154.

Abdali, N., Parks, J. M., Haynes, K. M., Chaney, J. L., Green, A. T., Wolloscheck, D., Walker, J. K., Rybenkov, V. V., Baudry, J., Smith, J. C. & Zgurskaya, H. I. 2017. Reviving Antibiotics: Efflux Pump Inhibitors That Interact with AcrA, a Membrane Fusion Protein of the AcrAB-TolC Multidrug Efflux Pump. *ACS Infect Dis,* 3**,** 89-98.

Abouzeed, Y. M., Baucheron, S. & Cloeckaert, A. 2008. *ramR* mutations involved in efflux-mediated multidrug resistance in *Salmonella enterica* serovar Typhimurium. *Antimicrob Agents Chemother,* 52**,** 2428-34.

Alav, I., Kobylka, J., Kuth, M. S., Pos, K. M., Picard, M., Blair, J. M. A. & Bavro, V. N. 2021. Structure, Assembly, and Function of Tripartite Efflux and Type 1 Secretion Systems in Gram-Negative Bacteria. *Chemical Reviews,* 121**,** 5479-5596.

Alav, I., Sutton, J. M. & Rahman, K. M. 2018. Role of bacterial efflux pumps in biofilm formation. *J Antimicrob Chemother,* 73**,** 2003-2020.

Alcalde-Rico, M., Olivares-Pacheco, J., Halliday, N., Camara, M. & Martinez, J. L. 2020. The impaired quorum sensing response of *Pseudomonas aeruginosa* MexAB-OprM efflux pump overexpressing mutants is not due to non-physiological efflux of 3-oxo-C12-HSL. *Environ Microbiol*.

Alon Cudkowicz, N. & Schuldiner, S. 2019. Deletion of the major *Escherichia coli* multidrug transporter AcrB reveals transporter plasticity and redundancy in bacterial cells. *PLoS One,* 14**,** e0218828.

Amann, E., Brosius, J. & Ptashne, M. 1983. Vectors bearing a hybrid *trp-lac* promoter useful for regulated expression of cloned genes in *Escherichia coli*. *Gene,* 25**,** 167-78.

Andersen, C., Koronakis, E., Bokma, E., Eswaran, J., Humphreys, D., Hughes, C. & Koronakis, V. 2002. Transition to the open state of the TolC periplasmic tunnel entrance. *Proc Natl Acad Sci U S A,* 99**,** 11103-8.

Anderson, C. J. & Kendall, M. M. 2017. *Salmonella enterica* Serovar Typhimurium Strategies for Host Adaptation. *Front Microbiol,* 8**,** 1983.

Aron, Z. & Opperman, T. J. 2018. The hydrophobic trap-the Achilles heel of RND efflux pumps. *Res Microbiol,* 169**,** 393-400.

Augustus, A. M., Celaya, T., Husain, F., Humbard, M. & Misra, R. 2004. Antibiotic-sensitive TolC mutants and their suppressors. *J Bacteriol,* 186**,** 1851-60.

Ayhan, D. H., Tamer, Y. T., Akbar, M., Bailey, S. M., Wong, M., Daly, S. M., Greenberg, D. E. & Toprak, E. 2016. Sequence-Specific Targeting of Bacterial Resistance Genes Increases Antibiotic Efficacy. *PLoS Biol,* 14**,** e1002552.

Bailey, A. M., Paulsen, I. T. & Piddock, L. J. 2008. RamA confers multidrug resistance in *Salmonella enterica* via increased expression of *acrB*, which is inhibited by chlorpromazine. *Antimicrob Agents Chemother,* 52**,** 3604-11.

Bassler, B. L. & Losick, R. 2006. Bacterially speaking. *Cell,* 125**,** 237-46.

Baucheron, S., Imberechts, H., Chaslus-Dancla, E. & Cloeckaert, A. 2002. The AcrB multidrug transporter plays a major role in high-level fluoroquinolone resistance in *Salmonella enterica* serovar typhimurium phage type DT204. *Microb Drug Resist,* 8**,** 281-9.

Baucheron, S., Tyler, S., Boyd, D., Mulvey, M. R., Chaslus-Dancla, E. & Cloeckaert, A. 2004. AcrAB-TolC directs efflux-mediated multidrug resistance in *Salmonella enterica* serovar typhimurium DT104. *Antimicrob Agents Chemother,* 48**,** 3729-35.

Baugh, S., Ekanayaka, A. S., Piddock, L. J. & Webber, M. A. 2012. Loss of or inhibition of all multidrug resistance efflux pumps of *Salmonella enterica* serovar Typhimurium results in impaired ability to form a biofilm. *J Antimicrob Chemother,* 67**,** 2409-17.

Bavro, V. N., Pietras, Z., Furnham, N., Perez-Cano, L., Fernandez-Recio, J., Pei, X. Y., Misra, R. & Luisi, B. 2008. Assembly and channel opening in a bacterial drug efflux machine. *Mol Cell,* 30**,** 114-21.

Bender, J. K., Wille, T., Blank, K., Lange, A. & Gerlach, R. G. 2013. LPS structure and PhoQ activity are important for *Salmonella* Typhimurium virulence in the *Galleria mellonella* infection model [corrected]. *PLoS One,* 8**,** e73287.

Berger, C. N., Sodha, S. V., Shaw, R. K., Griffin, P. M., Pink, D., Hand, P. & Frankel, G. 2010. Fresh fruit and vegetables as vehicles for the transmission of human pathogens. *Environ Microbiol,* 12**,** 2385-97.

Bernal, J. C., El-Delik, J., Göttig, S. & Pos, K. M. 2021. Characterization and Molecular Determinants for β-Lactam Specificity of the Multidrug Efflux Pump AcrD from *Salmonella* Typhimurium. *Antibiotics,* 10**,** 1494.

Betts, M. J. & Russell, R. B. 2003. Amino Acid Properties and Consequences of Substitutions. *Bioinformatics for Geneticists.*

Bhattacharyya, S., Walker, D. M. & Harshey, R. M. 2020. Dead cells release a 'necrosignal' that activates antibiotic survival pathways in bacterial swarms. *Nat Commun,* 11**,** 4157.

Bina, X. R., Provenzano, D., Nguyen, N. & Bina, J. E. 2008. *Vibrio cholerae* RND family efflux systems are required for antimicrobial resistance, optimal virulence factor production, and colonization of the infant mouse small intestine. *Infect Immun,* 76**,** 3595-605.

Bjarnsholt, T. 2013. The role of bacterial biofilms in chronic infections. *APMIS Suppl***,** 1-51.

Blair, J. M., Bavro, V. N., Ricci, V., Modi, N., Cacciotto, P., Kleinekathfer, U., Ruggerone, P., Vargiu, A. V., Baylay, A. J., Smith, H. E., Brandon, Y., Galloway, D. & Piddock, L. J. 2015a. AcrB drug-binding pocket substitution confers clinically relevant resistance and altered substrate specificity. *Proc Natl Acad Sci U S A,* 112**,** 3511-6.

Blair, J. M., La Ragione, R. M., Woodward, M. J. & Piddock, L. J. 2009. Periplasmic adaptor protein AcrA has a distinct role in the antibiotic resistance and virulence of *Salmonella enterica* serovar Typhimurium. *J Antimicrob Chemother,* 64**,** 965-72.

Blair, J. M. & Piddock, L. J. 2016. How to Measure Export via Bacterial Multidrug Resistance Efflux Pumps. *MBio,* 7.

Blair, J. M., Smith, H. E., Ricci, V., Lawler, A. J., Thompson, L. J. & Piddock, L. J. 2015b. Expression of homologous RND efflux pump genes is dependent upon AcrB expression: implications for efflux and virulence inhibitor design. *J Antimicrob Chemother,* 70**,** 424-31.

Blair, J. M., Webber, M. A., Baylay, A. J., Ogbolu, D. O. & Piddock, L. J. 2015c. Molecular mechanisms of antibiotic resistance. *Nat Rev Microbiol,* 13**,** 42-51.

Bnf 2021. *British National Formulary (BNF) 82*, BMJ Publishing Group Ltd and Royal Pharmaceutical Society.

Bohnert, J. A. & Kern, W. V. 2005. Selected arylpiperazines are capable of reversing multidrug resistance in *Escherichia coli* overexpressing RND efflux pumps. *Antimicrob Agents Chemother,* 49**,** 849-52.

Bohnert, J. A., Schuster, S., Seeger, M. A., Fahnrich, E., Pos, K. M. & Kern, W. V. 2008. Site-directed mutagenesis reveals putative substrate binding residues in the *Escherichia coli* RND efflux pump AcrB. *J Bacteriol,* 190**,** 8225-9.

Borges-Walmsley, M. I., Beauchamp, J., Kelly, S. M., Jumel, K., Candlish, D., Harding, S. E., Price, N. C. & Walmsley, A. R. 2003. Identification of oligomerization and drug-binding domains of the membrane fusion protein EmrA. *J Biol Chem,* 278**,** 12903-12.

Boyer, E., Dessolin, J., Lustig, M., Decossas, M., Phan, G., Cece, Q., Durand, G., Dubois, V., Sansen, J., Taveau, J.-C., Broutin, I., Daury, L. & Lambert, O. 2022. Molecular Determinants for OMF Selectivity in Tripartite RND Multidrug Efflux Systems. *Antibiotics,* 11**,** 126.

Brauner, A., Fridman, O., Gefen, O. & Balaban, N. Q. 2016. Distinguishing between resistance, tolerance and persistence to antibiotic treatment. *Nat Rev Microbiol,* 14**,** 320-30.

Brenner, F. W., Villar, R. G., Angulo, F. J., Tauxe, R. & Swaminathan, B. 2000. *Salmonella* nomenclature. *J Clin Microbiol,* 38**,** 2465-7.

Brooks, L. E., Ul-Hasan, S., Chan, B. K. & Sistrom, M. J. 2018. Quantifying the Evolutionary Conservation of Genes Encoding Multidrug Efflux Pumps in the ESKAPE Pathogens To Identify Antimicrobial Drug Targets. *mSystems,* 3.

Buckley, A. M., Webber, M. A., Cooles, S., Randall, L. P., La Ragione, R. M., Woodward, M. J. & Piddock, L. J. 2006. The AcrAB-TolC efflux system of *Salmonella enterica* serovar Typhimurium plays a role in pathogenesis. *Cell Microbiol,* 8**,** 847-56.

Buckner, M. M., Blair, J. M., La Ragione, R. M., Newcombe, J., Dwyer, D. J., Ivens, A. & Piddock, L. J. 2016. Beyond Antimicrobial Resistance: Evidence for a Distinct Role of the AcrD Efflux Pump in *Salmonella* Biology. *mBio,* 7.

Cacciotto, P., Basciu, A., Oliva, F., Malloci, G., Zacharias, M., Ruggerone, P. & Vargiu, A. V. 2022. Molecular rationale for the impairment of the MexAB-OprM efflux pump by a single mutation in MexA. *Comput Struct Biotechnol J,* 20**,** 252-260.

Canton, R., Gonzalez-Alba, J. M. & Galan, J. C. 2012. CTX-M Enzymes: Origin and Diffusion. *Front Microbiol,* 3**,** 110.

Casin, I., Hanau-Bercot, B., Podglajen, I., Vahaboglu, H. & Collatz, E. 2003. *Salmonella enterica* serovar Typhimurium bla(PER-1)-carrying plasmid pSTI1 encodes an extended-spectrum aminoglycoside 6'-N-acetyltransferase of type Ib. *Antimicrob Agents Chemother,* 47**,** 697-703.

Centers for Disease Control and Prevention. *National Outbreak Reporting System Dashboard* [Online]. Atlanta, Georgia: U.S. Department of Health and Human Services. Available: wwwn.cdc.gov/norsdashboard [Accessed 28th April 2022 2022].

Cha, H. J., Muller, R. T. & Pos, K. M. 2014. Switch-loop flexibility affects transport of large drugs by the promiscuous AcrB multidrug efflux transporter. *Antimicrob Agents Chemother,* 58**,** 4767-72.

Chacon, K. N., Mealman, T. D., Mcevoy, M. M. & Blackburn, N. J. 2014. Tracking metal ions through a Cu/Ag efflux pump assigns the functional roles of the periplasmic proteins. *Proc Natl Acad Sci U S A,* 111**,** 15373-8.

Chan, W., Costantino, N., Li, R., Lee, S. C., Su, Q., Melvin, D., Court, D. L. & Liu, P. 2007a. A recombineering based approach for high-throughput conditional knockout targeting vector construction. *Nucleic Acids Res,* 35**,** e64.

Chan, Y. Y., Bian, H. S., Tan, T. M., Mattmann, M. E., Geske, G. D., Igarashi, J., Hatano, T., Suga, H., Blackwell, H. E. & Chua, K. L. 2007b. Control of quorum sensing by a *Burkholderia pseudomallei* multidrug efflux pump. *J Bacteriol,* 189**,** 4320-4.

Chang, A. C. & Cohen, S. N. 1978. Construction and characterization of amplifiable multicopy DNA cloning vehicles derived from the P15A cryptic miniplasmid. *J Bacteriol,* 134**,** 1141-56.

Chaudhuri, R. R., Morgan, E., Peters, S. E., Pleasance, S. J., Hudson, D. L., Davies, H. M., Wang, J., Van Diemen, P. M., Buckley, A. M., Bowen, A. J., Pullinger, G. D., Turner, D. J., Langridge, G. C., Turner, A. K., Parkhill, J., Charles, I. G., Maskell, D. J. & Stevens, M. P. 2013. Comprehensive assignment of roles for *Salmonella* Typhimurium genes in intestinal colonization of food-producing animals. *PLoS Genet,* 9**,** e1003456.

Chen, M., Shi, X., Yu, Z., Fan, G., Serysheva, Ii, Baker, M. L., Luisi, B. F., Ludtke, S. J. & Wang, Z. 2021. *In situ* structure of the AcrAB-TolC efflux pump at subnanometer resolution. *Structure*.

Clsi 2020. *Performance standards for antimicrobial susceptibility testing, 30th edition,* Wayne, PA, Clinical and Laboratory Standards Institute

Colclough, A. L., Alav, I., Whittle, E. E., Pugh, H. L., Darby, E. M., Legood, S. W., Mcneil, H. E. & Blair, J. M. 2020. RND efflux pumps in Gram-negative bacteria; regulation, structure and role in antibiotic resistance. *Future Microbiol,* 15**,** 143-157.

Colclough, A. L., Scadden, J. & Blair, J. M. A. 2019. TetR-family transcription factors in Gram-negative bacteria: conservation, variation and implications for efflux-mediated antimicrobial resistance. *BMC Genomics,* 20**,** 731.

Conroy, O., Kim, E. H., Mcevoy, M. M. & Rensing, C. 2010. Differing ability to transport nonmetal substrates by two RND-type metal exporters. *FEMS Microbiol Lett,* 308**,** 115-22.

Costerton, J. W., Ingram, J. M. & Cheng, K. J. 1974. Structure and function of the cell envelope of gram-negative bacteria. *Bacteriol Rev,* 38**,** 87-110.

Crucello, A., Furtado, M. M., Chaves, M. D. R. & Sant'ana, A. S. 2019. Transcriptome sequencing reveals genes and adaptation pathways in *Salmonella* Typhimurium inoculated in four low water activity foods. *Food Microbiol,* 82**,** 426-435.

Cuthbertson, L. & Nodwell, J. R. 2013. The TetR family of regulators. *Microbiol Mol Biol Rev,* 77**,** 440-75.

Dalton, J. P., Uy, B., Swift, S. & Wiles, S. 2017. A Novel Restraint Device for Injection of *Galleria mellonella* Larvae that Minimizes the Risk of Accidental Operator Needle Stick Injury. *Front Cell Infect Microbiol,* 7**,** 99.

Daniel, N., Nuria, C., Sun, P., Sugden, D. & Aldin, V. 2020. The Burden of Foodborne Disease in the UK 2018. UK: Food Standards Agency.

Darzynkiewicz, Z. M., Green, A. T., Abdali, N., Hazel, A., Fulton, R. L., Kimball, J., Gryczynski, Z., Gumbart, J. C., Parks, J. M., Smith, J. C. & Zgurskaya, H. I. 2019. Identification of Binding Sites for Efflux Pump Inhibitors of the AcrAB-TolC Component AcrA. *Biophys J,* 116**,** 648-658.

Datsenko, K. A. & Wanner, B. L. 2000. One-step inactivation of chromosomal genes in *Escherichia coli* K-12 using PCR products. *Proc Natl Acad Sci U S A,* 97**,** 6640-5.

Daury, L., Orange, F., Taveau, J. C., Verchere, A., Monlezun, L., Gounou, C., Marreddy, R. K., Picard, M., Broutin, I., Pos, K. M. & Lambert, O. 2016. Tripartite assembly of RND multidrug efflux pumps. *Nat Commun,* 7**,** 10731.

De Angelis, F., Lee, J. K., O'connell, J. D., 3rd, Miercke, L. J., Verschueren, K. H., Srinivasan, V., Bauvois, C., Govaerts, C., Robbins, R. A., Ruysschaert, J. M., Stroud, R. M. & Vandenbussche, G. 2010. Metal-induced conformational changes in ZneB suggest an active role of membrane fusion proteins in efflux resistance systems. *Proc Natl Acad Sci U S A,* 107**,** 11038-43.

De Duve, C. & Wattiaux, R. 1966. Functions of lysosomes. *Annu Rev Physiol,* 28**,** 435-92.

Delcour, A. H. 2009. Outer membrane permeability and antibiotic resistance. *Biochim Biophys Acta,* 1794**,** 808-16.

Dhamdhere, G., Krishnamoorthy, G. & Zgurskaya, H. I. 2010. Interplay between drug efflux and antioxidants in *Escherichia coli* resistance to antibiotics. *Antimicrob Agents Chemother,* 54**,** 5366-8.

Dönhöfer, A., Franckenberg, S., Wickles, S., Berninghausen, O., Beckmann, R. & Wilson, D. N. 2012. Structural basis for TetM-mediated tetracycline resistance. *Proceedings of the National Academy of Sciences,* 109**,** 16900-16905.

Dorea, F. C., Cole, D. J., Hofacre, C., Zamperini, K., Mathis, D., Doyle, M. P., Lee, M. D. & Maurer, J. J. 2010. Effect of *Salmonella* vaccination of breeder chickens on contamination of broiler chicken carcasses in integrated poultry operations. *Appl Environ Microbiol,* 76**,** 7820-5.

Du, D., Neuberger, A., Orr, M. W., Newman, C. E., Hsu, P. C., Samsudin, F., Szewczak-Harris, A., Ramos, L. M., Debela, M., Khalid, S., Storz, G. & Luisi, B. F. 2020. Interactions of a Bacterial RND Transporter with a Transmembrane Small Protein in a Lipid Environment. *Structure,* 28**,** 625-634 e6.

Du, D., Wang, Z., James, N. R., Voss, J. E., Klimont, E., Ohene-Agyei, T., Venter, H., Chiu, W. & Luisi, B. F. 2014. Structure of the AcrAB-TolC multidrug efflux pump. *Nature,* 509**,** 512-5.

Du, D., Wang-Kan, X., Neuberger, A., Van Veen, H. W., Pos, K. M., Piddock, L. J. V. & Luisi, B. F. 2018. Multidrug efflux pumps: structure, function and regulation. *Nat Rev Microbiol,* 16**,** 523-539.

Duy, P. T., Dongol, S., Giri, A., Nguyen To, N. T., Dan Thanh, H. N., Nhu Quynh, N. P., Duc Trung, P., Thwaites, G. E., Basnyat, B., Baker, S., Rabaa, M. A. & Karkey, A. 2020. The emergence of azithromycin-resistant *Salmonella* Typhi in Nepal. *JAC Antimicrob Resist,* 2**,** dlaa109.

Eaves, D. J., Ricci, V. & Piddock, L. J. 2004. Expression of *acrB, acrF, acrD, marA*, and *soxS* in *Salmonella enterica* serovar Typhimurium: role in multiple antibiotic resistance. *Antimicrob Agents Chemother,* 48**,** 1145-50.

Economou, V. & Gousia, P. 2015. Agriculture and food animals as a source of antimicrobial-resistant bacteria. *Infect Drug Resist,* 8**,** 49-61.

Eda, S., Maseda, H., Yoshihara, E. & Nakae, T. 2006. Assignment of the outer-membrane-subunit-selective domain of the membrane fusion protein in the tripartite xenobiotic efflux pump of *Pseudomonas aeruginosa*. *FEMS Microbiol Lett,* 254**,** 101-7.

Eguchi, Y., Oshima, T., Mori, H., Aono, R., Yamamoto, K., Ishihama, A. & Utsumi, R. 2003. Transcriptional regulation of drug efflux genes by EvgAS, a two-component system in *Escherichia coli*. *Microbiology,* 149**,** 2819-2828.

Eicher, T., Cha, H. J., Seeger, M. A., Brandstatter, L., El-Delik, J., Bohnert, J. A., Kern, W. V., Verrey, F., Grutter, M. G., Diederichs, K. & Pos, K. M. 2012. Transport of drugs by the multidrug transporter AcrB involves an access and a deep binding pocket that are separated by a switch-loop. *Proc Natl Acad Sci U S A,* 109**,** 5687-92.

El Meouche, I. & Dunlop, M. J. 2018. Heterogeneity in efflux pump expression predisposes antibiotic-resistant cells to mutation. *Science,* 362**,** 686-690.

Elkins, C. A. & Mullis, L. B. 2006. Mammalian steroid hormones are substrates for the major RND- and MFS-type tripartite multidrug efflux pumps of *Escherichia coli*. *J Bacteriol,* 188**,** 1191-5.

Elkins, C. A. & Nikaido, H. 2002. Substrate specificity of the RND-type multidrug efflux pumps AcrB and AcrD of *Escherichia coli* is determined predominantly by two large periplasmic loops. *J Bacteriol,* 184**,** 6490-8.

Elkins, C. A. & Nikaido, H. 2003. Chimeric analysis of AcrA function reveals the importance of its C-terminal domain in its interaction with the AcrB multidrug efflux pump. *J Bacteriol,* 185**,** 5349-56.

Elnekave, E., Hong, S., Mather, A. E., Boxrud, D., Taylor, A. J., Lappi, V., Johnson, T. J., Vannucci, F., Davies, P., Hedberg, C., Perez, A. & Alvarez, J. 2018. *Salmonella enterica* Serotype 4,[5],12:i:- in Swine in the United States Midwest: An Emerging Multidrug-Resistant Clade. *Clin Infect Dis,* 66**,** 877-885.

Eng, S. K., Pusparajah, P., Ab Mutalib, N. S., Ser, H. L., Chan, K. G. & Lee, L. H. 2015. *Salmonella*: A review on pathogenesis, epidemiology and antibiotic resistance. *Frontiers in Life Science,* 8**,** 284-293.

Erridge, C., Bennett-Guerrero, E. & Poxton, I. R. 2002. Structure and function of lipopolysaccharides. *Microbes Infect,* 4**,** 837-51.

Eucast 2021. Routine and extended internal quality control for MIC determination and disk diffusion as recommended by EUCAST. Version 11.0. 11 ed.: European Society of Clinical Microbiology and Infectious Diseases.

European Centre for Disease Prevention and Control and European Food Safety Authority and European Medicines, A. 2017. ECDC/EFSA/EMA second joint report on the integrated analysis of the consumption of antimicrobial agents and occurrence of antimicrobial resistance in bacteria from humans and food-producing animals. *EFSA Journal,* 15.

Fang, J., Yu, L., Wu, M. & Wei, Y. 2013. Dissecting the function of a protruding loop in AcrB trimerization. *J Biomol Struct Dyn,* 31**,** 385-92.

Feasey, N. A., Dougan, G., Kingsley, R. A., Heyderman, R. S. & Gordon, M. A. 2012. Invasive non-typhoidal *Salmonella* disease: an emerging and neglected tropical disease in Africa. *Lancet,* 379**,** 2489-2499.

Fernandez-Recio, J., Walas, F., Federici, L., Venkatesh Pratap, J., Bavro, V. N., Miguel, R. N., Mizuguchi, K. & Luisi, B. 2004. A model of a transmembrane drug-efflux pump from Gram-negative bacteria. *FEBS Lett,* 578**,** 5-9.

Ferrari, R. G., Rosario, D. K. A., Cunha-Neto, A., Mano, S. B., Figueiredo, E. E. S. & Conte-Junior, C. A. 2019. Worldwide Epidemiology of *Salmonella* serovars in Animal-Based Foods: a Meta-analysis. *Appl Environ Microbiol,* 85.

Flemming, H. C. & Wingender, J. 2010. The biofilm matrix. *Nat Rev Microbiol,* 8**,** 623-33.

Flemming, H. C., Wingender, J., Szewzyk, U., Steinberg, P., Rice, S. A. & Kjelleberg, S. 2016. Biofilms: an emergent form of bacterial life. *Nat Rev Microbiol,* 14**,** 563-75.

Fraser, A., Paul, M., Goldberg, E., Acosta, C. J. & Leibovici, L. 2007. Typhoid fever vaccines: systematic review and meta-analysis of randomised controlled trials. *Vaccine,* 25**,** 7848-57.

Gal-Mor, O., Boyle, E. C. & Grassl, G. A. 2014. Same species, different diseases: how and why typhoidal and non-typhoidal *Salmonella enterica* serovars differ. *Front Microbiol,* 5**,** 391.

Gasteiger, G., D'osualdo, A., Schubert, D. A., Weber, A., Bruscia, E. M. & Hartl, D. 2017. Cellular Innate Immunity: An Old Game with New Players. *J Innate Immun,* 9**,** 111-125.

Ge, Q., Yamada, Y. & Zgurskaya, H. 2009. The C-terminal domain of AcrA is essential for the assembly and function of the multidrug efflux pump AcrAB-TolC. *J Bacteriol,* 191**,** 4365-71.

Gebreyes, W. A. & Altier, C. 2002. Molecular characterization of multidrug-resistant *Salmonella enterica* subsp. enterica serovar Typhimurium isolates from swine. *J Clin Microbiol,* 40**,** 2813-22.

Gerken, H. & Misra, R. 2004. Genetic evidence for functional interactions between TolC and AcrA proteins of a major antibiotic efflux pump of *Escherichia coli*. *Mol Microbiol,* 54**,** 620-31.

Giammanco, G. M., Pignato, S., Mammina, C., Grimont, F., Grimont, P. A., Nastasi, A. & Giammanco, G. 2002. Persistent endemicity of *Salmonella bongori* 48:z(35):--in Southern Italy: molecular characterization of human, animal, and environmental isolates. *J Clin Microbiol,* 40**,** 3502-5.

Gibani, M. M., Britto, C. & Pollard, A. J. 2018. Typhoid and paratyphoid fever: a call to action. *Curr Opin Infect Dis,* 31**,** 440-448.

Gilardi, A., Bhamidimarri, S. P., Bronstrup, M., Bilitewski, U., Marreddy, R. K. R., Pos, K. M., Benier, L., Gribbon, P., Winterhalter, M. & Windshugel, B. 2017. Biophysical characterization of *E. coli* TolC interaction with the known blocker hexaamminecobalt. *Biochim Biophys Acta Gen Subj,* 1861**,** 2702-2709.

Glavier, M., Puvanendran, D., Salvador, D., Decossas, M., Phan, G., Garnier, C., Frezza, E., Cece, Q., Schoehn, G., Picard, M., Taveau, J. C., Daury, L., Broutin, I. & Lambert, O. 2020. Antibiotic export by MexB multidrug efflux transporter is allosterically controlled by a MexA-OprM chaperone-like complex. *Nat Commun,* 11**,** 4948.

Goel, A. K., Rajagopal, L., Nagesh, N. & Sonti, R. V. 2002. Genetic locus encoding functions involved in biosynthesis and outer membrane localization of xanthomonadin in *Xanthomonas oryzae* pv. oryzae. *J Bacteriol,* 184**,** 3539-48.

Gorecki, K. & Mcevoy, M. M. 2020. Phylogenetic analysis reveals an ancient gene duplication as the origin of the MdtABC efflux pump. *PLoS One,* 15**,** e0228877.

Green, A. T., Moniruzzaman, M., Cooper, C. J., Walker, J. K., Smith, J. C., Parks, J. M. & Zgurskaya, H. I. 2020. Discovery of multidrug efflux pump inhibitors with a novel chemical scaffold. *Biochim Biophys Acta Gen Subj,* 1864**,** 129546.

Grimsey, E. M., Fais, C., Marshall, R. L., Ricci, V., Ciusa, M. L., Stone, J. W., Ivens, A., Malloci, G., Ruggerone, P., Vargiu, A. V. & Piddock, L. J. V. 2020a. Chlorpromazine and Amitriptyline Are Substrates and Inhibitors of the AcrB Multidrug Efflux Pump. *mBio,* 11.

Grimsey, E. M. & Piddock, L. J. V. 2019. Do phenothiazines possess antimicrobial and efflux inhibitory properties? *FEMS Microbiol Rev,* 43**,** 577-590.

Grimsey, E. M., Weston, N., Ricci, V., Stone, J. W. & Piddock, L. J. V. 2020b. Overexpression of RamA, Which Regulates Production of the Multidrug Resistance Efflux Pump AcrAB-TolC, Increases Mutation Rate and Influences Drug Resistance Phenotype. *Antimicrob Agents Chemother,* 64.

Guan, L. & Nakae, T. 2001. Identification of essential charged residues in transmembrane segments of the multidrug transporter MexB of *Pseudomonas aeruginosa*. *J Bacteriol,* 183**,** 1734-9.

Gupta, A., Matsui, K., Lo, J. F. & Silver, S. 1999. Molecular basis for resistance to silver cations in *Salmonella*. *Nat Med,* 5**,** 183-8.

Hancock, R. E., Egli, C., Benz, R. & Siehnel, R. J. 1992. Overexpression in *Escherichia coli* and functional analysis of a novel PPi-selective porin, *oprO*, from *Pseudomonas aeruginosa*. *J Bacteriol,* 174**,** 471-6.

Hannula, M. & Hanninen, M. L. 2008. Effect of putative efflux pump inhibitors and inducers on the antimicrobial susceptibility of *Campylobacter jejuni* and *Campylobacter coli*. *J Med Microbiol,* 57**,** 851-5.

Hassan, J. O. & Curtiss, R., 3rd 1994. Development and evaluation of an experimental vaccination program using a live avirulent *Salmonella* Typhimurium strain to protect

immunized chickens against challenge with homologous and heterologous *Salmonella* serotypes. *Infect Immun,* 62**,** 5519-27.

Hayashi, K., Nakashima, R., Sakurai, K., Kitagawa, K., Yamasaki, S., Nishino, K. & Yamaguchi, A. 2016. AcrB-AcrA Fusion Proteins That Act as Multidrug Efflux Transporters. *J Bacteriol,* 198**,** 332-42.

Haynes, K. M., Abdali, N., Jhawar, V., Zgurskaya, H. I., Parks, J. M., Green, A. T., Baudry, J., Rybenkov, V. V., Smith, J. C. & Walker, J. K. 2017. Identification and Structure-Activity Relationships of Novel Compounds that Potentiate the Activities of Antibiotics in *Escherichia coli*. *J Med Chem,* 60**,** 6205-6219.

Heisig, P. 1993. High-Level Fluoroquinolone Resistance in a *Salmonella* Typhimurium Isolate Due to Alterations in Both *gyrA* and *gyrB* Genes. *Journal of Antimicrobial Chemotherapy,* 32**,** 367-377.

Henderson, P. J. F., Maher, C., Elbourne, L. D. H., Eijkelkamp, B. A., Paulsen, I. T. & Hassan, K. A. 2021. Physiological Functions of Bacterial "Multidrug" Efflux Pumps. *Chem Rev*.

Higgins, M. K., Eswaran, J., Edwards, P., Schertler, G. F., Hughes, C. & Koronakis, V. 2004. Structure of the ligand-blocked periplasmic entrance of the bacterial multidrug efflux protein TolC. *J Mol Biol,* 342**,** 697-702.

Hilbert, F., Smulders, F. J. M., Chopra-Dewasthaly, R. & Paulsen, P. 2012. *Salmonella* in the wildlife-human interface. *Food Research International,* 45**,** 603-608.

Hirakawa, H., Takumi-Kobayashi, A., Theisen, U., Hirata, T., Nishino, K. & Yamaguchi, A. 2008. AcrS/EnvR represses expression of the *acrAB* multidrug efflux genes in *Escherichia coli*. *J Bacteriol,* 190**,** 6276-9.

Hiyoshi, H., Tiffany, C. R., Bronner, D. N. & Baumler, A. J. 2018. Typhoidal *Salmonella* serovars: ecological opportunity and the evolution of a new pathovar. *FEMS Microbiol Rev,* 42**,** 527-541.

Hobbs, E. C., Yin, X., Paul, B. J., Astarita, J. L. & Storz, G. 2012. Conserved small protein associates with the multidrug efflux pump AcrB and differentially affects antibiotic resistance. *Proc Natl Acad Sci U S A,* 109**,** 16696-701.

Hocquet, D., Roussel-Delvallez, M., Cavallo, J. D. & Plesiat, P. 2007. MexAB-OprM- and MexXY-overproducing mutants are very prevalent among clinical strains of *Pseudomonas aeruginosa* with reduced susceptibility to ticarcillin. *Antimicrob Agents Chemother,* 51**,** 1582-3.

Hoffmann, S., Batz, M. B. & Morris, J. G., Jr. 2012. Annual cost of illness and quality-adjusted life year losses in the United States due to 14 foodborne pathogens. *J Food Prot,* 75**,** 1292-302.

Hofmann, A. F. & Eckmann, L. 2006. How bile acids confer gut mucosal protection against bacteria. *Proc Natl Acad Sci U S A,* 103**,** 4333-4.

Hohmann, E. L. 2001. Nontyphoidal salmonellosis. *Clin Infect Dis,* 32**,** 263-9.

Holden, E. R. & Webber, M. A. 2020. MarA, RamA, and SoxS as Mediators of the Stress Response: Survival at a Cost. *Front Microbiol,* 11**,** 828.

Holmqvist, E. & Vogel, J. 2018. RNA-binding proteins in bacteria. *Nat Rev Microbiol,* 16**,** 601-615.

Hooda, Y., Sajib, M. S. I., Rahman, H., Luby, S. P., Bondy-Denomy, J., Santosham, M., Andrews, J. R., Saha, S. K. & Saha, S. 2019. Molecular mechanism of azithromycin resistance among typhoidal *Salmonella* strains in Bangladesh identified through passive pediatric surveillance. *PLoS Negl Trop Dis,* 13**,** e0007868.

Horiyama, T. & Nishino, K. 2014. AcrB, AcrD, and MdtABC multidrug efflux systems are involved in enterobactin export in *Escherichia coli*. *PLoS One,* 9**,** e108642.

Horiyama, T., Yamaguchi, A. & Nishino, K. 2010. TolC dependency of multidrug efflux systems in *Salmonella enterica* serovar Typhimurium. *J Antimicrob Chemother,* 65**,** 1372-6.

Housden, N. G., Webby, M. N., Lowe, E. D., El-Baba, T. J., Kaminska, R., Redfield, C., Robinson, C. V. & Kleanthous, C. 2021. Toxin import through the antibiotic efflux channel TolC. *Nat Commun,* 12**,** 4625.

Hsu, R. B. & Lin, F. Y. 2005. Risk factors for bacteraemia and endovascular infection due to non-typhoid *Salmonella*: a reappraisal. *QJM,* 98**,** 821-7.

Huang, J., Wang, M., Ding, H., Ye, M., Hu, F., Guo, Q., Xu, X. & Wang, M. 2013. New Delhi metallo-beta-lactamase-1 in carbapenem-resistant *Salmonella* strain, China. *Emerg Infect Dis,* 19**,** 2049-51.

Husain, F., Humbard, M. & Misra, R. 2004. Interaction between the TolC and AcrA proteins of a multidrug efflux system of *Escherichia coli*. *J Bacteriol,* 186**,** 8533-6.

Ikonomidis, A., Tsakris, A., Kanellopoulou, M., Maniatis, A. N. & Pournaras, S. 2008. Effect of the proton motive force inhibitor carbonyl cyanide-m-chlorophenylhydrazone (CCCP) on *Pseudomonas aeruginosa* biofilm development. *Lett Appl Microbiol,* 47**,** 298-302.

Janganan, T. K., Bavro, V. N., Zhang, L., Matak-Vinkovic, D., Barrera, N. P., Venien-Bryan, C., Robinson, C. V., Borges-Walmsley, M. I. & Walmsley, A. R. 2011. Evidence for the assembly of a bacterial tripartite multidrug pump with a stoichiometry of 3:6:3. *J Biol Chem,* 286**,** 26900-12.

Jawad, I., Luksic, I. & Rafnsson, S. B. 2012. Assessing available information on the burden of sepsis: global estimates of incidence, prevalence and mortality. *J Glob Health,* 2**,** 010404.

Jeong, H., Kim, J. S., Song, S., Shigematsu, H., Yokoyama, T., Hyun, J. & Ha, N. C. 2016. Pseudoatomic Structure of the Tripartite Multidrug Efflux Pump AcrAB-TolC Reveals the Intermeshing Cogwheel-like Interaction between AcrA and TolC. *Structure,* 24**,** 272-6.

Johnson, R. M., Fais, C., Parmar, M., Cheruvara, H., Marshall, R. L., Hesketh, S. J., Feasey, M. C., Ruggerone, P., Vargiu, A. V., Postis, V. L. G., Muench, S. P. & Bavro, V. N. 2020. Cryo-EM Structure and Molecular Dynamics Analysis of the Fluoroquinolone Resistant Mutant of the AcrB Transporter from *Salmonella*. *Microorganisms,* 8**,** 943.

Joo, H. S., Fu, C. I. & Otto, M. 2016. Bacterial strategies of resistance to antimicrobial peptides. *Philos Trans R Soc Lond B Biol Sci,* 371.

Jumper, J., Evans, R., Pritzel, A., Green, T., Figurnov, M., Ronneberger, O., Tunyasuvunakool, K., Bates, R., Zidek, A., Potapenko, A., Bridgland, A., Meyer, C., Kohl, S. a. A., Ballard, A. J., Cowie, A., Romera-Paredes, B., Nikolov, S., Jain, R., Adler, J., Back, T., Petersen, S., Reiman, D., Clancy, E., Zielinski, M., Steinegger, M., Pacholska, M., Berghammer, T., Bodenstein, S., Silver, D., Vinyals, O., Senior, A. W., Kavukcuoglu, K., Kohli, P. & Hassabis, D. 2021. Highly accurate protein structure prediction with AlphaFold. *Nature,* 596**,** 583-589.

Kaatz, G. W., Moudgal, V. V., Seo, S. M., Hansen, J. B. & Kristiansen, J. E. 2003. Phenylpiperidine selective serotonin reuptake inhibitors interfere with multidrug efflux pump activity in *Staphylococcus aureus*. *Int J Antimicrob Agents,* 22**,** 254-61.

Kaila, V. R. I. & Wikstrom, M. 2021. Architecture of bacterial respiratory chains. *Nat Rev Microbiol,* 19**,** 319-330.

Kapach, G., Nuri, R., Schmidt, C., Danin, A., Ferrera, S., Savidor, A., Gerlach, R. G. & Shai, Y. 2020. Loss of the Periplasmic Chaperone Skp and Mutations in the Efflux Pump

AcrAB-TolC Play a Role in Acquired Resistance to Antimicrobial Peptides in *Salmonella* Typhimurium. *Front Microbiol,* 11**,** 189.

Karatan, E. & Watnick, P. 2009. Signals, regulatory networks, and materials that build and break bacterial biofilms. *Microbiol Mol Biol Rev,* 73**,** 310-47.

Katayama, Y., Ito, T. & Hiramatsu, K. 2000. A new class of genetic element, staphylococcus cassette chromosome *mec*, encodes methicillin resistance in *Staphylococcus aureus*. *Antimicrob Agents Chemother,* 44**,** 1549-55.

Kawabe, T., Fujihira, E. & Yamaguchi, A. 2000. Molecular construction of a multidrug exporter system, AcrAB: molecular interaction between AcrA and AcrB, and cleavage of the N-terminal signal sequence of AcrA. *J Biochem,* 128**,** 195-200.

Kawakami, V. M., Bottichio, L., Angelo, K., Linton, N., Kissler, B., Basler, C., Lloyd, J., Inouye, W., Gonzales, E., Rietberg, K., Melius, B., Oltean, H., Wise, M., Sinatra, J., Marsland, P., Li, Z., Meek, R., Kay, M., Duchin, J. & Lindquist, S. 2016. Notes from the Field: Outbreak of Multidrug-Resistant *Salmonella* Infections Linked to Pork--Washington, 2015. *MMWR Morb Mortal Wkly Rep,* 65**,** 379-81.

Kikuchi, T., Mizunoe, Y., Takade, A., Naito, S. & Yoshida, S. 2005. Curli fibers are required for development of biofilm architecture in *Escherichia coli* K-12 and enhance bacterial adherence to human uroepithelial cells. *Microbiol Immunol,* 49**,** 875-84.

Kim, H. B., Wang, M., Park, C. H., Kim, E. C., Jacoby, G. A. & Hooper, D. C. 2009. *oqxAB* encoding a multidrug efflux pump in human clinical isolates of Enterobacteriaceae. *Antimicrob Agents Chemother,* 53**,** 3582-4.

Kim, H. M., Xu, Y., Lee, M., Piao, S., Sim, S. H., Ha, N. C. & Lee, K. 2010. Functional relationships between the AcrA hairpin tip region and the TolC aperture tip region for the formation of the bacterial tripartite efflux pump AcrAB-TolC. *J Bacteriol,* 192**,** 4498-503.

Kim, J. S., Jeong, H., Song, S., Kim, H. Y., Lee, K., Hyun, J. & Ha, N. C. 2015. Structure of the tripartite multidrug efflux pump AcrAB-TolC suggests an alternative assembly mode. *Mol Cells,* 38**,** 180-6.

Kim, J. S., Song, S., Lee, M., Lee, S., Lee, K. & Ha, N. C. 2016. Crystal Structure of a Soluble Fragment of the Membrane Fusion Protein HlyD in a Type I Secretion System of Gram-Negative Bacteria. *Structure,* 24**,** 477-85.

Klein, E. Y., Van Boeckel, T. P., Martinez, E. M., Pant, S., Gandra, S., Levin, S. A., Goossens, H. & Laxminarayan, R. 2018. Global increase and geographic convergence in antibiotic consumption between 2000 and 2015. *Proc Natl Acad Sci U S A,* 115**,** E3463-E3470.

Klemm, E. J., Shakoor, S., Page, A. J., Qamar, F. N., Judge, K., Saeed, D. K., Wong, V. K., Dallman, T. J., Nair, S., Baker, S., Shaheen, G., Qureshi, S., Yousafzai, M. T., Saleem, M. K., Hasan, Z., Dougan, G. & Hasan, R. 2018. Emergence of an Extensively Drug-Resistant *Salmonella enterica* Serovar Typhi Clone Harboring a Promiscuous Plasmid Encoding Resistance to Fluoroquinolones and Third-Generation Cephalosporins. *MBio,* 9.

Kobayashi, K., Tsukagoshi, N. & Aono, R. 2001. Suppression of hypersensitivity of *Escherichia coli acrB* mutant to organic solvents by integrational activation of the *acrEF* operon with the IS1 or IS2 element. *J Bacteriol,* 183**,** 2646-53.

Kobayashi, N., Tamura, N., Van Veen, H. W., Yamaguchi, A. & Murakami, S. 2014. beta-Lactam selectivity of multidrug transporters AcrB and AcrD resides in the proximal binding pocket. *J Biol Chem,* 289**,** 10680-90.

Koebnik, R., Locher, K. P. & Van Gelder, P. 2000. Structure and function of bacterial outer membrane proteins: barrels in a nutshell. *Mol Microbiol,* 37**,** 239-53.

Krishnamoorthy, G., Tikhonova, E. B., Dhamdhere, G. & Zgurskaya, H. I. 2013. On the role of TolC in multidrug efflux: the function and assembly of AcrAB-TolC tolerate significant depletion of intracellular TolC protein. *Mol Microbiol,* 87**,** 982-97.

Krishnamoorthy, G., Tikhonova, E. B. & Zgurskaya, H. I. 2008. Fitting periplasmic membrane fusion proteins to inner membrane transporters: mutations that enable *Escherichia coli* AcrA to function with *Pseudomonas aeruginosa* MexB. *J Bacteriol,* 190**,** 691-8.

Kroger, C., Colgan, A., Srikumar, S., Handler, K., Sivasankaran, S. K., Hammarlof, D. L., Canals, R., Grissom, J. E., Conway, T., Hokamp, K. & Hinton, J. C. 2013. An infection-relevant transcriptomic compendium for *Salmonella enterica* serovar Typhimurium. *Cell Host Microbe,* 14**,** 683-95.

Kvist, M., Hancock, V. & Klemm, P. 2008. Inactivation of efflux pumps abolishes bacterial biofilm formation. *Appl Environ Microbiol,* 74**,** 7376-82.

Lacroix, F. J., Cloeckaert, A., Grepinet, O., Pinault, C., Popoff, M. Y., Waxin, H. & Pardon, P. 1996. *Salmonella* typhimurium *acrB*-like gene: identification and role in resistance to biliary salts and detergents and in murine infection. *FEMS Microbiol Lett,* 135**,** 161-7.

Lamers, R. P., Cavallari, J. F. & Burrows, L. L. 2013. The efflux inhibitor phenylalanine-arginine beta-naphthylamide (PAbetaN) permeabilizes the outer membrane of gram-negative bacteria. *PLoS One,* 8**,** e60666.

Lamut, A., Peterlin Masic, L., Kikelj, D. & Tomasic, T. 2019. Efflux pump inhibitors of clinically relevant multidrug resistant bacteria. *Med Res Rev,* 39**,** 2460-2504.

Lennen, R. M., Politz, M. G., Kruziki, M. A. & Pfleger, B. F. 2013. Identification of transport proteins involved in free fatty acid efflux in *Escherichia coli*. *J Bacteriol,* 195**,** 135-44.

Lewis, K. 2008. Multidrug tolerance of biofilms and persister cells. *Curr Top Microbiol Immunol,* 322**,** 107-31.

Li, L., Liao, X., Yang, Y., Sun, J., Li, L., Liu, B., Yang, S., Ma, J., Li, X., Zhang, Q. & Liu, Y. 2013. Spread of *oqxAB* in *Salmonella enterica* serotype Typhimurium predominantly by IncHI2 plasmids. *J Antimicrob Chemother,* 68**,** 2263-8.

Li, X. Z. & Nikaido, H. 2009. Efflux-mediated drug resistance in bacteria: an update. *Drugs,* 69**,** 1555-623.

Li, X. Z., Plesiat, P. & Nikaido, H. 2015. The challenge of efflux-mediated antibiotic resistance in Gram-negative bacteria. *Clin Microbiol Rev,* 28**,** 337-418.

Lien, E., Means, T. K., Heine, H., Yoshimura, A., Kusumoto, S., Fukase, K., Fenton, M. J., Oikawa, M., Qureshi, N., Monks, B., Finberg, R. W., Ingalls, R. R. & Golenbock, D. T. 2000. Toll-like receptor 4 imparts ligand-specific recognition of bacterial lipopolysaccharide. *J Clin Invest,* 105**,** 497-504.

Lin, M. F., Lin, Y. Y., Tu, C. C. & Lan, C. Y. 2017. Distribution of different efflux pump genes in clinical isolates of multidrug-resistant *Acinetobacter baumannii* and their correlation with antimicrobial resistance. *J Microbiol Immunol Infect,* 50**,** 224-231.

Lin, X. M., Yang, M. J., Li, H., Wang, C. & Peng, X. X. 2014. Decreased expression of LamB and Odp1 complex is crucial for antibiotic resistance in *Escherichia coli*. *J Proteomics,* 98**,** 244-53.

Lobedanz, S., Bokma, E., Symmons, M. F., Koronakis, E., Hughes, C. & Koronakis, V. 2007. A periplasmic coiled-coil interface underlying TolC recruitment and the assembly of bacterial drug efflux pumps. *Proc Natl Acad Sci U S A,* 104**,** 4612-7.

Lomovskaya, O. & Bostian, K. A. 2006. Practical applications and feasibility of efflux pump inhibitors in the clinic--a vision for applied use. *Biochem Pharmacol,* 71**,** 910-8.

Lomovskaya, O., Warren, M. S., Lee, A., Galazzo, J., Fronko, R., Lee, M., Blais, J., Cho, D., Chamberland, S., Renau, T., Leger, R., Hecker, S., Watkins, W., Hoshino, K., Ishida,

H. & Lee, V. J. 2001. Identification and characterization of inhibitors of multidrug resistance efflux pumps in *Pseudomonas aeruginosa*: novel agents for combination therapy. *Antimicrob Agents Chemother,* 45**,** 105-16.

Lomovskaya, O., Zgurskaya, H. I., Totrov, M. & Watkins, W. J. 2007. Waltzing transporters and 'the dance macabre' between humans and bacteria. *Nat Rev Drug Discov,* 6**,** 56-65.

Long, F., Su, C. C., Lei, H. T., Bolla, J. R., Do, S. V. & Yu, E. W. 2012. Structure and mechanism of the tripartite CusCBA heavy-metal efflux complex. *Philos Trans R Soc Lond B Biol Sci,* 367**,** 1047-58.

Lu, S. & Zgurskaya, H. I. 2013. MacA, a periplasmic membrane fusion protein of the macrolide transporter MacAB-TolC, binds lipopolysaccharide core specifically and with high affinity. *J Bacteriol,* 195**,** 4865-72.

Lv, L., Wan, M., Wang, C., Gao, X., Yang, Q., Partridge, S. R., Wang, Y., Zong, Z., Doi, Y., Shen, J., Jia, P., Song, Q., Zhang, Q., Yang, J., Huang, X., Wang, M. & Liu, J. H. 2020. Emergence of a Plasmid-Encoded Resistance-Nodulation-Division Efflux Pump Conferring Resistance to Multiple Drugs, Including Tigecycline, in *Klebsiella pneumoniae*. *mBio,* 11.

Maclennan, C. A., Martin, L. B. & Micoli, F. 2014. Vaccines against invasive *Salmonella* disease: current status and future directions. *Hum Vaccin Immunother,* 10**,** 1478-93.

Magiorakos, A. P., Srinivasan, A., Carey, R. B., Carmeli, Y., Falagas, M. E., Giske, C. G., Harbarth, S., Hindler, J. F., Kahlmeter, G., Olsson-Liljequist, B., Paterson, D. L., Rice, L. B., Stelling, J., Struelens, M. J., Vatopoulos, A., Weber, J. T. & Monnet, D. L. 2012. Multidrug-resistant, extensively drug-resistant and pandrug-resistant bacteria: an international expert proposal for interim standard definitions for acquired resistance. *Clin Microbiol Infect,* 18**,** 268-81.

Marineli, F., Tsoucalas, G., Karamanou, M. & Androutsos, G. 2013. Mary Mallon (1869-1938) and the history of typhoid fever. *Ann Gastroenterol,* 26**,** 132-134.

Marquez, B. 2005. Bacterial efflux systems and efflux pumps inhibitors. *Biochimie,* 87**,** 1137-47.

Marshall, R. L., Lloyd , G. S., Lawler, A. J., Element, S. J., Kaur, J., Ciusa, M. L., Ricci, V., Tschumi, A., Kühne, H., Alderwick, L. J. & Piddock, L. 2020. New Multidrug Efflux Inhibitors for Gram-Negative Bacteria. *MBio,* 11.

Matsumura, K., Furukawa, S., Ogihara, H. & Morinaga, Y. 2011. Roles of multidrug efflux pumps on the biofilm formation of *Escherichia coli* K-12. *Biocontrol Sci,* 16**,** 69-72.

Mcewen, S. A. & Fedorka-Cray, P. J. 2002. Antimicrobial use and resistance in animals. *Clin Infect Dis,* 34 Suppl 3**,** S93-S106.

Mcneil, H. E., Alav, I., Torres, R. C., Rossiter, A. E., Laycock, E., Legood, S., Kaur, I., Davies, M., Wand, M., Webber, M. A., Bavro, V. N. & Blair, J. M. A. 2019. Identification of binding residues between periplasmic adapter protein (PAP) and RND efflux pumps explains PAP-pump promiscuity and roles in antimicrobial resistance. *PLoS Pathog,* 15**,** e1008101.

Medeiros, A. A., O'brien, T. F., Rosenberg, E. Y. & Nikaido, H. 1987. Loss of OmpC porin in a strain of *Salmonella* typhimurium causes increased resistance to cephalosporins during therapy. *J Infect Dis,* 156**,** 751-7.

Michael, B., Smith, J. N., Swift, S., Heffron, F. & Ahmer, B. M. 2001. SdiA of *Salmonella enterica* is a LuxR homolog that detects mixed microbial communities. *J Bacteriol,* 183**,** 5733-42.

Micoli, F., Bagnoli, F., Rappuoli, R. & Serruto, D. 2021. The role of vaccines in combatting antimicrobial resistance. *Nat Rev Microbiol,* 19**,** 287-302.

Mikolosko, J., Bobyk, K., Zgurskaya, H. I. & Ghosh, P. 2006. Conformational flexibility in the multidrug efflux system protein AcrA. *Structure,* 14**,** 577-87.

Miller, S. I. & Salama, N. R. 2018. The gram-negative bacterial periplasm: Size matters. *PLoS Biol,* 16**,** e2004935.

Mitchell, P. 2011. Chemiosmotic coupling in oxidative and photosynthetic phosphorylation. 1966. *Biochim Biophys Acta,* 1807**,** 1507-38.

Monack, D. M. 2012. *Salmonella* persistence and transmission strategies. *Curr Opin Microbiol,* 15**,** 100-7.

Motta, S. S., Cluzel, P. & Aldana, M. 2015. Adaptive resistance in bacteria requires epigenetic inheritance, genetic noise, and cost of efflux pumps. *PLoS One,* 10**,** e0118464.

Munita, J. M. & Arias, C. A. 2016. Mechanisms of Antibiotic Resistance. *Microbiol Spectr,* 4.

Murakami, S., Nakashima, R., Yamashita, E., Matsumoto, T. & Yamaguchi, A. 2006. Crystal structures of a multidrug transporter reveal a functionally rotating mechanism. *Nature,* 443**,** 173-9.

Murakami, S., Nakashima, R., Yamashita, E. & Yamaguchi, A. 2002. Crystal structure of bacterial multidrug efflux transporter AcrB. *Nature,* 419**,** 587-93.

Murray, C. J. L., Ikuta, K. S., Sharara, F., Swetschinski, L., Robles Aguilar, G., Gray, A., Han, C., Bisignano, C., Rao, P., Wool, E., Johnson, S. C., Browne, A. J., Chipeta, M. G., Fell, F., Hackett, S., Haines-Woodhouse, G., Kashef Hamadani, B. H., Kumaran, E. a. P., Mcmanigal, B., Agarwal, R., Akech, S., Albertson, S., Amuasi, J., Andrews, J., Aravkin, A., Ashley, E., Bailey, F., Baker, S., Basnyat, B., Bekker, A., Bender, R., Bethou, A., Bielicki, J., Boonkasidecha, S., Bukosia, J., Carvalheiro, C., Castañeda-Orjuela, C., Chansamouth, V., Chaurasia, S., Chiurchiù, S., Chowdhury, F., Cook, A. J., Cooper, B., Cressey, T. R., Criollo-Mora, E., Cunningham, M., Darboe, S., Day, N. P. J., De Luca, M., Dokova, K., Dramowski, A., Dunachie, S. J., Eckmanns, T., Eibach, D., Emami, A., Feasey, N., Fisher-Pearson, N., Forrest, K., Garrett, D., Gastmeier, P., Giref, A. Z., Greer, R. C., Gupta, V., Haller, S., Haselbeck, A., Hay, S. I., Holm, M., Hopkins, S., Iregbu, K. C., Jacobs, J., Jarovsky, D., Javanmardi, F., Khorana, M., Kissoon, N., Kobeissi, E., Kostyanev, T., Krapp, F., Krumkamp, R., Kumar, A., Kyu, H. H., Lim, C., Limmathurotsakul, D., Loftus, M. J., Lunn, M., Ma, J., Mturi, N., Munera-Huertas, T., Musicha, P., Mussi-Pinhata, M. M., Nakamura, T., Nanavati, R., Nangia, S., Newton, P., Ngoun, C., Novotney, A., Nwakanma, D., Obiero, C. W., Olivas-Martinez, A., Olliaro, P., Ooko, E., et al. 2022. Global burden of bacterial antimicrobial resistance in 2019: a systematic analysis. *The Lancet*.

Nabarro, L. E., Mccann, N., Herdman, M. T., Dugan, C., Ladhani, S., Patel, D., Morris-Jones, S., Balasegaram, S., Heyderman, R. S., Brown, M., Parry, C. M. & Godbole, G. 2022. British infection association guidelines for the diagnosis and management of enteric fever in England. *J Infect*.

Nakashima, R., Sakurai, K., Yamasaki, S., Hayashi, K., Nagata, C., Hoshino, K., Onodera, Y., Nishino, K. & Yamaguchi, A. 2013. Structural basis for the inhibition of bacterial multidrug exporters. *Nature,* 500**,** 102-6.

Nakashima, R., Sakurai, K., Yamasaki, S., Nishino, K. & Yamaguchi, A. 2011. Structures of the multidrug exporter AcrB reveal a proximal multisite drug-binding pocket. *Nature,* 480**,** 565-9.

Nehme, D., Li, X. Z., Elliot, R. & Poole, K. 2004. Assembly of the MexAB-OprM multidrug efflux system of *Pseudomonas aeruginosa*: identification and characterization of mutations in *mexA* compromising MexA multimerization and interaction with MexB. *J Bacteriol,* 186**,** 2973-83.

Nehme, D. & Poole, K. 2005. Interaction of the MexA and MexB components of the MexAB-OprM multidrug efflux system of *Pseudomonas aeruginosa*: identification of MexA extragenic suppressors of a T578I mutation in MexB. *Antimicrob Agents Chemother,* 49**,** 4375-8.

Nehme, D. & Poole, K. 2007. Assembly of the MexAB-OprM multidrug pump of *Pseudomonas aeruginosa*: component interactions defined by the study of pump mutant suppressors. *J Bacteriol,* 189**,** 6118-27.

Neuberger, A., Du, D. & Luisi, B. F. 2018. Structure and mechanism of bacterial tripartite efflux pumps. *Res Microbiol,* 169**,** 401-413.

Ni, R. T., Onishi, M., Mizusawa, M., Kitagawa, R., Kishino, T., Matsubara, F., Tsuchiya, T., Kuroda, T. & Ogawa, W. 2020. The role of RND-type efflux pumps in multidrug-resistant mutants of *Klebsiella pneumoniae*. *Scientific Reports,* 10**,** 10876.

Nicoloff, H. & Andersson, D. I. 2013. Lon protease inactivation, or translocation of the *lon* gene, potentiate bacterial evolution to antibiotic resistance. *Mol Microbiol,* 90**,** 1233-48.

Nies, D. H. 2003. Efflux-mediated heavy metal resistance in prokaryotes. *FEMS Microbiol Rev,* 27**,** 313-39.

Nikaido, E., Shirosaka, I., Yamaguchi, A. & Nishino, K. 2011. Regulation of the AcrAB multidrug efflux pump in *Salmonella enterica* serovar Typhimurium in response to indole and paraquat. *Microbiology,* 157**,** 648-655.

Nikaido, E., Yamaguchi, A. & Nishino, K. 2008. AcrAB multidrug efflux pump regulation in *Salmonella enterica serovar* Typhimurium by RamA in response to environmental signals. *J Biol Chem,* 283**,** 24245-53.

Nikaido, H. 1992. Porins and specific channels of bacterial outer membranes. *Mol Microbiol,* 6**,** 435-42.

Nikaido, H. 2018. RND transporters in the living world. *Res Microbiol,* 169**,** 363-371.

Nishino, K. 2016. Antimicrobial drug efflux pumps in *Salmonella*. 261-279.

Nishino, K., Hayashi-Nishino, M. & Yamaguchi, A. 2009. H-NS modulates multidrug resistance of *Salmonella enterica* serovar Typhimurium by repressing multidrug efflux genes *acrEF*. *Antimicrob Agents Chemother,* 53**,** 3541-3.

Nishino, K., Latifi, T. & Groisman, E. A. 2006. Virulence and drug resistance roles of multidrug efflux systems of *Salmonella enterica* serovar Typhimurium. *Mol Microbiol,* 59**,** 126-41.

Nishino, K., Nikaido, E. & Yamaguchi, A. 2007. Regulation of multidrug efflux systems involved in multidrug and metal resistance of *Salmonella enterica* serovar Typhimurium. *J Bacteriol,* 189**,** 9066-75.

Nishino, K. & Yamaguchi, A. 2001. Overexpression of the response regulator *evgA* of the two-component signal transduction system modulates multidrug resistance conferred by multidrug resistance transporters. *J Bacteriol,* 183**,** 1455-8.

Nishino, K. & Yamaguchi, A. 2002. EvgA of the two-component signal transduction system modulates production of the *yhiUV* multidrug transporter in *Escherichia coli*. *J Bacteriol,* 184**,** 2319-23.

Nishino, K. & Yamaguchi, A. 2004. Role of histone-like protein H-NS in multidrug resistance of *Escherichia coli*. *J Bacteriol,* 186**,** 1423-9.

Nolivos, S., Cayron, J., Dedieu, A., Page, A., Delolme, F. & Lesterlin, C. 2019. Role of AcrAB-TolC multidrug efflux pump in drug-resistance acquisition by plasmid transfer. *Science,* 364**,** 778-782.

Normark, B. H. & Normark, S. 2002. Evolution and spread of antibiotic resistance. *J Intern Med,* 252**,** 91-106.

Ntreh, A. T., Weeks, J. W., Nickels, L. M. & Zgurskaya, H. I. 2016. Opening the Channel: the Two Functional Interfaces of *Pseudomonas aeruginosa* OpmH with the Triclosan Efflux Pump TriABC. *J Bacteriol,* 198**,** 3176-3185.

O'Brien, S. J. 2013. The "decline and fall" of nontyphoidal *Salmonella* in the United kingdom. *Clin Infect Dis,* 56**,** 705-10.

O'Neill, J. 2016. Tackling drug-resistant infections globally: final report and recommendations.

Oethinger, M., Kern, W. V., Jellen-Ritter, A. S., Mcmurry, L. M. & Levy, S. B. 2000. Ineffectiveness of topoisomerase mutations in mediating clinically significant fluoroquinolone resistance in *Escherichia coli* in the absence of the AcrAB efflux pump. *Antimicrob Agents Chemother,* 44**,** 10-3.

Oh, E., Zhang, Q. & Jeon, B. 2014. Target optimization for peptide nucleic acid (PNA)-mediated antisense inhibition of the CmeABC multidrug efflux pump in *Campylobacter jejuni*. *J Antimicrob Chemother,* 69**,** 375-80.

Okusu, H., Ma, D. & Nikaido, H. 1996. AcrAB efflux pump plays a major role in the antibiotic resistance phenotype of *Escherichia coli* multiple-antibiotic-resistance (Mar) mutants. *J Bacteriol,* 178**,** 306-8.

Olliver, A., Valle, M., Chaslus-Dancla, E. & Cloeckaert, A. 2004. Role of an *acrR* mutation in multidrug resistance of in vitro-selected fluoroquinolone-resistant mutants of *Salmonella enterica* serovar Typhimurium. *FEMS Microbiol Lett,* 238**,** 267-72.

Olliver, A., Valle, M., Chaslus-Dancla, E. & Cloeckaert, A. 2005. Overexpression of the multidrug efflux operon *acrEF* by insertional activation with IS1 or IS10 elements in *Salmonella enterica* serovar Typhimurium DT204 *acrB* mutants selected with fluoroquinolones. *Antimicrob Agents Chemother,* 49**,** 289-301.

Onwuezobe, I. A., Oshun, P. O. & Odigwe, C. C. 2012. Antimicrobials for treating symptomatic non-typhoidal *Salmonella* infection. *Cochrane Database Syst Rev,* 11**,** CD001167.

Opperman, T. J., Kwasny, S. M., Kim, H. S., Nguyen, S. T., Houseweart, C., D'souza, S., Walker, G. C., Peet, N. P., Nikaido, H. & Bowlin, T. L. 2014. Characterization of a novel pyranopyridine inhibitor of the AcrAB efflux pump of *Escherichia coli*. *Antimicrob Agents Chemother,* 58**,** 722-33.

Opperman, T. J. & Nguyen, S. T. 2015. Recent advances toward a molecular mechanism of efflux pump inhibition. *Front Microbiol,* 6**,** 421.

Oswald, C., Tam, H. K. & Pos, K. M. 2016. Transport of lipophilic carboxylates is mediated by transmembrane helix 2 in multidrug transporter AcrB. *Nat Commun,* 7**,** 13819.

Padilla, E., Llobet, E., Domenech-Sanchez, A., Martinez-Martinez, L., Bengoechea, J. A. & Alberti, S. 2010. *Klebsiella pneumoniae* AcrAB efflux pump contributes to antimicrobial resistance and virulence. *Antimicrob Agents Chemother,* 54**,** 177-83.

Paixao, L., Rodrigues, L., Couto, I., Martins, M., Fernandes, P., De Carvalho, C. C., Monteiro, G. A., Sansonetty, F., Amaral, L. & Viveiros, M. 2009. Fluorometric determination of ethidium bromide efflux kinetics in *Escherichia coli*. *J Biol Eng,* 3**,** 18.

Pannek, S., Higgins, P. G., Steinke, P., Jonas, D., Akova, M., Bohnert, J. A., Seifert, H. & Kern, W. V. 2006. Multidrug efflux inhibition in *Acinetobacter baumannii*: comparison between 1-(1-naphthylmethyl)-piperazine and phenyl-arginine-beta-naphthylamide. *J Antimicrob Chemother,* 57**,** 970-4.

Parveen, S., Taabodi, M., Schwarz, J. G., Oscar, T. P., Harter-Dennis, J. & White, D. G. 2007. Prevalence and antimicrobial resistance of *Salmonella* recovered from processed poultry. *J Food Prot,* 70**,** 2466-72.

Paulsen, I. T., Brown, M. H. & Skurray, R. A. 1996. Proton-dependent multidrug efflux systems. *Microbiol Rev,* 60**,** 575-608.

Pearce, M. E., Langridge, G. C., Lauer, A. C., Grant, K., Maiden, M. C. J. & Chattaway, M. A. 2021. An evaluation of the species and subspecies of the genus *Salmonella* with whole genome sequence data: Proposal of type strains and epithets for novel *S. enterica* subspecies VII, VIII, IX, X and XI. *Genomics,* 113**,** 3152-3162.

Pearson, J. P., Van Delden, C. & Iglewski, B. H. 1999. Active efflux and diffusion are involved in transport of *Pseudomonas aeruginosa* cell-to-cell signals. *J Bacteriol,* 181**,** 1203-10.

Pereira, M. F., Rossi, C. C., Da Silva, G. C., Rosa, J. N. & Bazzolli, D. M. S. 2020. *Galleria mellonella* as an infection model: an in-depth look at why it works and practical considerations for successful application. *Pathog Dis,* 78.

Pettersen, E. F., Goddard, T. D., Huang, C. C., Meng, E. C., Couch, G. S., Croll, T. I., Morris, J. H. & Ferrin, T. E. 2021. UCSF ChimeraX: Structure visualization for researchers, educators, and developers. *Protein Sci,* 30**,** 70-82.

Piddock, L. J. 2006a. Clinically relevant chromosomally encoded multidrug resistance efflux pumps in bacteria. *Clin Microbiol Rev,* 19**,** 382-402.

Piddock, L. J. 2006b. Multidrug-resistance efflux pumps - not just for resistance. *Nat Rev Microbiol,* 4**,** 629-36.

Piddock, L. J., White, D. G., Gensberg, K., Pumbwe, L. & Griggs, D. J. 2000. Evidence for an efflux pump mediating multiple antibiotic resistance in *Salmonella enterica s*erovar Typhimurium. *Antimicrob Agents Chemother,* 44**,** 3118-21.

Pieters, Z., Saad, N. J., Antillon, M., Pitzer, V. E. & Bilcke, J. 2018. Case Fatality Rate of Enteric Fever in Endemic Countries: A Systematic Review and Meta-analysis. *Clin Infect Dis,* 67**,** 628-638.

Ple, C., Tam, H. K., Vieira Da Cruz, A., Compagne, N., Jimenez-Castellanos, J. C., Muller, R. T., Pradel, E., Foong, W. E., Malloci, G., Ballee, A., Kirchner, M. A., Moshfegh, P., Herledan, A., Herrmann, A., Deprez, B., Willand, N., Vargiu, A. V., Pos, K. M., Flipo, M. & Hartkoorn, R. C. 2022. Pyridylpiperazine-based allosteric inhibitors of RND-type multidrug efflux pumps. *Nat Commun,* 13**,** 115.

Pletzer, D. & Weingart, H. 2014. Characterization of AcrD, a resistance-nodulation-cell division-type multidrug efflux pump from the fire blight pathogen *Erwinia amylovora*. *BMC Microbiol,* 14**,** 13.

Pontel, L. B., Audero, M. E., Espariz, M., Checa, S. K. & Soncini, F. C. 2007. GolS controls the response to gold by the hierarchical induction of *Salmonella*-specific genes that include a CBA efflux-coding operon. *Mol Microbiol,* 66**,** 814-25.

Poole, K. 2005. Efflux-mediated antimicrobial resistance. *J Antimicrob Chemother,* 56**,** 20-51.

Poomchuchit, S., Kerdsin, A., Chopjitt, P., Boueroy, P., Hatrongjit, R., Akeda, Y., Tomono, K., Nuanualsuwan, S. & Hamada, S. 2021. Fluoroquinolone resistance in non-typhoidal *Salmonella enterica* isolated from slaughtered pigs in Thailand. *J Med Microbiol,* 70.

Pos, K. M. 2009. Drug transport mechanism of the AcrB efflux pump. *Biochim Biophys Acta,* 1794**,** 782-93.

Post, A. S., Diallo, S. N., Guiraud, I., Lompo, P., Tahita, M. C., Maltha, J., Van Puyvelde, S., Mattheus, W., Ley, B., Thriemer, K., Rouamba, E., Derra, K., Deborggraeve, S., Tinto, H. & Jacobs, J. 2019. Supporting evidence for a human reservoir of invasive non-Typhoidal *Salmonella* from household samples in Burkina Faso. *PLoS Negl Trop Dis,* 13**,** e0007782.

Prajapati, J. D., Kleinekathöfer, U. & Winterhalter, M. 2021. How to Enter a Bacterium: Bacterial Porins and the Permeation of Antibiotics. *Chemical Reviews,* 121**,** 5158-5192.

Qin, X., Liu, Y. & Shi, X. 2021. Resistance-Nodulation-Cell Division (RND) Transporter AcrD Confers Resistance to Egg White in *Salmonella enterica* Serovar Enteritidis. *Foods,* 11.

Raetz, C. R. & Whitfield, C. 2002. Lipopolysaccharide endotoxins. *Annu Rev Biochem,* 71**,** 635-700.

Rahmati, S., Yang, S., Davidson, A. L. & Zechiedrich, E. L. 2002. Control of the AcrAB multidrug efflux pump by quorum-sensing regulator SdiA. *Mol Microbiol,* 43**,** 677-85.

Ramaswamy, V. K., Vargiu, A. V., Malloci, G., Dreier, J. & Ruggerone, P. 2017. Molecular Rationale behind the Differential Substrate Specificity of Bacterial RND Multi-Drug Transporters. *Sci Rep,* 7**,** 8075.

Ramirez, M. S. & Tolmasky, M. E. 2010. Aminoglycoside modifying enzymes. *Drug Resist Updat,* 13**,** 151-71.

Rampioni, G., Pillai, C. R., Longo, F., Bondi, R., Baldelli, V., Messina, M., Imperi, F., Visca, P. & Leoni, L. 2017. Effect of efflux pump inhibition on *Pseudomonas aeruginosa* transcriptome and virulence. *Sci Rep,* 7**,** 11392.

Rasko, D. A. & Sperandio, V. 2010. Anti-virulence strategies to combat bacteria-mediated disease. *Nat Rev Drug Discov,* 9**,** 117-28.

Reading, E., Ahdash, Z., Fais, C., Ricci, V., Wang-Kan, X., Grimsey, E., Stone, J., Malloci, G., Lau, A. M., Findlay, H., Konijnenberg, A., Booth, P. J., Ruggerone, P., Vargiu, A. V., Piddock, L. J. V. & Politis, A. 2020. Perturbed structural dynamics underlie inhibition and altered efflux of the multidrug resistance pump AcrB. *Nat Commun,* 11**,** 5565.

Redgrave, L. S., Sutton, S. B., Webber, M. A. & Piddock, L. J. 2014. Fluoroquinolone resistance: mechanisms, impact on bacteria, and role in evolutionary success. *Trends Microbiol,* 22**,** 438-45.

Reens, A. L., Crooks, A. L., Su, C. C., Nagy, T. A., Reens, D. L., Podoll, J. D., Edwards, M. E., Yu, E. W. & Detweiler, C. S. 2018. A cell-based infection assay identifies efflux pump modulators that reduce bacterial intracellular load. *PLoS Pathog,* 14**,** e1007115.

Renau, T. E., Leger, R., Filonova, L., Flamme, E. M., Wang, M., Yen, R., Madsen, D., Griffith, D., Chamberland, S., Dudley, M. N., Lee, V. J., Lomovskaya, O., Watkins, W. J., Ohta, T., Nakayama, K. & Ishida, Y. 2003. Conformationally-restricted analogues of efflux pump inhibitors that potentiate the activity of levofloxacin in *Pseudomonas aeruginosa*. *Bioorg Med Chem Lett,* 13**,** 2755-8.

Ricci, V., Attah, V., Overton, T., Grainger, D. C. & Piddock, L. J. V. 2017. CsrA maximizes expression of the AcrAB multidrug resistance transporter. *Nucleic Acids Res,* 45**,** 12798-12807.

Ricci, V., Blair, J. M. & Piddock, L. J. 2014. RamA, which controls expression of the MDR efflux pump AcrAB-TolC, is regulated by the Lon protease. *J Antimicrob Chemother,* 69**,** 643-50.

Rosenberg, E. Y., Ma, D. & Nikaido, H. 2000. AcrD of *Escherichia coli* is an aminoglycoside efflux pump. *J Bacteriol,* 182**,** 1754-6.

Ruiz, N., Kahne, D. & Silhavy, T. J. 2006. Advances in understanding bacterial outer-membrane biogenesis. *Nat Rev Microbiol,* 4**,** 57-66.

Saier, M. H., Jr., Tam, R., Reizer, A. & Reizer, J. 1994. Two novel families of bacterial membrane proteins concerned with nodulation, cell division and transport. *Mol Microbiol,* 11**,** 841-7.

Saier, M. H., Reddy, V. S., Moreno-Hagelsieb, G., Hendargo, K. J., Zhang, Y., Iddamsetty, V., Lam, K. J. K., Tian, N., Russum, S., Wang, J. & Medrano-Soto, A. 2021. The Transporter Classification Database (TCDB): 2021 update. *Nucleic Acids Res,* 49**,** D461-D467.

Saw, H. T., Webber, M. A., Mushtaq, S., Woodford, N. & Piddock, L. J. 2016. Inactivation or inhibition of AcrAB-TolC increases resistance of carbapenemase-producing Enterobacteriaceae to carbapenems. *J Antimicrob Chemother,* 71**,** 1510-9.

Schindelin, J., Arganda-Carreras, I., Frise, E., Kaynig, V., Longair, M., Pietzsch, T., Preibisch, S., Rueden, C., Saalfeld, S., Schmid, B., Tinevez, J. Y., White, D. J., Hartenstein, V., Eliceiri, K., Tomancak, P. & Cardona, A. 2012. Fiji: an open-source platform for biological-image analysis. *Nat Methods,* 9**,** 676-82.

Schrödinger, L. 2022. The PyMOL Molecular Graphics System. 2.5.2 ed.: Schrödinger LLC.

Schumacher, A., Steinke, P., Bohnert, J. A., Akova, M., Jonas, D. & Kern, W. V. 2006. Effect of 1-(1-naphthylmethyl)-piperazine, a novel putative efflux pump inhibitor, on antimicrobial drug susceptibility in clinical isolates of Enterobacteriaceae other than *Escherichia coli*. *J Antimicrob Chemother,* 57**,** 344-8.

Schumacher, A., Trittler, R., Bohnert, J. A., Kummerer, K., Pages, J. M. & Kern, W. V. 2007. Intracellular accumulation of linezolid in *Escherichia coli*, *Citrobacter freundii* and *Enterobacter aerogenes*: role of enhanced efflux pump activity and inactivation. *J Antimicrob Chemother,* 59**,** 1261-4.

Schuster, S., Vavra, M. & Kern, W. V. 2016. Evidence of a Substrate-Discriminating Entrance Channel in the Lower Porter Domain of the Multidrug Resistance Efflux Pump AcrB. *Antimicrob Agents Chemother,* 60**,** 4315-23.

Seeger, M. A., Schiefner, A., Eicher, T., Verrey, F., Diederichs, K. & Pos, K. M. 2006. Structural asymmetry of AcrB trimer suggests a peristaltic pump mechanism. *Science,* 313**,** 1295-8.

Sennhauser, G., Amstutz, P., Briand, C., Storchenegger, O. & Grutter, M. G. 2007. Drug export pathway of multidrug exporter AcrB revealed by DARPin inhibitors. *PLoS Biol,* 5**,** e7.

Shaio, M. F. & Rowland, H. 1985. Bactericidal and opsonizing effects of normal serum on mutant strains of *Salmonella* typhimurium. *Infect Immun,* 49**,** 647-53.

Shen, J., Yang, B., Gu, Q., Zhang, G., Yang, J., Xue, F., Shao, J., Yi, X. & Jiang, Y. 2017. The Role of AcrAB-TolC Efflux Pump in Mediating Fluoroquinolone Resistance in Naturally Occurring *Salmonella* Isolates from China. *Foodborne Pathog Dis,* 14**,** 728-734.

Shi, X., Chen, M., Yu, Z., Bell, J. M., Wang, H., Forrester, I., Villarreal, H., Jakana, J., Du, D., Luisi, B. F., Ludtke, S. J. & Wang, Z. 2019. *In situ* structure and assembly of the multidrug efflux pump AcrAB-TolC. *Nat Commun,* 10**,** 2635.

Silhavy, T. J., Kahne, D. & Walker, S. 2010. The bacterial cell envelope. *Cold Spring Harb Perspect Biol,* 2**,** a000414.

Singh, M., Sykes, E. M. E., Li, Y. & Kumar, A. 2020. MexXY RND pump of P*seudomonas aeruginosa* PA7 effluxes bi-anionic beta-lactams carbenicillin and sulbenicillin when it partners with the outer membrane factor OprA but not with OprM. *Microbiology (Reading),* 166**,** 1095-1106.

Sjuts, H., Vargiu, A. V., Kwasny, S. M., Nguyen, S. T., Kim, H. S., Ding, X., Ornik, A. R., Ruggerone, P., Bowlin, T. L., Nikaido, H., Pos, K. M. & Opperman, T. J. 2016. Molecular basis for inhibition of AcrB multidrug efflux pump by novel and powerful pyranopyridine derivatives. *Proc Natl Acad Sci U S A,* 113**,** 3509-14.

Smith, H. E. & Blair, J. M. 2014. Redundancy in the periplasmic adaptor proteins AcrA and AcrE provides resilience and an ability to export substrates of multidrug efflux. *J Antimicrob Chemother,* 69**,** 982-7.

Song, S., Lee, B., Yeom, J. H., Hwang, S., Kang, I., Cho, J. C., Ha, N. C., Bae, J., Lee, K. & Kim, Y. H. 2015. MdsABC-mediated pathway for pathogenicity in *Salmonella enterica* serovar Typhimurium. *Infect Immun,* 83**,** 4266-76.

Spengler, G., Kincses, A., Gajdacs, M. & Amaral, L. 2017. New Roads Leading to Old Destinations: Efflux Pumps as Targets to Reverse Multidrug Resistance in Bacteria. *Molecules,* 22.

Springer. 2011. *Drug Profile: MP 601205* [Online]. Adis Insight. Available: https://adisinsight.springer.com/drugs/800023056 [Accessed 1st May 2022].

Srikumar, S., Kroger, C., Hebrard, M., Colgan, A., Owen, S. V., Sivasankaran, S. K., Cameron, A. D., Hokamp, K. & Hinton, J. C. 2015. RNA-seq Brings New Insights to the Intra-Macrophage Transcriptome of *Salmonella* Typhimurium. *PLoS Pathog,* 11**,** e1005262.

Stanaway, J. D., Parisi, A., Sarkar, K., Blacker, B. F., Reiner, R. C., Hay, S. I., Nixon, M. R., Dolecek, C., James, S. L., Mokdad, A. H., Abebe, G., Ahmadian, E., Alahdab, F., Alemnew, B. T. T., Alipour, V., Allah Bakeshei, F., Animut, M. D., Ansari, F., Arabloo, J., Asfaw, E. T., Bagherzadeh, M., Bassat, Q., Belayneh, Y. M. M., Carvalho, F., Daryani, A., Demeke, F. M., Demis, A. B. B., Dubey, M., Duken, E. E., Dunachie, S. J., Eftekhari, A., Fernandes, E., Fouladi Fard, R., Gedefaw, G. A., Geta, B., Gibney, K. B., Hasanzadeh, A., Hoang, C. L., Kasaeian, A., Khater, A., Kidanemariam, Z. T., Lakew, A. M., Malekzadeh, R., Melese, A., Mengistu, D. T., Mestrovic, T., Miazgowski, B., Mohammad, K. A., Mohammadian, M., Mohammadian-Hafshejani, A., Nguyen, C. T., Nguyen, L. H., Nguyen, S. H., Nirayo, Y. L., Olagunju, A. T., Olagunju, T. O., Pourjafar, H., Qorbani, M., Rabiee, M., Rabiee, N., Rafay, A., Rezapour, A., Samy, A. M., Sepanlou, S. G., Shaikh, M. A., Sharif, M., Shigematsu, M., Tessema, B., Tran, B. X., Ullah, I., Yimer, E. M., Zaidi, Z., Murray, C. J. L. & Crump, J. A. 2019a. The global burden of non-typhoidal salmonella invasive disease: a systematic analysis for the Global Burden of Disease Study 2017. *The Lancet Infectious Diseases,* 19**,** 1312-1324.

Stanaway, J. D., Reiner, R. C., Blacker, B. F., Goldberg, E. M., Khalil, I. A., Troeger, C. E., Andrews, J. R., Bhutta, Z. A., Crump, J. A., Im, J., Marks, F., Mintz, E., Park, S. E., Zaidi, A. K. M., Abebe, Z., Abejie, A. N., Adedeji, I. A., Ali, B. A., Amare, A. T., Atalay, H. T., Avokpaho, E. F. G. A., Bacha, U., Barac, A., Bedi, N., Berhane, A., Browne, A. J., Chirinos, J. L., Chitheer, A., Dolecek, C., El Sayed Zaki, M., Eshrati, B., Foreman, K. J., Gemechu, A., Gupta, R., Hailu, G. B., Henok, A., Hibstu, D. T., Hoang, C. L., Ilesanmi, O. S., Iyer, V. J., Kahsay, A., Kasaeian, A., Kassa, T. D., Khan, E. A., Khang, Y.-H., Magdy Abd El Razek, H., Melku, M., Mengistu, D. T., Mohammad, K. A., Mohammed, S., Mokdad, A. H., Nachega, J. B., Naheed, A., Nguyen, C. T., Nguyen, H. L. T., Nguyen, L. H., Nguyen, N. B., Nguyen, T. H., Nirayo, Y. L., Pangestu, T., Patton, G. C., Qorbani, M., Rai, R. K., Rana, S. M., Ranabhat, C. L., Roba, K. T., Roberts, N. L. S., Rubino, S., Safiri, S., Sartorius, B., Sawhney, M., Shiferaw, M. S., Smith, D. L., Sykes, B. L., Tran, B. X., Tran, T. T., Ukwaja, K. N., Vu, G. T., Vu, L. G., Weldegebreal, F., Yenit, M. K., Murray, C. J. L. & Hay, S. I. 2019b. The global burden of typhoid and paratyphoid fevers: a systematic analysis for the Global Burden of Disease Study 2017. *The Lancet Infectious Diseases,* 19**,** 369-381.

Stegmeier, J. F., Polleichtner, G., Brandes, N., Hotz, C. & Andersen, C. 2006. Importance of the adaptor (membrane fusion) protein hairpin domain for the functionality of multidrug efflux pumps. *Biochemistry,* 45**,** 10303-12.

Stock, J. B., Rauch, B. & Roseman, S. 1977. Periplasmic space in *Salmonella* typhimurium and *Escherichia coli*. *J Biol Chem,* 252**,** 7850-61.

Sturge, C. R., Felder-Scott, C. F., Pifer, R., Pybus, C., Jain, R., Geller, B. L. & Greenberg, D. E. 2019. AcrAB-TolC Inhibition by Peptide-Conjugated Phosphorodiamidate Morpholino Oligomers Restores Antibiotic Activity *in vitro* and *in vivo*. *ACS Infect Dis,* 5**,** 1446-1455.

Su, C. C., Li, M., Gu, R., Takatsuka, Y., Mcdermott, G., Nikaido, H. & Yu, E. W. 2006. Conformation of the AcrB multidrug efflux pump in mutants of the putative proton relay pathway. *J Bacteriol,* 188**,** 7290-6.

Su, C. C., Long, F., Zimmermann, M. T., Rajashankar, K. R., Jernigan, R. L. & Yu, E. W. 2011. Crystal structure of the CusBA heavy-metal efflux complex of *Escherichia coli*. *Nature,* 470**,** 558-62.

Su, C. C., Rutherford, D. J. & Yu, E. W. 2007. Characterization of the multidrug efflux regulator AcrR from *Escherichia coli*. *Biochem Biophys Res Commun,* 361**,** 85-90.

Su, L. H., Wu, T. L. & Chiu, C. H. 2012. Development of carbapenem resistance during therapy for non-typhoid *Salmonella* infection. *Clin Microbiol Infect,* 18**,** E91-4.

Sulavik, M. C., Houseweart, C., Cramer, C., Jiwani, N., Murgolo, N., Greene, J., Didomenico, B., Shaw, K. J., Miller, G. H., Hare, R. & Shimer, G. 2001. Antibiotic susceptibility profiles of *Escherichia coli* strains lacking multidrug efflux pump genes. *Antimicrob Agents Chemother,* 45**,** 1126-36.

Sun, J., Deng, Z. & Yan, A. 2014. Bacterial multidrug efflux pumps: mechanisms, physiology and pharmacological exploitations. *Biochem Biophys Res Commun,* 453**,** 254-67.

Symmons, M. F., Bokma, E., Koronakis, E., Hughes, C. & Koronakis, V. 2009. The assembled structure of a complete tripartite bacterial multidrug efflux pump. *Proc Natl Acad Sci U S A,* 106**,** 7173-8.

Symmons, M. F., Marshall, R. L. & Bavro, V. N. 2015. Architecture and roles of periplasmic adaptor proteins in tripartite efflux assemblies. *Front Microbiol,* 6**,** 513.

Takatsuka, Y. & Nikaido, H. 2006. Threonine-978 in the transmembrane segment of the multidrug efflux pump AcrB of *Escherichia coli* is crucial for drug transport as a probable component of the proton relay network. *J Bacteriol,* 188**,** 7284-9.

Takaya, A., Suzuki, M., Matsui, H., Tomoyasu, T., Sashinami, H., Nakane, A. & Yamamoto, T. 2003. Lon, a stress-induced ATP-dependent protease, is critically important for systemic *Salmonella enterica* serovar Typhimurium infection of mice. *Infect Immun,* 71**,** 690-6.

Takeshita, S., Sato, M., Toba, M., Masahashi, W. & Hashimoto-Gotoh, T. 1987. High-copy-number and low-copy-number plasmid vectors for *lacZ* alpha-complementation and chloramphenicol- or kanamycin-resistance selection. *Gene,* 61**,** 63-74.

Tam, H. K., Foong, W. E., Oswald, C., Herrmann, A., Zeng, H. & Pos, K. M. 2021. Allosteric drug transport mechanism of multidrug transporter AcrB. *Nat Commun,* 12**,** 3889.

Tam, H. K., Malviya, V. N., Foong, W. E., Herrmann, A., Malloci, G., Ruggerone, P., Vargiu, A. V. & Pos, K. M. 2020. Binding and Transport of Carboxylated Drugs by the Multidrug Transporter AcrB. *J Mol Biol,* 432**,** 861-877.

Tamura, K., Stecher, G. & Kumar, S. 2021. MEGA11: Molecular Evolutionary Genetics Analysis Version 11. *Mol Biol Evol,* 38**,** 3022-3027.

Tamura, N., Murakami, S., Oyama, Y., Ishiguro, M. & Yamaguchi, A. 2005. Direct interaction of multidrug efflux transporter AcrB and outer membrane channel TolC detected via site-directed disulfide cross-linking. *Biochemistry,* 44**,** 11115-21.

Tanner, J. R. & Kingsley, R. A. 2018. Evolution of *Salmonella* within hosts. *Trends Microbiol,* 26**,** 986-998.

Tatsumi, R. & Wachi, M. 2008. TolC-dependent exclusion of porphyrins in *Escherichia coli*. *J Bacteriol,* 190**,** 6228-33.
Teelucksingh, T., Thompson, L. K. & Cox, G. 2020. The Evolutionary Conservation of Escherichia coli Drug Efflux Pumps Supports Physiological Functions. *J Bacteriol*.
Tegel, H., Ottosson, J. & Hober, S. 2011. Enhancing the protein production levels in *Escherichia coli* with a strong promoter. *FEBS J,* 278**,** 729-39.
Thanassi, D. G., Cheng, L. W. & Nikaido, H. 1997. Active efflux of bile salts by *Escherichia coli*. *J Bacteriol,* 179**,** 2512-8.
Tikhonova, E. B., Dastidar, V., Rybenkov, V. V. & Zgurskaya, H. I. 2009. Kinetic control of TolC recruitment by multidrug efflux complexes. *Proc Natl Acad Sci U S A,* 106**,** 16416-21.
Tikhonova, E. B., Yamada, Y. & Zgurskaya, H. I. 2011. Sequential mechanism of assembly of multidrug efflux pump AcrAB-TolC. *Chem Biol,* 18**,** 454-63.
Tikhonova, E. B. & Zgurskaya, H. I. 2004. AcrA, AcrB, and TolC of Escherichia coli Form a Stable Intermembrane Multidrug Efflux Complex. *J Biol Chem,* 279**,** 32116-24.
Toro, C. S., Lobos, S. R., Calderon, I., Rodriguez, M. & Mora, G. C. 1990. Clinical isolate of a porinless *Salmonella* Typhi resistant to high levels of chloramphenicol. *Antimicrob Agents Chemother,* 34**,** 1715-9.
Touze, T., Eswaran, J., Bokma, E., Koronakis, E., Hughes, C. & Koronakis, V. 2004. Interactions underlying assembly of the *Escherichia coli* AcrAB-TolC multidrug efflux system. *Mol Microbiol,* 53**,** 697-706.
Tsai, C. J., Loh, J. M. & Proft, T. 2016. *Galleria mellonella* infection models for the study of bacterial diseases and for antimicrobial drug testing. *Virulence,* 7**,** 214-29.
Tsutsumi, K., Yonehara, R., Ishizaka-Ikeda, E., Miyazaki, N., Maeda, S., Iwasaki, K., Nakagawa, A. & Yamashita, E. 2019. Structures of the wild-type MexAB-OprM tripartite pump reveal its complex formation and drug efflux mechanism. *Nat Commun,* 10**,** 1520.
Uk Health Security Agency 2021. Non-typhoidal *Salmonella* data 2010 to 2019. UK Health Security Agency.
Vaara, M. 1993. Antibiotic-supersusceptible mutants of *Escherichia coli* and *Salmonella* Typhimurium. *Antimicrob Agents Chemother,* 37**,** 2255-60.
Varadi, M., Anyango, S., Deshpande, M., Nair, S., Natassia, C., Yordanova, G., Yuan, D., Stroe, O., Wood, G., Laydon, A., Zidek, A., Green, T., Tunyasuvunakool, K., Petersen, S., Jumper, J., Clancy, E., Green, R., Vora, A., Lutfi, M., Figurnov, M., Cowie, A., Hobbs, N., Kohli, P., Kleywegt, G., Birney, E., Hassabis, D. & Velankar, S. 2021. AlphaFold Protein Structure Database: massively expanding the structural coverage of protein-sequence space with high-accuracy models. *Nucleic Acids Res*.
Vargiu, A. V. & Nikaido, H. 2012. Multidrug binding properties of the AcrB efflux pump characterized by molecular dynamics simulations. *Proc Natl Acad Sci U S A,* 109**,** 20637-42.
Vargiu, A. V., Ruggerone, P., Opperman, T. J., Nguyen, S. T. & Nikaido, H. 2014. Molecular mechanism of MBX2319 inhibition of *Escherichia coli* AcrB multidrug efflux pump and comparison with other inhibitors. *Antimicrob Agents Chemother,* 58**,** 6224-34.
Ventola, C. L. 2015. The antibiotic resistance crisis: part 1: causes and threats. *P T,* 40**,** 277-83.
Vergalli, J., Bodrenko, I. V., Masi, M., Moynie, L., Acosta-Gutierrez, S., Naismith, J. H., Davin-Regli, A., Ceccarelli, M., Van Den Berg, B., Winterhalter, M. & Pages, J. M. 2020. Porins and small-molecule translocation across the outer membrane of Gram-negative bacteria. *Nat Rev Microbiol,* 18**,** 164-176.

Viegas, S. C., Mil-Homens, D., Fialho, A. M. & Arraiano, C. M. 2013. The virulence of *Salmonella enterica* Serovar Typhimurium in the insect model *Galleria mellonella* is impaired by mutations in RNase E and RNase III. *Appl Environ Microbiol,* 79**,** 6124-33.

Vollmer, W. & Bertsche, U. 2008. Murein (peptidoglycan) structure, architecture and biosynthesis in *Escherichia coli*. *Biochim Biophys Acta,* 1778**,** 1714-34.

Wang, Y., Venter, H. & Ma, S. 2016. Efflux Pump Inhibitors: A Novel Approach to Combat Efflux-Mediated Drug Resistance in Bacteria. *Curr Drug Targets,* 17**,** 702-19.

Wang, Z., Fan, G., Hryc, C. F., Blaza, J. N., Serysheva, Ii, Schmid, M. F., Chiu, W., Luisi, B. F. & Du, D. 2017. An allosteric transport mechanism for the AcrAB-TolC multidrug efflux pump. *Elife,* 6.

Wang-Kan, X., Blair, J. M. A., Chirullo, B., Betts, J., La Ragione, R. M., Ivens, A., Ricci, V., Opperman, T. J. & Piddock, L. J. V. 2017. Lack of AcrB Efflux Function Confers Loss of Virulence on *Salmonella enterica* Serovar Typhimurium. *mBio,* 8.

Wang-Kan, X., Rodriguez-Blanco, G., Southam, A. D., Winder, C. L., Dunn, W. B., Ivens, A. & Piddock, L. J. V. 2021. Metabolomics Reveal Potential Natural Substrates of AcrB in Escherichia coli and *Salmonella enterica* Serovar Typhimurium. *mBio,* 12.

Warner, D. M. & Levy, S. B. 2010. Different effects of transcriptional regulators MarA, SoxS and Rob on susceptibility of *Escherichia coli* to cationic antimicrobial peptides (CAMPs): Rob-dependent CAMP induction of the *marRAB* operon. *Microbiology,* 156**,** 570-8.

Watkins, W. J., Landaverry, Y., Leger, R., Litman, R., Renau, T. E., Williams, N., Yen, R., Zhang, J. Z., Chamberland, S., Madsen, D., Griffith, D., Tembe, V., Huie, K. & Dudley, M. N. 2003. The relationship between physicochemical properties, *in vitro* activity and pharmacokinetic profiles of analogues of diamine-containing efflux pump inhibitors. *Bioorg Med Chem Lett,* 13**,** 4241-4.

Webber, M. A., Bailey, A. M., Blair, J. M., Morgan, E., Stevens, M. P., Hinton, J. C., Ivens, A., Wain, J. & Piddock, L. J. 2009. The global consequence of disruption of the AcrAB-TolC efflux pump in *Salmonella enterica* includes reduced expression of SPI-1 and other attributes required to infect the host. *J Bacteriol,* 191**,** 4276-85.

Weeks, J. W., Celaya-Kolb, T., Pecora, S. & Misra, R. 2010. AcrA suppressor alterations reverse the drug hypersensitivity phenotype of a TolC mutant by inducing TolC aperture opening. *Mol Microbiol,* 75**,** 1468-83.

Wehmeier, C., Schuster, S., Fahnrich, E., Kern, W. V. & Bohnert, J. A. 2009. Site-directed mutagenesis reveals amino acid residues in the *Escherichia coli* RND efflux pump AcrB that confer macrolide resistance. *Antimicrob Agents Chemother,* 53**,** 329-30.

Weisblum, B. 1995. Erythromycin resistance by ribosome modification. *Antimicrob Agents Chemother,* 39**,** 577-85.

Wellcome Trust & The Boston Consulting Group 2018. Vaccines to tackle drug resistant infections. An evaluation of R&D opportunities.

Wielders, C. L., Fluit, A. C., Brisse, S., Verhoef, J. & Schmitz, F. J. 2002. *mecA* gene is widely disseminated in *Staphylococcus aureus* population. *J Clin Microbiol,* 40**,** 3970-5.

Williams, K. J. 2009. The introduction of 'chemotherapy' using arsphenamine - the first magic bullet. *J R Soc Med,* 102**,** 343-8.

Wilson, D. N., Hauryliuk, V., Atkinson, G. C. & O'neill, A. J. 2020. Target protection as a key antibiotic resistance mechanism. *Nature Reviews Microbiology,* 18**,** 637-648.

Wiriyathanawudhiwong, N., Ohtsu, I., Li, Z. D., Mori, H. & Takagi, H. 2009. The outer membrane TolC is involved in cysteine tolerance and overproduction in *Escherichia coli*. *Appl Microbiol Biotechnol,* 81**,** 903-13.

Wray, C. & Sojka, W. J. 1978. Experimental *Salmonella* Typhimurium infection in calves. *Res Vet Sci,* 25**,** 139-43.

Wylie, J. L. & Worobec, E. A. 1995. The OprB porin plays a central role in carbohydrate uptake in *Pseudomonas aeruginosa*. *J Bacteriol,* 177**,** 3021-6.

Xu, Y., Lee, M., Moeller, A., Song, S., Yoon, B. Y., Kim, H. M., Jun, S. Y., Lee, K. & Ha, N. C. 2011a. Funnel-like hexameric assembly of the periplasmic adapter protein in the tripartite multidrug efflux pump in gram-negative bacteria. *J Biol Chem,* 286**,** 17910-20.

Xu, Y., Sim, S. H., Song, S., Piao, S., Kim, H. M., Jin, X. L., Lee, K. & Ha, N. C. 2010. The tip region of the MacA alpha-hairpin is important for the binding to TolC to the Escherichia coli MacAB-TolC pump. *Biochem Biophys Res Commun,* 394**,** 962-5.

Xu, Y., Song, S., Moeller, A., Kim, N., Piao, S., Sim, S. H., Kang, M., Yu, W., Cho, H. S., Chang, I., Lee, K. & Ha, N. C. 2011b. Functional implications of an intermeshing cogwheel-like interaction between TolC and MacA in the action of macrolide-specific efflux pump MacAB-TolC. *J Biol Chem,* 286**,** 13541-9.

Yamagishi, A., Nakano, S., Yamasaki, S. & Nishino, K. 2020. An efflux inhibitor of the MacAB pump in *Salmonella enterica* serovar Typhimurium. *Microbiol Immunol,* 64**,** 182-188.

Yamanaka, H., Izawa, H. & Okamoto, K. 2001. Carboxy-terminal region involved in activity of *Escherichia coli* TolC. *J Bacteriol,* 183**,** 6961-4.

Yamanaka, H., Kobayashi, H., Takahashi, E. & Okamoto, K. 2008. MacAB is involved in the secretion of *Escherichia coli* heat-stable enterotoxin II. *J Bacteriol,* 190**,** 7693-8.

Yamanaka, H., Nomura, T., Fujii, Y. & Okamoto, K. 1998. Need for TolC, an *Escherichia coli* outer membrane protein, in the secretion of heat-stable enterotoxin I across the outer membrane. *Microb Pathog,* 25**,** 111-20.

Yamanaka, H., Nomura, T., Morisada, N., Shinoda, S. & Okamoto, K. 2002. Site-directed mutagenesis studies of the amino acid residue at position 412 of *Escherichia coli* TolC which is required for the activity. *Microb Pathog,* 33**,** 81-9.

Yamanaka, H., Tadokoro, S., Miyano, M., Takahashi, E., Kobayashi, H. & Okamoto, K. 2007. Studies on the region involved in the transport activity of *Escherichia coli* TolC by chimeric protein analysis. *Microb Pathog,* 42**,** 184-92.

Yamasaki, S., Nagasawa, S., Hayashi-Nishino, M., Yamaguchi, A. & Nishino, K. 2011. AcrA dependency of the AcrD efflux pump in *Salmonella enterica* serovar Typhimurium. *J Antibiot (Tokyo),* 64**,** 433-7.

Yoshida, K., Nakayama, K., Ohtsuka, M., Kuru, N., Yokomizo, Y., Sakamoto, A., Takemura, M., Hoshino, K., Kanda, H., Nitanai, H., Namba, K., Yoshida, K., Imamura, Y., Zhang, J. Z., Lee, V. J. & Watkins, W. J. 2007. MexAB-OprM specific efflux pump inhibitors in *Pseudomonas aeruginosa*. Part 7: highly soluble and in vivo active quaternary ammonium analogue D13-9001, a potential preclinical candidate. *Bioorg Med Chem,* 15**,** 7087-97.

Yum, S., Xu, Y., Piao, S., Sim, S. H., Kim, H. M., Jo, W. S., Kim, K. J., Kweon, H. S., Jeong, M. H., Jeon, H., Lee, K. & Ha, N. C. 2009. Crystal structure of the periplasmic component of a tripartite macrolide-specific efflux pump. *J Mol Biol,* 387**,** 1286-97.

Zechini, B. & Versace, I. 2009. Inhibitors of multidrug resistant efflux systems in bacteria. *Recent Pat Antiinfect Drug Discov,* 4**,** 37-50.

Zgurskaya, H. I., Krishnamoorthy, G., Ntreh, A. & Lu, S. 2011. Mechanism and Function of the Outer Membrane Channel TolC in Multidrug Resistance and Physiology of Enterobacteria. *Front Microbiol,* 2**,** 189.

Zgurskaya, H. I. & Nikaido, H. 1999. AcrA is a highly asymmetric protein capable of spanning the periplasm. *J Mol Biol,* 285**,** 409-20.

Zgurskaya, H. I. & Nikaido, H. 2000. Cross-linked complex between oligomeric periplasmic lipoprotein AcrA and the inner-membrane-associated multidrug efflux pump AcrB from *Escherichia coli*. *J Bacteriol,* 182**,** 4264-7.

Zgurskaya, H. I., Yamada, Y., Tikhonova, E. B., Ge, Q. & Krishnamoorthy, G. 2009. Structural and functional diversity of bacterial membrane fusion proteins. *Biochim Biophys Acta,* 1794**,** 794-807.

Zhang, C. Z., Chang, M. X., Yang, L., Liu, Y. Y., Chen, P. X. & Jiang, H. X. 2018. Upregulation of AcrEF in Quinolone Resistance Development in *Escherichia coli* When AcrAB-TolC Function Is Impaired. *Microb Drug Resist,* 24**,** 18-23.

Zmarlicka, M. T., Nailor, M. D. & Nicolau, D. P. 2015. Impact of the New Delhi metallo-beta-lactamase on beta-lactam antibiotics. *Infect Drug Resist,* 8**,** 297-309.

Zwama, M. & Nishino, K. 2021. Ever-Adapting RND Efflux Pumps in Gram-Negative Multidrug-Resistant Pathogens: A Race against Time. *Antibiotics (Basel),* 10.

Zwama, M. & Yamaguchi, A. 2018. Molecular mechanisms of AcrB-mediated multidrug export. *Res Microbiol,* 169**,** 372-383.

Zwama, M., Yamasaki, S., Nakashima, R., Sakurai, K., Nishino, K. & Yamaguchi, A. 2018. Multiple entry pathways within the efflux transporter AcrB contribute to multidrug recognition. *Nat Commun,* 9**,** 124.

Appendix I. List of drugs used for antimicrobial susceptibility testing.

Drug	Chemical class	Supplier	Solvent
Acriflavine	Dye	Acros Organics	SDW
Aztreonam	Monobactam	Acros Organics	DMSO
Benzalkonium chloride	QAC	Alfa Aesar	SDW
Berberine	QAC	Alfa Aesar	DMSO
Carbenicillin	β-lactam	Alfa Aesar	SDW
CCCP	Ionophore	Sigma-Aldrich	DMSO + SDW
Chloramphenicol	Phenicol	Sigma-Aldrich	70% ethanol
Ciprofloxacin	Fluoroquinolone	Acros Organics	SDW + acetic acid
Cloxacillin	β-lactam	Cayman Chemical	SDW
Clindamycin	Lincosamide	TCI	SDW
Crystal violet	Dye	Sigma-Aldrich	SDW
Doxorubicin	Anthracycline	TCI	SDW
Ethidium bromide	Dye	Acros Organics	SDW
Erythromycin	Macrolide	Acros Organics	70% ethanol
Fusidic acid	Fusidane	Sigma-Aldrich	SDW
Gentamicin	Aminoglycoside	Fisher Scientific	SDW
Hygromycin B	Aminoglycoside	Sigma-Aldrich	SDW
Kanamycin	Aminoglycoside	Sigma-Aldrich	SDW
Linezolid	Oxazolidinone	Acros Organics	DMSO
Methylene blue	Dye	Fisher Scientific	SDW
Minocycline	Tetracycline	TCI	SDW
Nafcillin	β-lactam	Sigma-Aldrich	SDW
Novobiocin	Aminocoumarin	Alfa Aesar	SDW
Oxacillin	β-lactam	Sigma-Aldrich	SDW
Rhodamine 6G	Dye	Sigma-Aldrich	SDW
Rifampicin	Ansamycin	Fisher Scientific	DMSO
Streptomycin	Aminoglycoside	Sigma-Aldrich	SDW
Spectinomycin	Aminoglycoside	Sigma-Aldrich	SDW
Tetracycline	Tetracycline	Sigma-Aldrich	SDW
Ticarcillin	β-lactam	Sigma-Aldrich	SDW
Tobramycin	Aminoglycoside	Acros Organics	SDW

CCCP, carbonyl cyanide-*m*-chlorophenyl hydrazone; DMSO, dimethyl sulphoxide; QAC, quaternary ammonium compound; SDW, sterile distilled water; TCI, Tokyo Chemical Industry.

Appendix II. List of primers used for site-directed mutagenesis reactions.

Primer ID	Primer name	Primer sequence
P366	AcrA_R59A_F	CTTCCGGGTGCTACCGTTGCTTACCGTATC
P367	AcrA_R59A_R	GCAACGGTAGCACCCGGAAGTTCAGTTGTG
P368	AcrA_T270A_F	GTTGACCAAGCCACCGGGTCTATTACTTTG
P369	AcrA_T270A_R	CCCGGTGGCTTGGTCAACGGTCACGTCGG
P370	AcrA_T270D_F	GACCGTTGACCAAGACACCGGGTCTATTAC
P371	AcrA_T270D_R	GACCCGGTGTCTTGGTCAACGGTCACGTCG
P372	AcrA_T271A_F	GTTGACCAAACCGCCGGGTCTATTACTTTGC
P373	AcrA_T271A_R	GTAATAGACCCGGCGGTTTGGTCAACGGTC
P374	AcrA_T271D_F	GTTGACCAAACCGACGGGTCTATTACTTTGC
P375	AcrA_T271D_R	GTAATAGACCCGTCGGTTTGGTCAACGGTC
P348	AcrA_G272A_S273A_F	CAAACCACCGCGGCTATTACTTTGCGCGCC
P349	AcrA_G272A_S273A_R	GTAATAGCCGCGGTGGTTTGGTCAACGGTCAC
P682	AcrA_G272F_F	TGGCGCGCAAAGTAATAGAGAAGGTGGTTTGGTCAACGGTC
P683	AcrA_G272F_R	GACCGTTGACCAAACCACCTTCTCTATTACTTTGCGCGCCA
P694	AcrA_S273F_F	GACCAAACCACCGGGTTTATTACTTTGCGCGCC
P695	AcrA_S273F_R	GGCGCGCAAAGTAATAAACCCGGTGGTTTGGTC
P684	AcrA_I274D_F	GATGGCGCGCAAAGTATCAGACCCGGTGGTTTGG
P685	AcrA_I274D_R	CCAAACCACCGGGTCTGATACTTTGCGCGCCATC
P346	AcrA_F292V_F	CCAGGAATGGTCGTTCGCGCACGTCTGC
P347	AcrA_F292V_R	CGAACGACCATTCCTGGCAATAAGGTGTG
P360	AcrA_Q310P_Q311P_F	CTGGTTCCACCACCGGGCGTTACCCGTACTC
P361	AcrA_Q310P_Q311P_R	GTAACGCCCGGTGGTGGAACCAGTAATGCCG
P356	AcrA_Q311F_F	GTTCCACAATTCGGCGTTACCCGTACTCC
P357	AcrA_Q311F_R	GTAACGCCGAATTGTGGAACCAGTAATGC
P354	AcrA_P317G_F	GTTACCCGTACTGGACGCGGCGATGCCAC
P355	AcrA_P317G_R	TCGCCGCGTCCAGTACGGGTAACGCCCT
P352	AcrA_P317F_F	GTTACCCGTACTTTCCGCGGCGATGCCACG
P353	AcrA_P317F_R	CGCCGCGGAAAGTACGGGTAACGCCCTGTTG
P362	AcrA_R318F_F	CGTACTCCATTCGGCGATGCCACGGTGCTG
P363	AcrA_R318F_R	CATCGCCGAATGGAGTACGGGTAACGCCCTG
P404	AcrA_I343F_G344F_F	GCCAGGCGTTCTTCGATAAGTGGCTGGTGAC
P405	AcrA_I343F_G344F_R	CACTTATCGAAGAACGCCTGGCTTGCGACG
P358	AcrA_Q365F_F	GCGGGCTGTTCAAAGTACGTCCTGGCGCAC
P359	AcrA_Q365F_R	GACGTACTTTGAACAGCCCGCTGACGACTAC

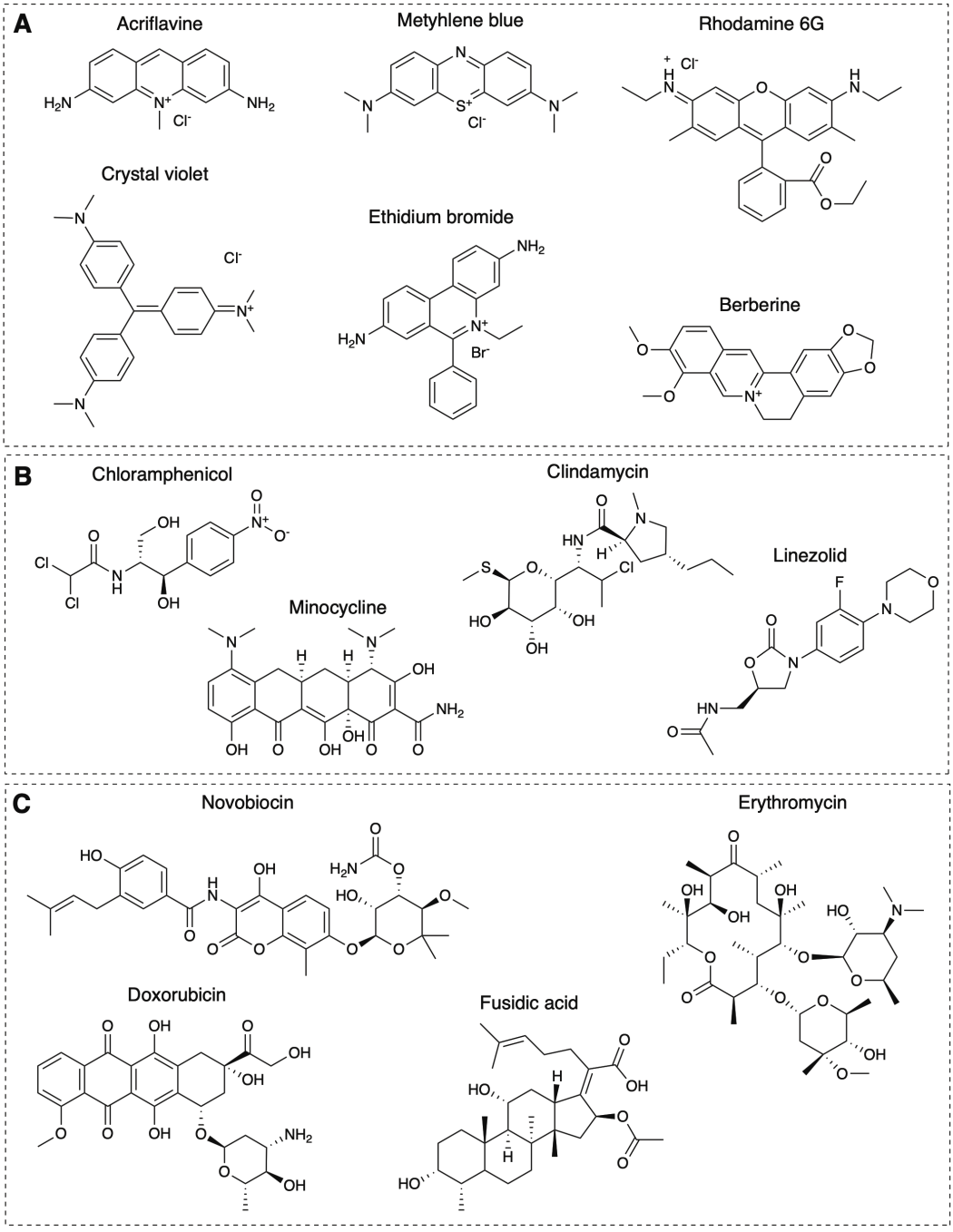
P462	AcrA_K346A_F	AGCCAGGCGATCGGCGATGCGTGGCTGGTG
P463	AcrA_K346A_R	CACCAGCCACGCATCGCCGATCGCCTGGCT
P350	AcrA_K366D_F	GGCTGCAAGATGTACGTCCTGGCGCACAGG
P351	AcrA_K366D_R	GGACGTACATCTTGCAGCCCGCTGACGAC
P468	AcrA_R368A_F	CAGCGGGCTGCAAAAAGTAGCTCCTGGCGCA
P469	AcrA_R368A_R	TGCGCCAGGAGCTACTTTTTGCAGCCCGCTG
P364	AcrA_R368F_F	GCAAAAAGTATTTCCTGGCGCACAGGTTAAAG
P365	AcrA_R368F_R	CGCCAGGAAATACTTTTTGCAGCCCGCTGAC
P604	AcrE_G57F_F	GTAACGACCGAACTTCCCTTCCGTACGTCCGCATTTCGC
P605	AcrE_G57F_R	GCGAAATGCGGACGTACGGAAGGGAAGTTCGGTCGTTAC
P606	AcrE_R58A_F	ACCGAACTTCCCGGAGCTACGTCCGCATTTCG
P607	AcrE_R58A_R	CGAAATGCGGACGTAGCTCCGGGAAGTTCGGT
P423	AcrE_T216F_F	CGATCCGATTTATGTCGACGTGTTCCAATCAAGCAACGACTTTATGC
P424	AcrE_T216F_F	GCATAAAGTCGTTGCTTGATTGGAACACGTCGACATAAATCGGATCG
P608	AcrE_T270D_F	GTTACCGTAGATGAAAGCGACGGCTCTATCACGCTCAG
P609	AcrE_T270D_R	CTGAGCGTGATAGAGCCGTCGCTTTCATCTACGGTAAC
P711	AcrE_S272F_F	ATGAAAGCACCGGCTTTATCACGCTCAGGGC
P712	AcrE_S272F_R	GCCCTGAGCGTGATAAAGCCGGTGCTTTCAT
P692	AcrE_I273D_F	AAAGCACCGGCTCTGACACGCTCAGGGCGG
P693	AcrE_I273D_R	CCGCCCTGAGCGTGTCAGAGCCGGTGCTTT
P417	AcrE_F291G_F	CTGCTTCCCGGTATGGGTGTTCGCGCCCGCAT
P418	AcrE_F291G_R	ATGCGGGCGCGAACACCCATACCGGGAAGCAG
P610	AcrE_R293F_F	GTCTGCTTCCCGGTATGTTTGTTTTCGCCCGCATTGA
P611	AcrE_R293F_R	TCAATGCGGGCGAAAACAAACATACCGGGAAGCAGAC
P421	AcrE_G362F_F	CGATAAGGTCATCGTCAGCTTCTTACAAAAAGCGCGACCG
P422	AcrE_G362F_R	CGGTCGCGCTTTTTGTAAGAAGCTGACGATGACCTTATCG
P612	AcrE_K365D_F	CATCGTCAGCGGCTTACAAGATGCGCGACCGG
P613	AcrE_K365D_R	CCGGTCGCGCATCTTGTAAGCCGCTGACGATG
P614	AcrE_R367D_F	CGGCTTACAAAAAGCGGATCCGGGCGTCCAGGTG
P615	AcrE_R367D_R	CACCTGGACGCCCGGATCCGCTTTTTGTAAGCCG
P574	AcrB_A33W_F	GCGATCCTCAAATTGCCGGTATGGCAATATCCGACGAT
P575	AcrB_A33W_R	ATCGTCGGATATTGCCATACCGGCAATTTGAGGATCGC
P576	AcrB_T37W_F	GGTATGGCAATATCCGTGGATTGCGCCACCAGCA
P577	AcrB_T37W_R	TGCTGGTGGCGCAATCCACGGATATTGCCATACC
P578	AcrB_N298W_F	TGGCTACCGGCGCCTGGGCGCTGGATACCGC
P579	AcrB_N298W_R	GCGGTATCCAGCGCCCAGGCGCCGGTAGCCA

Appendix III. Antimicrobial susceptibility of the *Salmonella* Typhimurium SL1344 Δ4PAP strain carrying different versions of AcrA on the pTrcHis2 plasmid.

	MIC (μg/mL)													
Strain	ACR	BZK	CHL	CIP	CLI	CV	DOX	EtBr	ERY	FA	MB	MIN	NOV	R6G
WT	256	64	4	0.015	512	64	1024	>1024	64	1024	1024	1	512	>1024
Δ4PAP	**16**	**4**	**0.5**	**0.008**	**1**	**2**	**2**	**16**	**4**	**4**	**8**	**0.25**	**1**	**8**
The following rows are Δ4PAP background strain + pTrcHis2 carrying different versions of AcrA														
WT AcrA complement	256	64	4	0.015	512	64	1024	>1024	64	512	1024	1	512	>1024
R59A AcrA	**16**	**4**	**0.5**	**0.008**	**4**	**1**	**2**	**16**	**4**	**4**	**8**	**0.25**	**2**	**8**
T271D AcrA	**16**	**4**	**0.5**	**0.008**	**4**	**1**	**2**	**16**	**4**	**4**	**8**	**0.25**	**2**	**8**
F292V AcrA	**16**	**4**	**0.5**	**0.008**	**4**	**1**	**2**	**16**	**4**	**4**	**8**	**0.25**	**2**	**8**
Q311F AcrA	256	64	4	0.015	128	32	512	>1024	64	1024	1024	1	512	>1024
Q310P-Q311P AcrA	**16**	**4**	**1**	**0.008**	**4**	**4**	**4**	**32**	**2**	**4**	**16**	**0.25**	**1**	**8**
K366D AcrA	256	64	**1**	**0.008**	**32**	64	**64**	>1024	**16**	**64**	1024	**0.25**	**64**	>1024

ACR, acriflavine; BZK, benzalkonium chloride; CHL, chloramphenicol; CIP, ciprofloxacin; CLI, clindamycin; CV, crystal violet; DOX, doxorubicin; EtBr, ethidium bromide; ERY, erythromycin; FA, fusidic acid; MB, methylene blue; MIN, minocycline; NOV, novobiocin; R6G, rhodamine 6G. Underlined values highlight values for the Δ4PAP strain complemented with pTrcHis2 *acrA*, which encodes wild type *S.* Typhimurium SL1344 *acrA* with a C-terminal His-tag (WT AcrA complement). Bold values indicate at least two-fold or more difference compared to the parent strain.

Appendix IV. Structural formulae of AcrB-substrates.



A) Planar aromatic cations (PACs) are dye compounds that consist of multiple planar rings and a cationic moiety. **B)** Low-molecular mass drugs are generally non-planar and uncharged with a molecular mass below 500 Da. **C)** High-molecular mass drugs are generally non-planar and uncharged with a molecular mass above 500 Da. Although doxorubicin and minocycline possess planar rings, they lack the cationic moiety required to be grouped with the PACs. Figure created using ChemDraw 20.0.

Appendix V. Mean generation times of the *Salmonella* Typhimurium SL1344 Δ4PAP strain carrying plasmid different versions of AcrA in the presence of AcrB-substrates.

	Mean generation time (minutes) ± standard deviation									
Strain	LB only	CHL	CLI	DOX	EtBr	ERY	FA	MIN	NOV	R6G
WT	25.82 ± 1.92	36.88 ± 2.22	29.43 ± 1.46	25.75 ± 1.23	26.69 ± 3.88	26.16 ± 1.76	27.15 ± 1.56	25.28 ± 0.3	24.94 ± 1.01	24.59 ± 2.13
Δ4PAP	27.6 ± 1.65	NC	NC	NC	NC	NC	NC	NC	NC	NC
The following rows are Δ4PAP background strain + pET-20b carrying different versions of AcrA										
WT AcrA	29.34 ± 2.1	85.55 ± 3.41	49.96 ± 5.84	31.12 ± 4.28	24.87 ± 1.84	47.50 ± 3.42	36.78 ± 2.61	54.05 ± 3.38	25.88 ± 1.42	28.12 ± 2.32
F292V AcrA	24.43 ± 6.82 (ns)	NC	NC	NC	NC	NC	NC	NC	NC	NC
K366D AcrA	24.76 ± 0.58 (ns)	117.9 ± 5.6 (**)	74.92 ± 5.11 (**)	NC	24.71 ± 1.25 (ns)	NC	96.70 ± 5.61 (**)	95.23 ± 5.05 (***)	64.18 ± 2.67 (***)	28.54 ± 3.53 (ns)
Q311F AcrA	28.74 ± 0.08 (ns)	87.58 ± 3.02 (ns)	51.84 ± 7.92 (ns)	32.97 ± 0.43 (ns)	27.46 ± 1.45 (ns)	46.99 ± 0.52 (ns)	40.88 ± 7.1 (ns)	62.72 ± 2.95 (ns)	24.54 ± 2.36 (ns)	24.22 ± 3.77 (ns)

The generation times listed are the mean of three independent biological replicates ± standard deviation. NC, not calculated. For these strains, there was no observable exponential phase at these concentrations to calculate a generation time. This is because the exponential phase is when the cells are dividing regularly, so for strains without an observable exponential phase, it was not possible to calculate a generation time. Abbreviations and concentrations of drugs used: CHL, 0.5 μg/mL chloramphenicol; CLI, 8 μg/mL clindamycin; DOX, 4 μg/mL doxorubicin; EtBr, 16 μg/mL ethidium bromide; ERY, 4 μg/mL erythromycin; FA, 8 μg/mL fusidic acid; MIN, 0.25 μg/mL minocycline; NOV, 4 μg/mL novobiocin; R6G, 16 μg/mL rhodamine 6G. The mean generation time of the Δ4PAP strains carrying the plasmid with the F292V, Q311F or K366D AcrA mutations were compared to that of the Δ4PAP strain complemented with WT AcrA by one-way ANOVA. ** ($P \leq 0.01$); *** ($P \leq 0.001$); ns, not significant.

Appendix VI. Mean generation times of the *Salmonella* Typhimurium SL1344 Δ4PAP strain carrying the plasmid with the K366D AcrA mutation in the presence of different linezolid concentrations.

	Mean generation time (minutes) ± standard deviation				
Strain	LB only	2 μg/mL LZD	4 μg/mL LZD	8 μg/mL LZD	16 μg/mL LZD
K366D AcrA	22.49 ± 2.92	56.77 ± 6.03 (***)	91.58 ± 4.98 (****)	NC	NC

The generation times listed are the mean of three independent biological replicates ± standard deviation. NC, not calculated. For these strains, there was no observable exponential phase at these concentrations to calculate a generation time. This is because the exponential phase is when cells are dividing regularly, so for strains without an observable exponential phase, it was not possible to calculate a generation time. The mean generation time for each concentration of linezolid was compared to the mean generation time for LB only using one-way ANOVA. *** ($P \leq 0.001$), **** ($P \leq 0.0001$).

Appendix VII. Mean generation times of the *Salmonella* Typhimurium Δ4PAP Δ*acrB* strain carrying the plasmid with the K366D AcrA and channel 4 (F380A) AcrB mutations in the presence of different fusidic acid concentrations.

	Mean generation time (minutes) ± standard deviation			
Strain	LB only	4 μg/mL FA	8 μg/mL FA	16 μg/mL FA
WT	23.73 ± 157	24.43 ± 1.87	26.11 ± 1.63	30.37 ± 2.1
Δ4PAP Δ*acrB*	24.44 ± 0.18	NC	NC	NC
The following rows are Δ4PAP Δ*acrB* background strain + pET-20b carrying different version of AcrAB.				
WT AcrAB complement	25.13 ± 0.39	28.2 ± 2.59	33.89 ± 5.29	55.73 ± 5.59
K366D AcrA + WT AcrB	25.66 ± 0.67 (ns)	43.66 ± 0.82 (**)	75.74 ± 2.96 (***)	NC
WT AcrA + CH4 AcrB mutation	24.54 ± 1.28 (ns)	27.62 ± 0.58 (ns)	35.26 ± 1.89 (ns)	50.25 ± 4.45 (ns)
K366D AcrA + CH4 AcrB mutation	23.56 ± 1.15 (ns)	64.31 ± 4.9 (***)	NC	NC

The generation times listed are the mean of three independent biological replicates ± standard deviation. NC, not calculated. For these strains, there was no observable exponential phase at these concentrations to calculate a generation time. This is because the exponential phase is when cells are dividing regularly, so for strains without an observable exponential phase, it was not possible to calculate a generation time. The mean generation time of the Δ4PAP Δ*acrB* strain carrying the plasmid with the K366D AcrA and/or the channel 4 (CH4) AcrB mutation was compared to that of the Δ4PAP Δ*acrB* strain complemented with WT AcrAB using one-way ANOVA. FA, fusidic acid; ns, not significant; ** ($P \leq 0.01$); *** ($P \leq 0.001$).